Entanglement and defect entropies in gauge/gravity duality

Mario Flory

München 2016

Entanglement and defect entropies in gauge/gravity duality

Mario Flory

Dissertation
an der Fakultät für Physik
der Ludwig–Maximilians–Universität
München

vorgelegt von
Mario Flory
aus Neustadt an der Aisch

München, den 5. April 2016

Erstgutachter: Prof. Dr. Johanna Erdmenger
Zweitgutachter: Prof. Dr. Dieter Lüst
Tag der mündlichen Prüfung: 13.07.2016

Contents

List of Figures

List of Tables

Zusammenfassung

In dieser Dissertation untersuchen und verwenden wir geometrische Methoden zur Berechnung von Verschränkungs-Entropie in Feldtheorien, die gemäß der Eichtheorie/Gravitations-Dualität über ein Gravitations-Dual verfügen. Die Hauptresultate dieser Arbeit ergeben sich aus der Anwendung unserer Ergebnisse auf die Untersuchung von Verschränkungs- und Defekt-Entropien in einem holographischen Modell des Kondo-Effektes.

Die Eichtheorie/Gravitations-Dualität ist eine wichtige Methode zur Untersuchung stark gekoppelter Systeme. Zunächst geben wir einen kurzen Überblick über die verwandten Ideen des holographischen Prinzips und die Realisierung der AdS/CFT-Korrespondenz in Stringtheorie (AdS steht hier für *Anti-de Sitter*, und CFT steht für *Konforme Feldtheorie*, englisch *conformal field theory*). Außerdem besprechen wir das Konzept der Verschränkungs-Entropie und erklären, wie diese Größe holographisch berechnet werden kann.

Anschließend wenden wir moderne Methoden zur Berechnung von Verschränkungs-Entropie in Gravitationstheorien mit Termen höherer Krümmungsordnung auf spezielle Raumzeiten, im Besonderen auf stationäre Schwarze Löcher, an. Dabei stoßen wir auf analytische Lösungen für die extremalen Hyperflächen, die die Verschränkungs-Entropie bestimmen, welche sich um das Schwarze Loch winden. Wir argumentieren, dass diese Hyperflächen unphysikalisch sind, indem wir aufzeigen, dass sie bestimmte Kausalitätsbedingungen verletzen.

Weiterhin untersuchen wir die geometrischen Eigenschaften bestimmter Modelle für Dualitäten zwischen AdS-Räumen und Grenzflächen-CFTs, mit einem besonderen Augenmerk auf ein kürzlich vorgeschlagenes holographisches Modell des Kondo-Effektes. Eines der Hauptresultate dieser Dissertation wird darin bestehen, ein Verständnis dafür zu erlangen, wie sich Energie-Bedingungen auf die möglichen Geometrien der höherdimensionalen Raumzeit auswirken. Wir wenden dann die Ergebnisse dieser Untersuchungen im Speziellen auf das Kondo-Modell an und insbesondere berechnen wir Verschränkungs- und Defekt-Entropien numerisch. Diese Größen können im Kontext des RG-Flusses, welchen das Kondo-Modell erfährt, interpretiert werden. Es wird im Detail erläutert, inwiefern das holographische Kondo-Modell Erwartungen aus Feldtheorie-Rechnungen erfüllt und wie es verbessert werden könnte. Weiterhin gehen wir auf aktuelle Vorschläge zur Definition eines holographischen Maßes für Komplexität ein. Dabei handelt es sich um einen Begriff aus der Quanteninformationstheorie. Die Arbeit endet mit einem Ausblick auf mögliche

zukünftige Forschungsrichtungen.

Diese Dissertation basiert auf der Arbeit die der Autor als Doktorand unter der Betreuung durch Prof. Dr. Johanna Erdmenger am Max-Planck-Institut für Physik in München im Zeitraum vom 2. April 2013 bis zum 31. März 2016 durchgeführt hat. Die einschlägigen Publikationen lauten wie folgt:

[1] J. Erdmenger, M. Flory and C. Sleight, *Conditions on holographic entangling surfaces in higher curvature gravity*, *JHEP* **1406** (2014) 104, `arXiv:1401.5075 [hep-th]`.

[2] J. Erdmenger, M. Flory and M. N. Newrzella, *Bending branes for DCFT in two dimensions*, *JHEP* **1501** (2015) 058, `arXiv:1410.7811 [hep-th]`.

[3] J. Erdmenger, M. Flory, C. Hoyos, M. N. Newrzella and J. M. S. Wu, *Entanglement Entropy in a Holographic Kondo Model*, *Fortsch. Phys.* **64** (2016) 109–130, `arXiv:1511.03666 [hep-th]`.

[4] J. Erdmenger, M. Flory, C. Hoyos, M. N. Newrzella, A. O'Bannon and J. Wu, *Holographic impurities and Kondo effect*, `arXiv:1511.09362 [hep-th]`

Abstract

In this thesis we investigate and use geometrical prescriptions for the calculation of entanglement entropy in field theories that have a gravity dual according to gauge/gravity duality. The main results of this work will arise from the application of our findings to the study of entanglement and defect entropies in a holographic model of the Kondo effect.

Gauge/gravity duality is an important tool for the study of strongly coupled systems. We give a short review over the related idea of the holographic principle and the realisation of the AdS/CFT correspondence in string theory. We also introduce the concept of entanglement entropy and review the methods of holographically calculating it.

We then apply recent prescriptions for calculating holographic entanglement entropy in gravitational theories with higher curvature terms to specific example spacetimes, such as stationary black holes, and obtain analytical solutions for extremal surfaces defining entanglement entropy that wrap around the black holes. We argue that these surfaces are unphysical by discussing how they violate certain well motivated causality constraints.

We then investigate the geometrical properties of certain models of dualities between AdS spaces and boundary CFTs, with a special interest in a recently proposed holographic model of the Kondo effect. Understanding the impact of energy conditions on the allowed bulk geometries will be one of the main results of this thesis. We then apply the knowledge gained from these studies to the specific Kondo model, and numerically calculate entanglement and impurity entropies. These quantities can be interpreted in terms of the RG flow that the Kondo model undergoes. It will also be discussed in detail to which extend the holographic model reproduces field theory expectations, and how it can be improved. Furthermore, we investigate recent proposals of defining holographic measures of complexity. This is a quantity in quantum information theory. We end with an outlook on possible future research directions.

This thesis is based on the research that the author carried out as a PhD student under the supervision of Prof. Dr. Johanna Erdmenger at the Max Planck Institute for Physics in Munich, Germany, between the 2nd of April 2013 and the 31st of March 2016. The relevant publications are:

[1] J. Erdmenger, M. Flory and C. Sleight, *Conditions on holographic entangling surfaces in higher curvature gravity*, *JHEP* **1406** (2014) 104, `arXiv:1401.5075 [hep-th]`.

[2] J. Erdmenger, M. Flory and M. N. Newrzella, *Bending branes for DCFT in two dimensions*, *JHEP* **1501** (2015) 058, arXiv:1410.7811 [hep-th].

[3] J. Erdmenger, M. Flory, C. Hoyos, M. N. Newrzella and J. M. S. Wu, *Entanglement Entropy in a Holographic Kondo Model*, *Fortsch. Phys.* **64** (2016) 109–130, arXiv:1511.03666 [hep-th].

[4] J. Erdmenger, M. Flory, C. Hoyos, M. N. Newrzella, A. O'Bannon and J. Wu, *Holographic impurities and Kondo effect*, arXiv:1511.09362 [hep-th]

Chapter 1

Introduction

From clockworks to geometry and information

The goal of natural sciences is to describe the world around us in exact scientific terms, often by uncovering fundamental laws of nature and phrasing them in an unambiguous mathematical language, thereby enabling scientists to make predictions about future events in nature or laboratory environments. Ultimately, the natural sciences, specifically physics, have to be applied to the universe as a whole. In this endeavour, it is not surprising that, instead of starting from scratch, people have often derived inspiration from the ideas of science and technology that were prevalent at the time. The deterministic laws of celestial motion and Newtonian mechanics have, for example, often caused scientists to liken the universe to a clockwork. In contrast, during the last century, the analogy of the universe as a (quantum) computer seems to have grown popular.

A little more than 100 years ago, Albert Einstein's general theory of relativity[1], introduced the idea into theoretical physics that events in the universe are not taking place on a fixed stage, but that spacetime itself is a dynamical quantity, and has to play an important part in the physics of the universe. This was already an enormous paradigm shift, but it didn't take long before scientists such as Oskar Klein and Theodor Kaluza proposed that the idea of dynamical spactime geometry could lead the way to a unification of general relativity and electromagnetism. Although due to certain problems of this approach and the rise of quantum field theory these early ideas have fallen somewhat out of favour shortly after their advent,[2] they have arguably seen a strong comeback with the necessity of handling the extra dimensions that string theory proposes.

In the 1950s, the idea of dynamical geometry as the fundamental property of nature made its return to (classical) theoretical physics with Wheelers idea of *geometrodynamics* [7, 8], culminating in the slogan "physics is geometry" [8]. This program proposed that, for

[1] Just recently confirmed once more by the direct detection of a gravitational wave [5].

[2] For an excellent overview over the early history of general relativity and Kaluza Klein theory, see [6].

example, point charges could be seen as the ends of tiny *wormholes* from which the field lines of a source-free electromagnetic field emerge.

These ideas attracted some amount of interest at the time, only to fall out of favour thereafter, only to be revived once more in a slightly different way under the modern slogan "ER=EPR" (see [9–13] for a partial list of references). This idea notes certain fundamental similarities between the physical properties of entangled particles (*EPR pairs*) and black holes (defined by the geometry of *Einstein-Rosen (ER) bridges*) and proposes that this is not a coincidence, but in fact a fundamental duality between these two phenomena. This would mean that entanglement, one of the core phenomena of quantum physics and quantum information theory, can be understood in terms of geometry and topology. How can such a bold claim be made with so much confidence? The reason is that this is not an isolated qualitative idea, but it is motivated and in some cases derived from a much broader, more fundamental and, most importantly, more quantitative framework, namely the ideas of *holography* and *gauge/gravity duality*.

Holography

The ideas of *holography* arise from the need to formulate a consistent theory of thermodynamics in a world that allows for *black holes* to exist. Black holes are solutions to the equations of Einstein's gravity (or similar theories) that have a non-trivial *causal structure*, i.e. there are regions in the black hole spacetime that cannot send a signal out to the region infinitely far away from the black hole. Such objects can *only* arise in a theory where the speed of communication has an upper bound (the speed of light in Einstein's theory) and the *spacetime metric* (the mathematical object determining the trajectories of information carrying signals) is a dynamical quantity, not being fixed to be a simple background structure. Even more, such objects are not only theoretical constructs allowed by the mathematics of Einstein's theory, but also have they likely been observed to exist in nature [5]. The consistency of the physics of such objects with the well known laws of thermodynamics is hence an interesting and important question, the study of which was started in [14–16]. The result of this work was the realisation that not only is it necessary to assign *entropy* to black holes, but that this entropy has to scale like the surface area of the black hole. This is in contrast to non-gravitational systems where the thermodynamic entropy, being an extensive quantity, scales like the volume. This groundbreaking result has led to deep investigations into the thermodynamics of black holes and quantum field theory in curved spacetimes. Also, it has led to the idea that there should be upper bounds on the amount of entropy (or information) that can be stored in physical systems, depending on the characteristics of the system such as energy content or size [17–19]. Simply speaking, whenever someone tries to violate these bounds by storing too much entropy in a given system, nature automatically intervenes by forming a black hole. This led to the proposal [18, 19] that a consistent theory unifying the laws of gravity and the laws of quantum physics should obey the *holographic principle*, the principle that the number

of degrees of freedom of a given spacetime region scales like its surface area, not like its volume.

The best current candidate for a unified theory of quantum gravity is *string theory* (see [20–24] for introductory texts), and indeed it has been shown [25–27] that the holographic principle is realised in string theory in the form of an *Anti-de Sitter/conformal field theory (AdS/CFT) correspondence*. Specifically, the most well known example studied in [25] proposes a *duality* between type IIB superstring theory on an $\mathrm{AdS}_5 \times \mathrm{S}^5$ background and $\mathcal{N} = 4$ $SU(N)$ super Yang-Mills theory in $3+1$ dimensions, which is a CFT. The former theory is (in general) a theory of quantum gravity and hence its foundational principles and properties must currently be considered to be mysterious, but the latter one, in contrast, is a quantum field theory and hence in principle well understood. This is how the AdS/CFT correspondence encodes the holographic principle, a quantum gravity theory in (after compactification) $(d+1)+1$ dimensions is formulated as a $d+1$-dimensional field theory, such that the entropies in both theories will scale as length^d.

Although we wrote above that in general the mathematical principles of quantum field theory are much better understood than those of quantum gravity, we will see later that the best understood form of Maldacena's $\mathrm{AdS}_5/\mathrm{CFT}_4$ correspondence requires us to work in a parameter range where the CFT is *strongly coupled*, making computations hard in practice. On the other hand, the quantum gravity theory becomes weakly coupled classical gravity in this case, and is hence tractable. The $\mathrm{AdS}_5/\mathrm{CFT}_4$ correspondence and similar models of AdS/CFT duality and generalisations thereof, going by the name *gauge/gravity dualities*, then provide a new way of studying strongly coupled systems. This topic is notoriously hard due to the inapplicability of perturbation theory and the shortcomings of lattice techniques. Successes of gauge/gravity duality techniques in this field involve, amongst many others, the following:

- Gauge/gravity duality naturally suggests an investigation of the *information paradox*, as the CFT that is dual to the quantum gravity theory in the bulk is manifestly unitary [28].
- Using gauge/gravity techniques, it has been possible to derive the ratio of shear viscosity η to entropy density s,

$$\frac{\eta}{s} = \frac{1}{4\pi}\frac{\hbar}{k_B}, \tag{1.1}$$

  for a wide class of holographic fluids [29,30]. Later, an entire field called *fluid/gravity correspondence* emerged in which the methods of holography, and in particular the physics of black holes and event horizons, were applied to the study of fluids [31], see also [32] for an overview.
- In fact, the result (1.1) has been conjectured to be a universal lower bound on η/s for realistic systems [29, 30] (see also the review [33]), an idea fuelled by the fact that of all experimentally known fluids in nature it is the (strongly coupled) *quark-gluon plasma* (QGP) that comes closest to this bound, but it does not violate it

[30, 33, 34]. Much work, often involving numerical simulations of dynamical bulk spacetimes, has been invested to apply gauge/gravity techniques to the study of strongly coupled plasmas and QGP phenomenology, which can experimentally be studied in heavy ion collisions at accelerators such as LHC or RHIC. Apart from this problem of heavy ion collisions, gauge/gravity methods have also been applied to other questions in *quantum chromodynamics (QCD)*. For overviews of the various attempts to create qualitative holographic duals of QCD see [33, 35–37]. Notable results are the holographic studies of *meson melting* and *meson spectra* (see [33, 38] for reviews) and of the QCD phase diagram (see [36] for a review). Very recently, holographic methods have also been applied to the study of *glueballs* [39].

- Gauge/gravity duality has also been applied to condensed matter physics, for example with the study of *holographic superconductors* pioneered in [40, 41]. A detailed overview over the vast landscape of holographic models and results concerning condensed matter physics is beyond the scope of this introduction, but see [42, 43] for reviews and references.

- Gauge/gravity duality and especially one of its features, the *UV/IR connection* [44], naturally suggest an application to the study of *renormalisation group* (RG) flows, both by constructing duals of specific flows (see e.g. [45]) or by proving general theorems about RG-flow monotones, such as the famous c-theorem or similar theorems [45–49].

Overviews of some of the above mentioned research directions as well as further references can also be found in the recent textbooks [50–53].

We see that the concrete realisation which the holographic principle has, due to string theory, found in the form of the AdS/CFT correspondence and gauge/gravity duality has transformed holography from a simple *property* of gravitational theories to a versatile *tool* that can be applied to many different research questions and topics. In the next section, we will focus on one additional important achievement of gauge/gravity duality research that was left out in our above enumeration, namely the holographic study of *entanglement entropy*.

Entanglement entropy

In its weak form, i.e. when taking the limit of strong coupling in the CFT and small bulk Newton's constant, the AdS/CFT duality is not only a *strong-weak duality* but also a *quantum-classical duality*. This means that quantum phenomena of the field theory, like for example entanglement, have to be somehow encoded in the classical bulk gravity theory.

There are different ways of quantifying the amount of entanglement between two quantum systems (see [54] for a basic introduction to quantum information theory), and one of the simplest ways to do so is by calculating a quantity called *entanglement entropy*. For

a quantum system A which is the subsystem of a larger quantum system, entanglement entropy is defined to be the *von Neumann entropy* of the *reduced density matrix* ρ_A of the system A, i.e.[3]

$$S_A = -k_B \mathrm{Tr}_A[\rho_A \log \rho_A]. \tag{1.2}$$

Ryu and Takayanagi proposed in [55, 56] that this field theory quantity has a very simple geometrical interpretation, namely that the holographically dual way to calculate this quantity is to calculate the area $\mathcal{A}$ of a certain extremal hypersurface in the curved bulk spacetime. The entanglement entropy is then

$$S_A = \frac{k_B c^3}{\hbar G_N} \frac{\mathcal{A}}{4}. \tag{1.3}$$

This encompasses the Bekenstein-Hawking formula for black hole entropy as a special case and generalises it. Holography thus naturally suggests to interpret black hole entropy as entanglement entropy for a division of the dual theory into two sectors. As the entropy of stationary black holes is determined by their geometrical properties (Killing horizons, bifurcation surfaces et cetera), this leads to a geometric interpretation of entanglement in holography and hence to the idea of "ER=EPR" mentioned earlier on. In fact, as the dual prescription (1.3) for calculating entanglement entropy is *only* dependent on the bulk geometry, and not on any other bulk field, it is the ideal subject to study in order to understand how gauge/gravity duality leads to a modern manifestation of the old slogan "physics is geometry".

Gauge/gravity models do not have to be derived from string theory, in fact it is quite common to propose *bottom-up models* that follow the spirit of stringy holography, but otherwise take some freedom. For example, such models may make use of asymptotically AdS spacetimes and interpret certain bulk objects as dual to certain objects in a conjectured dual field theory, but otherwise freely fix the field content of the bulk theory without having a concrete derivation of that field content from a string theory model in mind. In such bottom-up models it may then occasionally be of interest to consider bulk gravitational theories which are not pure Einstein-Hilbert gravity, but contain *higher curvature terms* in their action. It is well known [57–59] that such higher curvature terms will lead to corrections to Bekenstein's area formula for black hole entropy and consequently there will also have to be corrections to the holographic entanglement entropy formula. These corrections have only recently been determined [60–63] and it will be one of the topics of this thesis to study geometrical properties of holographic entanglement entropy when such higher curvature corrections are present. In particular, we will investigate the geometrical impact of the *causal influence argument* [64], which has to hold for simple physical reasons.

[3] In contrast to many sources that are concerned with information theory, we explicitly include the factor k_B here.

Holographic impurities and the Kondo effect

Above, we have seen that holographic techniques have been successfully applied to topics in condensed matter physics. One phenomenon out of this broad field that will be studied in this thesis is what is known as the *Kondo effect*. See [65] for the original source, [66, 67] for a modern perspective and [68] for a brief historical overview.

This effect has first been observed by measuring the resistivity of metal probes with a low concentration of impurity atoms as a function of temperature. For example, when investigating the resistivity of a gold probe with dilute iron impurities it is clearly visible that as the temperature is lowered, the resistivity first attains a minimum at a certain temperature and then *increases* [69]. This increase of resistivity at low temperatures was surprising as it was qualitatively different from the expected decrease in normal metals or even superconductors [65, 66, 68]. As the effect was only observed in the presence of magnetic impurities and was found to be proportional to the concentration of the impurity atoms, it was quickly realised that the phenomenon had to be due to the interaction of conduction electrons with localised single magnetic impurities [65, 68]. A perturbative second order calculation by Jun Kondo then showed in [65] that due to the spin-spin interaction between impurities and electrons, the resistivity ρ at low temperatures follows an equation of the form

$$\rho(T) = a_1 T^5 + c a_2 - c a_3 \log\left(\frac{T}{T_F}\right), \tag{1.4}$$

where c is the concentration of the impurity atoms, T_F is the Fermi temperature and the a_i are model dependent positive parameters. The term $\sim -\log(T)$ explains the rise of resistivity at low temperatures. However, the prediction of a *divergence* of the resistivity at low temperatures is unphysical, and signifies a breakdown of the perturbation theory, used to derive (1.4), below a certain temperature T_K, the *Kondo temperature* [65–67, 70]. The desire to understand the correct behaviour of these impurity systems at temperatures below the Kondo temperature T_K, the *Kondo problem* [67], inspired the application and development of a variety of different physical methods [66], including renormalisation group methods [70, 71]. The modern understanding of the solution of this problem is that at low temperatures the impurity is screened from the rest of the system by conduction electrons that form the *Kondo screening cloud* [72], see also [66, 67, 73, 74]. As pointed out in [66, 67], interest in the Kondo effect has increased recently with the advent of nanotechnology and *quantum dots* [75].

The Kondo effect has attracted a large amount of attention from the theoretical physics community, and the works cited above only give a small glimpse of the extensive literature that is available on this topic. There is even a sizeable amount of holographic models describing Kondo impurities or related physics, see [76–86]. What interesting things can such holographic models still teach us about a phenomenon that is so well researched in the condensed matter literature? In the closing section of [66], three mayor topics concerning the physics of the Kondo effect were outlined that still warrant further research:

- The properties of the Kondo cloud, and ways to measure and manipulate it.
- Time-dependent phenomena in Kondo systems.
- Interactions between different magnetic impurities.

Excitingly, all three of these items can be studied based on a holographic Kondo model proposed in [86] and sketched in figure 1.1. This model will be explained in more detail later, for the moment it is only important to note that the asymptotically AdS bulk spacetime is a $2+1$-dimensional black hole, and the localised magnetic impurity is holographically described by an infinitely thin massive hypersurface, referred to as *brane* in the following. The two impurity case of this model was holographically studied in [87], and a numerical study of time-dependent phenomena in the model of [86] is currently under way. Results on the Kondo cloud based on this model have been published in [3, 4] and will be a central issue of this thesis in chapter 6.

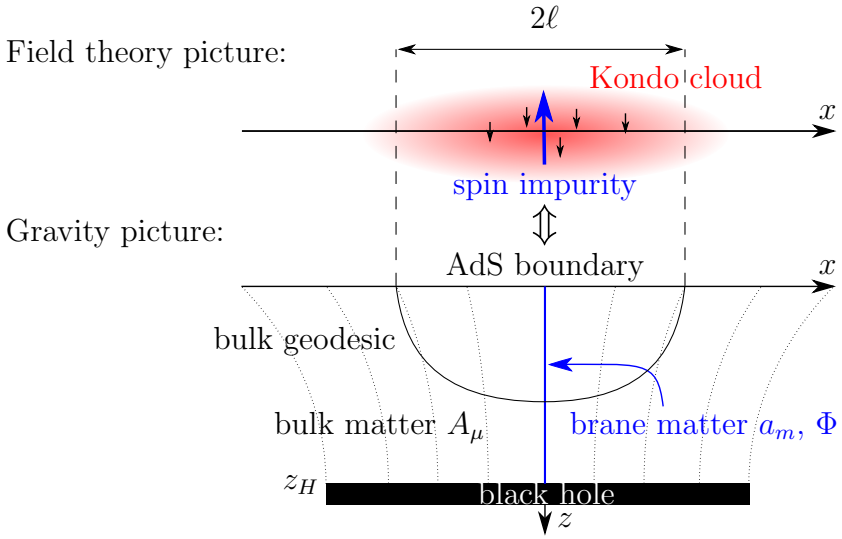

Figure 1.1: A sketch of the holographic bottom-up Kondo model of [86]. On the field theory side, we have conduction electrons interacting with a localised impurity via spin-spin interaction. At low temperatures these electrons will form a Kondo cloud bound to the impurity. In the dual gravity model, the localised impurity is mapped to a localised codimension one hypersurface, called *brane*, embedded into the ambient spacetime. A Chern-Simons field A_μ is defined throughout the bulk spacetime, while a scalar field Φ and a gauge field a_m are confined to the worldvolume of the hypersurface. The entanglement entropy of a boundary interval of length 2ℓ centered around the impurity will be holographically given by the length of a spacelike geodesic crossing the brane. The figure is presented as in [3].

Specifically, we will study the Kondo cloud using holographic calculations of entanglement entropy. As said above, the Kondo effect comes about due to the spin-spin interaction of conduction electrons and impurity, creating entanglement between the impurity and the

conduction electrons [74]. Entanglement entropy can hence be used to study the Kondo cloud and its length scale, as has been done in the field theory literature in [88–91]. We carry out similar computations using the holographic Kondo model, but to do so we need to consistently take into account the backreaction of the brane onto the bulk geometry. The necessary mathematical formalism to do so is given by the *Israel junction conditions*, which will be studied in detail. Proposals for holographic duals of field theories with boundaries, or field theories interacting with impurities or defects, based on these junction conditions have been proposed already in [92–94]. Towards the end of this thesis, it will become clear how the geometrical properties of the model of [86] and the Israel junction conditions combine in a non-trivial way to yield new insights into holographic Kondo physics.

Results of this thesis

In this thesis, we present several new results that have been published in [1–4]. Of course these papers were not written without the help of the coauthors listed on these papers, and hence we will in this thesis focus on presenting the contributions that the present author made to these publications. In particular, the original results to be presented in this thesis will be the following:

- Following [1], we will demonstrate the importance that causality constraints have in the calculation of holographic entanglement entropy. We will do so by explicitly calculating closed holographic entangling surfaces in black hole spacetimes in new massive gravity (NMG) and Gauss-Bonnet gravity, demonstrating that the standard prescriptions proposed in the literature [60–63] would lead to unphysical results. The imposition of causality constraints is then sufficient to exclude the unphysical hypersurfaces both in NMG and Gauss-Bonnet gravity.

- In a framework proposed by Takayanagi [92–94] for constructions of bottom-up models of AdS/boundary CFT duality, we provide a geometrical theorem that greatly constrains the possible geometries of bulk spacetimes in models of this type, depending on the energy conditions satisfied by the bulk matter [2].

- Furthermore, as in [2], we present a variety of exact solutions to a simple toy model of this kind, showcasing the content of the above mentioned geometrical theorem.

- We then apply these geometrical methods to the specific bottom-up model of the Kondo effect proposed in [86]. From the resulting bulk geometry, we holographically calculate entanglement entropy and impurity entropy and show that the holographic model satisfies the g-theorem, as expected. These results have been published in [3,4].

- For AdS/BCFT models such as the Kondo model of [86], we develop a geometrical approximation method that is valid when calculating the entanglement entropy of large boundary regions [3, 4]. We will compare the analytical formula following from this approximation scheme to an analytical result published in the field theory

literature [90], finding good agreement.

- We will also comment on a quantity referred to as *computational complexity* [95–101] and present results on this quantity in the holographic Kondo model that have not yet been published elsewhere. We will discuss both the possible physical interpretation of this quantity in the light of the RG flow of the Kondo model, as well as certain issues concerning the definition and holographic computation of complexity.
- Finally, we will analyse the low temperature features of the holographic Kondo model. It is then shown by analytical arguments [3] that the potential of the scalar field Φ needs to be equipped with terms of at least quartic order for the model to show realistic behaviour at very low temperatures.

Outline of this thesis

The structure of this thesis is as follows:

- Chapter 2 will deal with the fundamental ideas behind holography and the AdS/CFT correspondence. Specifically, section 2.1 will summarise how the physics and thermodynamics of black holes leads to the holographic principle. In section 2.2 we will then encounter a first realisation of the holographic principle due to the asymptotic symmetries of three-dimensional Anti-de Sitter space. The following section 2.3 will contain a detailed look at how the to this date best understood manifestation of the holographic idea, namely Maldacena's AdS_5/CFT_4 correspondence, arises from string theory. The chapter closes with a few musings on the similarities and differences between gravitational holography and optical holography in section 2.4.
- In chapter 3 we will then encounter what arguably is (besides the idea of holography itself) the main topic of this thesis: entanglement entropy. The basic definition of this quantity in quantum mechanical terms will be given in section 3.1, followed by a discussion of how to calculate this quantity in a holographic way in section 3.2. In section 3.3 it will be explained how holographic entanglement entropy is related to and generalises the idea of black hole entropy. This will enable us to understand the basic motivation of the ER=EPR proposal mentioned earlier. The replica trick, an important method for calculating and understanding entanglement entropy, will then be briefly discussed in section 3.4.
- In chapter 4 we will then begin to delve into the new results presented in this thesis. After a quick introduction to the topic of holographic entanglement entropy in the presence of higher curvature terms in section 4.1 we will study explicit calculations concerning holographic entanglement entropy in two higher curvature theories, namely new massive gravity in section 4.2 and Gauss-Bonnet gravity in section 4.3. In both cases we will encounter problems when following the standard prescription for the holographic calculation of entanglement entropy in these higher curvature

theories. These problems will be resolved in section 4.4 by imposing a causality requirement on the prescription for calculating entanglement entropy.

- Bottom-up models for dualities between AdS spaces containing dynamical boundary surfaces and *boundary CFTs (BCFTs)* will be discussed in chapter 5. After introducing the geometric setup in section 5.1, we will in detail study the relation between energy conditions and geometry for these models in section 5.2. Specifically, we will present a useful decomposition of the energy-momentum tensor in section 5.2.1, state the various energy conditions in section 5.2.2 and discuss their implications in conjunction with the *barrier theorem* in section 5.2.3. We will then discuss the special cases of AdS and BTZ background spacetimes in section 5.2.4. Exact analytical solutions to the equations of motion defined in section 5.1 will then be discussed in section 5.3, where in subsection 5.3.1 we deal with constant tension models and in subsection 5.3.2 we assume the matter content to be described by a perfect fluid.

- Chapter 6 will then be denoted to an application of the results developed in the previous chapter to the holographic Kondo model of [86]. The Kondo effect itself will be briefly reviewed from a field theory perspective in section 6.1.1, before explaining the top-down holographic Kondo model of [86] in section 6.1.2. The main results of this chapter will however be obtained working with the bottom-up model of [86] to be summarised in section 6.2. The inclusion of backreaction into this model and its equations of motion will be discussed in section 6.3. The numerical results on this model will then be explained in section 6.4, with a focus on energy conditions (section 6.4.1), entanglement entropy (section 6.4.2) and the g-theorem (section 6.4.3). A semi-analytical approximation formula for the impurity entropy will be discussed in section 6.5, before the behaviour of a measure of complexity in the holographic Kondo model is studied in section 6.6. The chapter then closes in section 6.7 with a discussion of the zero-temperature behaviour of the holographic bottom-up Kondo model, and ways to improve it.

- The main text of this thesis concludes with chapter 7, where we give an outlook on possible future research directions related to the topics discussed in this work.

- A number of technical details will be relegated to the appendices. In particular, in appendix A we will discuss geometrical definitions such as extrinsic curvature and induced metrics for hypersurfaces of both codimension two (appendix A.1) and codimension one (appendix A.2). The corollary to the barrier theorem presented in section 5.2.3 for 2+1-dimensional ambient spaces will be extended to 3+1 dimensions in appendix B. Finally, appendix C will discuss junction conditions for Chern-Simons fields similar to the Israel junction conditions for the metric discussed in section 6.3.1. In this appendix, we will also apply these Chern-Simons junction conditions to a simple and pedagogical toy model in order to illustrate them.

Conventions

Most of the time we will be setting the speed of light c, the reduced Planck constant $\hbar$ and the Boltzmann constant k_B to one,

$$c = \hbar = k_B \equiv 1, \tag{1.5}$$

leaving only Newton's constant G_N as a dimensionfull independent natural constant. This is sometimes referred to as *quantum units*, see e.g. [102]. This in particular means that all hypervolumes of d-dimensional hypersurfaces (referred to as *areas* for codimension two hypersurfaces) will be measured in units of the Planck length ℓ_P^d. In four spacetime dimensions, $\ell_P = \sqrt{G_N}$. We will occasionally also make use of the reduced Newton's constant $\kappa_N^2 \equiv 8\pi G_N$ and the 10-dimensional reduced Planck length $\ell_{P,10}^8 \equiv \kappa_N^2$.

For Lorentzian spacetimes or induced metrics, we use the mostly plus sign convention. A vector v^μ is then called *timelike* if $v^\mu v_\mu < 0$, *spacelike* if $v^\mu v_\mu > 0$ and *null* if $v^\mu v_\mu = 0$. Any worldvolume, submanifold or hypersurface in a larger spacetime that includes a timelike vector field is also referred to as timelike, irrespective of how many spacelike dimensions it may also have. A $d+1$-dimensional spacetime is then a spacetime with one timelike and d spacelike dimension.

Chapter 2

Holography

In the following, we will lay the foundations for the later chapters by discussing the holographic principle and its realisations in the form of AdS/CFT. To do so, we will summarise how the existence of a general holographic principle can be inferred from thought experiments concerning the physics of black holes in section 2.1. In section 2.2 we will have a look at the famous result due to Brown and Henneaux [103] that established a possible relation between gravity on three-dimensional asymptotically Anti-de Sitter (AdS) spaces and two-dimensional CFTs already in 1986. Section 2.3 will then be devoted to the so far best understood manifestation of the holographic principle, namely Maldacena's derivation of an AdS_5/CFT_4 correspondence from string theory [25]. There will also be a short epilogue 2.4 in which we compare the holographic principle and its realisations to optical holography.

2.1 Holography and the laws of gravity

In this section we will briefly summarise how thought experiments concerning the physics of black holes show the necessity of some kind of holographic principle. To do so, we will mainly follow the outline of these ideas presented in [50, 104].

2.1.1 Black hole thermodynamics and entropy bounds

Black holes are solutions to general relativity[1] which exhibit a non-trivial causal structure that includes *event horizons*, i.e. null hypersurfaces that distinguish between such points from which signals can be sent to some notion of asymptotic infinity (or far away outside

[1] Or any other gravitational theory of curved spaces, such as higher curvature theories. See section 4 for more details. Throughout the reminder of this section, we will always assume gravity to be described by the Einstein-Hilbert action, with no or only negligible corrections.

region) and such points from which this is not possible. See e.g. [105] for the precise mathematical definition. The presence of such event horizons then means, almost by definition, that from the point of view of an outside observer which remains near infinity, other observers may fall into the black hole and vanish from sight. This raises the question: What happens to the entropy of an object that falls into the black hole from the point of view of an outside observer? Will the second law of thermodynamics be violated, or will the object's entropy be effectively transferred onto the black hole? Based on thought experiments like this, Bekenstein proposed that a black hole should indeed be assigned an entropy proportional to its area [14–16][2]

$$S_{BH} = \frac{\mathcal{A}}{4G_N} \tag{2.1}$$

While the precise nature of the microstates that may give rise to an entropy of the form (2.1) is still an open question up to this day, there are good reasons to believe in this formula at least as a good approximation to black hole entropy. The first reason is the existence of *Hawking radiation* corresponding to the *Hawking temperature* [106, 107]

$$T_{BH} = \frac{\kappa}{2\pi} \tag{2.2}$$

where κ is the *surface gravity* of the black hole horizon. Equations (2.1) and (2.2) together allow for a first law of black hole thermodynamics[3] to be formulated in the form [108]

$$dM = T_{BH} dS_{BH} = \frac{\kappa}{8\pi G_N} d\mathcal{A} \tag{2.3}$$

where M is the black hole mass. Indeed it is only equation (2.3) together with (2.2) that fixes the prefactor in (2.1) to be 1/4. It is easy to check the validity of equation (2.3) on concrete examples such as the Schwarzschild solution.

The second mayor reason to believe in the validity of equation (2.1) is that, due to the *area theorem* $dS_{BH} \geq 0$ proven by Hawking for classical processes in general relativity in [109, 110], it suggests an extension of the second law of thermodynamics to what is called the *generalised second law*. This law purports that in any physical process, the combination of matter entropy S_{mat} and black hole entropy S_{BH} can only grow, i.e. [14–16]

$$dS_{tot} = d(S_{mat} + S_{BH}) \geq 0. \tag{2.4}$$

In the absence of black holes, this reduces to the ordinary second law of thermodynamics, $dS_{mat} \geq 0$, while in the absence of thermodynamic matter it reduces to the area law. The remaining question is then: Will in any physical process the apparent loss of thermodynamic entropy be outweighed by the corresponding increase in black hole entropy, such

[2] The prefactor 1/4 was only fixed in hindsight by Hawking's calculation of black hole temperature in [106, 107].

[3] The "zeroth" law of black hole thermodynamics is often stated to claim that on the event horizon of a stationary black hole, κ is a constant [108].

that the generalised second law (2.4) holds? This leads directly to a thought experiment discussed by Bekenstein in [17]. This thought experiment is concerned with a process in which a thermodynamic system with energy E, entropy S_{mat} and size R is lowered into a Schwarzschild black hole with radius $r_S \gg R$ in two steps: First the system's center of mass is slowly lowered from infinity to a position located at a distance of R above the horizon, and then in the second step it is let loose to fall into the black hole. Taking the redshifting of the energy E in step one of the process properly into account, one finds $dM = \frac{ER}{4G_N M}$. Then, using (2.3) as well as $T_{BH} = \frac{1}{8\pi G_N M}$ for the Schwarzschild black hole [107], this implies that the generalised second law (2.4) only holds when [17]

$$S_{mat} \leq 2\pi ER \tag{2.5}$$

for any physical thermodynamic system. This equation (2.5) is known as the *Bekenstein bound*, not to be confused with the *Bekenstein formula* (2.1). See also [104] for a short discussion of this result and its general validity. The relevance of the Bekenstein bound in the context of holography is that, assuming that black holes exist and behave in a physical thermodynamic way, it sets an upper limit on the amount of information that can be stored in a physical system with finite size and energy content. In this context, it is interesting to note that Schwarzschild black holes in 4 dimensions actually saturate this bound when setting $E = M, R = r_S$ [104]. The Bekenstein bound also exemplifies the *species problem* [104,111,112] which is ubiquitous in discussions of the holographic principle and black hole information: If one just allows for a large number of particle species to be present in the theory, then information can efficiently be encoded in the types of particles present in a certain system, with no significant increase in energy cost. This way the bound (2.5) can in principle easily be violated. An arbitrarily large number of particle species is hence considered unphysical, see [104] for a more in depth discussion.

In a different kind of thought experiment, first analysed by Susskind in [19] (see also [50, 104]), an approximately spherical matter system (smaller than a sphere with surface area $\mathcal{A}$, and with an entropy S_{mat}) is turned into a black hole with area precisely equal to $\mathcal{A}$ by collapsing a spherical shell of matter onto the central matter system. Demanding the generalised second law (2.4) to hold then straightforwardly yields the *spherical entropy bound* [19]

$$S_{mat} \leq \frac{\mathcal{A}}{4G_N} \tag{2.6}$$

which, due to (2.1), is saturated by black holes. Again, simply by requiring the existence of thermodynamically well behaved black hole solutions in the universe (i.e. equation (2.4)) a bound was derived that limits the amount of information that can be stored in a finite physical system. This yields the motivation for the formulation of the *holographic principle*, to be discussed in the next section.

2.1.2 The holographic principle

In the above discussion, we have mentioned that entropy bounds such as (2.5) and (2.6) (and consequently (2.4)) can easily be violated by invoking the species problem, i.e. by allowing the matter part of the theory under consideration to contain an arbitrarily large number of particle species. However, it was estimated in [104] that the number of species would have to exceed 10^{40} in order to violate (2.6) for proton sized black holes. This means that the holographic principle cannot be derived as a consequence of quantum field theory (QFT) or classical general relativity (GR), instead it may be proposed as a law of nature that should be respected by any physical theory of the universe [104].

What is then the holographic principle? For a quantum field theory, a naive estimate of the amount of information that can be stored in a given volume $\mathcal{V}$ goes as follows [18,19,50,104]: To obtain a finite result, approximate the quantum field theory of interest by a lattice of harmonic oscillators, the lattice spacing being of the order of the Planck scale. The finiteness of the volume in question precludes any IR divergencies, and UV divergencies are avoided by imposing a UV cutoff on the oscillator spectrum at the Planck scale. The spectrum of each oscillator at each lattice point is then discrete and finite as well as bounded from below and above. The number of possible states of this system is then naturally exponential in $\mathcal{V}$, and consequently the amount of information that can be stored in this system, the maximal entropy, is proportional to the volume, $S_{max} \sim \mathcal{V}$. But taking the effects of gravitational physics into account, we find that a lot of these seemingly different configurations of quantum fields in the volume $\mathcal{V}$ would collapse to indistinguishable black holes, due to the property of stationary black holes to be described only by very few macroscopic quantities. This is known as the *no-hair theorem*, see e.g. [113, 114] and references therein for an overview. The arguments discussed in the previous section, and especially the bounds (2.5) and (2.6), then imply that the maximal entropy can at most scale like the surface area $\mathcal{A}$ of the system.

Hence the *holographic principle* is a proposed principle of nature, assumed to be valid in any physical theory consistently incorporating gravitational physics and hence the physics and thermodynamics of black holes in a way similar to Einstein's GR, that states that the logarithm of the number of possible states of a physical system in a certain region, and hence its maximal entropy, is proportional to the area $\mathcal{A}$ of the boundary of that region, and *not* its volume $\mathcal{V}$ [18, 19, 50, 104]. Any attempt to store more information in a given physical system than allowed by this principle must either result in a system that does not have the desired properties (in terms of entropy-density versus energy density), or must be interrupted by the formation of a black hole. For concreteness, we can state the holographic principle in the following formulation:

> *A region with boundary of area $\mathcal{A}$ is fully described by no more than $\mathcal{A}/4G_N$ degrees of freedom[4], or $1/\ln 2$ bits of information per Planck area [18, 104].*

[4] In [104], the term *degree of freedom* means that N degrees of freedom yield a maximal entropy $S_{max} = N$.

It has been argued (see [18, 19, 50, 104, 115] amongst others) that this holographic principle, tentatively proposed as a fundamental principle of nature, might lead the way towards a better understanding of (quantum) gravity. It is hence of immediate interest to study theories or systems in which this holographic principle is not only satisfied, but in which it is in some sense manifest, formulated in a more quantitative way, and/or derived from underlying principles. The most prominent realisation of the holographic principle to this day is without any doubt the *AdS/CFT correspondence* (and more generally the *gauge/gravity duality* in the case of broken conformal symmetry) which will be outlined in sections 2.1.4, 2.2 and 2.3. These will in fact be the foundation of the results presented in the later chapters 4-6, but it is important to note that there are also other manifestations of the holographic principle. For example, in the original paper [18], it was proposed to construct a fundamental theory obeying the holographic principle based on *constrained cellular automata*, see also [116] for further investigations in this direction. Holographic entropy bounds on lightlike surfaces have been discussed in [19], see also [50] and references therein. In [117, 118] and references therein, it was discussed what role holography may play in thermodynamical approaches to gravitational physics. For four-dimensional vacuum solutions to GR of Petrov type D with certain symmetry properties, a form of the holographic principle was proven in [119] by relating it to initial value theorems.

In the next section, we will briefly summarise the *covariant entropy bound* or *Bousso bound*, and in section 2.1.4 we will see how the geometry of *Anti-de Sitter (AdS) spaces* naturally invites the use of holographic techniques. This will set the stage for the discussions in the later sections 2.2 and 2.3.

2.1.3 Covariant entropy bound

The entropy bounds of the previous section were derived via very specific thought experiments, e.g. the assumption of spherical symmetry was important in the derivation of (2.6). See [104] for a more in depth discussion of the explicit and implicit assumptions made in the derivations of these entropy bounds. It is hence of interest to study whether there is a general kind of entropy bound from which bounds like (2.5) and (2.6) can be derived as special cases. One proposal in this direction is the *covariant entropy bound* or *Bousso bound* (see [50, 104, 120]) to be briefly discussed in this section.

The geometrical setup underlying the formulation of the Bousso bound is depicted in figure 2.1. We start with a spacelike orientable codimension two hypersurface B. It can be thought of as the surface or boundary of a spacelike codimension one hypersurface C, $B = \partial C$. The light cone of any point P on B includes four light rays that leave P perpendicularly to B. Of these four light rays, two are ingoing, outgoing, future pointing and past pointing, respectively, see figure 2.1 *a*). If we construct these four light rays for every point on B, we obtain four null hypersurfaces, see figure 2.1 *b*) and *c*). These null hypersurfaces can be interpreted as the light fronts that emerge from a light emitting surface B (upon time reversal for the past pointing rays). Again, two of these surfaces

can be classified as ingoing while the other two are said to be outgoing. So far, these notions and definitions are independent of the specific spacetime geometry. If we imagine that B is e.g. a sphere in flat Minkowski space, it is clear that the ingoing light fronts will have decreasing area along the congruence and shrink to a point (the tips of the cones in figure 2.1 *b*)) while the outgoing light fronts will have increasing area along the light front. This, however, is not true in generic spacetimes. If the hypersurface B is e.g. inside of a Schwarzschild black hole, then both null hypersurfaces constructed from future pointing null rays will have an area decreasing with the affine parameter. In this case, B is called a *trapped surface* [104, 121].

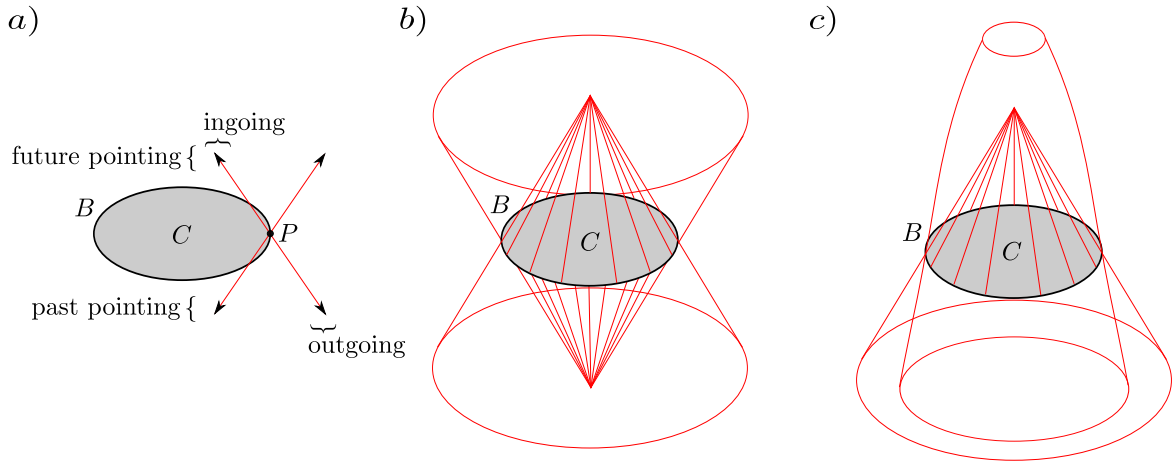

Figure 2.1: *a*): Construction of light rays perpendicular to a surface $B = \partial C$, starting from a point P. *b*): Correspondingly constructed null hypersurfaces, here shown for the example on an approximately flat spacetime. *c*): Similar construction, this time for a trapped surface B, e.g. a sphere inside of a black hole. See also figure 3 in [104].

Mathematically, this is related to the definition of the *expansion* θ of the null congruences in question.[5] Assume that the light rays starting from B are all affinely parameterised by a parameter λ, such that $\lambda \equiv 0$ defines B. For all four types of light rays in figure 2.1 *a*), we assume that the affine parameter increases away from B. The condition $\lambda \equiv \lambda_0 > 0$ then defines spacelike slices $B'(\lambda_0)$ (with area $\mathcal{A}(\lambda_0)$) of the null hypersurfaces generated by the null geodesics as in figure 2.1 *b*) and *c*). For any of the four null hypersurfaces, the expansion is defined to be [104, 120]

$$\theta(\lambda_0) = \frac{1}{\mathcal{A}} \frac{d\mathcal{A}}{d\lambda_0}. \tag{2.7}$$

As pointed out in [104, 120], one does not need to make the assumption that B is closed as in figure 2.1, in fact this procedure also holds for open surfaces B.[6] Hence we will from now

[5] This definition is also important in the definitions of apparent and trapping horizons [121].

[6] The terms *ingoing* and *outgoing* then become interchangeable, but can, after fixing a convention, still be distinguished as B is orientable.

on assume the expansion of all four null hypersurfaces to not change sign when varying the coordinate on B. If this is not the case, one can split B up into parts and carry out the analysis piece by piece. The null hypersurfaces constructed accordingly are referred to as *lightsheets* in [104, 120] if the expansion at B, as defined in (2.7), is non-positive: $\theta(\lambda = 0) \leq 0$. Furthermore, lightsheets are defined to terminate where the expansion becomes positive ($\theta(\lambda) > 0$) [104, 120]. This will e.g. be the case when the null congruence in question forms *caustics* or *focal points* [104, 120].

Due to a vanishing expansion being allowed in the definition of lightsheets, there are at least two lightsheets constructed from any B. In figure 2.1 *c*), the null hypersurfaces constructed from the future pointing in- and outgoing light rays are lightsheets, while in the middle example only the null hypersurfaces constructed by ingoing future and past pointing light rays are lightsheets.

Having clarified the necessary terminology and definitions above, we can now state the Bousso bound as in [50, 104, 120]: The entropy $S(L)$ passing through any lightsheet L constructed from a surface B is conjectured to be bounded by

$$S(L) \leq \frac{\mathcal{A}(B)}{4G_N} \tag{2.8}$$

where $\mathcal{A}(B)$ is the area of B. For further details, tests and a discussion of validity see [50, 104, 120]. A priori, this conjecture concerns the entropy flowing through a certain null hypersurface, and not the entropy of a spacelike region as the previous bounds (2.5) and (2.6). Yet, looking at figure 2.1, we see that there are examples where any worldline passing through the spacelike region C necessarily also passes through the lightsheet constructed from future pointing light rays. Then, invoking the second law of thermodynamics, it can be argued that the same bound (2.8) also applies to the entropy $S(C)$ assigned to the region C [50, 104, 120].

This closes our discussion of the motivation for and the general formulation of the holographic principle. In the next section, we will introduce the geometry of Anti-de Sitter (AdS) spacetime, and investigate it in light of the entropy bounds discussed so far. Then, in the later chapters 2.2 and 2.3 we will study the more concrete manifestation of the holographic principle in the form of the AdS/CFT correspondence.

2.1.4 Anti-de Sitter spacetime

The Anti-de sitter (AdS) spacetime is the globally maximally symmetric Lorentzian solution to Einstein's vacuum equations

$$R_{\mu\nu} - \frac{1}{2}Rg_{\mu\nu} + \Lambda g_{\mu\nu} = 0 \tag{2.9}$$

with a negative cosmological constant Λ. In the $d+1$-dimensional case, the line element can be written as

$$ds^2 = -\left(1+\frac{r^2}{L^2}\right)dt^2 + \frac{1}{1+\frac{r^2}{L^2}}dr^2 + r^2 d\Omega_{d-1}^2, \tag{2.10}$$

where $t \in]-\infty, +\infty[$, $r \in [0, +\infty]$ and $d\Omega_{d-1}^2$ is the line element of the $d-1$ sphere. Here, L is the *AdS scale* or *AdS radius*, and using (2.9) it is easy to derive $\Lambda = -\frac{d(d-1)}{2L^2}$. The coordinates used above are called *global coordinates* as they cover the entire spacetime. Via a particular coordinate transformation[7], one finds the line element

$$ds^2 = \frac{L^2}{z^2}(-d\tau^2 + d\vec{x}^2 + dz^2) \tag{2.11}$$

with $\tau, x^i \in]-\infty, +\infty[$, $z \in [0, +\infty]$. This coordinate system is geodesically incomplete due to the coordinate singularity at $z \to \infty$, and hence does not cover the entire AdS spacetime. The region covered by these coordinates is called the *Poincaré patch*.

Returning to the global coordinates (2.10), we see that AdS space has the topology of a d-dimensional disk times the real (time) axis, $D^d \times \mathbb{R}^{(t)}$, i.e. the topology of a full cylinder. This is similar to $d+1$-dimensional Minkowski space written as $ds^2 = -dt^2 + dr^2 + r^2 d\Omega_{d-1}^2$, yet there is a very important difference: In Minkowski space, the asymptotic infinity (i.e. the boundary of the conformal diagram) can be reached by light rays only after infinite coordinate time t. Contrarily, it can be shown that in AdS space an observer in the spacetime (from now on called the *bulk*) can send a light ray towards infinity (i.e. the cylinder at $r \to \infty$, henceforth called the *boundary*) and receive an answer in finite coordinate time t, hence establishing a back and forth communication with the boundary.[8] This motivates the question about the role that the boundary will play in the light of the holographic principle. Can for example the entropy bounds derived in the earlier sections 2.1.1-2.1.3 be applied to the AdS space?

This is indeed the case [50, 104, 122]: Taking the surface B used in the formulation of the Bousso bound (2.8) to be a sphere in global AdS space (2.10) specified by the restriction $t = t_0, r = r_0$, it is easy to calculate the corresponding light rays and sheets as described in section 2.1.3. Indeed, the result will look qualitatively similar to figure 2.1 *b*), with the two null surfaces constructed from ingoing light rays, which terminate at a focal point, satisfying the definition of a lightsheet. The difference from the Minkowski case is that the outgoing light rays reach infinity in finite coordinate time. As discussed in section 2.1.3, in this situation the Bousso bound (2.8) implies the spherical entropy bound (2.6) $S(C) \leq \mathcal{A}(B)/4$ on the entropy of the spacelike region C. As we take the limit $r_0 \to 1/\epsilon$

[7] Details on the geometry of AdS and its different coordinate systems can be found in [51].

[8] In this discussion we have been using the coordinate t (similarly we could have used τ for the Poincaré patch (2.11)) as a measure of physical time. This makes sense, as the corresponding vector ∂_t (similarly ∂_τ) is a Killing vector, and the spacetimes under consideration are static. The coordinates t and τ are then natural and well-defined measures of time.

with a small cutoff ϵ, C becomes an equal time slice of the AdS space, and due to the entropy bound the information stored on this slice is bounded by the area of a spacelike slice of the AdS boundary. The information on this surface C, together with boundary conditions imposed at the cutoff surface (which is interpreted as the AdS boundary) then determines the evolution of all fields in the bulk spacetime. The interesting aspect of this is that the induced metric on the AdS boundary is Lorentzian and nondegenerate. Specifically, it is the *Einstein static universe* for (2.10) and Minkowski space for (2.11) [51]. Consequently, it might be possible to define an ordinary QFT (without gravitational sector) to live on this boundary, and the maximal entropy and information storage capacity of this theory would scale like the area of the boundary, just as is the case for the gravitational bulk theory. Hence it may in principle be possible to describe the bulk dynamics entirely in terms of such a boundary theory. In the next sections 2.2 and 2.3 we will see in detail how this is indeed possible.

2.2 The AdS$_3$/CFT$_2$ duality

Gravitational theory in $2+1$ dimensions, i.e. in one dimension lower than in the observable universe, has often been described as an interesting field of research as it is technically simpler than $3+1$-dimensional gravity while at the same time still posing similar problems to quantisation attempts. See [123] for an overview over this topic. In this section we will very briefly recapitulate the connection found in [103] between gravity in $2+1$ dimensions in the presence of a negative cosmological constant and $1+1$-dimensional CFTs. See also [124–126] for important further work and [127, 128] for useful reviews.

In section 2.1.4, we have seen that Einstein's equations with a negative cosmological constant Λ are solved by AdS space. For $2+1$ bulk dimensions in particular, the line element of global AdS (2.10) reads

$$ds^2 = -\left(1+\frac{r^2}{L^2}\right)dt^2 + \frac{1}{1+\frac{r^2}{L^2}}dr^2 + r^2 d\phi^2, \quad \Lambda = -\frac{1}{L^2}, \tag{2.12}$$

where the angular coordinate $\phi \in [0, 2\pi[$ is periodically identified. This metric is maximally symmetric, and its symmetry group is $SL(2,\mathbb{R}) \times SL(2,\mathbb{R}) \cong SO(2,2)$. This can be explicitly seen [129] by deriving the Killing vectors

$$l_0 = \frac{i}{2}(L\partial_t + \partial_\phi), \tag{2.13}$$

$$l_{-1} = \frac{i}{2}e^{-i\left(\frac{t}{L}+\phi\right)}\left[\frac{Lr}{\sqrt{L^2+r^2}}\partial_t + \frac{\sqrt{L^2+r^2}}{r}\partial_\phi + i\sqrt{L^2+r^2}\partial_r\right], \tag{2.14}$$

$$l_{+1} = \frac{i}{2}e^{+i\left(\frac{t}{L}+\phi\right)}\left[\frac{Lr}{\sqrt{L^2+r^2}}\partial_t + \frac{\sqrt{L^2+r^2}}{r}\partial_\phi - i\sqrt{L^2+r^2}\partial_r\right], \tag{2.15}$$

$$\bar{l}_0 = \frac{i}{2}(L\partial_t - \partial_\phi), \tag{2.16}$$

$$\bar{l}_{-1} = \frac{i}{2}e^{-i\left(\frac{t}{L}-\phi\right)}\left[\frac{Lr}{\sqrt{L^2+r^2}}\partial_t - \frac{\sqrt{L^2+r^2}}{r}\partial_\phi + i\sqrt{L^2+r^2}\partial_r\right], \tag{2.17}$$

$$\bar{l}_{+1} = \frac{i}{2}e^{+i\left(\frac{t}{L}-\phi\right)}\left[\frac{Lr}{\sqrt{L^2+r^2}}\partial_t - \frac{\sqrt{L^2+r^2}}{r}\partial_\phi - i\sqrt{L^2+r^2}\partial_r\right], \tag{2.18}$$

and verifying their algebra

$$\begin{aligned} &[l_0, l_{\pm1}] = \mp l_{\pm1}, \quad [l_{+1}, l_{-1}] = 2l_0, \\ &[\bar{l}_0, \bar{l}_{\pm1}] = \mp \bar{l}_{\pm1}, \quad [\bar{l}_{+1}, \bar{l}_{-1}] = 2\bar{l}_0, \\ &[l_m, \bar{l}_n] = 0, \end{aligned} \tag{2.19}$$

where for vector fields $l_m, \bar{l}_n$ the bracket $[\cdot,\cdot]$ is simply the Lie bracket.

Although pure gravity in $2+1$ dimensions does not have propagating bulk degrees of freedom [103, 123], it is known [103, 130, 131] to exhibit non-trivial solutions that are locally equivalent to (2.12), but not globally. This hence motivated the study [103] of the boundary conditions (as $r \to \infty$) that a metric should have to satisfy in order to be called *asymptotically AdS*:[9]

$$g_{tt} = -\frac{r^2}{L^2} + \mathcal{O}(1), \tag{2.20}$$

$$g_{tr} = \mathcal{O}\left(\frac{1}{r^3}\right), \tag{2.21}$$

$$g_{t\phi} = \mathcal{O}(1), \tag{2.22}$$

$$g_{rr} = \frac{L^2}{r^2} + \mathcal{O}\left(\frac{1}{r^4}\right), \tag{2.23}$$

$$g_{r\phi} = \mathcal{O}\left(\frac{1}{r^3}\right), \tag{2.24}$$

$$g_{\phi\phi} = r^2 + \mathcal{O}\left(1\right). \tag{2.25}$$

Of course diffeomorphisms are generated by vector fields ζ^μ according to the formula $\delta g_{\mu\nu} = \nabla_\mu\zeta_\nu + \nabla_\nu\zeta_\mu$, and the vector fields that generate diffeomorphisms that leave the conditions

[9] Indeed, two sets of possible boundary conditions were studied in [103]. Here, we only consider the laxer ones which lead to a larger asymptotic symmetry group.

(2.20)-(2.25) invariant can be shown [103, 125, 128] to be of the form

$$\zeta^t = L\left(f^+ + f^-\right) + \frac{L^3}{2r^2}\left(\partial_+^2 f^+ + \partial_-^2 f^-\right) + \mathcal{O}\left(\frac{1}{r^4}\right), \tag{2.26}$$

$$\zeta^r = -r\left(\partial_+ f^+ + \partial_- f^-\right) + \mathcal{O}\left(\frac{1}{r}\right), \tag{2.27}$$

$$\zeta^\phi = f^+ - f^- - \frac{L^2}{2r^2}\left(\partial_+^2 f^+ - \partial_-^2 f^-\right) + \mathcal{O}\left(\frac{1}{r^4}\right), \tag{2.28}$$

where $f^\pm$ is a function of $\frac{t}{L} \pm \phi$ and $\partial_\pm = \frac{1}{2}\left(L\partial_t \pm \partial_\phi\right)$. Introducing the basis

$$l_n = \zeta\left(f^+ \equiv \frac{i}{2}e^{in\left(\frac{t}{L}+\phi\right)}, f^- \equiv 0\right), \tag{2.29}$$

$$\bar{l}_n = \zeta\left(f^+ \equiv 0, f^- \equiv \frac{i}{2}e^{in\left(\frac{t}{L}-\phi\right)}\right), \tag{2.30}$$

we see that these contain the globally defined Killing vectors (2.13)-(2.18), and the resulting algebra

$$\begin{aligned}
[l_m, l_n] &= (m-n)l_{m+n}, \\
[\bar{l}_m, \bar{l}_n] &= (m-n)\bar{l}_{m+n}, \\
[l_m, \bar{l}_n] &= 0,
\end{aligned} \tag{2.31}$$

contains the $SL(2,\mathbb{R}) \times SL(2,\mathbb{R})$ algebra (2.19) as a subalgebra [103, 125, 128][10]. These are two commuting copies of the *Witt algebra* and are known to describe the algebra of infinitesimal conformal transformations in two dimensions, see e.g. the monograph [132].

Due to a careful Hamiltonian analysis of GR in $2+1$ dimensions and its boundary terms, which will not be repeated here, it was also shown in [103] that the Dirac bracket algebra of the associated charges $L_n, \bar{L}_m$ reads [103, 125, 128]

$$\begin{aligned}
[L_m, L_n] &= (m-n)L_{m+n} + \frac{c}{12}(m^3 - m)\delta_{m+n,0}, \\
[\bar{L}_m, \bar{L}_n] &= (m-n)\bar{L}_{m+n} + \frac{c}{12}(m^3 - m)\delta_{m+n,0}, \\
[L_m, \bar{L}_n] &= 0,
\end{aligned} \tag{2.32}$$

which is similar to (2.31), but *centrally extended* with a *central charge*

$$c = \frac{3L}{2G_N}. \tag{2.33}$$

The algebra (2.32) is easily recognised to be composed of two commuting copies of the *Virasoro algebra* [103], see also [132]. This suggests that the boundary dynamics of GR in $2+1$ dimensions can be phrased in terms of a $1+1$-dimensional (quantum) conformal field theory. In fact, this theory was argued to be *Liouville theory* in [124].

[10] In the normalisation of the vectors (2.13)-(2.18) and (2.29)-(2.30) we have followed the convention of [129] in contrast to [103, 125, 128], leading to slightly different factors in the algebra.

2.3 Maldacena's AdS_5/CFT_4 duality

Having seen in chapters 2.1.4 and 2.2 how Anti-de Sitter space naturally seems like a good starting point for an implementation of holographic ideas (see section 2.1), we will now proceed to describe how *string theory* implements the holographic principle in the form of the AdS/CFT duality. We will not give a detailed introduction to string theory, referring the reader to the many excellent text books on the subject [20–24]. For the outline of how the AdS_5/CFT_4 correspondence was obtained in [25], we will mostly follow [51] throughout this section, although other textbooks on the subject matter exist [52,53], as well as a large number of review papers [133–139] focusing on a variety of aspects of the topic.

The motivation of the AdS_5/CFT_4 correspondence from superstring theory is based on the fact that string theory not only contains strings as dynamical objects, but also *Dirichlet branes* [140, 141]. These D-branes can be described both from an open and from a closed string perspective [141], and the existence of these two complementary perspectives is what ultimately motivates the AdS/CFT correspondence in string theory. In the following, we will hence describe a certain configuration of D-branes from an open string point of view in section 2.3.1, and from a closed string point of view in section 2.3.2. In section 2.3.3, we will then bring these two perspectives together.

2.3.1 Open string construction

Conventionally, D-branes are introduced as hypersurfaces on which open strings can end, i.e. as surfaces where *Dirichlet boundary conditions* are imposed on the endpoints of the open string, in contrast to the more simple *Neumann boundary conditions*. As an example, we can take type IIB superstring theory in which $D3$-branes may be studied. By nomenclature, such a $D3$-brane is then a $3+1$-dimensional hypersurface in the $9+1$-dimensional target space of the superstring theory. Specifically, using standard coordinates x^M ($M \in \{0,..,9\}$) for the 10-dimensional Minkowski space, the simplest $D3$-brane can be taken to extend along the directions $M \in \{0,1,2,3\}$. Brane embeddings like this are conventionally depicted in the form of tables such as table 2.1:

Direction	x^M, $M=$	0	1	2	3	4	5	6	7	8	9
	$D3$	•	•	•	•	-	-	-	-	-	-

Table 2.1: Embedding of a $D3$-brane into 10-dimensional Minkowski space.

This means that for an open string with both endpoints on this $D3$-brane, the coordinates x^4-x^9 of both endpoints are fixed to be zero, while they can still freely move in the directions x^0-x^3. See also figure 2.2 which depicts an entire stack of coincident $D3$-branes.

We now study a setup of N coincident $D3$-branes in type IIB superstring theory such as depicted in table 2.1 or figure 2.2. To be able to view the strings as small perturbations,

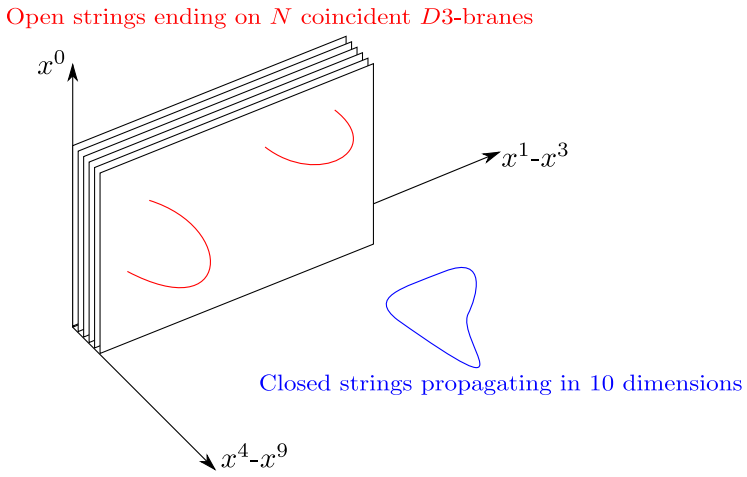

Figure 2.2: N coincident $D3$-branes in a 10-dimensional Minkowski space, embedded as in table 2.1.

we will choose to work in the regime

$$g_s N \ll 1, \tag{2.34}$$

where g_s is the closed string coupling constant. Furthermore, we will work with massless excitations, i.e. low energies

$$E \ll 1/\sqrt{\alpha'}, \tag{2.35}$$

where α' is related to the string length ℓ_s and tension T_s by $\alpha' = \ell_s^2$, $T_s = \frac{1}{2\pi\alpha'}$.

In order to understand the theory described by this setup, we have to note two things: First of all, the excitations of the open strings give rise to a gauge theory living in the world-volume of the $D3$-branes. Specifically, the bosonic excitations of the open strings parallel to the D-brane directions give rise to a $U(N)$ gauge (vector) field A_μ while the bosonic excitations perpendicular to the brane, not carrying any worldsheet indices, are described by scalar fields of the worldvolume theory. As the number of perpendicular directions is six, there will be precisely six real scalar fields emerging this way. Similarly, the fermionic excitations of the open strings will contribute fermions to the effective brane worldsheet action, allowing for a certain amount of supersymmetry to be preserved. Second of all, it is important to point out that any string theory containing open strings consequently also has to contain closed strings, but not vice versa. This means that closed strings can be emitted from the $D3$-branes and propagate into the full 10-dimensional Minkowski space. We hence find that the effective low energy action for string theory in this setup takes the form

$$\mathcal{S} = \mathcal{S}_{closed,\ 10d} + \mathcal{S}_{open,\ 4d} + \mathcal{S}_{int}, \tag{2.36}$$

where $\mathcal{S}_{int}$ is the interaction term between the two sectors and

$$\mathcal{S}_{closed,\,10d} = \frac{1}{2\kappa_N^2}\int d^{10}x\sqrt{-g}R + ..., \tag{2.37}$$

$$2\kappa_N^2 = (2\pi)^7 g_s^2 \alpha'^4, \tag{2.38}$$

is the (Einstein frame) action of 10-dimensional ($\mathcal{N}=1$) supergravity including higher derivative corrections of order α' and higher. For the open strings, one finds to leading order in α':

$$\mathcal{S}_{open,\,4d} = \frac{-1}{2\pi g_s}\int d^4x \left(\frac{1}{4}\mathrm{Tr}\left[F_{\mu\nu}F^{\mu\nu}\right] + \text{fermions, scalars} + \mathcal{O}(\alpha')\right). \tag{2.39}$$

We now ignore terms of order α' and higher, i.e. we take the limit $\alpha' \to 0$. To do this limit consistently, we will at the same time send any distance ℓ to zero such that ℓ/α' is kept fixed. This is known as the *Maldacena limit*. The action (2.39) then becomes the action of $\mathcal{N}=4$ *Super Yang-Mills (SYM) theory* with a coupling[11]

$$g_{YM}^2 = 4\pi g_s \tag{2.40}$$

and a $U(N)$ gauge group. In fact, this $U(N)$ symmetry group can be split into $SU(N)$ and $U(1)$, such that the $U(1)$ part decouples [27, 136, 143]. In the $\alpha' \to 0$ limit, the terms in $\mathcal{S}_{int}$ vanish and hence the open and closed string sectors decouple. Later on, it will be useful to note that instead of using the coupling constant g_{YM} for the Yang-Mills field, we can also define the *'t Hooft coupling* [144]

$$\lambda \equiv g_{YM}^2 N. \tag{2.41}$$

2.3.2 Closed string construction

Following [25, 51] in the previous section, using the limit $g_s N \ll 1$, we discussed a stack of N $D3$-branes as a geometrical manifestation of boundary conditions on open strings, viewing both the branes and the strings from a perturbative point of view. In this section on the other hand, using the regime

$$g_s N \gg 1, \tag{2.42}$$

we will view the D-branes as massive non-perturbative solutions to (closed) string theory and its supergravity low-energy limit, again following [25, 51]. This alternative view of D-branes was introduced in [141]. The solution of type IIB supergravity (ignoring higher

[11] This seems to be the most common convention in the literature, although [25, 51] use $g_{YM}^2 = 2\pi g_s$. See [142] for a detailed discussion of how a convention on the normalisation of the non-abelian generators influences this factor.

curvature terms of order $\mathcal{O}(\alpha')$) that preserves the same symmetries as the brane embedding depicted in table 2.1[12] contains a constant dilaton field

$$e^{2\phi(r)} = g_s^2, \tag{2.43}$$

a *black brane* line element

$$ds^2 = \frac{1}{\sqrt{H(r)}}\eta_{\mu\nu}dx^\mu dx^\nu + \sqrt{H(r)}\delta_{ij}dx^i dx^j, \tag{2.44}$$

$$r = \sqrt{x^i x_i}, \tag{2.45}$$

$$H(r) = 1 + \left(\frac{L}{r}\right)^4, \tag{2.46}$$

with brane worldvolume directions x^μ, $\mu, \nu \in \{0, ..., 3\}$, and perpendicular directions x^i, $i, j \in \{4, ..., 9\}$, as well as a non-trivial four-form field

$$C_{(4)} = \left(1 - \frac{1}{H(r)}\right) dx^0 \wedge dx^1 \wedge dx^2 \wedge dx^3 + ... \ . \tag{2.47}$$

The flux of the corresponding five-form $F_{(5)} = dC_{(4)}$ through the five-sphere spanned by the perpendicular coordinates x^i around the black brane has to be quantized, yielding the number N of coincident $D3$-branes. This fixes the relation

$$L^4 = 4\pi g_s N \alpha'^2. \tag{2.48}$$

Consequently, using (2.42) we find

$$\frac{L^4}{\alpha'^2} = \frac{L^4}{\ell_s^4} \gg 1, \tag{2.49}$$

i.e. the curvature scale of the black brane should be large compared to the string scale, resulting in a weak curvature regime $R_{MN}R^{MN} \sim \frac{1}{L^4}$. We could also make use of the 10-dimensional *reduced Planck constant* $\ell_{P,10}^8 \equiv \kappa_N^2$ and (2.38) to deduce from (2.48) that [136]

$$\frac{L}{\ell_{P,10}} = 2^{-\frac{1}{4}}\pi^{-\frac{5}{8}}N^{\frac{1}{4}}, \tag{2.50}$$

so that large N implies a classical spacetime description.

In section 2.3.2, an important part of the calculations relied on taking the low energy limit of the excitations. What does a low energy limit mean in the background spacetime (2.44)? To answer this, consider that an observer at infinity, far away from the black branes, will see two kinds of low energy excitations: On the one hand closed strings propagating through

[12] I.e. Poincaré symmetry $\mathbb{R}^{3+1} \rtimes SO(3,1)$ in the brane worldvolume directions, rotations $SO(6)$ in the remaining directions and the correct amount of supersymmetry.

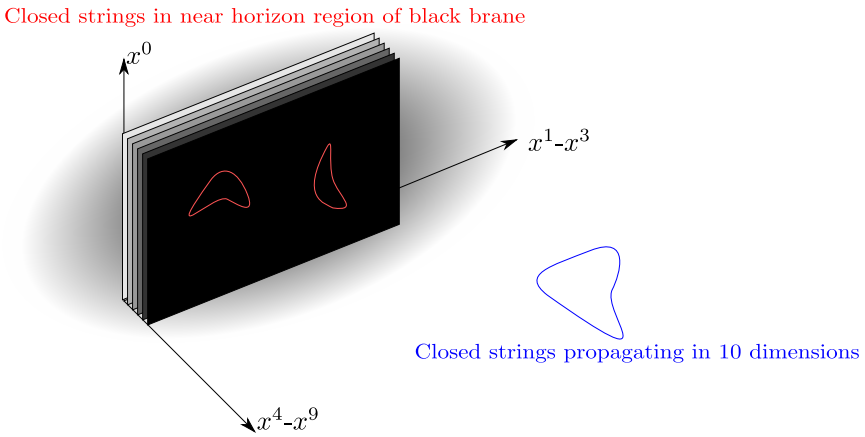

Figure 2.3: Black brane in a 10-dimensional asymptotically flat space.

the asymptotically flat space far away from the branes and on the other hand closed strings living near the black brane horizon, which will appear redshifted to the observer due to the redshift factor $\sqrt{-g_{tt}} = H(r)^{-1/4}$. See also figure 2.3.

The low energy limit hence splits the theory into two decoupled sectors: low energy modes of type IIB supergravity propagating in 10-dimensional Minkowski space far away from the brane, and excitations near the horizon of the black brane. In order to study the latter, we will take the *near horizon limit*

$$r \ll L \Rightarrow H(r) \sim \frac{L^4}{r^4} \tag{2.51}$$

of the line element (2.44). From (2.48), we know that $L^4/r^4 \sim g_s N(\alpha'^4/r^4)\alpha'^{-2}$, hence keeping $\lambda \sim g_s N$ fixed, this limit is consistent with the Maldacena limit (introduced in section 2.3.1) of taking $\alpha' \to 0$ such that α'/r is fixed. Taking the limit in this way means that energies measured at infinity

$$[E_\infty] \sim \left[\frac{r}{\alpha'}\right] [E(r)\sqrt{\alpha'}] \tag{2.52}$$

are kept fixed if the energy of the near horizon excitations is kept fixed with respect to the string length, i.e. if $E(r)\sqrt{\alpha'}$ is kept fixed. In (2.52), fixed quantities in the Maldacena limit are grouped in square brackets [...]. Performing this limit, we obtain

$$ds^2 = \frac{r^2}{L^2}\eta_{\mu\nu}dx^\mu dx^\nu + \frac{L^2}{r^2}\delta_{ij}dx^i dx^j. \tag{2.53}$$

Let us next introduce a coordinate $z = L^2/r$ as well as S^5 coordinates in the six directions perpendicular to the brane. The line element then takes the familiar form

$$ds^2 = \frac{L^2}{z^2}\left(\eta_{\mu\nu}dx^\mu dx^\nu + dz^2\right) + L^2 ds^2_{S^5}, \tag{2.54}$$

which is a product spacetime built out of the sphere S^5 and a five-dimensional Poincaré AdS space (2.11). This is the spacetime on which the near horizon low energy excitations effectively live.

2.3.3 The duality

Let us now bring the results of sections 2.3.1 and 2.3.2 into a common framework. Both times we have studied type IIB superstring theory in the presence of branes, once in the perturbative limit $g_sN \ll 1$ and once in the non-perturbative limit $g_sN \gg 1$. In the former case, we have taken the Maldacena limit and obtained type IIB supergravity in flat space together with $\mathcal{N} = 4$ $SU(N)$ SYM theory. In the latter case, we have taken the near horizon limit and obtained type IIB supergravity in flat space together with type IIB superstring theory on $AdS_5 \times S^5$. Assuming that these respective low energy limits commute with adiabatic variations of g_s [136], this observation motivates the AdS_5/CFT_4 correspondence [25]:

$$\begin{gathered}\text{Type IIB superstring theory on } \mathrm{AdS}_5\times\mathrm{S}^5 \text{ with } N \text{ units of } F_{(5)} \text{ flux on } \mathrm{S}^5\\ \text{is dual to}\\ \mathcal{N}=4 \text{ SYM theory with gauge group } SU(N) \text{ in four dimensions.}\end{gathered} \tag{2.55}$$

As in section 2.1.4, the $AdS_5 \times S^5$ spacetime is called the *bulk* spacetime. Both theories in (2.55) are each described by three constants of which one is redundant, these are the string coupling g_s, the string length $\ell_s = \sqrt{\alpha'}$ and the reduced Planck length $\ell_{P,10}^8 = \frac{1}{2}(2\pi)^7 g_s^2 \alpha'^4$ in the string theory on $AdS_5 \times S^5$ and the number N, the coupling g_{YM} and the 't Hooft coupling $\lambda = g_{YM}^2 N$ in the YM theory. The relations between these parameters are, according to (2.40),(2.41),(2.48) and (2.50):

$$N^{\frac{1}{4}} = 2^{\frac{1}{4}} \pi^{\frac{5}{8}} \frac{L}{\ell_{P,10}}, \tag{2.56}$$

$$g_{YM}^2 = 4\pi g_s, \tag{2.57}$$

$$\lambda = \frac{L^4}{\alpha'^2}. \tag{2.58}$$

Consequently, taking the limit $N \to \infty$ will allow for a classical treatment of the AdS background geometry, while assuming λ to be large will allow us to neglect (classical) string corrections. While it is known how to mathematically formulate the $\mathcal{N} = 4$ SYM theory of (2.55) at least in principle, this is not the case for the type IIB superstring theory (in a non-perturbative target space formalism). The equations (2.56)-(2.58) hence suggest different forms of the conjectured duality (2.55):

- The *weak form* of the AdS/CFT correspondence proposes that (2.55) only holds for the limit $N \to \infty$ while λ is assumed to be fixed and large, consequently $g_s \to 0$.

This means that (2.55) reduces to a correspondence between classical supergravity and $\mathcal{N} = 4$ SYM theory in the large N limit and for large 't Hooft coupling. This is certainly the form of the correspondence which is best motivated by the description above, and in which the gravity side of the duality is best understood. Consequently, this is also the best tested form of the correspondence, see e.g. [51,52] for an overview of tests of the correspondence. Relating a strongly coupled ($\lambda \gg 1$) theory to a weakly coupled theory, this weak form of the correspondence (2.55) is an example of a *strong-weak duality*. Given the reliance of many modern physics calculations on perturbative methods and the scarcity of adequate methods to tackle strongly coupled theories, such strong-weak dualities are obviously very useful[13].

- The *strong form* of the AdS/CFT correspondence proposes that (2.55) requires the large N limit $N \to \infty$, but is valid for any fixed value of λ. This still implies $g_s \to 0$. The gravity side of the duality is then described by classical type IIB string theory on $AdS_5 \times S^5$. What is the significance of the large N limit in both the weak and strong versions of the duality? This question leads us to work by 't Hooft, who studied $U(N)$ gauge theories in the limit $N \to \infty, \lambda = g_{YM}^2 N$ fixed in [144]. He found that in this limit, the Feynman diagrams of the theory can be rearranged in an expansion in $1/N$, in such a way that each diagram contributes with a factor N^χ, where χ is the *Euler characteristic* of the corresponding diagram. This topological expansion suggests a similarity with string theory, where $1/N$ takes the role of the string coupling constant g_s. In fact, as the 't Hooft parameter λ is assumed to be held fixed in the large N or *'t Hooft limit*, from (2.41) and (2.57) we immediately find $\frac{1}{N} \sim \frac{g_s}{\lambda}$. This means that the strong form of the AdS/CFT correspondence (2.55), together with the relations (2.56)-(2.58), identifies the precise string theory describing the 't Hooft limit of $\mathcal{N} = 4$ SYM theory to be type IIB string theory on $AdS_5 \times S^5$.

- Taking into account $1/N$ corrections then leads to the *strongest form* of the AdS/CFT correspondence, i.e. the conjecture that (2.55) is valid for any choice of the parameters N and λ, or $\frac{L}{\ell_{P,10}}$ and $\frac{L^4}{\alpha'^2}$ respectively.

In the remaining part of this subsection, we will discuss some of the aspects of the correspondence (2.55) which make it more concrete, or which are important for carrying out concrete calculations. The first important aspect to note is that of global symmetries, which have to match on both sides of the duality (2.55) [25]. This is indeed the case as shown in table 2.2:

The next important thing that we need to understand is how precisely we can make use of the correspondence (2.55). What does the result of a certain calculation on one side of the

[13] We should also note that the correspondence (2.55) evades the famous Weinberg Witten theorem [145] in a rather elegant way: According to this theorem, a dynamical graviton cannot arise effectively in a gauge theory. The AdS/CFT correspondence evades this theorem as the gauge theory describes a graviton that lives in a higher-dimensional background spacetime.

Gravity side	Symmetry	Field theory side
Isometries of AdS_5	$SO(2,4) \sim SU(2,2)$	Conformal group in 4 dimensions
Isometries of S^5	$SO(6) \sim SU(4)$	R-Symmetry
Bosonic subgroup of full supergroup	$SO(2,4) \times SU(4)$ $\subset$ $SU(2,2\|4)$	Bosonic subgroup of full supergroup

Table 2.2: Global symmetries in AdS_5/CFT_4, following e.g. [133].

correspondence mean in terms of the theory on the other side of the correspondence? To answer this, one needs to establish a *holographic dictionary* that relates certain quantities on the two sides of the correspondence. This was done in [26, 27], where it was argued that in an AdS_{d+1}/CFT_d duality such as (2.55) the boundary generating functional should be related to the bulk partition function according to what is sometimes called, after the names of the authors of [26, 27], the *GKPW formula*

$$\left\langle e^{\int d^d x \mathcal{O}\varphi_{(0)}} \right\rangle_{CFT} = Z_{string}\big|_{\lim_{z\to 0} z^{\Delta-d}\varphi(z,x)\to\varphi_{(0)}(x)}. \tag{2.59}$$

Let us explain the notation used in this formula. First of all, this formula is presented for the Euclidean case for simplicity. On the left hand side we have a CFT generating functional, with the CFT expectation value defined in the usual way via the path integral. We are interested in a CFT operator $\mathcal{O}$ with conformal dimension Δ, such that $\varphi_{(0)}$ on the left hand side of (2.59) is the *source* for that operator. On the right hand side, we have the string theory partition function with the restriction that the bulk field $\varphi(z,x)$ must have a certain asymptotic behaviour given by $\varphi_{(0)}$. This means that the boundary source enters the bulk calculation as a boundary condition. In the weak form of the correspondence (2.55), the bulk theory becomes classical and we can use the *saddle point approximation* [26, 27]

$$\left\langle e^{\int d^d x \mathcal{O}\varphi_{(0)}} \right\rangle_{CFT} = e^{-\mathcal{S}_{SUGRA}|_{\lim_{z\to 0} z^{\Delta-d}\varphi(z,x)\to\varphi_{(0)}(x)}}, \tag{2.60}$$

where now $\varphi(z,x)$ is a solution to the classical supergravity equations of motion. This equation can then be used to holographically calculate n-point functions of operators $\mathcal{O}$ and compare them to CFT expectations [26, 27], which is an important check of the AdS/CFT correspondence.

In the above formulas (2.59) and (2.60), the bulk field φ is said to be the field *dual* to the boundary operator $\mathcal{O}$. But which kinds of operators have such dual fields, and how can one determine which bulk field is the dual one to a given $\mathcal{O}$? Just like the global symmetries of the two theories of the duality match according to table 2.2, it is clear that

in such a *field-operator map*, the entries on both sides of the duality should transform in the same representations of the global symmetry group. Comparing then the gauge invariant operators present in the field theory to the fields present in the bulk theory after the Kaluza-Klein (KK) reduction on the S^5 leads to the expectation that certain operators on the field theory side with conformal dimension Δ are related by the holographic dictionary to fields on the AdS^5 background with mass determined by Δ [27]. As an example, this dictionary will relate the scalar 1/2 BPS operator

$$\mathcal{O}_\Delta(x) \equiv C^\Delta_{i_1\ldots i_\Delta} Tr\left[\phi^{i_1}\ldots\phi^{i_\Delta}\right] \tag{2.61}$$

to a scalar field φ that satisfies a Klein-Gordon equation on the AdS$_5$ background (the S^5 being gone due to KK reduction) with mass

$$m^2L^2 = \Delta(\Delta-4) \tag{2.62}$$

for the correspondence (2.55) [27]. Similar formulas exist for fields with different spins and general dimensions, see e.g. the overview given in [51,52]. For the model building in chapter 6, it will be useful to note that the field-operator map relates, in particular, fluctuations of the bulk metric to the CFT stress energy tensor, and fluctuations of a gauge field on the gravity side to a corresponding current on the field theory side.

Let us consider the example of a scalar bulk field φ and its dual operator $\mathcal{O}$ in more detail. The Klein-Gordon equation in Poincaré AdS$_{d+1}$ (see the first term in (2.54)) reads, following the notation of [51],

$$0 = \frac{1}{\sqrt{-g}}\partial_m\left(\sqrt{-g}g^{mn}\partial_n\varphi\right) - m^2\varphi \tag{2.63}$$

$$= \frac{1}{L^2}\left(z^2\partial_z^2\varphi - (d-1)z\partial_z\varphi + z^2\partial_\mu\partial^\mu\varphi\right) - m^2\varphi. \tag{2.64}$$

It is now a standard exercise to make the ansatz $\varphi(z,x) = \varphi_k(z)e^{ikx}$ and find from the above equation that

$$0 = z^2\partial_z^2\varphi_k - (d-1)z\partial_z\varphi_k - \left(m^2L^2 + k^2z^2\right)\varphi_k. \tag{2.65}$$

The solution of this equation is given in terms of two modes whose near-boundary ($z\to 0$) asymptotic behaviour is

$$\varphi_k(z) \sim z^{\Delta_+} \quad \text{respectively} \quad \varphi_k(z) \sim z^{\Delta_-}. \tag{2.66}$$

Here $\Delta_\pm$ are the solutions to equation (2.62) (with 4 replaced by the general dimension d), i.e.

$$\Delta_\pm = \frac{d}{2} \pm \sqrt{\frac{d^2}{4} + m^2L^2}, \quad \Delta_- = d - \Delta_+, \tag{2.67}$$

and an expansion of the bulk solution $\varphi(z,x)$ will yield

$$\varphi(z,x) = \varphi_{(0)}(x)z^{\Delta_-} + \varphi_+(x)z^{\Delta_+} + ..., \tag{2.68}$$

where ... stands for other terms. In fact, comparing (2.68) to the boundary condition imposed in the GKPW formula (2.59),(2.60) we see that this field has the right near-boundary behaviour to define the source $\varphi_{(0)}$ for an operator $\mathcal{O}$ of dimension Δ_+ [27]. Even more, using (2.60) to calculate the expectation value and taking care of bulk IR divergencies one can identify the coefficient φ_+ with the expectation value $\langle\mathcal{O}\rangle$ [146, 147], see also the overview given in [51, 52].

We have just seen what an important role the near-boundary behaviour of bulk fields plays in the concrete formulation of the holographic dictionary of the AdS/CFT correspondence (2.55). Indeed, this, as well as our studies in sections 2.1.4 and 2.1.4, suggest the common picture that in an AdS/CFT correspondence, the CFT lives on the conformal boundary of the AdS space. An interesting aspect of this geometrical picture is the so called *UV/IR connection* motivated in [44], see also [50]. This connection states that IR effects in the bulk theory will be holographically related to UV effects in the field theory. For concreteness, let's take another look at the $AdS_5\times S^5$ line element (2.54). Technically, the conformal boundary is located at $z = 0$, but in order to regulate the infinite volume of the AdS space (and IR effects of the bulk theory), we can cut off the spacetime at the regulating surface $z = \epsilon \ll 1$. As we lower ϵ towards zero, we see that the Minkowski part of the induced boundary metric

$$ds^2 = \frac{L^2}{\epsilon^2}\left(\eta_{\mu\nu}dx^\mu dx^\nu\right) + L^2 ds^2_{S^5} \tag{2.69}$$

seems to diverge. But of course the CFT assumed to live on the boundary is scale invariant, so the effect is that overall, the size of the sphere S^5 shrinks to zero compared to the Minkowski space [50]. This is the reason why in (2.55) we are dealing with a *boundary theory* that lives on four-dimensional Minkowski space $\mathcal{M}^4$, not on $\mathcal{M}^4\times S^5$. As argued in [44], the role of ϵ in the field theory is that of a UV cutoff. This can be seen by studying a variety of quantities, such as for example entanglement entropy which will be investigated in section 3, see [44, 50] for other examples. As argued in [44, 50], this knowledge of how the field theory UV cutoff is related to the bulk geometry allows to verify that the correspondence (2.55) indeed satisfies a holographic bound as already argued in 2.1.4. To see this, we remind ourselves that we are dealing with a theory with fields in the adjoint representation of $SU(N)$. For a UV cutoff ϵ, we then expect that the number of bits N_{bits} that can be stored in the CFT in a spacelike unit volume ($\Delta x^\mu = 1$) goes as

$$N_{bits} \sim \frac{N^2}{\epsilon^3}. \tag{2.70}$$

From the bulk point of view, the corresponding area (calculated from (2.69)) will scale as (dropping the part of the sphere)

$$\mathcal{A} = \frac{L^3}{\epsilon^3}. \tag{2.71}$$

Hence (2.70) can be written as

$$N_{bits} \sim \frac{N^2}{\epsilon^3} \sim \frac{\mathcal{A}N^2}{L^3} \overset{N\sim\frac{L^4}{g_s\alpha'^2}}{\sim} \frac{\mathcal{A}L^5}{\alpha'^4 g_s^2} \sim \frac{\mathcal{A}}{G_{5,N}}. \tag{2.72}$$

Here, we have used (2.58) and in the last step we have identified the five-dimensional Newton's constant $G_{5,N}$. Following [44,50], we hence reproduced the expected holographic bound of section (2.1.2) up to a factor.

This shows that the correspondence (2.55), if any of the three forms discussed above holds true, is without a doubt the most concrete realisation of the holographic principle discussed in this thesis. However, it should be pointed out that the correspondence (2.55) is not the only holographic duality that has been shown to arise from brane constructions in string theory or more generally M-theory. Notable other instances include the $AdS_3\times S^3\times T^4/CFT_3$ correspondence of [25] and the ABJM $AdS_4\times S^7/\mathbb{Z}_k$ $/CFT_3$ duality [148], amongst others. Attempts to change the brane constructions in such a way that the conjectured dual field theories resemble more realistic field theories, with less conformal and supersymmetry, have led to a variety of models, the famous Sakagi-Sugimoto model [149, 150] for a holographic dual of a QCD-like field theory being only one example. Such models, that have a precise definition in the form of a brane setup in string or M-theory, are commonly referred to as *top-down* models. In section 6 we will encounter a top-down model [86] for a holographic dual of the Kondo effect. Unfortunately, such top-down models are notoriously complicated, and as the findings of sections 2.1 and 2.2 suggest, a holographic duality between two theories may be possible even without a formal derivation from string theory. Conjectured dualities between certain field theories and gravitational theories, in which the bulk fields are chosen in such a way that a holographic dictionary between the bulk theory and the field theory of interest can be established, are then referred to as *bottom-up* models. Such bottom-up models predominantly include classical gravity in the bulk, i.e. are based on the weak form of the AdS/CFT correspondence. Chapters 4 and 5 will be denoted to the investigation of general classes of holographic bottom-up models. In chapter 6, we will study in detail a specific holographic bottom-up model [86] for the Kondo effect, and compare it to the top-down model for the same effect proposed in the same paper.

Before moving on to the definition and study of *entanglement entropy*, an important and useful entry in the holographic dictionary, in chapter 3, we will now close this chapter with a short epilogue contrasting gravitational holography with its namesake, optical holography.

2.4 Epilogue: comparison to optical holography

In the past sections 2.1-2.3 we have studied the *holographic principle* and examples of its manifestation in theories of gravitation. To end this chapter, we will leave strings and

curved spaces aside for a moment to go back to the very beginnings and ask: Why is it called the "holographic principle"? The origin of this name goes back to the paper [18], where 't Hooft proposed this principle and pointed out some superficial similarities between this putative feature of (quantum) gravity and properties of *optical holograms*. Even a good analogy should never be overstrained, but it may prove insightful to briefly recap the principles of optical holography (following [151, 152]) and then point out both similarities and discrepancies between the two phenomena going by the name "holography"[14].

Optical holography is based on the insight that a light wave carries information not only in its amplitude, but also in its phase. An ordinary photograph records an intensity pattern only, but no phase information, hence information is lost in the photographic process. In optical holography, in contrast, the key to recording both intensity and phase information on a two-dimensional photographic plate is the introduction of a reference wave, with known amplitude, phase and direction. It is then the interference pattern caused by both the *reference wave* and the *object wave* that is recorded by a photographic screen, and that allows for the reconstruction of three-dimensional data in a later step.

Specifically, let us assume that we want to produce a holographic image of a certain object. To do so, we produce a reference wave of coherent light with known intensity, wavelength et cetera. Apart of this reference wave directly falls onto the photographic screen, while another one is first scattered from the object of interest. We are then faced with two *wave fields*[15] [152]

$$E_{R/O} = A_{R/O}(x, y, z) \cos 2\pi(\nu t + \Phi_{R/O}(x, y, z)), \tag{2.73}$$

where index R stands for the reference wave and O stands for the *object wave*. The position dependent functions A and Φ give amplitude and phase, respectively. As neither the amplitude A nor the phase Φ are time dependent, we see that this derivation assumes a stationary wave field, at least on the time scales that it takes to produce one holographic "snapshot". Assume furthermore that a photographic screen is placed at the position $x = 0$, extending infinitely along the y, z-plane. On this holographic screen, the intensity distribution will be

$$I(y, z) \propto [E_O + E_R]^2 \big|_{x=0} = \left[A_O^2 + A_R^2 + 2A_O A_R \cos 2\pi(\Phi_O - \Phi_R)\right] \big|_{x=0}, \tag{2.74}$$

where we also implicitly assumed a time averaging over one period $1/\nu$. This intensity distribution will determine the blackening on the photographic plate (as a negative), and as this plate is processed we assume to obtain a holographic image which shows a structure of blackened stripes on a transparent background (for example on a glass plate), such that the transmittance is proportional to the original function $I(y, z)$. If now the same reference

[14] It was pointed out in [153] that metamaterials may be used to test certain bottom-up models of holographic dualities in a laboratory environment, and that the methods of optical holography may then be of use.

[15] Holography, as an interference phenomenon, can be done with transversal as well as longitudinal waves, e.g. light waves as well as sound waves. Hence for simplicity we work with scalar wave fields in this section.

wave as before falls on this hologram, it will be refracted by the complicated pattern of black stripes that make up the hologram.[16] The wave field obtained this way in the y, z-plane is

$$E(y,z) \propto I(y,z)E_R(y,z) \tag{2.75}$$

$$\propto \big[A_R(A_O^2 + A_R^2)\cos 2\pi(\nu t + \Phi_R) + A_O A_R^2 \cos 2\pi(\nu t + \Phi_O) + A_O A_R^2 \cos 2\pi(\nu t - \Phi_O + 2\Phi_R)\big]\big|_{x=0}. \tag{2.76}$$

Knowing the wave field $E(y,z)$ in the plane of the holographic plate, we can now predict the wavefield behind the holographic plate as it is completely determined by $E(y,z)$ via the Huygens-Fresnel principle. In fact, in (2.76) we see that this wavefield behind the holographic plate will be a superposition of three wavefields: one ($\sim \cos 2\pi(\nu t + \Phi_R)$) that reproduces the original reference wave, one ($\sim \cos 2\pi(\nu t + \Phi_O)$) that reproduces the original object wave[17] and creates the impression of a three-dimensional object for an observer (i.e. the hologram) and one ($\sim \cos 2\pi(\nu t - \Phi_O + 2\Phi_R)$)) that creates a kind of twin image of the original object.

We can now see what motivated 't Hooft's original analogy [18] between optical holography and his own holographic principle: Information about a higher-dimensional region can be stored on its lower-dimensional boundary. In the gravitational case, it is the physics of black holes as we have seen in section 2.1 that seemingly restricts the scaling of the information storage capacity of a physical theory to be proportional to the surface area, not the bulk volume. In the optical case, it is the Huygens-Fresnel principle combined with the assumption of a stationary wave field that allows the reconstruction of the object image. Even further, 't Hooft pointed out that in both cases of holography there is a fundamental limit on the length scales that can be resolved on the boundary/ holographic plate: In the gravitational case this is the Planck length, in the optical case it is the wavelength of the light.

Interestingly, there is one aspect in which the analogy fails, and this is the issue of causality and bulk reconstruction. It is known [151, 152] that if you take a holographic plate and smash it into pieces, you can still produce a comparably good holographic image by sending the reference wave through one of the pieces only. The smaller the piece (compared to the original holographic plate), the worse the spacial resolution of the hologram will be. This is the reason why it is often said that an optical hologram stores information about every part of the image object in every part of the hologram. In contrast, in the case of the holographic principle as a property of gravitational theories, this will not be possible, as the gravitational (bulk) theory necessarily needs to contain notions of causality, such as light cones et cetera. In section 4 we will discuss things like *domains of dependence* and the *causal influence argument*, and we will see that for causality reasons it must not be possible to reconstruct certain parts of the bulk spacetime if only a too small part of the boundary

[16] For example a Fresnel zone plate can be considered to be a simple hologram of an approximately point-like object.

[17] We see that ideally the reference wave should be chosen such that A_R is approximately constant [151].

information is known. Indeed, in the recent literature this topic of *bulk reconstruction* has received much attention, especially with the introduction of the idea of *quantum error correcting codes*, see [154–158].

Chapter 3

Entanglement entropy and holography

The AdS/CFT duality (2.55) is, in its weak form, not only a duality between a strongly and a weakly coupled theory, but also between a quantum and a classical theory. It is hence particularly interesting to study the quantum properties of a field theory via holographic techniques, and one phenomenon of fundamental meaning to quantum theory is *entanglement*. There are several quantities that can be used to investigate or quantify entanglement in quantum systems (see e.g. [54]), but due to its simplicity, *entanglement entropy* has received the most attention in the holography literature. We will hence introduce the definition of entanglement entropy in this chapter, as well as its calculation and interpretation in holographic terms. This will provide the basis for the work to be presented in chapters 4-6. Due to its prominence in holography, there is as lot of literature on entanglement entropy. Reference [54] contains a thorough review of entanglement, entropy and other topics of quantum theory. Reviews of entanglement entropy from a holographic viewpoint can be found in [52, 159], amongst others.

3.1 Definition

We start by presenting the definition and basic properties of entanglement entropy following [52, 54]. The definition of entanglement entropy starts by describing the quantum state of a certain quantum system via a *density matrix* ρ. In case of a pure state $|\Psi\rangle$, we find $\rho = |\Psi\rangle\langle\Psi|$, but in more general cases the density matrix may describe a system in a mixed state, or an ensemble of states. For example, in the thermal canonical ensemble with inverse temperature β the density matrix takes the form

$$\rho = \frac{1}{Z(\beta)} e^{-\beta \hat{H}} = \frac{1}{Z} \sum_i e^{-\beta E_i} |\psi_i\rangle \langle\psi_i| , \tag{3.1}$$

where $\hat{H}$ is the Hamiltonian operator with energy eigenstates $|\psi_i\rangle$ and eigenvalues E_i, and the partition function $Z(\beta)$ serves as a normalisation to ensure $\mathrm{Tr}\,[\,\rho] = 1$.

Using the density matrix of a system, a generalisation of *Shannon entropy* to quantum states can be defined [54]. This is called *von Neumann entropy* and reads

$$S = -\mathrm{Tr}\,[\,\rho \log \rho]. \tag{3.2}$$

Entanglement entropy now extends this definition onto subsystems of the total quantum system. To do so, one divides the total system into complementary subsystems A and $\bar{A}$, such that the Hilbert space factorises as $\mathcal{H} = \mathcal{H}_A \otimes \mathcal{H}_{\bar{A}}$.[1] One can then define the *reduced density matrix* of the subsystem A, ρ_A, by tracing out the states on the Hilbert space $\mathcal{H}_{\bar{A}}$:

$$\rho_A = \mathrm{Tr}_{\bar{A}}[\rho]. \tag{3.3}$$

The *entanglement entropy of* A, S_A, is then defined as the von Neumann entropy (3.2) of the reduced density matrix ρ_A on $\mathcal{H}_A$, i.e.

$$S_A = -\mathrm{Tr}_A[\rho_A \log \rho_A]. \tag{3.4}$$

This quantity has the following properties [52, 54]:

- Von Neumann entropies and consequently entanglement entropies are non-negative, $S \geq 0$.
- Von Neumann entropy (3.2) is zero if and only if the density matrix ρ describes a pure state.
- Entanglement entropies of subsystems (A, B, C) of a larger system satisfy a number inequalities. These are the *subadditivity*

  $$S_{A\cup B} \leq S_A + S_B, \tag{3.5}$$

  indicating that entanglement entropy is not extensive, *strong subadditivity*

  $$S_{A\cup B\cup C} + S_B \leq S_{A\cup B} + S_{B\cup C}, \tag{3.6}$$

  and the *triangle* or *Araki-Lieb inequality* [54, 161]

  $$S_{A\cup B} \geq |S_A - S_B|. \tag{3.7}$$

  This implies that in the case of a pure total state, $S_{A\cup\bar{A}} = 0$, the entanglement entropy will be symmetric: $S_A = S_{\bar{A}}$.

As a consequence of the above, we see why entanglement entropy can be used as a rough

[1] The assumption that the Hilbert space always factorises in this nice way is indeed non-trivial for gauge theories. See [160] for a detailed discussion.

measure for entanglement: If we find $S_A = 0$, then the reduced density matrix ρ_A is in a pure state, even after tracing out the degrees of freedom in the Hilbertspace $\mathcal{H}_{\bar{A}}$. This indicates that no information about subsystem A is lost when tracing out $\bar{A}$, hence there is no entanglement between A and $\bar{A}$ present in the total state ρ. Unfortunately, the converse is not true: $S_A \neq 0$ does not necessarily imply entanglement between A and $\bar{A}$ in the initial state ρ. Entanglement entropy is hence not a perfect quantifier of entanglement in any generic situation, nevertheless it can be used as a practical indicator of entanglement in many cases.

To illustrate this point, let us consider two spins A and B which are together in the pure *EPR state*

$$|\Psi\rangle = \frac{1}{\sqrt{2}} \left(|\uparrow\rangle_A |\uparrow\rangle_B + |\downarrow\rangle_A |\downarrow\rangle_B \right). \tag{3.8}$$

It is then an easy task to calculate the reduced density matrix

$$\rho_A = \frac{1}{2} \left(|\uparrow\rangle_A \langle\uparrow|_A + |\downarrow\rangle_A \langle\downarrow|_A \right), \tag{3.9}$$

which describes a mixed state with entanglement entropy

$$S = \log 2. \tag{3.10}$$

This shows that the two states in the EPR state (3.8) are entangled. In fact they are maximally entangled because in a Hilbert space $\mathcal{H}_A$ with finite dimension d the entanglement entropy is bounded from above by $\log d$ [54].

Via the *replica trick* to be studied in section 3.4, entanglement entropy can not only be calculated for simple systems in quantum information theory, but also for more complicated setups. In particular, for conformal field theories in two dimensions, there are a number of analytic results, see [162]. In many other cases, nevertheless, the calculation of entanglement entropy can be notoriously difficult. This makes it a very interesting quantity to be studied holographically. In the next two sections, we will hence discuss holographic techniques of calculating entanglement entropy, and the way in which entanglement entropy leads to a generalisation of the Bekenstein-Hawking formula (2.1).

3.2 Holographic entanglement entropy

A prescription for the calculation of entanglement entropy in the AdS/CFT correspondence was first proposed by Ryu and Takayanagi (RT) in [55, 56]. This proposal rests on the assumptions that the gravitational bulk theory is described by Einstein-Hilbert gravity coupled to matter, and that the (asymptotically AdS) bulk spacetime $\mathcal{M}$ is static, i.e. there exists a timelike hypersurface orthogonal Killing vector field. Then this Killing vector field

defines a foliation of both the spacetime $\mathcal{M}$ and its conformal boundary $\partial\mathcal{M}$ into equal time slices. Via holography, we assume a quantum field theory to live on the asymptotic boundary $\partial\mathcal{M}$, and we divide the equal time slice of $\partial\mathcal{M}$ into two spacelike regions, A and its complement $\bar{A}$. According to the RT prescription, the entanglement entropy for the CFT subsystem defined on the region A can be calculated via the formula

$$S(A) = \frac{\text{area}(\mathcal{E}(A))}{4G_N}, \tag{3.11}$$

where $\mathcal{E}(A)$ is an extremal surface[2] in the (static) bulk spacetime which is anchored to the boundary of the region A on the AdS boundary, i.e. $\partial\mathcal{E}(A) = \partial A$. See figure 3.1 for the geometrical setup. Here, the extremal surface $\mathcal{E}(A)$ will be referred to as the *holographic* or *bulk entangling surface*, while ∂A, the boundary of the region A on $\partial\mathcal{M}$, is often called the *entangling surface*.

As shown in [163], the RT prescription has to be amended with a topological constraint that we refer to as *homology condition*: $\mathcal{E}(A)$ has to be required to be homologous to A, i.e. there has to be a spacelike codimension one surface $\mathcal{F}$ (see figure 3.1) such that the boundary $\partial\mathcal{F}$ is the union of $\mathcal{E}(A)$ and A.

It was already shown in [55, 56] that this prescription reproduces results known for CFTs from field theory calculations [162], and much more evidence for the correctness of (3.11) has been aggregated since. In particular, a simple proof for the strong subadditivity (3.6) of holographic entanglement entropy was given using the RT prescription in [164]. A first general proof of this formula was attempted in [163], but see [165]. A universally accepted proof of the RT prescription was then given in [166], see section 3.4. Attempted proofs for the special case of $2+1$-dimensional bulk spacetimes can be found in [167, 168].

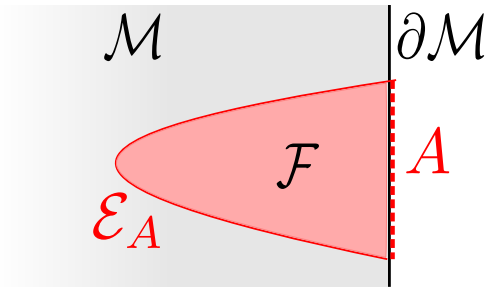

Figure 3.1: The geometrical setup for the Ryu-Takayanagi prescription. The bulk spacetime $\mathcal{M}$ is assumed to be static. The time direction is suppressed in this figure, i.e. only a spacelike slice of $\mathcal{M}$ is shown. The figure is presented as in [1].

One of its shortcomings is that the RT prescription is by definition only valid for static bulk spacetimes, but a covariant extension to general cases, with non-static bulk spacetimes, was given by Hubeny, Rangamani and Takayanagi (HRT) in [169]. According to

[2]Particularly, a spacelike codimension two surface embedded in the equal time slice of the geometry that minimises its surface area.

this prescription, in order to holographically calculate the entanglement entropy of the subsystem of the boundary CFT defined on a spacelike codimension one region A of the boundary $\partial\mathcal{M}$, one searches for bulk surfaces $\mathcal{E}(A)$ that are anchored to ∂A and satisfy the homology constraint as before, but now *extremise* the area. Then, out of all surfaces that satisfy these conditions, the one with *minimal* area is chosen, and the entanglement entropy is calculated as

$$S(A) = \min_X \frac{\text{area}(\mathcal{E}(A))}{4G_N} \text{ for } X = \{\mathcal{E}(A) : \partial\mathcal{E}(A) = \partial A, \exists\mathcal{F} \text{ s.t. } \partial\mathcal{F} = \mathcal{E}(A) \cup A\}. \quad (3.12)$$

The reason that the HRT prescription searches for curves extremising the area is the following [169]: In the RT prescription, the bulk entangling curves are by definition embedded in a spacelike time slice, and on this spacelike slice a unique minimal area surface should exist. In the covariant case however, the length of a spacelike curve for example can always be made arbitrarily small by deforming it closer and closer to a piecewise null curve. The minimisation of the area in a Lorentzian background will hence not yield a well-defined spacelike surface. This is why in the HRT prescription, one first constructs the set of all well-defined spacelike extremal surfaces, and then takes the minimal area surface in this set.

As remarked in [170, 171], the homology constraint has to be refined for the covariant prescription (3.12), e.g. by requiring that the codimension one surface $\mathcal{F}$ has to be spacelike. In the RT approach, this is the case by construction. In [64], it was discussed that the bulk entangling curves should satisfy certain causality constraints, and that this is automatically the case in the HRT prescription when the null energy condition is satisfied. These causality conditions will play a major role in our discussion of entanglement entropy in higher curvature theories, where we show that they are not automatically satisfied even in physical background spacetimes, see section 4.

We will end this section by showing a very simple example of the calculation of entanglement entropy using these holographic methods that was originally already presented in [55]. Specifically, we will take $2+1$-dimensional Poincaré AdS (2.11) as the background spacetime, and we will be interested in calculating the entanglement entropy of a boundary interval A defined to be a subset of the equal time slice $\tau = 0$ and ranging from $x = -\Delta x/2$ to $x = +\Delta x/2$. The bulk spacetime is static and the equal time slice $\tau = 0$ is the Euclidean hyperbolic space

$$ds^2 = \frac{L^2}{z^2}(dx^2 + dz^2). \quad (3.13)$$

It is well known that the geodesics in this space are half-circles, and consequently the bulk-entangling surface needed to calculate the entanglement entropy can be given in a

simple non-affine parametrisation

$$z(s) = \frac{\Delta x}{2}\sin(s), \tag{3.14}$$

$$x(s) = \frac{\Delta x}{2}\cos(s), \tag{3.15}$$

with $s \in]0, \pi[$. See figure 3.2 for an illustration of the geometric setup. By (3.11), the entanglement entropy will be defined by the *area* of this codimension two hypersurface, which is in case of such a one-dimensional curve only its length. Strictly speaking, this length will be infinite due to the contribution of the part of the curve near the boundary and we hence have to impose a cutoff at $z = \epsilon$. As explained in section 2.3.3, this cutoff acts as an IR regulator for the bulk theory (regulating infinite volume effects), but as a UV regulator in terms of the boundary CFT. Using (3.11), the entanglement entropy is then

$$S = \frac{L}{4G_N}\int_{\arcsin\left(\frac{2\epsilon}{\Delta x}\right)}^{\pi-\arcsin\left(\frac{2\epsilon}{\Delta x}\right)} \frac{ds}{\sin(s)} \approx \frac{c}{3}\log\left(\frac{\Delta x}{\epsilon}\right) + \dots\,, \tag{3.16}$$

where ... stands for terms of higher order in $\frac{\epsilon}{\Delta x}$ and we used the result (2.33) to express G_N in terms of the central charge c. As expected, (3.16) reproduces the field theory result of [162].

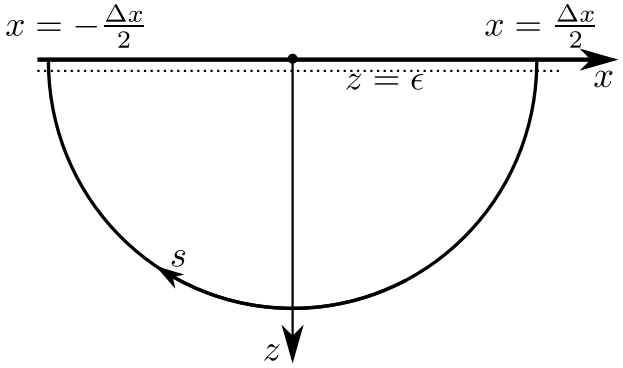

Figure 3.2: Geometric setup for the calculation of entanglement entropy of an interval $A = [-\frac{\Delta x}{2}, \frac{\Delta x}{2}]$. In the hyperbolic space (3.13), the spacelike geodesics are half-circles.

3.3 Black hole entropy and thermofield double states

As we can clearly see by comparing equations (2.1), (3.11) and (3.12), the holographic prescription for calculating entanglement entropy is a generalisation of the Bekenstein-Hawking formula for black hole entropy. Indeed, we can see that in the AdS/CFT correspondence the entropy of a static bulk black hole can be calculated as entanglement

entropy. To do so, we have to distinguish two possible cases.

In the first case, we are working in an asymptotically Poincaré black hole background, where the event horizon extends infinitely in the spacelike directions x^μ. When we then calculate the entanglement entropies of certain boundary systems (e.g. infinite strips) $A(R)$ with size R, and take the limit $R \to \infty$, we find that the corresponding holographic entangling surfaces in the bulk approach the event horizon more and more closely, see figure 3.3. For example, the generalisation of (3.16) to the background-spacetime given by the BTZ black hole [130, 131] with temperature T will play an important role in chapter 6 and reads [55, 162][3]

$$S = \frac{c}{3} \log \left(\frac{1}{\pi \epsilon T} \sinh (\pi R T) \right). \tag{3.17}$$

Apart from the divergence $\sim \log(\epsilon)$ caused by the near-boundary part of these surfaces, which can be subtracted, the entanglement entropy will then be dominated by the increasing parts of the surfaces that are close to the horizon. For large R, the renormalised entanglement entropy S_{ren} can then be approximated by the area of the part of the curve $\mathcal{E}_{A(R)}$ which is near the event horizon, or equivalently by the area of $A(R)$ (measured at the boundary) times the entropy density of the event horizon times some constant. In the limit $R \to \infty$ the entanglement entropy hence reproduces the black hole entropy. We also see that in this limit the entanglement entropy becomes extensive, as expected for a thermodynamic entropy. For example, in the limit $R \to \infty$ equation (3.17) yields

$$S_{ren} \approx \frac{c}{6} \pi T R. \tag{3.18}$$

These considerations will later become very useful in our study of entanglement entropy and impurity entropy in the Kondo effect, see chapter 6.

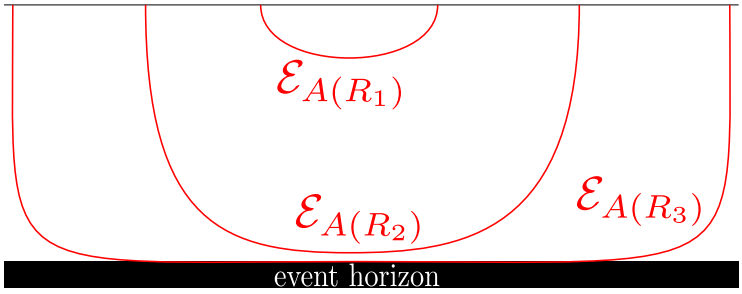

Figure 3.3: Typical holographic entangling surfaces for three boundary regions $A(R_i)$ with sizes $R_1 < R_2 < R_3$. With increasing size, the surfaces approach the event horizon closer and closer.

In the second case we deal with black holes in asymptotically global AdS, where the boundary is compactified to a (hyper-) sphere. The analogous situation to the first case

[3] With Δx in (3.16) renamed to R in this context.

is a bit more complicated here, as bulk entangling curves still tend to approach the event horizon, but due to the finiteness of the boundary volume, the limit $R \to \infty$ is now not possible anymore. To investigate this case more closely, we should consider the conformal diagram of a static asymptotically AdS black hole as it is sketched in figure 3.4. Outside of the event horizons, this spacetime is static, and hence equal time slices can be constructed. In such cases, as we have seen in section 3.2, we can calculate entanglement entropy holographically using the Ryu-Takayanagi prescription[4]. The corresponding holographic entangling surfaces are then extremal surfaces on the geometry defined by the equal time slice, which is known as an *Einstein-Rosen (ER) bridge* or also *Euclidean wormhole*. See figure 3.5 for a sketch of the geometry of such an equal time slice.

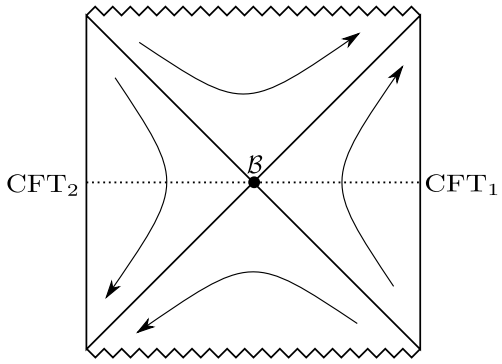

Figure 3.4: Conformal diagram for a static asymptotically AdS black hole. The spacetime has *two* boundaries, with CFTs 1 and 2 living on it. The flow of the (asymptotically) timelike Killing vector field ∂_t is indicated with arrows. The event horizons (diagonal lines) are Killing horizons, and the bifurcation surface $\mathcal{B}$ is defined to be the locus where the Killing vector field vanishes. An equal time slice with respect to the Killing field is a straight line through the center of this diagram, shown as a dotted line. The figure is presented as in [1].

Assume we start with a subregion A of CFT_1 which has a small angular extend $\Delta\phi$ on the boundary sphere.[5] The corresponding bulk entangling surface used in the RT prescription will then be of the qualitative form of $\mathcal{C}$ in figure 3.5. As $\Delta\phi$ grows beyond π, this will smoothly transform into a hypersurface of the shape $\mathcal{D}$, which increasingly approaches the bifurcation surface $\mathcal{B}$, which is the equal time slice of the black hole event horizon. But now we have to take into account that according to the RT prescription, the bulk entangling surface need not necessarily be connected. Then, for $\Delta\phi \to 2\pi$, there are two possibilities for extremal bulk surfaces that satisfy the homology constraint and are anchored at ∂A on the boundary. One possibility is the surface $\mathcal{D}$ sketched in figure 3.5, the other possibility is that the entanglement entropy is described by the *union* of the curves $\mathcal{B}$ and $\mathcal{C}$.[6] Note

[4]Assuming that the boundary subsystem in question is also defined on an equal time slice.

[5]This is a generalisation of the size scale R that we used for the case of a flat boundary.

[6]For the moment, we ignore surfaces of the type $\mathcal{A}$, i.e. closed surfaces wrapping around the black hole event horizon. In Einstein-Hilbert gravity, these are excluded by the null energy condition [172].

that $\mathcal{C}$ alone would not satisfy the homology constraint with respect to the boundary region A. According to the RT prescription, the entanglement entropy is given by the extremal surfaces with smallest area, subject to the correct boundary conditions and the homology constraint. Hence, as $\Delta\phi$ is increased from 0 to 2π, there will generically be a transition from the entanglement entropy being defined by one surface for small $\Delta\phi$ to the entanglement entropy being defined by the union of a surface anchored at the boundary and the bifurcation surface $\mathcal{B}$ for large $\Delta\phi$.[7] Especially, we see that if we take the limit $B \to 0$ such that the subregion A encompasses the entirety of the right boundary, where CFT_1 lives, the (renormalised) entanglement entropy is given by the area of the bifurcation surface $\mathcal{B}$,[8] i.e. the area of a slice of the event horizon. This means that the two CFTs on the two boundaries of the eternal black hole are entangled, and the entanglement entropy between them is exactly the Bekenstein-Hawking entropy (2.1), or in the nomenclature of this section [169, 170]

$$S = \frac{\mathrm{area}(\mathcal{B})}{4G_N}. \tag{3.19}$$

This implies that after tracing out the degrees of freedom of CFT_2, CFT_1 is left in a thermal state with density matrix (3.1) and an entropy (3.19) that could be interpreted as thermal entropy from a viewpoint of the CFT_1, but that is an entanglement entropy from a viewpoint that takes into account both CFT_1 and CFT_2.

The remaining question is: What is the total state of CFT_1 and CFT_2 dual to the eternal black hole? The answer was given by Maldacena in [173], where he proposed that in the weak form of the AdS/CFT conjecture, the total state of the two CFTs dual to the large static eternal black hole[9] is the (pure) *thermofield double state*

$$|\Psi\rangle = \frac{1}{\sqrt{Z(\beta)}} \sum_i e^{-\frac{1}{2}\beta E_i} |E_i\rangle_1 |E_i\rangle_2 \ , \tag{3.20}$$

where the notation is similar to equation (3.1) and the states $|E_i\rangle_{1/2}$ are energy eigenstates of $\mathrm{CFT}_{1/2}$ respectively. Starting from this state (3.20), it is then easy to take the trace on the Hilbertspace of CFT_2 and find that the reduced density matrix for CFT_1 will be the thermal one (3.1). This pure thermofield double state describing two entangled CFTs is hence analogous to the EPR state (3.8) describing two entangled spins. This is one manifestation of the ER=EPR proposal mentioned in section 1.

The fact that the entropy of the bulk black hole holographically describes the entropy of the CFT on one of the boundaries, described by the density matrix of a thermal state, was already derived without the use of entanglement entropy in [27, 174]. To understand this result, we should note that for a thermal canonical ensemble, the CFT thermodynamics

[7] This also leads to the phenomenon of *entanglement plateaux* studied in [170].

[8] As $\mathrm{area}(\mathcal{C}) \to 0$ in this limit.

[9] The AdS-black hole is assumed to be *large* compared to the AdS-scale in order to have positive specific heat and be the dominant contribution to the canonical thermodynamic ensemble [173].

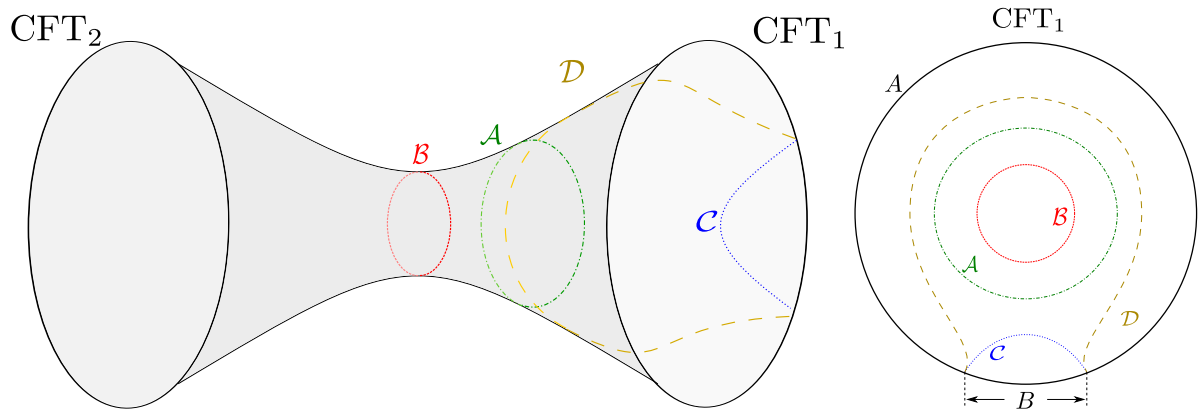

Figure 3.5: Left: The geometry of an Einstein-Rosen bridge, which is the equal time slice signified in figure 3.4 by a dotted line. Several types of possible curves on such a time slice are shown as $\mathcal{A}, \mathcal{B}, \mathcal{C}, \mathcal{D}$. $\mathcal{B}$ is the bifurcation surface, which is the throat of the wormhole, where the circumference of the geometry is the smallest. Curves of the type of $\mathcal{A}$ are usually not possible in Einstein-Hilbert gravity [172], but will play a role in higher curvature theories, see chapter 4. Right: A similar sketch, showing only the spacetime region between the bifurcation surface and the right boundary (divided into regions A and B), where CFT$_1$ is assumed to live via the holographic duality. The figures are presented as in [1].

can be inferred from the (canonical) partition function $Z(\beta) = \mathrm{Tr}\left[e^{-\beta \hat{H}}\right]$. Then, one can define quantities such as the free energy $\beta F = -\log Z(\beta)$ and the field theory entropy $S_{CFT} = \beta^2 \partial_\beta F$. Holographically, the weak form GKPW formula (2.60) equates the CFT partition function with the saddle point approximation of the gravity partition function, i.e.

$$Z = e^{-\mathcal{S}_E(\beta)}, \tag{3.21}$$

where $\mathcal{S}_E$ is the Euclidean on-shell action of the dominant bulk saddle for a given temperature. This dominant saddle will be a black hole, at least for large temperatures [27, 174]. It then follows that $\beta F = \mathcal{S}$ and the CFT thermal entropy can be calculated from the gravity on-shell action to be [27, 174]

$$S_{CFT} = \beta^2 \partial_\beta \left(\frac{1}{\beta}\mathcal{S}\right). \tag{3.22}$$

This on-shell action approach to black hole entropy reduces to the area formula (3.19) [27, 174], and hence we find

$$S_{CFT} = S_{BH} = \frac{\mathrm{area}(\mathcal{B})}{4G_N}, \tag{3.23}$$

reproducing the result derived via entanglement entropy above.

3.4 The replica method

So far, we have seen concrete examples of how entanglement entropy can be calculated for simple spin-systems, as well as in holographic contexts. To gain a deeper understanding of entanglement entropy in field theory terms, in this section we present a brief overview over the *replica trick* or *replica method*. Although this method has been developed in the context of *spin glasses* (see e.g. [175]), we will in this section follow the outline presented in [162] as well as the summary of [52].

The first step towards understanding the replica method is to write the entanglement entropy (3.4) in the form

$$S_A = -\mathrm{Tr}_A[\rho_A \log \rho_A] = -\lim_{n\to 1} \frac{\partial}{\partial n} \mathrm{Tr}\left[\rho_A^n\right]. \tag{3.24}$$

S_A can hence be calculated by the detour of calculating $\mathrm{Tr}\left[\rho_A^n\right]$ for any integer $n > 1$, analytically continuing to general $n > 1$ and taking the appropriate limit [162]. The virtue of the replica method is that the quantity $\mathrm{Tr}\left[\rho_A^n\right]$ can be calculated via path integral methods. For simplicity, we will now restrict our discussion to Euclidean two-dimensional quantum field theories, with a Euclidean time coordinate t and a space coordinate x. We will also assume this Euclidean space to be simply a cylinder where the time is compactified with a period $\beta = 1/T$.

The path integral can now for example be used to calculate transition probabilities between two states at different Euclidean times, or the thermal partition function

$$Z = \int \mathcal{D}[\phi]\big|_{t\sim t+\beta}\, e^{-\mathcal{S}_E}, \tag{3.25}$$

where we have collectively called the fields of the theory ϕ, and the Euclidean action $\mathcal{S}_E$. The integration is over all field configurations that satisfy the appropriate periodicity conditions for finite temperature. In the following, we consider the case where a subsystem A is defined to be an interval on the $t = 0$ line of the Euclidean space. The reduced density matrix ρ_A then reads [162]:

$$\rho = \frac{1}{Z} \int \mathcal{D}[\phi]\big|_{t\sim t+\beta \text{ for } x\in\bar{A}} \prod_{x\in A} \delta(\phi(x,0^+) - \phi'(x)) \prod_{x\in A} \delta(\phi(x,0^-) - \phi''(x))\, e^{-\mathcal{S}_E}. \tag{3.26}$$

The interpretation of this formula is that the periodicity conditions are only imposed on the fields outside of A, while in the subsystem A we impose the boundary condition $\phi'(x)$ at an infinitesimal time-step to the future and $\phi''(x)$ at an infinitesimal time step to the past. This implements the tracing out of the complement $\bar{A}$ ($\rho_A = \mathrm{Tr}_{\bar{A}}[\rho]$), and the functions ϕ' and ϕ'' can be seen as indices of the reduced density matrix, $(\rho_A)_{\phi'\phi''}$. It is now straightforward to understand how the quantity $\mathrm{Tr}\left[\rho_A^n\right]$ can be calculated by introducing n copies, also called *replicas*, of the manifold on which the QFT lives. See figure 3.6 for an

illustration. One simply sews together the n copies of the spacetime along the subsystem A in a cyclic way, always identifying the state on the 0^+-line of replica i with the state on the 0^--line of replica $i+1$. Taking the overall trace is then implemented by identifying the state on the 0^+-line of replica n with the state on the 0^--line of replica 1.

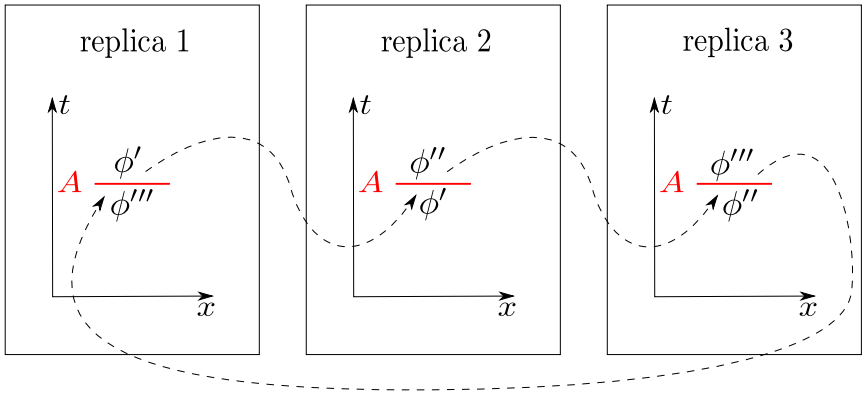

Figure 3.6: An illustration of the replica method, here for the case $n = 3$. The subsystem A is seen as a cut in the space on which the field theory lives, and n replicas of the space are sewn together along this cut in a cyclic manner.

This means that we are effectively working with an n-sheeted Riemann surface R_n, and the reduced density matrix is related to the partition function $Z_n(A)$ of the QFT on this Riemann surface via the equation [162]

$$\mathrm{Tr}\,[\rho_A^n] = \frac{Z_n(A)}{Z^n}. \tag{3.27}$$

Thus, the replica trick suggests a possible way to calculate entanglement entropy by calculating the expressions $Z_n(A)$ for integer $n > 1$. Unfortunately, this is still a non-trivial task in general, but analytic results such as (3.17) can be derived for two dimensional CFTs [162]. We will not go into the details of this, instead we will in the rest of this section give a brief overview over how the replica trick was used for a holographic derivation of the Ryu-Takayanagi prescription (3.11) in [166], see also [163, 165, 167, 168] for earlier work. To do so, we will follow the overviews presented in [52] and [62].

The idea behind the proof given in [166] is to extend the replica trick into the bulk spacetime. Specifically, for the case of n replicas, there should be a bulk spacetime B_n such that R_n is the conformal boundary of this bulk spacetime, and B_n is a solution to Einstein's equations. The generalisation of (3.21) then reads

$$Z_n(A) = e^{-\mathcal{S}_{E,\,bulk}(B_n)}. \tag{3.28}$$

For integer n, the boundary manifold R_n has a cyclic $\mathbb{Z}_n$ symmetry (of shifting the replicas $i \to i + m$ modulo n), and this is conjectured to be also the case for B_n [166]. The set of points that are invariant under this $\mathbb{Z}_n$ symmetry is very interesting: On the boundary R_n,

these points will be the boundary ∂A of the subsystem A, i.e. the endpoints of the cut along which the replicas are sewn together. In the bulk spacetime B_n, the set of fixed points will form a codimension two surface that reaches to the boundary R_n and is anchored there at ∂A. For simplicity, we refer to this set of fixed points as $\mathcal{E}(A)$, as in the limit $n \to 1$ it will become the holographic entangling surface defined in section 3.2. Instead of B_n, it is now useful to look at the orbifold

$$\widehat{B}_n = B_n/\mathbb{Z}_n. \tag{3.29}$$

The hypersurface $\mathcal{E}(A)$ is then the locus of a *conical defect* in $\widehat{B}_n$. Excluding boundary terms of the action at the locus of this conical defect, one can then write $\mathcal{S}_{E,\,bulk}(B_n) = n\mathcal{S}_{E,\,bulk}(\widehat{B}_n)$ [62, 166]. Furthermore, as $\mathrm{Tr}[\rho] = 1$, (3.24), (3.27), (3.28) and (3.29) can be used to derive [62, 166]

$$S_A = -\lim_{n\to 1}\partial_n \mathrm{Tr}\left[\rho_A^n\right] = -\lim_{n\to 1}\partial_n \log \mathrm{Tr}\left[\rho_A^n\right] = \lim_{n\to 1}\frac{1}{1-n}\log \mathrm{Tr}\left[\rho_A^n\right] \tag{3.30}$$

$$= \lim_{n\to 1}\frac{n}{n-1}\left(\mathcal{S}_{E,\,bulk}(\widehat{B}_n) - \mathcal{S}_{E,\,bulk}(\widehat{B}_1 = B_1)\right) = \lim_{n\to 1}\partial_n \mathcal{S}_{E,\,bulk}(\widehat{B}_n) \tag{3.31}$$

As shown in [62, 166], the metric in the vicinity of this hypersurface can be written as

$$ds^2 = \rho^{-2\epsilon}\left(d\rho^2 + \rho^2 d\tau^2\right) + \left(h_{ij} + 2k_{ij}^{(\alpha)}x^\alpha\right)dy^i dy^j + ..., \tag{3.32}$$

where the y^i are coordinates along $\mathcal{E}$ while $x^\alpha \in \{\rho, \tau \sim \tau + 2\pi\}$ are polar coordinates in the plane normal to the conical defect surface. The conical defect is parameterised by $\epsilon = 1 - 1/n$, and the $k_{ij}^{(\alpha)}$ are extrinsic curvature tensors, see appendix A. The terms ... are terms in higher order of ρ. The virtue of this approach of introducing $\widehat{B}_n$ and the metric (3.32) is that this setup can easily be generalised to non-integer n.

As shown in [166], imposing Einstein's equations to be satisfied by the metric (3.32) leads, in the limit $n \to 1$, to the condition

$$k^{(\alpha)i}_{\ \ i} = 0, \tag{3.33}$$

i.e. the traces of the extrinsic curvature tensors have to vanish. This means nothing else than that the surface $\mathcal{E}(A)$ has to be an extremal surface[10], as expected from the holographic prescriptions discussed in section 3.2. This is a very important result, as in chapter 4 we will be concerned with locating the extremal surfaces that define entanglement entropy in higher curvature theories. Furthermore, a detailed analysis of the terms arising in the action $\mathcal{S}_{E,\,bulk}(\widehat{B}_n)$, which will not be repeated here for the sake of brevity, confirms that the correct entropy functional is indeed (3.11) [166].

As we have seen in this chapter, entanglement entropy is a widely studied topic in the AdS/CFT literature and it would lead too far to summarise here all the ways in which

[10] In the sense of extremising its area.

the study of entanglement entropy has lead to new insights into the nature of holography. Instead, we will devote the remaining chapters of this thesis to highlighting the contributions that the author made to the understanding of holographic entanglement entropy in certain contexts. In chapter 4, we study how prescriptions for calculating entanglement entropy in bulk theories with higher curvature terms in the action will be constrained by requirements of causality. In chapters 5 and 6 we will study bottom-up models of boundary CFTs (BCFTs), and how entanglement entropy can be used in such models to define *defect entropy* and monitor the behaviour of this quantity under holographic RG flows.

Chapter 4

Entanglement entropy in higher curvature theories

4.1 Introduction

In the following chapter, we will present the results obtained by the present author in [1]. In section 3.3 we have seen that in AdS/CFT, the entropy of eternal black holes is interpreted as the entanglement entropy between two CFTs living on the two AdS boundaries. While, as we discussed in section 2.1.1, the entropy of a black hole in Einstein-Hilbert gravity should be given by the Bekenstein-Hawking formula (2.1), the generalisation of this formula to gravitational theories with higher curvature terms in the action (e.g. $R^2, R_{\mu\nu}R^{\mu\nu}$ et cetera) was given by Wald and others in [57–59]. There, it was derived that for a stationary black hole in a higher curvature theory with action

$$\mathcal{S} = \frac{1}{16\pi G_N}\int d^{d+1}x\sqrt{-g}\mathcal{L}, \tag{4.1}$$

the black hole entropy can be calculated by evaluating a certain entropy functional on the bifurcation surface $\mathcal{B}$ (see section 3.3) of the black hole [57–59]:

$$S_{Wald} = \frac{-1}{8G_N}\int\limits_{\mathcal{B}} d^{d-1}y\sqrt{\gamma}\frac{\partial\mathcal{L}}{\partial R_{\alpha\beta\gamma\delta}}\epsilon_{\alpha\beta}\epsilon_{\gamma\delta}. \tag{4.2}$$

Here $\epsilon_{\alpha\beta}$ is called the *binormal* and, using $\epsilon^{\alpha\beta}\epsilon_{\alpha\beta} = -2$, (2.1) follows as the special case for Einstein-Hilbert gravity [57–59]. Now as we have seen in sections 3.2 and 3.3 the holographic prescriptions for the calculation of entanglement entropy can be considered to be a straightforward generalisation of the entropy formula (2.1) for black holes. Will holographic entanglement entropy calculations in higher curvature bulk theories then be a straightforward generalisation of (4.2)? The answer is both yes and no. "Yes" because, as

explained in section 3.3, the prescription for calculating holographic entanglement entropy has to reproduce the correct black hole entropy. "No" because the necessary generalisation of (4.2) will not be straightforward. In the derivation of [57–59], there where several possible ambiguities that did not matter as the corresponding terms always vanish when evaluated on a bifurcation surface $\mathcal{B}$ [176]. Nevertheless, holographic entanglement entropy in higher curvature theories has been an active field of research in holography, starting already with [163,176,177] for specific theories, continuing with [60,61] for general theories with higher curvature terms of order R^2 and reaching the most general result up to date with [62,63]. Specifically, for a higher curvature theory of the form

$$\mathcal{S} = \frac{1}{16\pi G_N}\int d^{d+1}x\,\sqrt{-g}\left[R + 2\Lambda + aR^2 + bR_{\mu\nu}R^{\mu\nu} + cR_{\mu\nu\alpha\beta}R^{\mu\nu\alpha\beta}\right], \tag{4.3}$$

the entropy functional proposed in [60–63] based on replica methods similar to the arguments discussed in section 3.4 reads:

$$S_{EE}(\Sigma) = \frac{1}{4G_N}\int\limits_{\Sigma} d^{d-1}y\sqrt{\gamma}\,\left[1 + 2aR + b\left(R_{\parallel} - \frac{1}{2}k^2\right) + 2c\left(R_{\parallel\parallel} - \mathrm{Tr}(k)^2\right)\right]. \tag{4.4}$$

This indeed reduces to (4.2) when evaluated on a black hole bifurcation surface [60–63]. For an explanation of the notation used in this formula, see appendix A.1.

The derivations done in [60–63] are a generalisation of the calculations of [166] (see section 3.4) to higher curvature theories, and as such are quite involved. However, just like the end result of [166] was the simple Ryu-Takayanagi prescription (3.11), the general prescription how to calculate holographic entanglement entropy using the functional (4.4) is thought to be simply a generalisation of the RT and HRT prescriptions studied in section 3.2. According to [62], in order to calculate the entanglement entropy of a boundary subregion A, one has to find a codimension two spacelike surface extremising the functional (4.4) and satisfying the same boundary conditions as the curve $\mathcal{E}(A)$ in the RT and HRT prescriptions, i.e. $\partial\Sigma = \partial A$ and the homology condition. If several extremal surfaces Σ satisfying these conditions exist, one would take the one yielding the smaller entropy (4.4) to be the one defining the physical holographic entanglement entropy.

In this chapter, however, we will apply this prescription to two different physical theories and find that there are special situations in which this prescription yields extremal surfaces Σ that satisfy all conditions described above and give the lowest entropy, but that should not be considered to be the correct physical surface defining entanglement entropy. In particular, following the thoughts of section 3.3 we will look for hypersurfaces extremising the functional (4.4) which are not anchored to the asymptotic boundary, but which are closed and wrap around a black hole, such as curve $\mathcal{A}$ in figure 3.5. If such a curve was to define entanglement entropy between the two CFTs on the boundaries of an eternal black hole, this would mean that the entanglement entropy ($S_{EE}(\mathcal{A})$) would no longer be equivalent to the black hole entropy ($S_{EE}(\mathcal{B}) = S_{Wald}$), violating the expectations from section 3.3 and, e.g., [27,174]. In section 4.4 we will show that the imposition of additional causality constraints serves to distinguish physical from unphysical extremal surfaces.

4.2 New massive gravity

The first higher curvature theory that we are going to work with is *new massive gravity* (NMG) which is a toy model of gravity in $2+1$ dimensions that was proposed in [178, 179] and studied in the holographic context in [180–187]. The action is written as

$$\mathcal{S} = \frac{1}{16\pi G_N}\int d^3x\sqrt{-g}\left[\sigma R - 2\lambda m^2 + \frac{1}{m^2}\left(R_{\mu\nu}R^{\mu\nu} - \frac{3}{8}R^2\right)\right]. \tag{4.5}$$

Here the mass parameter m^2 may take any sign, λ is a cosmological constant parameter and $\sigma = \pm 1$ allows us to choose the sign of the Einstein-Hilbert term. The parameter space of this theory is quite complicated and we will now summarise the most important aspects of it following [179].

First of all, we are interested in whether the corresponding equations of motion allow for AdS solutions. This can be shown to be the case if the AdS radius L satisfies the equation

$$\frac{1}{L^2} = 2m^2\left(\sigma \pm \sqrt{1+\lambda}\right), \tag{4.6}$$

i.e. only for $\lambda \geq -1$ [179]. Unfortunately, NMG is known to be plagued by several problems that cast doubt on its validity as a *physical* theory[1]. First of all, *ghosts*, i.e. negative energy gravitons, are only absent when

$$m^2(\Lambda - 2m^2\sigma) > 0 \tag{4.7}$$

where we defined $\Lambda = -1/L^2$ [179]. As a second constraint, we have to impose the Breitenlohner-Freedman bound [179, 197]

$$-2m^2\sigma \geq \Lambda. \tag{4.8}$$

Furthermore, one can determine the central charge of the assumed CFT dual of NMG to be [179, 198]

$$c = \frac{3L}{2G_N}\left(\sigma + \frac{1}{2m^2L^2}\right), \tag{4.9}$$

which should ideally be positive. Unfortunately, (4.7) and the condition $c \geq 0$ in (4.9) are mutually exclusive. An overview over the parameter space of NMG and the different conditions discussed above is given in figure 4.2 at the end of this subsection.

[1] Nevertheless, as a model of gravity in 3 dimensions with propagating degrees of freedom this theory has received much attention, just like the (similarly problematic) *topologically massive gravity* [188, 189]. In the recent years, much effort has been invested into two theories that are hoped to be just as interesting, yet in many aspects physically better behaved. These are *zwei-dreibein gravity* [190–193] and *minimal massive gravity* [194–196]. Unfortunately, these theories are not of the form (4.3) and hence (4.4) does not apply. How to calculate entanglement entropy in these theories seems to be an open problem.

As AdS_3 is a solution to NMG for certain parameters, the same holds for the BTZ black hole [130, 131] which is constructed via global identifications of an AdS_3 background. In Schwarzschild like coordinates, the line element for the non-rotating case reads[2]

$$ds^2 = -\left(-M + \frac{r^2}{L^2}\right) dt^2 + \left(-M + \frac{r^2}{L^2}\right)^{-1} dr^2 + r^2 d\phi^2. \tag{4.10}$$

The event horizon is obviously located at $r_H = L\sqrt{M}$. The entropy of this black hole in NMG can then be shown to be [179, 198]

$$S_{BTZ} = \frac{2\pi r_H}{4G_N}\left(\sigma + \frac{1}{2m^2L^2}\right). \tag{4.11}$$

Positivity of the black hole entropy is hence tied to positivity of the central charge (4.9).

As shown in [199], in NMG the functional (4.4) takes the form

$$S_{EE} = \frac{1}{4G_N}\int d\tau \sqrt{g_{\tau\tau}}\left[\sigma + \frac{1}{m^2}\left(R_{\parallel} - \frac{1}{2}k^2 - \frac{3}{4}R\right)\right], \tag{4.12}$$

where $\sqrt{g_{\tau\tau}} = \sqrt{g_{\mu\nu}\frac{dx^\mu}{d\tau}\frac{dx^\nu}{d\tau}}$ and τ is the parameter along the curve.[3] In [1] we studied curves extremising this functional both anchored at the boundary and closed in the bulk. In this thesis, we will for simplicity only present the closed curve solutions in the following.[4] As we have seen in section 3.3, such closed extremal curves should holographically describe the entanglement between the two CFTs living on the two boundaries of an eternal black hole.

In order to find such extremal curves, we would usually have to vary the functional (4.12) in order to obtain equations of motion, just as the geodesic equations can be found by varying the length functional $\int d\tau \sqrt{g_{\tau\tau}}$. Unfortunately, the resulting equations of motion are notoriously complicated. To simplify things, on can make something like a minisuperspace ansatz, i.e. assume that the solutions will have certain symmetry properties, plug a corresponding ansatz for the curve into the functional (4.12) and obtain simplified equations of motion by varying with respect to the remaining functions respectively the remaining parameters of the ansatz. The solutions that are obtained this way can then be plugged into the full equations of motion (i.e. using a computer program like *Mathematica*) to be checked for their validity. So to be specific, we will make two assumptions about potential closed surfaces extremising (4.12) in a BTZ background (4.10). First of all, as the spacetime is static outside of the horizon, we will assume our putative extremal surfaces to be

[2] In this thesis we will restrict ourselves to the nonrotating BTZ case. Rotating BTZ black holes and Lifshitz black holes in NMG have also been briefly investigated in [1].

[3] As NMG is a theory in three bulk dimensions, the codimension two hypersurfaces that define entanglement entropy are one-dimensional curves in this case. See also the example in section 3.2.

[4] Besides [1], extremal curves anchored at the boundary have also been studied in NMG in [186, 200, 201]. In [200], special boundary conditions were proposed to restrict the holographic entangling curves. In [201], field redefinitions where used to obtain the correct physical extremal surfaces.

embedded in constant time slices, i.e. $t(\tau) = const.$ Also, we will assume these curves to be invariant under translations generated by the angular Killing vector field ∂_ϕ, hence our ansatz is $r(\tau) = const.$, $\phi(\tau) \propto \tau$.

One technical problem that we encounter immediately is that the Schwarzschild coordinates used in (4.10) are not valid on the event horizon of the black hole. This problem could easily be solved by going to the *Kruskal coordinates* for the BTZ black hole [130, 131], yet these make computations significantly more complicated. For the sake of a concise presentation, just as in [1] we will hence continue to work in Schwarzschild coordinates. All our results can be, and were, checked for correctness by calculations in Kruskal coordinates, both in the Lorentzian and Euclidean BTZ metric where applicable.

As, however, the Schwarzschild coordinates do not cover the bifurcation surface $\mathcal{B}$, defined by

$$r_{\mathcal{B}} = r_H = L\sqrt{M}, \tag{4.13}$$

we have to be careful not to overlook this curve as an extremal curve of the entropy functional (4.12). In fact, the bifurcation surface of a black hole extremises not only the area functional, but in fact any physical functional like (4.4). The reason for this lies in the symmetries of the black hole spacetime, see figure 3.4 again. We expect that if some functional is evaluated on a given surface in the black hole spacetime, then if we move this surface along the flow of the Killing vector field ∂_t, the resulting surface yields the same value when the functional is evaluated on it. But the bifurcation surface $\mathcal{B}$ is the surface on which the two Killing horizons in figure 3.4 cross and hence it is the set of fixed points under the flow of the Killing vector field. Also, the maximally extended static black hole spacetimes are time inversion symmetric as well as symmetric under exchange of the left and the right side. These symmetries of a conformal diagram as figure 3.4 imply that the bifurcation surface $\mathcal{B}$ will always be a local saddle point to any functional of the form (4.4) on a static black hole background. This means that, if no other closed solutions do exist, the entanglement between the two CFTs on the two boundaries of the eternal black hole will always be given by the black hole entropy (4.11), as the functional (4.4) by definition reduces to Wald's result (4.2) on a bifurcation surface. This would be the physically expected result.

The problem that we will be concerned with in this chapter, and that was studied in [1], is that generically functionals of the form (4.4) *do* allow for additional closed extremal curves in black hole backgrounds. The first example that we encounter is NMG, where upon inserting our symmetric ansatz for a potential closed surface the functional (4.12) takes the form

$$S \propto \sigma r + \frac{M}{2m^2 r} \tag{4.14}$$

for a closed curve of radius r. This means that apart from the bifurcation surface (4.13),

we find a closed curve extremising (4.12) at radius

$$r = \sqrt{\frac{M}{2\sigma m^2}}. \tag{4.15}$$

Comparing this to the event horizon located at $r = r_H$ (4.13), we see that this additional extremal surface will be outside of (or exactly on) the event horizon for $\sigma m^2 L^2 \leq \frac{1}{2}$, which is precisely the Breitenlohner-Freedman bound (4.8). For $\sigma m^2 L^2 < 0$, this solution is ill defined and no additional extremal surfaces exist.[5] Due to the symmetry generated by the timelike Killing vector field ∂_t (see figure 3.4), these additional curves do not appear as solitary codimension two surfaces, but they foliate codimension one hypersurfaces invariant under flows of ∂_t. Depending on $\sigma m^2 L^2$, we hence find one of the four possible configurations shown in figure 4.1. In figure 4.2 we compare these different possible configurations with the restrictions imposed on NMG by the Breitenlohner-Freedman bound (4.8), the condition of unitarity ($c \geq 0$) and the absence of ghosts (4.7). As already said earlier, the latter two conditions are mutually exclusive, but it is interesting to point out that none of the possible pathologies of NMG seems to be in a one to one correspondence with the appearance of additional extremal surfaces.

Of course, according to the RT and HRT prescriptions, we would be required to take that extremal curve to define the entanglement entropy between the two CFTs on the two boundaries that yields the lowest value for the entanglement entropy. By definition, the entropy functional (4.12) evaluated on the bifurcation surface $\mathcal{B}$ will yield the Wald entropy (4.11). In contrast, the additional surface (4.15) yields an entropy

$$S_a = \frac{2\pi\sigma}{4G_N}\sqrt{\frac{2M}{\sigma m^2}}. \tag{4.16}$$

In the parameter regime where (4.15) is a real solution, we then find $|S_{BTZ}| \geq |S_a|$ with equality for $\sigma m^2 L^2 = 1/2$, where the additional extremal surfaces are slices of the event horizon. This is depicted as case c) in figures 4.1 and 4.2.

For positive black hole entropy S_{BTZ} (equivalent to positive central charge (4.9)), the RT and HRT like prescriptions for higher curvature theories discussed at the beginning of this chapter would then suggest that the entanglement entropy between the two CFTs on the two boundaries is in fact not given by the black hole entropy S_{BTZ}, but by the entropy S_a associated with the additional extremal closed curve. On physical grounds, this would be a very counterintuitive result, as it would mean that the black hole entropy (calculated on the bifurcation surface via Wald's formula (4.2)) would no longer be the entanglement entropy between the two CFTs. In fact, we will see in section 4.4 that the additional extremal surfaces found in this section have to be discarded for reasons of causality. Yet before studying these causality conditions, we will leave the topic of NMG and study another higher curvature theory instead, namely the well known Gauss-Bonnet gravity. This is

[5] Remember that we formally allow m^2 to have any sign, but L^2 is positive.

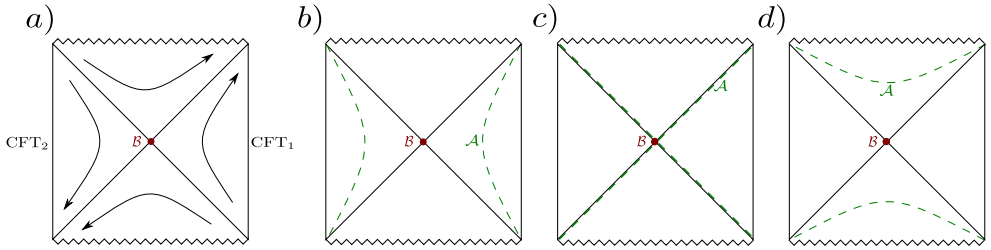

Figure 4.1: Four possible configurations of additional extremal surfaces (4.15), depending on the value of $\sigma m^2 L^2$. The bifurcation surface $\mathcal{B}$ is always an extremal curve of the entropy functional. *a*): $\sigma m^2 L^2 < 0$, no additional closed extremal curves exist in the BTZ geometry. The flow of the Killing vector field ∂_t is sketched by arrows. *b*): $0 \leq \sigma m^2 L^2 < \frac{1}{2}$, and the additional curves lie outside the event horizon. They are spacelike slices of a timelike hypersurface invariant under flows of ∂_t. *c*): $\sigma m^2 L^2 = \frac{1}{2}$, the additional surfaces are slices of the event horizon. *d*): $\sigma m^2 L^2 > \frac{1}{2}$, the additional extremal surfaces are inside of the event horizon. The figure is presented as in [1].

worthwhile as, as stated above and shown in figure 4.2, NMG is plagued by numerous pathologies. We will show that Gauss-Bonnet gravity, although being much better behaved as a physical theory than NMG, will also give rise to additional extremal closed surfaces that pose a problem for the calculation of entanglement entropy. We hence expect that problems of this kind for prescriptions for the calculation of entanglement entropy based on functionals like (4.4) may to a certain extend be generic to higher curvature theories.

4.3 Gauss-Bonnet gravity

Gauss-Bonnet gravity is a special case of *Lovelock gravity* [202] (see also [203]) and its action in five dimensions can be written as [177]

$$\mathcal{S} = \frac{1}{16\pi G_N} \int d^5x \sqrt{-g} \left[R + \frac{12}{L^2} + \lambda \frac{L^2}{2} \left(R_{\mu\nu\alpha\beta} R^{\mu\nu\alpha\beta} - 4 R_{\mu\nu} R^{\mu\nu} + R^2 \right) \right]. \tag{4.17}$$

This corresponds to the special choice of the parameters a, b, c in (4.3) such that the action and the corresponding equations of motion contain higher curvature terms, but can be written without higher derivatives of the metric [202, 203]. This means that the equations of motion for the metric are still second order, in contrast to NMG for example. Gauss-Bonnet and Lovelock theories of gravity are hence frequently studied models of higher curvature gravity in higher dimensions[6] both in general gravitational physics [202, 203] and AdS/CFT research [176, 177, 204, 205]. Just as it was the case for NMG, the parameter space for Gauss-Bonnet theory (4.17) has been studied in much detail in the literature. To

[6] In four or less bulk dimensions, the *Gauss-Bonnet* term $R_{\mu\nu\alpha\beta} R^{\mu\nu\alpha\beta} - 4 R_{\mu\nu} R^{\mu\nu} + R^2$ would be a topological invariant.

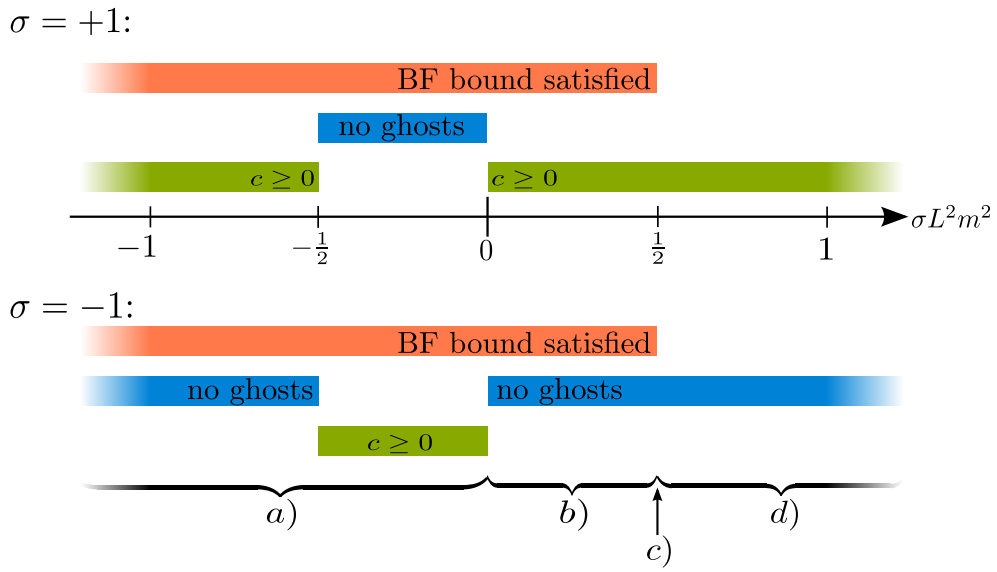

Figure 4.2: An overview over the parameter-space of NMG, where $\sigma L^2 m^2$ and $\sigma = \pm 1$ are used as variables. The conditions of absence of ghosts (equation (4.7)) and positivity of the central charge (equation (4.9)) are mutually exclusive. It is also shown for which parameters the Breitenlohner-Freedman bound (4.8) is satisfied. The brackets indicate which of the four cases shown in figure 4.1 appear for which parameter range. The figure is presented as in [1].

summarise these results, the presumed boundary theory for Gauss-Bonnet holography is causal for the parameter range [206–209][7]

$$-\frac{7}{36} \leq \lambda \leq \frac{9}{100}. \tag{4.18}$$

As shown in [211], this parameter choice will also guarantee the positivity of holographic relative entropy. It is also possible to choose an AdS vacuum such that the conjectured dual CFT is unitary [204, 205] and the bulk theory is free of ghosts [212].

Gauss-Bonnet theories (4.17) were the first higher curvature models for which holographic entanglement entropy was studied [60, 163, 176, 177] using the *Jacobson-Myers entropy functional* [213]

$$S_{EE} = \frac{1}{4G_N} \int_\Sigma d^3y \sqrt{\gamma} \left(1 + \lambda L^2 \mathcal{R}\right). \tag{4.19}$$

This is indeed the form that the functional (4.4) takes for the theory (4.17) if the extrinsic curvature quantities defined in appendix A.1 are re-expressed in terms of the intrinsic curvature scalar $\mathcal{R}$ of the hypersurface Σ using the *Gauss-Codazzi equations* (see e.g. chapter

[7] After the publication of [1], on which this chapter is based, it was shown in [210] that certain causality problems can arise in Gauss-Bonnet gravity for any non-perturbative value of λ. We will very briefly comment on this in section 4.4.

10.2 of [105]). The fact that the entropy functional (4.4) can be expressed completely in terms of intrinsic curvature quantities as in (4.19) is one of the many special properties of Gauss-Bonnet gravity.

Just as earlier for NMG, we will now try to find out whether Gauss-Bonnet gravity also allows for the existence of closed hypersurfaces (other than bifurcation surfaces) extremising the entropy functional (4.19). To begin this investigation, we will consider the background spacetime $g_{\mu\nu}$ to be a spherically symmetric static black hole solution of Gauss-Bonnet gravity [214–217]. As the functional (4.19) is only dependent on intrinsic curvature quantities, we see that the specific form of the background metric is not important at all. Suppose that the spherically symmetric background metric is given in terms of a time coordinate t, a radial coordinate r, and the angular coordinates θ, ϕ, ψ. Similar to the symmetric ansatz that we made in the NMG case, we can again assume that our putative extremal surface Σ is extended in the angular directions and defined by a choice of r and $t = const.$[8] The induced metric of Σ will hence be the one of a 3-sphere, with $\mathcal{R} = 6/r^2$. Consequently, (4.19) simplifies to

$$S_{EE} = \frac{\pi^2}{2G_N}\left(r^3 + 6\lambda L^2 r\right). \tag{4.20}$$

Again, just as discussed for the NMG case in section 4.2, we should not forget that by symmetry the bifurcation surface $\mathcal{B}$ will always be a saddle point of the entropy functional (4.19), even if the formula (4.20) does not make this manifest due to the shortcomings of Schwarzschild coordinates.

We easily see that the functional (4.20) indeed allows for additional extremal surfaces if the parameter λ is negative. These additional extremal surfaces will then be defined by

$$r = r_a = \sqrt{-2\lambda}L, \tag{4.21}$$

and the entropy functional evaluated on this surface will take the value

$$S_a = \frac{2\pi^2 L^3}{G_N}\sqrt{-2\lambda}\lambda < 0 \tag{4.22}$$

as $\lambda < 0$. This would be problematic, not only because the existence of additional closed extremal surfaces collides with the holographic interpretation of black hole entropy as entanglement entropy between two CFTs (as we discussed already for NMG), but also because clearly no entropy should be negative. These additional extremal surfaces that arise in RT or HRT like prescriptions (i.e. based on extremising an entropy functional) to calculate entanglement entropy in Gauss-Bonnet gravity are hence clearly unphysical, and it is desirable to have a tool that allows to identify such unphysical solutions and discard

[8] Due to ∂_t being a Killing vector, we expect that the value of the constant will not be important, and that this value can indeed be shifted at will. The extremal codimension two surfaces found this way will then define a foliation of a codimension one hypersurface invariant under the flow of the Killing vector field, just as it was the case for NMG. See again figure 4.1.

them. In the discussion of the above result (4.22) we could easily invoke the argument that this result (and the corresponding extremal surface) are unphysical in the context of calculating holographic entanglement entropy as the result is negative, but the reader should be reminded that this argument would not work in the NMG case studied earlier. Likewise, the problems encountered in the study of NMG (unitarity, ghosts) are absent in Gauss-Bonnet gravity. In section 4.4 we will hence investigate causality arguments that serve as a tool to rule out such unphysical extremal surfaces both in NMG and Gauss-Bonnet gravity alike, and that can easily be applied to any other higher curvature theory in which entanglement entropy is to be studied.[9]

But before we do so, a few comments are in order. First of all, we should check whether the solution (4.21) derived via the symmetric ansatz actually satisfies the full equations of motion for the extremal surface that can be derived from the functional (4.19) without any prior symmetry assumptions. Luckily, these equations of motion were explicitly worked out in [199, 218–220] and take the form

$$X^{ij}k^{(\alpha)}_{ij} \equiv \left(\frac{1}{2}\gamma^{ij} + \lambda L^2\left(\frac{1}{2}\gamma^{ij}\mathcal{R} - \mathcal{R}^{ij}\right)\right)k^{(\alpha)}_{ij} = 0, \tag{4.23}$$

which is the Gauss-Bonnet generalisation of (3.33). The spherical hypersurface Σ with radius (4.21) then indeed solves this equation with $X^{ij} = 0$. This is an interesting contrast to the black hole bifurcation surface, which solves this equation due to $k^{(\alpha)}_{ij} = 0$.

As a second comment, we should point out that while the case $\lambda < 0$ is not unphysical according to (4.18), it is a case that is studied much less commonly than $\lambda > 0$. This is because one motivation to study Gauss-Bonnet gravity models is that such higher curvature terms appear as corrections in string theory [206,212,221]. In such a context, the parameter λ in (4.17) should then be positive and perturbatively small. Interestingly, if we had studied background spacetimes with hyperbolic symmetries instead of spherical symmetries above, then we would have found $\mathcal{R} = -6/r$ for a symmetric ansatz and additional surfaces with radial coordinate $r_a = \sqrt{2\lambda}L$ would have appeared for positive λ.

The third and most important remark that we have to make at the end of this section concerns the existence of black holes that are sufficiently small to allow for the additional solutions described by (4.21) to exist in the spacetime at all. In Einstein-Hilbert gravity, the singularity of the (AdS) Reissner-Nordström black holes is located at $r = 0$, and hence a spherical surface of fixed positive radius could always exist in the spacetime. Even more, by tuning the mass and charge, we could always find a black hole for which the event horizon would lie below any spherical surface of fixed radius. Unfortunately, this is not so easy in Gauss-Bonnet gravity: There can be shown [216, 217, 222] to be a lower bound on the event horizon radius for Gauss-Bonnet vacuum spherical and charged hyperbolic black holes that coincides exactly with our result for the radius of the additional extremal surface.

[9] In [1] we also investigated an approach of constraining additional extremal surfaces by deriving constraints from a conical boundary conditions method. Unfortunately, there are examples where these additional constraints are *too* restrictive, hence we will not discuss this ansatz in this thesis.

Hence these additional surfaces could never exist outside of the black hole event horizon, ruling out situations of the type *b*) depicted in figure 4.1. Furthermore, there may even be a lower bound on the radial coordinate of the singularity, and in the vacuum case [216,217] this completely rules out our additional extremal surfaces: Not only would they have to appear below the event horizon, but also below the singularity, i.e. they are not part of the physical spacetime. For the charged case [222] the lower bound on the singularity is reduced sufficiently to allow the extremal surfaces derived above to appear in the spacetime region between singularity and outer event horizon, similar to the case *d*) depicted in figure 4.1. Anyhow, our computations above were based only on the intrinsic curvature of the putative extremal surfaces, and hence not sensitive to the presence of a wormhole throat (as in figure 3.5) at all. Consequently, the additional extremal surfaces derived above would also be problematic in global AdS space or boson star spacetimes [223, 224][10], where due to the absence of a bifurcation surface we would expect the functional prescriptions for calculating entanglement entropy for the boundary CFT to yield zero, corresponding to a pure boundary state.

To close this section, it is interesting to note that after the publication of [1], there where also other papers that found unexpected phenomena in Gauss-Bonnet gravity for $\lambda < 0$ [225, 226]. See also [227] for an earlier study.

4.4 The causal influence argument

In this section, we will present a simple physical argument that can be applied to NMG, Gauss-Bonnet gravity and any other gravitational theory to determine certain putative bulk entangling surfaces to be unphysical. This is what we will refer to as the *causal influence argument*, presented in [64].

The gist of the causal influence argument is to avoid causal paradoxes. After all, we demand a certain quantity in the bulk (an entropy functional evaluated on a given spacelike extremal surface) to be equal to a corresponding quantity on the boundary (entanglement entropy of a certain subsystem on the boundary). If it was possible to influence (and hence change) the bulk quantity at a time where the boundary quantity is already fixed, this would lead to a causal paradox.

Let us be more specific. Assume we are trying to calculate the entanglement entropy of a CFT subregion A using the bulk entangling curve $\mathcal{E}(A)$. As usual in the RT prescription, we assume that there is a well-defined notion of equal time slices, and that A is a subregion of such an equal time slice on the boundary. Without loss of generality, we assume that A lies on the $t = 0$ slice. If we know the CFT state at $t = 0$, we can calculate the value of the entanglement entropy $S(A)$ by field theory techniques, i.e. the value is fixed at $t = 0$ as

[10]These papers only study boson stars for $\lambda > 0$, yet the authors of those papers confirmed in private correspondence that similar solutions can be found for $\lambda < 0$.

we said above. If it was possible for an observer at or arbitrarily close to the boundary to send a signal into the bulk at a time $t = \delta > 0$ such that this signal still reaches the curve $\mathcal{E}(A)$ in the bulk, this signal could, due to its backreaction on the geometry, change $\mathcal{E}(A)$ and hence the holographically calculated value of $S(A)$. This would lead to the paradox described above. A first putative version of the causal influence argument could hence be formulated to demand that there should be no causal curve from the boundary region A to the bulk entangling curve $\mathcal{E}(A)$. Likewise, by time reflection symmetry there should be no causal curve going from $\mathcal{E}(A)$ to A, and as for a pure total state $S(A) = S(\bar{A})$ (section 3.1), there should be no causal curves connecting $\mathcal{E}(A)$ and the complement $\bar{A}$. In a choice of nomenclature differing from [64], we will refer to the set of points in the bulk spacetime that are not in causal contact with a boundary region A to be the *causal shadow of* A. See the left of figure 4.3 for an illustration. As the extremal surfaces used in the RT prescription are calculated on the equal time slice we see that the RT prescription satisfies this causality constraint by definition.

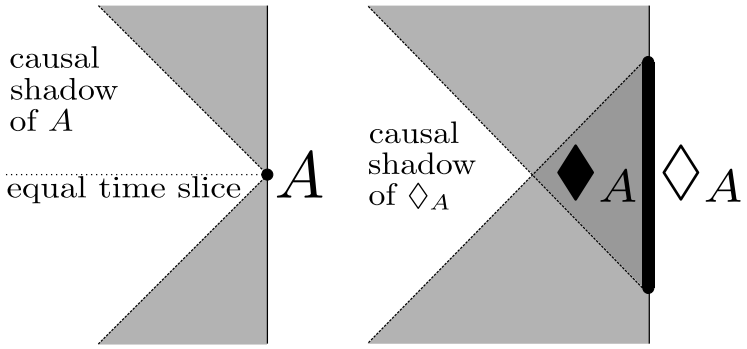

Figure 4.3: Left: The causal shadow of a (spacelike codimension one) boundary region A defined on an equal time slice is the set of all bulk points that are not in causal contact with this region. The time increases upwards in this figure. Right: In general, it is not possible to uniquely define equal time slices. Hence, the entanglement entropy of a boundary region A should be assigned to its entire domain of dependence $\Diamond_A$, see also figure 4.4. Demanding the bulk entangling curve $\mathcal{E}(A)$ to lie in the causal shadow of $\Diamond_A$ instead of A is then a much severer restriction. This is the causal influence argument. The region $\blacklozenge_A$ is called the *causal wedge* of A, see [228, 229]. The figure is presented as in [1].

Let us now extend this causality requirement to the case where the bulk spacetime is not static, and equal time slices cannot be defined. This is when the HRT prescription or its generalisations to higher curvature theories are assumed to be applicable. From (3.12), we remember that the important thing about the boundary region A that enters the calculation of the holographic entangling surface $\mathcal{E}(A)$ is the boundary ∂A. Apart from that, as we cannot assume unique spacelike slices to be well-defined, we could imagine to deform A into different spacelike surfaces A' with the same boundary $\partial A = \partial A'$ as shown in figure 4.4. This would not influence the calculation of entanglement entropy according to the HRT prescription. We hence see that instead of assigning entanglement entropy to

be a property of the arbitrarily defined spacelike slice A, we should better consider it to be a property of the *domain of dependence of* A, signified as $\Diamond_A$ [228]. All the possible spacelike slices A, A', A'' of $\Diamond_A$ with the same boundary ∂A act as Cauchy surfaces of $\Diamond_A$, explaining why they should all be assigned the same entanglement entropy. With this definition at hand, we then formulate the causal influence argument of [64] as we did in [1]:

> $\mathcal{E}(A)$ should be required to lie in the causal shadows of any possible spacelike deformations $(A', \bar{A}', A'', \bar{A}''...)$ of both A and $\bar{A}$ which leave the boundaries ∂A and $\partial \bar{A}$ invariant,

or equivalently,

> $\mathcal{E}(A)$ should be required to lie in the causal shadows of the interiors of both $\Diamond_A$ and $\Diamond_{\bar{A}}$.

This is illustrated on the right hand side of figure 4.3. In [64], it was proven that this condition is always satisfied by the HRT prescription in Einstein-Hilbert gravity, assuming the null energy condition and other technical details.

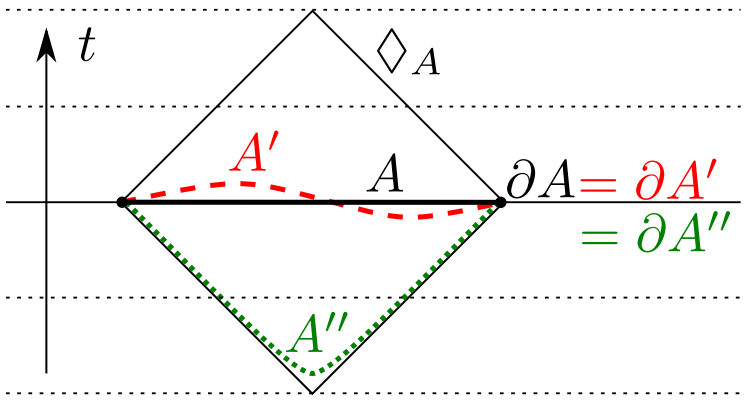

Figure 4.4: In general cases, it may not be possible to uniquely define an equal time slice, and via the HRT prescription it should be possible to calculate the entanglement entropy for any spacelike codimension one boundary region. The regions A, A' and A'' in the above figure will have the same entanglement entropy as in the HRT prescription only the boundary ∂A is important for determining the bulk entangling surface $\mathcal{E}(A)$. This makes sense, as the surfaces A, A' and A'' in the above image are all Cauchy surfaces for the same domain of dependence $\Diamond_A$. The entanglement entropy $S(A)$ should then be interpreted as a property of the physically well-defined object $\Diamond_A$, and not only of the arbitrarily chosen slice A. The figure is presented as in [1].

For higher curvature theories in contrast, our work of the last sections has shown that this causality condition is not automatically satisfied in physical background spacetimes. In fact, we will turn the argument of [64] around in this section: Instead of attempting to *derive* the causal influence argument (as done in 4.3 for the Einstein-Hilbert case), we *impose* it to distinguish physical from unphysical extremal surfaces.

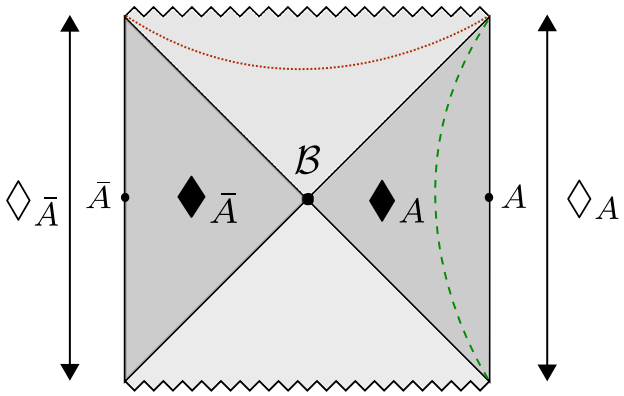

Figure 4.5: Application of the causal influence argument to a black hole spacetime. For a spacelike slice A that is an entire equal time slice of the right boundary, only the bifurcation surface $\mathcal{B}$ satisfies the causal influence argument. The green dashed and red dotted lines show possible configurations of additional extremal surfaces as the cases b) and d) in figure 4.1. The figure is presented as in [1].

In the case of a static black hole spacetime, such as the BTZ black hole studied in section 4.2, this argument is sketched in figure 4.5. The region A is assumed to be an entire spacelike slice of the right boundary, consequently the complement $\bar{A}$ is a slice of the left boundary. The domains of dependence $\Diamond_A$ and $\Diamond_{\bar{A}}$ are then the entireties of the right and the left boundaries, respectively. The sets of points that can both receive signals from and send signals to the interiors of $\Diamond_A$ or $\Diamond_{\bar{A}}$ are called the *causal wedges* $\blacklozenge_A$ and $\blacklozenge_{\bar{A}}$, respectively [228, 229]. See also figure 4.3. By definition, these causal wedges $\blacklozenge_A$ and $\blacklozenge_{\bar{A}}$ reach all the way from the boundary to the event horizon of the black hole. Additionally, all the points inside of the black hole event horizon are in one way causal contact with both $\Diamond_A$ and $\Diamond_{\bar{A}}$, and are hence also excluded by the causal influence argument. This argument hence rules out any possible closed extremal surface of the types $b), c)$ and $d)$ in figure 4.1. Only the bifurcation surface $\mathcal{B}$ is left over as a surface determining the physically correct entanglement between the two boundary CFTs. We hence recover the notion, explained in section 3.3, that the black hole entropy, calculated from the geometry of the bifurcation surface $\mathcal{B}$ according to Wald's formula (4.2), should have the holographic interpretation of being the entanglement entropy between the two CFTs living on the two conformal boundaries of the eternal black hole spacetime.

In section 4.3, we also mentioned that technically closed extremal surfaces may also appear in spacetimes with only one asymptotic boundary, such as global AdS or boson star spacetimes. These surfaces satisfy the homology condition, and when attempting to determine the entropy of the entire boundary CFT state via holographically calculating entanglement entropy, the only other option would be the *empty surface*, i.e. no surface at all. As these spacetimes do not have event horizons, every point in the bulk is in causal contact with the boundary, and consequently any possible closed extremal curve in the bulk would be ruled out due to the causal influence argument. Consequently, the entanglement entropy is

trivially defined by the empty surface to be zero, which is the result physically demanded for a pure state (see section 3.1).

We hence obtain the desired result, namely that the causal influence argument introduced above is a reliable tool to, at least in the concrete examples studied in sections 4.2 and 4.3, distinguish the physical surfaces extremising the entropy functional (4.4) from the unphysical additional extremal surfaces that we have found to occur. However, after the publication of [1], doubt on the physical validity of Gauss-Bonnet gravity for any non-perturbative λ has been cast by [210]. Consequently, it may be necessary to turn the logic of the above chapter around: Instead of using the causal influence argument to distinguish between physical and unphysical curves, one might hold the viewpoint that the existence of entangling curves violating the causal influence argument is a general sign of an unphysical bulk theory. This viewpoint was indeed advocated for in [64], but investigations into this topic are still ongoing [201, 225, 226]. This closes our investigation of holographic entanglement entropy in bulk theories with higher curvature terms. In the remaining chapters 5 and 6 we will investigate the geometry and entanglement entropy of toy models of holographic duals of boundary CFTs.

Chapter 5

Backreaction in holographic models of boundary CFTs

5.1 Holographic models of boundary CFTs

In the past sections we have studied models, both top-down and bottom-up, of dualities between gravitational theories on asymptotically AdS spacetimes and conformal field theories (CFTs) on the conformal boundary of these spacetimes, i.e. either on flat Minkowski space or the (spacially compact) Einstein static universe. It is, however, also possible to define CFTs on manifolds that have themselves a boundary, and these are called *boundary CFTs* or in short *BCFTs* [230,231]. The study of BCFTs with codimension one boundaries is related to the study of CFTs with *defects* and *interfaces* as often such CFTs can be formulated as a BCFT [232]. By now, it should not come as a surprise to the reader that there is a large variety of holographic models of such BCFTs or defect CFTs (see [233–236] for a partial list of references), and in the following we will especially focus on the bottom-up approach introduced by Takayanagi et al. in [92–94].

The idea behind this type of model is sketched in figure 5.1. Here, N is an asymptotically AdS spacetime which, as before, we will call the bulk spacetime. The asymptotic conformal boundary of N is called M in figure 5.1, and this is where holographically the CFT is understood to live. So far, this is an ansatz just as in the regular AdS/CFT correspondence. Now, for a BCFT the manifold M on which this theory lives has to have a boundary for itself, namely $P = \partial M$. According to the bottom-up models of [92–94], this boundary extends from M into the bulk spacetime N as a hypersurface Q, at which the spacetime N abruptly ends. For reasons that will become fully clear in section 6, we refer to this hypersurface as the *brane*, but the reader should be aware that it is not any of the string theoretic branes used in 2.3 for example. Also, there is often confusion about the meaning of the words "boundary" and "bulk" in the context of BCFT. Pure field theory papers often use "boundary" for P and "bulk" for M in figure 5.1, but in holography this nomenclature

is usually avoided because it would conflict with the standard AdS/CFT convention to call M the boundary and N the bulk. We will hence refer to P as the *defect*. When discussing the embedding of Q into N, will also refer to the latter as the *ambient spacetime*.

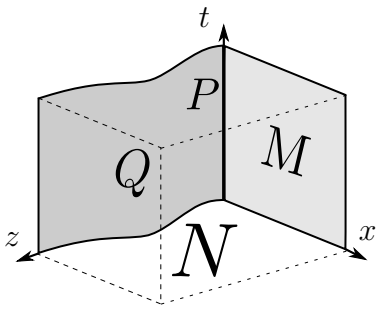

Figure 5.1: Geometric setup for a bottom-up AdS/BCFT model according to [92–94]. The (asymptotically) AdS bulk spacetime N has the usual conformal boundary M as well as the timelike hypersurface Q on which the spacetime ends. The intersection of Q and M is referred to as P. The coordinates t, x, z follow the usual conventions for the Poincaré patch (2.11). The figure is presented as in [2].

The proposal of [92–94] suggests that the action for the bulk metric $g_{\mu\nu}$ should be amended with the usual Gibbons-Hawking boundary term [237] and counter term $\Sigma^{(h)}$ [126, 146] on M (where h is the induced metric on M), but also with boundary terms on Q (induced metric γ) and P:

$$\begin{aligned}\mathcal{S} = &\frac{1}{2\kappa_N^2}\int_N d^{d+1}x\,\sqrt{-g}\,(R-2\Lambda) + \frac{1}{\kappa_N^2}\int_M d^dx\,\sqrt{-h}\left(K^{(h)}-\Sigma^{(h)}\right) \\ &- \frac{1}{\kappa_N^2}\int_Q d^dx\,\sqrt{-\gamma}K^{(\gamma)} + \int_Q d^dx\,\sqrt{-\gamma}\,\mathcal{L}_Q + S_P.\end{aligned} \tag{5.1}$$

In this formula, the quantities $K^{(h)}$ and $K^{(\gamma)}$ are the traces (with respect to the induced metrics h_{ij} and γ_{ij}) of the extrinsic curvature tensors of M and Q, respectively. The sign of K has to be fixed by a convention on where the normal vector to the surface in question points, for M we conventionally assume that the normal vector is oriented to the *outside* of the spacetime, while on the brane Q we choose the normal vector to be pointing *into* the bulk. This will be the more convenient convention later is chapter 6. See appendix A.2 for definitions and further explanations. In (5.1), we have omitted terms for possible matter fields living in N.

The model (5.1) explicitly includes the term $\sim \mathcal{L}_Q$ which describes matter fields living on the worldvolume of the brane Q. These matter fields together with the embedding of the brane Q into the ambient spacetime N will in these models (5.1) then constitute the holographic description of the defect P and the BCFT degrees of freedom potentially

restricted to it. Imposing *Neumann boundary conditions* on the bulk metric $g_{\mu\nu}$ at Q, we obtain the equations of motion [92–94]

$$K_{ij} - \gamma_{ij} K = -\kappa_N^2 \, S_{ij}, \tag{5.2}$$

where γ_{ij} is the induced metric on Q and S_{ij} is the energy-momentum tensor derived from the matter Lagrangian $\mathcal{L}_Q$. The letter S was chosen to mean "surface" or "shell". This way, we also distinguish the energy-momentum tensor on Q, S_{ij}, from the bulk energy-momentum tensor, conventionally denoted $T_{\mu\nu}$. Equation (5.2), together with the equations of motion for the matter fields described by $\mathcal{L}_Q$, has to be combined with the equations of motion of bulk fields, such as for example the bulk metric $g_{\mu\nu}$, for a full description of the classical bulk theory that is holographically dual to the BCFT defined on M and P. For the moment this prescription may seem rather abstract, but we will see a concrete and well motivated realisation of this setup in chapter 6, other work on setups of the type (5.1) was presented in [238–245]. In the remainder of this chapter, we will collect a number of results on general setups of this type that were discussed in [2].

5.2 Energy conditions and their impact on the bulk geometry

5.2.1 Decomposition of the energy-momentum tensor

In this section, we will in detail study the equations of motion (5.2). Specifically, we will consider the case of a $2+1$-dimensional bulk spacetime, such that both the AdS boundary and the brane Q are $1+1$ dimensional, as this is the relevant case for the holographic Kondo model to be discussed in section 6.2.

As we will see now, in this case the equations (5.2) can be considerably simplified and made tractable. The reason for this is that when Q is a $1+1$-dimensional timelike brane, its worldsheet *lightcone* degenerates into two distinct null directions. We make use of this by defining the worldvolume null vectors

$$l_i l^i = 0 = r_i r^i, \quad l_i r^i = -1, \tag{5.3}$$

where l stands for left pointing and r stands for right pointing. Note that this definition does not completely fix the two vectors l^i, r^i for a given induced metric γ_{ij}, as there is still a residual boost symmetry: $l^i \to a l^i$, $r^i \to \frac{1}{a} r^i$. Many of the expressions that we derive in the following will be invariant under such boosts, but later we will restrict our interest to static cases, where both the ambient spacetime N and the brane Q have a timelike Killing vector field ∂_t. One can then fix the boost symmetry by demanding $l^i + r^i \sim \delta^i_t$.

The use of defining this null vector basis is that we can now decompose the energy-

momentum tensor into scalar quantities by writing

$$S_{ij} = \frac{S}{2}\gamma_{ij} + S_L l_i l_j + S_R r_i r_j \text{ with} \tag{5.4}$$

$$S = \gamma^{ij} S_{ij}, \quad S_L = r^i r^j S_{ij}, \quad S_R = l^i l^j S_{ij}. \tag{5.5}$$

Obviously, S is the trace of S_{ij} while S_L and S_R parametrise the non-trace part of the energy-momentum tensor. These three scalars then define the symmetric $(0,2)$ tensor S_{ij}.

5.2.2 Energy conditions

In a next step we can now formulate energy conditions for S_{ij} using the decomposition (5.4)[1]. Often in general relativity, it is of interest to derive certain results concerning solutions of Einstein's equations even when the specific form of the energy-momentum tensor is not known. In these cases, one usually uses *energy conditions*, i.e. conditions imposed on the energy-momentum tensor that seem physically reasonable, for example the condition that no observer should ever measure a negative energy density. It should be pointed out that there are many different energy conditions, some stricter than others, and not all of them are satisfied even by physical matter models as we will see. For a review on this fascinating topic, see [246, 247]. We will use:

- The *null energy condition (NEC)*: For every null vector m^i in the worldvolume of the brane we have

  $$S_{ij} m^i m^j \geq 0 \ \ \forall\ m^i m_i = 0. \tag{5.6}$$

  The interpretation of the NEC is that a hypothetical null-observer will never measure a negative local energy density [247]. Using (5.4) it is easy to show that this implies

  $$S_{ij} l^i l^j \geq 0 \text{ and } S_{ij} r^i r^j \geq 0 \quad \Rightarrow \quad S_L \geq 0 \text{ and } S_R \geq 0. \tag{5.7}$$

- The *weak energy condition (WEC)* generalises the NEC to timelike vectors:

  $$S_{ij} m^i m^j \geq 0 \ \ \forall\ m^i m_i < 0. \tag{5.8}$$

  The interpretation of the WEC is that no physical observer will ever measure a negative local energy density [247]. By continuity, the WEC implies the NEC. Parameterising $m^i = \alpha l^i + \beta r^i$ with $\alpha \cdot \beta > 0$ (this ensures that m^i is timelike by (5.3)) we then find

  $$S_L \geq 0, \quad S_R \geq 0, \quad S\alpha\beta \leq S_L \alpha^2 + S_R \beta^2 \ \ \forall \alpha \cdot \beta > 0. \tag{5.9}$$

[1] Note that we will only formulate conditions on S_{ij} in terms of the intrinsic geometry, i.e. the induced metric γ_{ij} and vector fields living in the worldvolume of Q.

Optimising the choice of α, β yields

$$S_L \geq 0, \quad S_R \geq 0, \quad S \leq 2\sqrt{S_L S_R}. \tag{5.10}$$

Note that these expressions are all invariant under the boosts of the null vectors mentioned above.

- The *strong energy condition (SEC)* is well known in the literature of 3+1-dimensional general relativity, but the generalisation to arbitrary dimensions is not straightforward. In our context, we will hence refer to the inequality

$$(S_{ij} - S\gamma_{ij})m^i m^j \geq 0 \ \ \forall\ m^i m_i < 0. \tag{5.11}$$

as the SEC. This will prove to be very useful as the expression on the left hand side appears when solving (5.2) for the extrinsic curvature:

$$K_{ij} = -\kappa_N^2 (S_{ij} - S\gamma_{ij}) \tag{5.12}$$

We have however no reason to believe that a physical matter field has to satisfy this energy condition, and in fact we will see later that in the holographic Kondo model of section 6.2 it is indeed important that the matter fields *violate* this condition. In terms of scalar quantities, (optimising again the choice of α and β in $m^i = \alpha l^i + \beta r^i$) this yields

$$S_L \geq 0, \quad S_R \geq 0, \ \ S \geq -2\sqrt{S_L S_R}. \tag{5.13}$$

We see that the SEC, just as the WEC, implies the NEC. On the other hand, WEC and SEC are unrelated. Not very surprisingly, the NEC is considered the most important and reliable energy condition. Indeed, in this thesis we have already encountered some geometric results that were proved using the NEC as a technical assumption in sections 3 and 4. Although there are classical matter models that do even violate the NEC [246,247], it can be proven to be satisfied in string theory [248].

5.2.3 A corollary to the barrier theorem

The ultimate reason why we are interested in understanding the geometrical properties of AdS/BCFT models is that eventually we would like to compute entanglement entropy in the holographic Kondo model, as we will do in chapter 6. As we have seen in chapter 3, entanglement entropy of the boundary CFT is holographically encoded in the geometry of extremal (codimension 2) surfaces in the bulk spacetime. In a $2+1$ dimensional bulk, entanglement entropy is hence defined by spacelike geodesics as we have already seen in section 3.2. In a setup such as the one shown in figure 5.1, it is obviously of interest whether spacelike geodesics anchored at the boundary will, when they go deeper into the bulk, encounter the brane Q or whether they will stay in the interior of N. An intersection

between the geodesics and the brane would potentially lead to a strong signature in the pattern of entanglement entropy measured at the boundary, explicit examples of this were discussed in [2].

In order to investigate this issue in more detail, we can make use of the work of Engelhardt and Wall [249]. In this paper, the authors define the term *extremal surface barrier* to be a codimension one hypersurface that is embedded in an asymptotically AdS bulk spacetime in such a way that extremal spacelike surfaces that are anchored on the AdS boundary to one side of the extremal surface barrier cannot cross it. In the course of this thesis we will see several explicit examples of surfaces that are extremal surface barriers, but in this section we will be interested in the general statement of the theorem, and the implications that it has on our models defined by (5.2). We state the result of [249] in our own nomenclature as introduced in figure 5.1, section 5.1 and appendix A.2. There are some subtleties related to whether an extremal surface may touch the extremal surface barrier or not, which will not concern us very much in the following. The theorem presented here as in [2] is a combined result of theorems 2.1, 2.2 and corollary 2.4 in [249].

Barrier Theorem (Engelhardt, Wall [249])
Let Q be a codimension one hypersurface embedded in the spacetime N, which is assumed to end on Q and the AdS boundary M. If

$$K_{ij}v^iv^j \leq 0 \quad \text{for any vector field } v^i \text{ on } Q, \tag{5.14}$$

then any Q-deformable spacelike extremal surface Υ which is anchored on the AdS boundary M remains in N, i.e. does not cross Q. By *Q-deformable* we mean that there is a family $\{\Upsilon_a\}$ of extremal spacelike surfaces such that all of those are anchored on M, and can be continuously deformed from some $\Upsilon_0 \in \{\Upsilon_a\}$ which is only located in N and does not touch Q.

Consequently, in the setup of figure 5.1, the geodesic defining the entanglement entropy for a boundary interval (which does not intersect with P) on M cannot cross Q if the extrinsic curvature on Q satisfies the assumption (5.14). See figure 5.2 for an illustration.

In [249] the authors were concerned with the geometric properties of general codimension one hypersurfaces, but we are working with models in which the embedding of a brane Q into an ambient spacetime is dynamically determined via the equation of motion (5.2). We will hence reformulate the assumption (5.14) made in the barrier theorem in terms of the energy-momentum tensor S_{ij} and express it in terms of energy conditions. This will be complicated by the fact that (5.14) is supposed to hold for any (including spacelike) vector field v^i while energy conditions are usually only phrased in terms of causal vector fields.

Using (5.12) and (5.4), we find that (5.14) can be written as

$$-\frac{S}{2}v_iv^i + S_L(l_iv^i)^2 + S_R(r_iv^i)^2 \geq 0. \tag{5.15}$$

The last two terms are nonnegative due to the NEC, only the first term is potentially problematic. We can now separately discuss this for the three different cases:

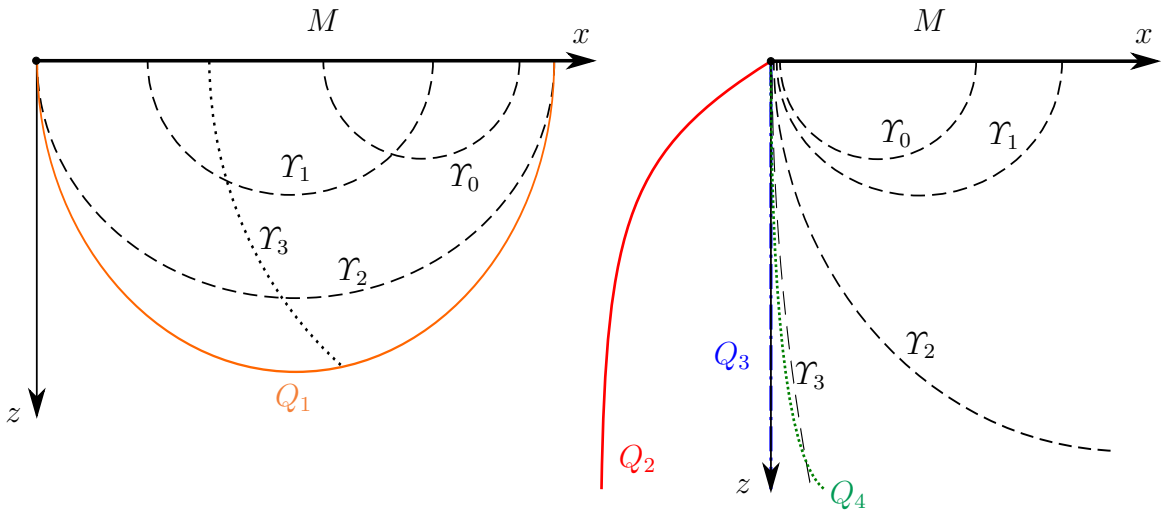

Figure 5.2: Compared to figure 5.1, we suppress the time direction t and assume a static embedding of the branes Q_i into a static background N. Left: Q can be an extremal surface barrier which bends back to the boundary in a $\cup$-shaped manner. No Q_1 deformable extremal surface can reach deeper into the bulk than Υ_2, and hence none of them can cross Q_1 if it is an extremal surface barrier. Note that the dotted geodesic Υ_3 would cross Q_1, but it is not anchored on M with both endpoints, hence the barrier theorem does not apply to it. Right: Three possible cases for which the brane Q_i is anchored to the boundary only once. We see that as we move the right anchoring point of the geodesics Υ on the boundary more and more to the right, they reach deeper and deeper into the bulk. Q_4 is not an extremal surface barrier as it is crossed by Υ_3, but Q_3 is an extremal surface barrier. In fact, it satisfies the assumption (5.14) trivially as $K_{ij}^{Q_3} = 0$. Q_2 is automatically an extremal surface barrier as it is completely behind the barrier Q_3, even if it does not satisfy (5.14). The figure is presented as in [2].

- $S = 0$: As said above, the NEC is enough to ensure (5.15) to be satisfied for any v^i.
- $S < 0$: For null and spacelike v^i, the NEC is again enough to ensure the validity of (5.15). For timelike vectors v^i, (5.15) is equivalent to the SEC as defined in section 5.2.2.
- $S > 0$: This is the least straightforward case, as here (5.15) is satisfied by null and timelike v^i (assuming NEC), but spacelike vectors need more investigation. Writing $v^i = -\alpha l^i + \beta r^i$ (with $\alpha \cdot \beta > 0$) this takes the form

$$-S\alpha\beta + S_L\beta^2 + S_R\alpha^2 \geq 0 \quad \text{for any } \alpha \cdot \beta > 0, \tag{5.16}$$

  which can be identified as the WEC introduced in section 5.2.2, see (5.9).

To summarise, we have shown that the condition of (5.14) is, using the equations of motion (5.2), equivalent to demand WEC and SEC (both implying the NEC) to hold at the same time. This means that the energy conditions satisfied or violated by the matter fields

defined to live in the worldvolume of Q will have profound implications on the possible embeddings of the brane Q into the ambient spacetime N. We will see this on specific examples in section 5.3.2 and chapter 6. In appendix B we will comment on the possible extension of the findings of this section to higher dimensions.

5.2.4 AdS and BTZ backgrounds

After having studied the equations of motion (5.2) in great generality, we will now specialise more to the specific cases that we will be interested in for the remainder of this thesis. Specifically, we will be interested in background spacetimes N with a static line element of the form

$$ds^2 = g_{\mu\nu}dx^\mu dx^\nu = \frac{1}{z^2}\left(-h(z)dt^2 + \frac{dz^2}{h(z)} + dx^2\right), \tag{5.17}$$

which is $2+1$-dimensional Poincaré AdS for $h(z)=1$ and the BTZ black hole [130, 131] in Poincaré coordinates for $h(z) = 1 - z^2/z_H^2$. For simplicity, we have set the AdS radius $L=1$. We will also be interested in static embeddings of the brane Q into this background spacetime, defined by a function $x(z)$ as for the examples in figure 5.2. On the worldsheet of the brane, we will then use the same coordinates t and z as in the bulk. The extrinsic curvature then reads:

$$\begin{aligned} K_{tt} &= \frac{1}{\mathcal{N}}\left(\partial_z x \frac{h}{2}\left(h' - \frac{2h}{z}\right)\right), \\ K_{tz} &= 0, \\ K_{zz} &= \frac{1}{\mathcal{N}}\left(-\partial_z^2 x + \partial_z x\left(\frac{h}{z}(\partial_z x)^2 + \frac{1}{z} - \frac{h'}{2h}\right)\right), \end{aligned} \tag{5.18}$$

where $\mathcal{N}$ comes from the normalisation of the normal vector n^μ, see also appendix A.2 for more information. For the induced metric we find

$$\gamma_{ij} = \begin{pmatrix} g_{tt} & 0 \\ 0 & g_{zz} + (\partial_z x)^2 g_{xx} \end{pmatrix} \equiv \begin{pmatrix} -a(z) & 0 \\ 0 & b(z) \end{pmatrix}. \tag{5.19}$$

where we have defined the positive functions $a(z)$ and $b(z)$. One can now easily write down the null vectors r^i and l^i (fixing their boost invariance by demanding $r^1 + l^1 = 0$) to find

$$S_{ij} = \frac{S}{2}\gamma_{ij} + S_L l_i l_j + S_R r_i r_j \tag{5.20}$$

$$= \frac{S}{2}\begin{pmatrix} -a & 0 \\ 0 & b \end{pmatrix} + \frac{S_L}{2}\begin{pmatrix} a & -\sqrt{ab} \\ -\sqrt{ab} & b \end{pmatrix} + \frac{S_R}{2}\begin{pmatrix} a & \sqrt{ab} \\ \sqrt{ab} & b \end{pmatrix}. \tag{5.21}$$

From (5.18) and (5.19) we see that, due to the equation of motion (5.2), also S_{ij} will have to be diagonal in the coordinate system of our choice, implying $S_L = S_R \equiv S_{L/R}$. This

makes sense, as it means that an observer at rest on the worldvolume of our brane at fixed z-coordinate should not see a net flux of energy from the left to the right, or vice versa. This should be a prerequisite for a static geometry. We hence find

$$S_{ij} = \frac{S}{2}\begin{pmatrix} -a & 0 \\ 0 & b \end{pmatrix} + S_{L/R}\begin{pmatrix} a & 0 \\ 0 & b \end{pmatrix}. \tag{5.22}$$

For later use, we will also define the traceless symmetric tensor appearing in this equation to be

$$\widehat{\gamma}_{ij} \equiv \begin{pmatrix} a & 0 \\ 0 & b \end{pmatrix}, \quad \widehat{\gamma}^{ij} = \begin{pmatrix} \frac{1}{a} & 0 \\ 0 & \frac{1}{b} \end{pmatrix}, \quad \widehat{\gamma}_{ij}\widehat{\gamma}^{ij} = 2 \tag{5.23}$$

which can also be written as $\widehat{\gamma}_{ij} = \gamma_{ij} + 2u_i u_j$ with the normalised timelike vector $u_i = \begin{pmatrix} \sqrt{a} \\ 0 \end{pmatrix}$ which satisfies

$$\nabla_i u^i = 0, \tag{5.24}$$

$$u^i \nabla_i u^j = \begin{pmatrix} 0 \\ \frac{1}{2}\gamma^{tt}\gamma^{zz}\partial_z \gamma_{tt} \end{pmatrix}. \tag{5.25}$$

Just as the energy-momentum tensor S_{ij} can in the static case be expressed in terms of two scalars S and $S_{L/R}$ in (5.22), the same decomposition can be applied to the extrinsic curvature. For this, we define (5.2) as

$$\mathcal{K}_{ij} = \frac{\mathcal{K}}{2}\gamma_{ij} + \mathcal{K}_{L/R}\widehat{\gamma}_{ij}, \tag{5.26}$$

$$\equiv -\left(K_{ij} - \gamma_{ij}K\right) = \kappa_N^2\, S_{ij}. \tag{5.27}$$

The equation of motion (5.2) then reads in scalar form

$$\mathcal{K} = \kappa_N^2 S \quad \text{and} \quad \mathcal{K}_{L/R} = \kappa_N^2 S_{L/R}. \tag{5.28}$$

While S and $S_{L/R}$ can be constrained by energy conditions as in section 5.2.2, the scalars $\mathcal{K}$ and $\mathcal{K}_{L/R}$ are dependent on the embedding profile $x(z)$. The impact of the different energy conditions on the embedding are summarised in table 5.1.

A further important result can be derived by demanding conservation of the energy-momentum tensor using (5.22) and (5.23):

$$0 = \nabla_i S^{ij} = \frac{1}{2}\partial_i S \gamma^{ij} + \partial_i S_{L/R}\widehat{\gamma}^{ij} + S_{L/R}\left(2u^j \nabla_i u^i + 2u^i \nabla_i u^j\right). \tag{5.29}$$

The term $u^j \nabla_i u^i$ vanishes immediately due to (5.24). There are now two cases for the index j:

BTZ: $h(z) = 1 - z^2/z_H^2, \quad z_H > z$	
$\mathcal{K}_{L/R}$	$\frac{z\left(z_H^2-z^2\right)\left(zx'^3+z_H^2x''\right)}{2z_H\left(z_H^2+\left(z_H^2-z^2\right)x'^2\right)^{3/2}}$
$\mathcal{K}$	$\frac{2z_H^4x'+\left(z^4-3z^2z_H^2+2z_H^4\right)x'^3+zz_H^2\left(z^2-z_H^2\right)x''}{z_H\left(z_H^2+\left(z_H^2-z^2\right)x'^2\right)^{3/2}}$
NEC ($\mathcal{K}_{L/R} \geq 0$)	$zx'^3 + z_H^2x'' \geq 0$
WEC ($2\mathcal{K}_{L/R} - \mathcal{K} \geq 0$)	$zz_H^2\left(z_H^2 - z^2\right)x'' - z_H^4x' - \left(z_H^2 - z^2\right)^2 x'^3 \geq 0$
SEC ($2\mathcal{K}_{L/R} + \mathcal{K} \geq 0$)	$x' \geq 0$

AdS: $h(z) = 1$	
$\mathcal{K}_{L/R}$	$\frac{zx''}{2(1+x'^2)^{3/2}}$
$\mathcal{K}$	$\frac{2x'+2x'^3-zx''}{(1+x'^2)^{3/2}}$
NEC ($\mathcal{K}_{L/R} \geq 0$)	$x'' \geq 0$
WEC ($2\mathcal{K}_{L/R} - \mathcal{K} \geq 0$)	$zx'' - x' - x'^3 \geq 0$
SEC ($2\mathcal{K}_{L/R} + \mathcal{K} \geq 0$)	$x' \geq 0$

Table 5.1: Impact of the energy conditions discussed in section 5.2.2 on the embedding profile $x(z)$ in a BTZ or AdS background (5.17). As the NEC is implied both by WEC and SEC, we only show those inequalities of WEC and SEC that are not redundant with NEC, i.e. in case of the WEC the NEC is satisfied and *additionally* $2\mathcal{K}_{L/R} - \mathcal{K} \geq 0$. We also give the extrinsic curvature scalars defined in (5.26). The table is presented as in [2].

- $j = t$: As we assume a static setting ($\partial_t(...) = 0$) and the diagonal metric (5.19) as well as a diagonal $\widehat{\gamma}^{ij}$, the first two terms in (5.29) vanish and we are left with $0 = S_{L/R}\left(2u^i\nabla_i u^j\right)$ which vanishes due to (5.25).

- $j = z$: This case is more interesting, as we find a non-trivial result due to (5.25). Using $\gamma^{zz} = \widehat{\gamma}^{zz}$ and setting $h(z) = 1$ as for the AdS space, we find

$$0 = \nabla_i S^{iz} = \frac{1}{2}S'\gamma^{zz} + S'_{L/R}\gamma^{zz} - \frac{2}{z}S_{L/R}\gamma^{zz} \tag{5.30}$$

$$\Rightarrow \left(S + 2S_{L/R}\right)' = \frac{4}{z}S_{L/R}. \tag{5.31}$$

  Equivalently, $h(z) = 1 - z^2/z_H^2$ yields the analogue result for the BTZ black hole:

$$\left(S + 2S_{L/R}\right)' = \frac{4}{z - \frac{z^3}{z_H^2}}S_{L/R} \tag{5.32}$$

These two equations are important for us because they have an interesting and straightforward interpretation: By NEC, the right hand side of both (5.31) and (5.32) should be positive, while the combination appearing in brackets on the left hand side is related to the SEC, see table 5.1 and section 5.2.2. Hence, the conservation of energy-momentum implies that if the NEC holds everywhere on the worldvolume of the brane and the SEC holds near the boundary, then the SEC will also hold deeper in the bulk, i.e. for larger z. This is also obvious from table 5.1: If $x'' > 0$ everywhere and $x' > 0$ near the boundary, then $x' > 0$ everywhere. The conservation of the energy-momentum tensor gives the deeper physical reason for this.

Let us apply the findings of table 5.1 to the example embedding curves $x(z)$ shown in figure 5.2, assuming for simplicity that the background spacetime there is the Poincaré AdS space. On the left hand side, we see that the embedding of Q_1 starts with positive $x'(z)$ and $x''(z)$, i.e. the SEC is satisfied by the matter fields on the brane. In our calculations so far and the results presented in 5.1 we were, by the choice of the direction of the normal vector n^μ, always implicitly assuming that if the brane is given by the embedding profile $x(z)$, then the bulk spacetime N is located to the right of it, i.e. in the region $x \geq x(z)$. Consequently, our calculations and results of table 5.1 can only be applied to Q_1 in figure 5.2 from the point $x = 0, z = 0$ up to the turning point of maximal z. In section 5.3.2 we will see explicit examples of solutions of this form. On the right hand side of figure 5.2 we see that all of the depicted example embeddings satisfy the NEC, while Q_2 clearly violates the SEC.

As an example of how the barrier theorem can be used in our context, let us propose the following question: Suppose we want to solve the equations of motion (5.2) with an energy-momentum tensor that is defined by some kind of matter model where we can analytically prove that it has to satisfy, say, NEC and SEC. How might the solution for the embedding qualitatively look like? Comparing to table 5.1, we immediately see that NEC and SEC imply $x' \geq 0$ and $x'' \geq 0$. This rules out an embedding of the type Q_2 shown in figure 5.2, and if we assume a non-trivial energy-momentum tensor $S_{ij} \neq 0$ this also rules out the trivial totally geodesic embedding Q_3. With NEC and SEC this is as far as we can go, but let us next also assume that in addition the WEC holds. Then the barrier theorem applies, and the brane is an extremal surface barrier. If it would start on the boundary at $x = z = 0$ and go into the bulk indefinitely with $x' > 0, x'' > 0$, as Q_4 in figure 5.2, then we could easily construct a spacelike geodesic anchored on M that intersects the brane somewhere in the bulk. All we would have to do is to move the one endpoint closer to the brane, and the other one farther and farther away, until the geodesics reaches so deep into the bulk spacetime that it intersects the brane. This would be in contradiction to the barrier theorem, and hence a behaviour of the type of Q_4 is also ruled out by SEC and WEC. The only possibility is a behaviour of the type of Q_1: The brane has to bend back to the boundary. This means that WEC and SEC together force the brane to bend in a $\cup$-shaped way. Conversely, if we want our brane to go deeper into the bulk without coming back to the boundary, either WEC or SEC has to be violated.

Suppose now that instead of a Poincaré background we are working with a BTZ back-

ground. A brane going from the boundary into the bulk, if it does not turn around and come back to the boundary, will then encounter the event horizon. To study this in more detail, let us take the entries of table 5.1 for the BTZ case and take the limit $z \to z_H$. Then we see that exactly at the horizon, WEC ($x'(z_H) \leq 0$) and SEC ($x'(z_H) \geq 0$) are mutually exclusive.[2] We have seen that when both WEC and SEC are satisfied the brane has to turn around and bend back to the boundary, and our discussion has just shown the converse: The brane (in the non-trivial case) can only enter the event horizon if either WEC or SEC is violated.

5.3 Exact solutions

Although the model (5.1) explicitly allows for generic matter fields to be defined on Q, most of the literature [92–94, 238–245] focuses on simple *constant tension* models, to be studied in subsection 5.3.1. Notable exceptions are [245] where a perfect fluid living on the hypersurface Q is defined, and [242] where the case of a non-linear sigma model as matter content on Q is qualitatively discussed, apart from this the literature on exact solutions of (5.1) with non-trivial $\mathcal{L}_Q$ is surprisingly sparse. In this section we will apply our analyses of the previous section in order to find simple analytical solutions of the equations of motion (5.2).

5.3.1 Constant tension solutions

The simplest possible model that can be studied using the equations (5.2) is the one where the energy-momentum tensor is defined by a constant tension λ:

$$S_{ij} = -\lambda\gamma_{ij} \;\Rightarrow\; S = -2\lambda, \quad S_{L/R} = 0. \tag{5.33}$$

For branes embedded in a global AdS_3 background this model has already been studied in [250], and we extensively commented on it in [2]. In this thesis we will only need the constant tension solutions in a Poincaré or BTZ background (5.17) which were studied in [92].

Let us begin with the case for a Poincaré background. From (5.28), (5.33) and table (5.1) we then find

$$0 = \mathcal{K} = \frac{zx''}{2\left(1+x'^2\right)^{3/2}}, \tag{5.34}$$

$$-2\lambda\kappa_N^2 = \mathcal{K} = \frac{2x' + 2x'^3 - zx''}{\left(1+x'^2\right)^{3/2}}. \tag{5.35}$$

[2] We have been assuming the general case $x' \neq 0$ and $x'' \neq 0$. Of course $x'(z_H) = 0$ would be a possible solution, but note that the NEC implies that $x'(z)$ is monotonously increasing. Hence, if the NEC holds and $x'(z_H) = 0$, then $x'(z) = 0$ for any z which is the trivial case.

This has the solution

$$x'(z) = \frac{-\lambda\kappa_N^2}{\sqrt{1-\lambda^2\kappa_N^4}} = const., \tag{5.36}$$

i.e. the corresponding embedding is just a straight line in Poincaré coordinates. We also see that no solutions to (5.2) for a brane anchored at the boundary and embedded in a Poincaré background exist when $|\lambda| \geq \kappa_N^{-2}$.

We see that for (5.33) with $\lambda \neq 0$, SEC and WEC are mutually exclusive: SEC would demand *negative tension* $\lambda < 0$ while WEC would demand *positive tension* $\lambda > 0$. This means that these solutions show a behaviour that was already anticipated in our discussion in section 5.2: $\lambda = 0$ would be the trivial case Q_3 in figure 5.2. The SEC satisfying but WEC violating case where $\lambda < 0$ and consequently $x'(z) > 0$ would be qualitatively similar to the curve Q_4[3] in this figure, as the curve would go to the right and be intersected by spacelike geodesics. The WEC satisfying and SEC violating case $\lambda > 0$, $x'(z) < 0$ would be qualitatively similar to Q_2, in that it does not satisfy the property (5.14) but still is an extremal surface barrier simply because it is entirely on the far side of the extremal surface barrier Q_3. The positive tension case is generally considered to be physical while the negative tension case is considered the unphysical one, for several reasons. Firstly, the WEC is considered to be better motivated as a condition on physical theories that what we termed the SEC in section 5.2.2 [247]. In fact we will see below that there are very sensible models of field theories living on the brane worldvolume that effectively lead to constant tension models with positive tension only. Secondly, as the brane can intersect geodesics in the negative tension case, it is not known how entanglement entropy for certain boundary regions would then have to be calculated holographically. A proposal was made in [2] which would however be in conflict with the causal influence argument discussed in section 4.4. This geometric situation may be similar to the case described in [251] in that there are *no* extremal codimension two surfaces in the bulk spacetime connecting two boundary points in certain cases.

This situation is qualitatively similar in a BTZ background spacetime (5.17) where $h(z) = 1 - z^2/z_H^2$. There one finds the solution [92]

$$x(z) = -z_H \text{arctanh}\left(\frac{\sinh(s(\lambda))}{\sqrt{\frac{z_H^2}{z^2} + \sinh(s(\lambda))^2}}\right), \quad \tanh(s(\lambda)) = \lambda\kappa_N^2. \tag{5.37}$$

Here we have chosen the boundary condition $x(0) = 0$. This can be done without loss of generality due to the translation invariance of (5.17) in the x-direction. As pointed out in [2, 92, 250], the solutions (5.36) and (5.37) can be geometrically constructed via a *geodesic normal flow*, see figure 5.3 for an illustration in the AdS case. This construction proceeds as follows: First, one determines the trivial embedding that solves the equations

[3] Except of course for the fact that Q_4 would then have to be a straight line.

(5.2) for zero tension $\lambda = 0$. By definition, this embedding will define a totally geodesic codimension one hypersurface in the bulk spacetime. Next one constructs the geodesics that go through this surface normally, and shifts every point of this surface along the flow of these geodesics by an affine distance s which is a function of λ. This way the embeddings (5.36) and (5.37) for $\lambda \neq 0$ can be constructed.

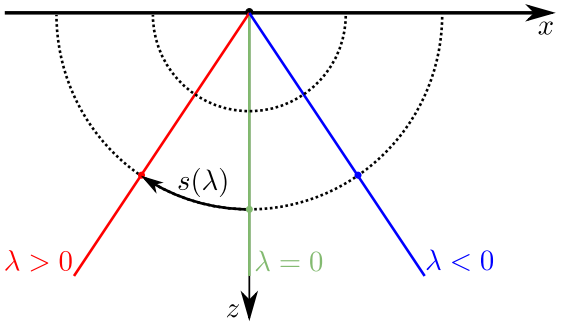

Figure 5.3: Geodesic normal flow construction of a constant tension brane embedding in a constant curvature background, here Poincaré AdS. Points on the trivial $\lambda = 0$ embedding are shifted along normal geodesics (dotted lines) by an affine distance $s(\lambda)$.

The constant tension solutions that we discussed in this section will be important for two reasons. First of all, the geodesic normal flow construction explained above makes it easy to obtain analytical results for embeddings such as (5.36) and (5.37), but also for the entanglement entropy of certain intervals. This is because the spacelike geodesics that are explicitly used in this construction define the entanglement entropy of certain boundary intervals, and increasing the tension, say, from $\lambda = 0$ to $\lambda = \lambda_0 > 0$, we see that all these geodesics get longer exactly by a distance $s(\lambda)$. Hence, according to the Ryu-Takayanagi prescription explained in section 3.2, the entanglement entropy of all these intervals will grow by the same amount $s(\lambda)/4$:

$$S(\lambda, \Delta x) = S(\lambda = 0, \Delta x) + \frac{s(\lambda)}{4}. \tag{5.38}$$

We will make use of this in sections 6.4.2 and 6.5.

The second reason why constant tension solutions will be important for us is that they can be mimicked by a gauge field as we will now see. If the two-dimensional action of the fields living on the brane only contains a $U(1)$ gauge field

$$\mathcal{S} = -\int d^2x \sqrt{-\gamma}\, \frac{1}{4} f_{mn} f^{mn}, \tag{5.39}$$

with no sources, then the energy-momentum tensor reads

$$S_{ij} = -\frac{1}{4} f^{mn} f_{mn} \gamma_{ij} + \gamma^{mn} f_{mi} f_{nj} \tag{5.40}$$

$$\Rightarrow S = \frac{1}{2} f^{mn} f_{mn} \tag{5.41}$$

and the traceless part of (5.40) reads

$$S_{ij} - \frac{S}{2}\gamma_{ij} = -\frac{1}{2}f^{mn}f_{mn}\gamma_{ij} + \gamma^{mn}f_{mi}f_{nj}. \tag{5.42}$$

The equation of motion in the absence of sources,

$$\partial_m\left(\sqrt{-\gamma}\gamma^{mp}\gamma^{nq}f_{pq}\right) = 0, \tag{5.43}$$

can then be shown to yield $\sqrt{-\gamma}f^{01} = \mathcal{C}$ with a constant $\mathcal{C}$. It should be noted that due to the antisymmetry of f^{mn} and the fact that we are working in two dimensions, f^{01} is the only independent component of the field strength tensor. Using this and assuming a static case with metric (5.19), it is then possible to show $f^{mn}f_{mn} = -2\mathcal{C}^2$ and $\gamma^{mn}f_{mi}f_{nj} = -\gamma_{ij}\mathcal{C}^2$. Consequently the traceless part (5.43) vanishes and the energy-momentum tensor (5.40) takes the form

$$S_{ij} = -\frac{1}{2}\gamma_{ij}\mathcal{C}^2. \tag{5.44}$$

We hence see that in the absence of charges, the $U(1)$ gauge field mimics a constant tension model with positive tension.

5.3.2 Perfect fluid models

Let us consider a toy model where the energy-momentum tensor S_{ij} on the brane is given by a perfect fluid[4]

$$S_{ij} = (\rho + p)u_iu_j + p\gamma_{ij}, \tag{5.45}$$

with $u_i \sim (1, 0)$ for staticity, and an equation of state

$$p = a \cdot \rho. \tag{5.46}$$

The usual decomposition into scalar quantities then tells us

$$S = p - \rho = \rho(a-1), \quad S_{L/R} = \frac{p+\rho}{2} = \rho\frac{1+a}{2}. \tag{5.47}$$

and consequently the energy conditions take the form (assuming $\rho \geq 0$)

$$\text{NEC: } a \geq -1, \quad \text{WEC: } a \geq -1, \quad \text{SEC: } a \geq 0. \tag{5.48}$$

[4]The ansatz that we follow in this section is different from the one presented in [245] in that we are working in one dimension less. Also, we will explicitly pick an equation of state, while in [245] the equation of state is fixed by the specific ansatz.

Let us now first work in a Poincaré background, i.e. (5.17) with $h(z) = 1$. A useful way to solve this equation is to use (5.31) which now reads[5]

$$\rho(z)' = \frac{1+a}{a}\frac{\rho(z)}{z} \quad \Rightarrow \quad \rho(z) = \frac{c}{\kappa_N^2} z^{1+\frac{1}{a}}, \tag{5.49}$$

where we introduced a constant c. Now (5.28) together with $\mathcal{K}$ from table 5.1 allows us to solve

$$x'(z) = \frac{a c z^{\frac{1}{2}\left(2+\frac{2}{a}\right)}}{\sqrt{1-a^2c^2z^{2+\frac{2}{a}}}}, \tag{5.50}$$

$$x(z) = \frac{a^2 c z^{2+\frac{1}{a}} {}_2F_1\left(\frac{1}{2}, \frac{1+2a}{2+2a}; \frac{3+4a}{2+2a}; a^2c^2z^{2+\frac{2}{a}}\right)}{1+2a}, \tag{5.51}$$

with the hypergeometric function ${}_2F_1(a,b;c;d)$. Studying these expressions we see that, demanding $x(z)$ to be real, these curves only reach the boundary for $a \geq 0$ (i.e. SEC) and $a \leq -1$. As we demand the NEC to be satisfied and the branes to be anchored at the boundary, we will from now on focus on $a \geq 0$, i.e. both WEC and SEC being satisfied. The solution (5.51) is only real for $0 \leq z \leq \left(\frac{1}{a^2c^2}\right)^{\frac{a}{2a+2}}$, and the derivative $x'(z)$ diverges as this limit is approached. This indicates that the embedding curves $x(z)$ turn around and go back to the boundary, which as we have seen in section 5.2 is demanded by the barrier theorem in the case where SEC and WEC are satisfied. The solution (5.51) hence describes an embedding similar to Q_1 in figure 5.2. See figure 5.4 for plots of these solutions for different values for a and c.

This calculation can easily be generalized in two ways. First of all, we can add a constant tension contribution Ω to the energy-momentum tensor:

$$S = -2\Omega + \rho(a-1), \quad S_{L/R} = \rho\frac{1+a}{2}. \tag{5.52}$$

Secondly, we can generalise the Poincaré background used above to a BTZ background (5.17), $h(z) = 1 - z^2/z_H^2$. Again, we can solve the equation (5.32) implying conservation of the energy-momentum tensor and find

$$\rho(z) = \frac{c}{\kappa_N^2}\left(\frac{z^2 z_H^2}{z_H^2 - z^2}\right)^{\frac{a+1}{2a}} \tag{5.53}$$

[5]This is basically the equation of motion for the perfect fluid. We could also look at the equation of particle number conservation, which in the static case is trivially satisfied as

$$\nabla_i\left(n(\rho(z))u^i\right) = u^i\partial_i n(\rho(z)) + n(\rho(z))\nabla_i u^i = 0,$$

where we can use (5.24), $u^z = 0$ and $\partial_t n(\rho(z)) = 0$ to show that this equation is satisfied. The particle number density n is related to the energy density ρ by the equation of state, see [252] for more information.

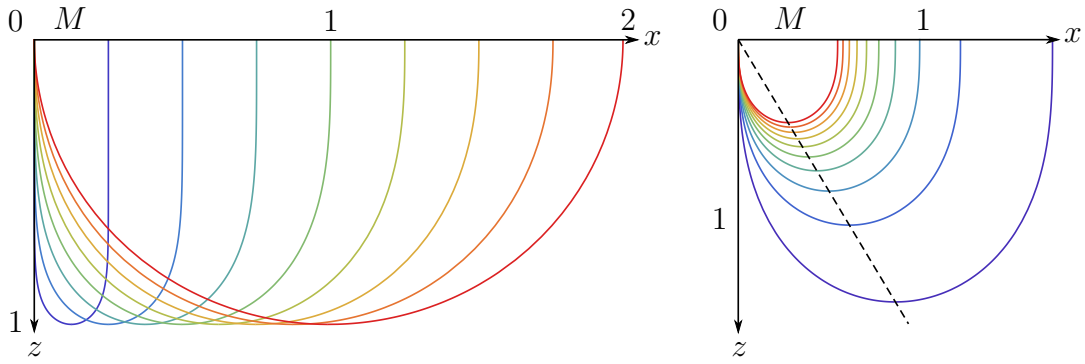

Figure 5.4: Left: Brane profiles (5.51) for $c = 1/a$ and, in order of increasing second intersection with the x-axis, $a \approx 0.1, 0.2, 0.4, 0.7, 1.1, 2.0, 4.8, 100$. Right: Brane profiles with $a = 1$ and, from outer to inner curve, $c = 0.5, 1, 1.5, ..., 5$. All the turning points lie on the dashed straight line. For clarity we added arcs leading back to the boundary in a symmetric way on both sides of the figure. We chose $\kappa_N^2 = 1$ for both the left and the right figure. The figure is presented as in [2].

which generalises (5.49). Interestingly, this result does not depend on the constant Ω. In the next step towards solving the equations of motion (5.28) for the given matter content (5.52), we use the results of table 5.1 to write

$$2a\rho(z) - 2\Omega = S + 2S_{L/R} = \mathcal{K} + 2\mathcal{K}_{L/R} = \frac{2z_H x'_+(z)}{\sqrt{(z_H^2 - z^2)x'_+(z)^2 + z_H^2}}, \tag{5.54}$$

where for simplicity we set $\kappa_N^2 = 1$ from now on. This combination of terms only includes $x'(z)$ but not $x''(z)$, hence it can be algebraically solved for $x'(z)$ to give

$$x'(z) = \frac{\mathfrak{F}(z) z_H}{\sqrt{\mathfrak{F}(z)^2 z^2 - \mathfrak{F}(z)^2 z_H^2 + 4z_H^2}}, \quad \mathfrak{F}(z) \equiv 2a\rho(z) - 2\Omega. \tag{5.55}$$

For the general case this can only be integrated numerically to give the embedding profile $x'(z)$, see the left hand side of figure 5.5. Even without an analytical solution for $x(z)$, the expression (5.55) gives us some information on the geometry of the brane embeddings, as we see that $x'(z)$ diverges to infinity at

$$z_\infty = \frac{\sqrt{\mathfrak{F}(z_\infty)^2 - 4}}{\mathfrak{F}(z_\infty)} z_H. \tag{5.56}$$

Solving this equation exactly is hard, but for $z \to z_H$, we see from (5.53) and (5.55) that $\mathfrak{F}$ diverges for $a > 0$, and hence (5.56) will always have a real solution $z_\infty \leq z_H$. Hence we expect that even in a BTZ background, and even in the presence of a cosmological constant term the branes will always turn around and bend back to the boundary. This is indeed the behaviour seen in figure 5.5.

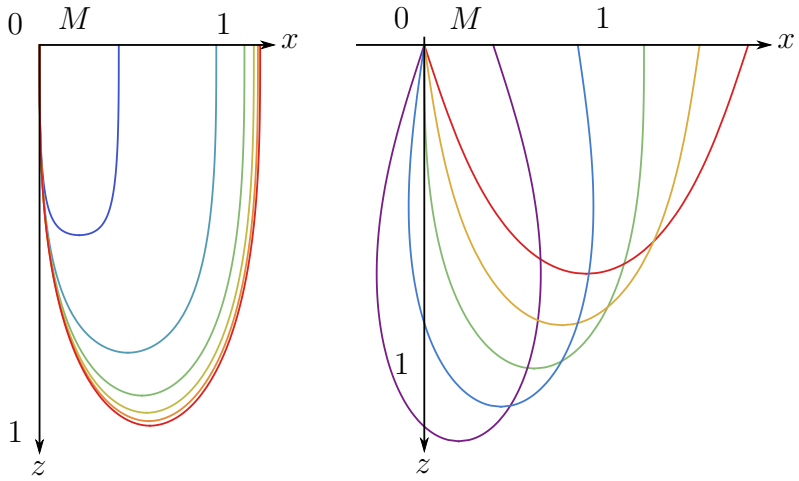

Figure 5.5: Left: Embedding functions for the brane with a perfect fluid in a BTZ background with $z_H = 1$. Depicted are the cases for $\Omega = 0$, $a = c = 1$ and, in order of increasing second intersection with the x-axis, $z_H = 0.5, 1, 1.5, ..., 3$. Additional symmetric branches leading back to the boundary after the turning point were added. Right: Embedding functions (5.57). Shown are the cases for $a = c = 1$ and, in order of increasing second intersection with the x-axis, $\Omega = 2, 1, 0, -1, -2$. We chose $\kappa_N^2 = 1$ for both the left and the right figure. The figure is presented as in [2].

Equation (5.55) simplifies on a Poincaré background, where $z_H \to \infty$. It can then actually be integrated analytically, and one finds for the embedding function

$$\begin{aligned} x(z) = {} & \frac{z}{(1+2a)2\sqrt{1-\Omega^2}} \\ & \times \left[\Omega(2a-2) F_1\left(\frac{a}{1+a}; \frac{1}{2}, \frac{1}{2}; \frac{1+2a}{1+a}; \frac{acz^{1+\frac{1}{a}}}{1+\Omega}, \frac{acz^{1+\frac{1}{a}}}{\Omega-1} \right) \right. \\ & \left. + 2a^2 c z^{1+\frac{1}{a}} F_1\left(\frac{2+a}{1+a}; \frac{1}{2}, \frac{1}{2}; \frac{3+2a}{1+a}; \frac{acz^{1+\frac{1}{a}}}{1+\Omega}, \frac{acz^{1+\frac{1}{a}}}{\Omega-1} \right) \right] \end{aligned} \tag{5.57}$$

where $F_1(a; b, c; d; e, f)$ is the Appell hypergeometric function. See the right hand side of figure 5.5 for a plot of such curves.

We have no specific boundary theory in mind that we hope this simple perfect fluid model studied in this section to be dual to, even on a qualitative bottom-up level. Nevertheless, we think that the investigations of this section were a worthwhile digression from our main interest (the holographic Kondo model) for two reasons: First of all, the exact solutions presented in this chapter demonstrate how tractable our analysis has made the equations of motion (5.2), and it nicely demonstrates the impact of the barrier theorem on the geometry of the embedding. Secondly, as we are now going to show, this perfect fluid can be reformulated as a massless free scalar when the equation of motion parameter is chosen to be $a = 1$.

Assume the action of the scalar field living on the brane worldvolume to be

$$\mathcal{L}_{matter,\,Q} = -\frac{1}{2}\gamma^{ij}\partial_i\phi\partial_j\phi. \tag{5.58}$$

The equations of motion that follow from this model are

$$\gamma'^{11}\phi' - \frac{2}{z}\gamma^{11}\phi' + 2\gamma^{11}\phi'' = 0 \tag{5.59}$$

and can be identified with (5.49) for $a = 1$ by setting

$$\rho \equiv \frac{1}{2}\gamma^{ij}\partial_i\phi\partial_j\phi = \frac{\gamma^{zz}}{2}\left(\phi'\right)^2. \tag{5.60}$$

Similarly, using this substitution and $a = 1$ the energy-momentum tensor derived from (5.58) takes the form (5.47).

This result is noteworthy because the scalar model (5.58) is a special case of the non-linear sigma models discussed in [242]. There, it was suggested that these models would have a holographic interpretation as describing a boundary RG flow. Unfortunately, we have seen that due to the consequences of the barrier theorem the branes in this model will have to bend back to the boundary as in figure 5.4, a behaviour that seems hard to interpret in terms of a holographic RG flow. In fact, from the results presented in this section this behaviour of bending back to the boundary seems quite generic as it happens both in Poincaré and BTZ backgrounds and even if due to the presence on a constant tension term the SEC is violated near the boundary. In chapter 6 on the other hand, we will study a specific model which does have an interpretation as the dual of a physical and well-defined holographic RG flow. In this model we will also find that the brane does not bend back to the boundary, which in itself should be considered a non-trivial feature after the experience gathered from the examples studied above.

Chapter 6

Entanglement entropy in a holographic Kondo model

We will now proceed to the central interest of this thesis, namely the Kondo effect and the holographic Kondo model of [86]. As we want to focus on presenting the contributions of the author to the study of entanglement entropy in the holographic Kondo effect carried out in [2–4], we will only give a very brief review of the field theory physics of the Kondo effect in section 6.1.1 following the overview given in [86]. The top-down model of [86] will then be recapitulated in section 6.1.2 before summarising the bottom-up model of [86] in section 6.2. Genuine new results will then be discussed in great detail in sections 6.4-6.7.

6.1 Field theory and top-down model

6.1.1 Field theory

As already outlined in the introduction, the Kondo effect is a consequence of the spin-spin interaction between conduction electrons and dilute magnetic impurities [65]. Using the notation of [86] in the following, the Kondo Hamiltonian describing the interaction of the electrons with one impurity can then be written as [65]

$$\widehat{H}_K = -\psi_\alpha^\dagger \frac{1}{2m}\nabla^2\psi_\alpha + \frac{1}{2}\lambda'_K\delta(\vec{x})\vec{S}\ \psi_\beta^\dagger \vec{T}_{\beta\alpha}\psi_\alpha. \tag{6.1}$$

In this formula, the first term is the standard kinetic term for the conduction electrons which are created and annihilated by the operators $\psi_\alpha^\dagger$ and ψ_α. The α, β indices are spin indices, and in the standard case of spin-$\frac{1}{2}$ particles with $SU(2)$ symmetry $\vec{T}$ is just the vector of Pauli matrices. The second term then describes the interaction between the electron spins and the spin $\vec{S}$ of the impurity localised at $\vec{x} = \vec{0}$. As we saw in

the introduction, the Kondo effect can be observed not only in traditional dilute alloys, but also in *quantum dot* systems. A unified description of the impurities that cause the Kondo effect in these diverse situations can be given in terms of the *Anderson impurity model* [253], reviewed in [66]. See also figure 6.1. In this model, one considers a localised site to which electrons can be bound. If one single electron is bound to this site, the corresponding energy level ϵ_d is below the Fermi energy ϵ_F of the surrounding conduction electrons. However, for two electrons bound to this site the Coulomb repulsion U between the two electrons raises the energy level above the Fermi energy. The state in which one single electron with an unpaired spin is bound to the localised site is hence energetically preferred, and the spin of this electron will act as magnetic impurity with respect to the surrounding conduction electrons.

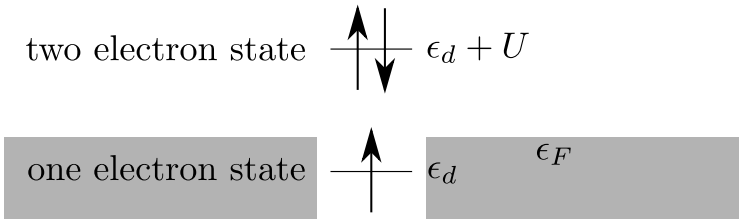

Figure 6.1: Illustration of the Anderson impurity model [253]. Electrons from a conduction band with Fermi energy ϵ_F can become bound to a localised site. Due to the Coulomb repulsion U, the state with one localised unpaired electron spin is energetically preferred.

As pointed out in [65], the Kondo effect is caused by an anti-ferromagnetic coupling $\lambda'_K > 0$. As the temperature of this system is lowered, it undergoes a *renormalisation group (RG)* flow which in the anti-ferromagnetic case leads to a growth and divergence of the running coupling at the dynamically generated *Kondo temperature* T_K [70]. At lower temperatures, the system flows to a state in which the impurity is effectively screened by conduction electrons forming the *Kondo screening cloud* [70, 72], see also [66, 67, 73, 74] for more information on this state.

In the following, in order to pave the way for a holographic description of the Kondo effect we will have to both simplify and generalise the model of (6.1). First of all, before applying the methods of the AdS/CFT duality to the Kondo system, we need to know whether and when CFT techniques can be used in the first place. Luckily, this topic has been studied extensively by Affleck and Ludwig in [254–258]. As shown in [254], by only considering the s-wave channel of electrons interacting with the impurity and linearising around the Fermi momentum k_F, the model (6.1) simplifies to

$$\widehat{H}_K = \frac{v}{2\pi}\psi_L^\dagger i\partial_x\psi_L + \frac{v}{2}\lambda_K\delta(x)\vec{S}\;\psi_L^\dagger\vec{T}\psi_L, \tag{6.2}$$

where we have still used the notation of [86]. Specifically, $v = k_F/m$ is the *Fermi velocity* and $\lambda_K = \frac{k_F^2}{2\pi^2 v}\lambda'_K$. The s-wave reduction leads to in- and out-going fermions moving on the radial coordinate $0 \leq r < +\infty$, but for (6.2) this is mapped to a system of chiral

left-moving fermions ψ_L on the real line $-\infty < x < +\infty$.[1]

This model (6.2) can then be treated by the methods of CFT and especially Kac-Moody algebras [254–258]. For us, the most important aspect of this is that the Kondo effect in $3+1$ dimensions, described by (6.1), obtains (at the fixed points) an additional conformal symmetry when reduced to the effectively $1+1$ dimensional model (6.2).

Furthermore, as in [86] we generalise the spin group from $SU(2)$ to $SU(N_s)$ and allow for k different *channels* or *flavours* of conduction electrons interacting with the impurity. As discussed in [86, 87], the symmetry group of (6.2) is then a $SU(N)_k \times SU(k)_N \times U(1)$ Kac-Moody symmetry. Here, the $U(1)$ part stands for the electromagnetic charge. One can also study different representations of the impurity spin under $SU(N_s)$ [259]. The benefit of promoting the spin group to $SU(N_s)$ is that this enables the use of large N_s techniques [259, 260]. It is known that in the large N_s limit, the formation of the Kondo cloud happens as a phase transition similar to the phase transitions observed in models of superconductivity, as part of the symmetry of the system is spontaneously broken [261–264]. In particular, the limit studied in [86] was the one where $N_s \to \infty$ and $\lambda_K \to 0$ such that $N_s\lambda_K$ is kept fixed. Assuming the impurity spin to be in a totally antisymmetric representation of $SU(N_s)$, it can be phrased as [265]

$$S^a = \chi^\dagger_\beta T^a_{\beta\alpha}\chi_\alpha, \tag{6.3}$$

where the auxiliary fermions χ_a trapped to the localised site are referred to as *slave fermions* or *Abrikosov pseudo-fermions*, see also [259,264]. In (6.3), the T^a ($a = 1, ..., N_s^2-1$) are the $SU(N_s)$ generators in the fundamental representation, under which the χ transform. These fermions introduce an additional $U(1)$ symmetry and unphysical states [265], a problem that can be dealt with by imposing the constraint [86, 259]

$$\chi^\dagger\chi = \widehat{\mathcal{Q}}. \tag{6.4}$$

This also means that the Young tableau of the impurity's representation is a single column with $\widehat{\mathcal{Q}} < N_s$ boxes [86, 259]. Now, using (6.3) and the identity

$$T^a_{\alpha\beta}T^a_{\gamma\delta} = \frac{1}{2}\delta_{\alpha\delta}\delta_{\beta\gamma} - \frac{1}{2N_s}\delta_{\alpha\beta}\delta_{\gamma\delta} \tag{6.5}$$

for the $SU(N_s)$ generators, we find as in [86] that the spin-spin coupling in (6.2) can be simplified to

$$\lambda_K\delta(x)\vec{S}\ \psi^\dagger_L\vec{T}\psi_L = \frac{1}{2}\lambda_K\delta(x)\left(\mathcal{O}\mathcal{O}^\dagger - \frac{\widehat{\mathcal{Q}}}{N_s}\psi^\dagger_L\psi_L\right), \tag{6.6}$$

where we defined the operator

$$\mathcal{O} = \psi^\dagger_L\chi. \tag{6.7}$$

[1] In [90], where (6.2) was modelled by a spin-chain, the s-wave reduction has been commented on in detail.

This operator has dimension 1/2, and hence the term $\mathcal{O}\mathcal{O}^\dagger$ is classically marginal, as it lives in $0+1$ dimensions only. In fact, in the Kondo model it is marginally relevant as discussed in [86, 266]. In the large N_s-limit, there will be a critical temperature $T_c < T_K$ below which the operator $\mathcal{O}$ condenses, i.e. gains a vacuum expectation value $\langle\mathcal{O}\rangle \neq 0$, while $\langle\mathcal{O}\rangle = 0$ at $T > T_c$ [261–264, 266]. This phase transition can be interpreted as a sign of the formation of the Kondo cloud.

6.1.2 Top-down model

There is a number of holographic models for the Kondo effect or similar impurity systems [76–86]. Specifically, in [86] *two* holographic models for the Kondo effect where proposed: One string theoretic top-down model, and one bottom-up model. In this section we will briefly summarise the top-down model, which is based on the setup of D-branes in type IIB string theory shown in table 6.1.

Direction	0	1	2	3	4	5	6	7	8	9
N_s $D3$	•	•	•	•	-	-	-	-	-	-
N_7 $D7$	•	•	-	-	•	•	•	•	•	•
N_5 $D5$	•	-	-	-	•	•	•	•	•	-

Table 6.1: Configuration of N_s $D3$, N_7 $D7$ and N_5 $D5$ branes in the top-down Kondo model of [86].

We see that this includes the same stack of N_s $D3$-branes as in Maldacena's original construction (see table 2.1), but also N_5 $D5$- and N_7 $D7$-branes. Just as in section 2.3, we can now investigate the open string and closed string perspective on this setup. Starting with the open string perspective, it is clear that strings can stretch between the different branes in table 6.1. This means there will be (up to orientation) $3-3$, $5-5$, $7-7$, $3-5$, $3-7$ and $5-7$ strings. The model of [86] is based on taking the usual Maldacena limit where $N_s \to \infty$, $g_s \to 0$ with $\lambda = 4\pi g_s N_s$ fixed, but keeping N_5 and N_7 finite at the same time, so that terms like N_5/N_s or N_7/N_s go to zero. This is called the *probe approximation*. The worldvolume theory of the $3-3$ strings will then describe $\mathcal{N}=4$ $SU(N_s)$ SYM theory as explained in section 2.3, while the worldvolume theories of the $5-5$ and $7-7$ strings decouple. Much more interesting for the holographic Kondo model will be the theories defined by the $3-5$, $3-7$ and $5-7$ strings, which live in the worldvolumes of the *intersections* of the respective branes.

For example, the $3-7$ strings are (in the low energy limit) confined to the $1+1$-dimensional intersection of the $D3$ and $D7$-branes. As can be seen from table 6.1, this means that in the $3+1$-dimensional flat space in which the $\mathcal{N}=4$ SYM theory lives (directions x^0-x^3), there is a $1+1$-dimensional hypersurface extending infinitely both in time (direction x^0) and one spacial direction (x^3). Detailed studies of the worldvolume theory on this intersection can be found in [267–270]. The important aspect in our context is that the $3-7$ strings

give rise to chiral fermions living in the $1+1$-dimensional brane intersection, and in the top-down Kondo model these are identified with the s-wave conduction electrons ψ_L in (6.2). In particular, the fermions arising in the top-down model yield a $SU(N_s)_{N_7} \times SU(N_7)_{N_s} \times U(1)$ Kac-Moody algebra [269]. We hence identify the number of $D7$-branes, N_7, with the number of channels k discussed in section 6.1.1. See [86] for more details. Similarly, we see that the $3-5$ strings give rise to a theory living in a $0+1$-dimensional worldvolume, i.e. on a localised point that extends only in time. Relevant references include [76, 78–82, 267, 271–276]. Again, the most important aspect of this is that the worldvolume theory of the $3-5$ strings gives rise to N_5 fermions on a $0+1$-dimensional space which, setting $N_5 = 1$, will be interpreted as the slave fermions of (6.3) [86]. In this picture, the $5-7$ strings are then responsible for the interaction between conduction fermions and slave fermions. The open string construction in table 6.1 can hence be interpreted as yielding a field theory system that has qualitatively similar features as the large N_s Kondo model discussed in section 6.1.1 [86].

The gravitational dual of this field theory system can then be obtained from the closed string construction of the setup of table 6.1 in the Maldacena limit. As in section 2.3.2, we will then obtain an $\mathrm{AdS}_5 \times \mathrm{S}^5$ background spacetime, the probe branes do not curve the spacetime in this setup. The probe brane worldvolumes hence become $\mathrm{AdS}_2 \times \mathrm{S}^4$ for the $D5$, $\mathrm{AdS}_3 \times \mathrm{S}^5$ for the $D7$, and $\mathrm{AdS}_2 \times \mathrm{S}^4$ for the $D5/D7$ intersection. From the fields living on $\mathrm{AdS}_3 \times \mathrm{S}^5$ one obtains a level-N_s $U(N_7)$ Chern-Simons (CS) field A living effectively on the AdS_3 [267–270]. This field is interpreted to be holographically dual to the current of the chiral fermions ψ_L on the field theory side [86]. Similarly, the fields living on the $\mathrm{AdS}_2 \times \mathrm{S}^4$ will yield both a $U(N_5 \equiv 1)$ gauge field a [267, 271, 272] and a charged scalar Φ [277, 278] living in the AdS_2. Holographically, the gauge field a will then be dual to the charge $\widehat{\mathcal{Q}}$ of the slave fermions χ, and the scalar field Φ, charged both under the AdS_2 field a and the AdS_3 field A, will be interpreted as the holographic dual of the operator $\mathcal{O}$ (6.7) [86]. Indeed, it is known [277, 278] that the scalar Φ is a *tachyon*, i.e. introduces an instability to the system. This instability leads to a condensation of Φ at low temperatures, which is holographically interpreted as the formation of the Kondo cloud [86].

In this section, we have only given a very brief overview over the top-down model outlined in table 6.1, and many more details can be found in [86]. Unfortunately, this model is very intricate and hard to work with. Consequently, in [86] the authors went one step further and designed a bottom-up model that was as close as possible to the top-down model in all aspects that are relevant for the interpretation as a genuine Kondo model, but on the other hand also as simple and tractable as possible. This bottom-up model will be discussed in the next section, and will be the basis of the original results of the present author to be presented in sections 6.4-6.7.

6.2 The bottom-up Kondo model

As said before, the bottom-up model of [86] is constructed in such a way as to be as simple as possible, while still providing a qualitative description of Kondo-like physics. Specifically, the holographic model will, by the limits discussed in sections 6.1.1 and 6.2 as well as by the nature of gauge/gravity duality, provide a description of a magnetic impurity (with large spin) interacting with a *strongly coupled* system.

To this end, the bottom-up model discards many of the features and fields of the top-down model, while retaining the following ingredients [86]:

- A $2+1$-dimensional asymptotically AdS bulk spacetime, such that the field theory model (6.2) can be interpreted as being the dual theory living on the AdS boundary. To describe the temperature dependence of the Kondo effect, the background spacetime will be chosen to be a BTZ black hole (5.17). If the event horizon is located at $z = z_H$ in the coordinate system of (5.17), the temperature then reads [130, 131]

$$T = \frac{1}{2\pi z_H}. \tag{6.8}$$

  Furthermore, we assume the bulk theory action to contain an Einstein-Hilbert term

$$\mathcal{S}_g = \frac{1}{2\kappa_N^2} \int d^3x \sqrt{-g} \left(R - 2\Lambda\right), \tag{6.9}$$

  with the Ricci scalar R, the negative cosmological constant $\Lambda = -1/L^2$ and the AdS radius L. In the following, we will set $L = 1$ for simplicity.

- A Chern-Simons (CS) field A_μ living in the $2+1$-dimensional bulk spacetime, dual to the current of the chiral fermions ψ_L on the boundary. The action reads

$$\mathcal{S}_A = -\frac{\mathcal{N}}{4\pi} \int \mathrm{Tr} \left(A \wedge dA + \frac{2}{3} A \wedge A \wedge A \right). \tag{6.10}$$

  The normalisation factor $\mathcal{N}$ is motivated from the action of the top-down model of section 6.1.2, and is proportional to N_s. In the following, we will for simplicity choose its gauge group to be $U(1)$, correspondingly there will only be one channel of conduction electrons, $k = 1$ [86].

- An asymptotically AdS_2 subspace embedded in the background spacetime, with one timelike direction and one radial direction. In the model of [86], this is simply taken to be the slice of the BTZ spacetime defined by $x \equiv 0$. As this hypersurface is the bottom-up remnant of the $D5/D7$ intersection in the top-down model, we will refer to it as the *brane*. The line element of the induced metric γ_{ij} reads

$$ds^2 = \gamma_{ij} dx^i dx^j = \frac{1}{z^2} \left(-h(z) dt^2 + \frac{dz^2}{h(z)} \right), \tag{6.11}$$

with $h(z) = 1 - \frac{z^2}{z_H^2}$. In the worldvolume of this brane, the model then includes the action

$$\mathcal{S}_{a,\Phi} = -\mathcal{N} \int d^2x \sqrt{-\gamma} \left(\frac{1}{4} f_{mn} f^{mn} + \gamma^{mn} (\mathcal{D}_m \Phi)^\dagger (\mathcal{D}_n \Phi) + V(\Phi\Phi^\dagger) \right) , \tag{6.12}$$

$$\mathcal{D}_m \Phi \equiv \partial_m \Phi + iqA_m \Phi - iqa_m \Phi \, , \tag{6.13}$$

for a $1+1$-dimensional gauge field a_m and a charged scalar $\Phi = \phi e^{i\psi}$. Similar to the nomenclature of chapter 5, we use Greek indices for quantities in the 2+1-dimensional bulk or ambient spacetime (e.g. $g_{\mu\nu}$ or A_μ) and Latin indices for quantities in the $1+1$-dimensional hypersurface $x \equiv 0$ (e.g. $a_m, \mathcal{D}_m\Phi$, or γ_{mn}). The gauge group of the field a_m (dual to the charge of the slave fermions χ) is chosen to be $U(1)$, which is adequate for the single impurity case [86]. See [87] for a study of the two-impurity case based on the same bottom-up model. The scalar field is charged both under the field a_m and the CS field A_m with opposite charges[2], and in (6.13) we have explicitly introduced the value of the charge q compared to [86]. These charges will become relevant in section 6.3.2. As in the top-down model explained in section 6.1.2, this scalar field will be interpreted to be holographically dual to the operator $\mathcal{O} = \psi_L^\dagger \chi$ and the condensation of this scalar at low temperatures will be interpreted as the formation of the Kondo cloud.

This model was sketched in figure 1.1. See [86,87] for an extensive discussion of this model, its features, and how good it describes Kondo physics via the holographic duality. Before we discuss how backreaction of the matter fields onto the bulk geometry can be taken into account in the bottom-up model in section 6.3, we will briefly summarise some of the results obtained in [86] for the case without backreaction that will be important later on. First of all, for high temperatures the system is in the *normal phase*, where the scalar Φ vanishes everywhere and only the gauge field a_m is non-zero on the brane. In the convenient gauge $a_z = 0$, the solution to the equations of motion then reads

$$a_t(z) = \frac{\mathcal{Q}}{z} + \mu, \tag{6.14}$$

where, holographically, $\mathcal{Q} \equiv \widehat{\mathcal{Q}}/N_s$ fixes the charge of the slave fermions defined in (6.4) [86]. When solving the equations of motion of the Kondo model, a fixed value of $\mathcal{Q}$ has to be given as a Neumann boundary condition [86], see also [279, 280] for related discussions of vector fields in low-dimensional bulk spacetimes. At low temperatures, the scalar field will condense, i.e. there will be a thermodynamically preferred solution to the equations of motion with $\phi(z) \neq 0$. In [86], the potential of the scalar appearing in (6.12) was chosen to be only a mass term

$$V(\Phi\Phi^\dagger) = M^2 \Phi\Phi^\dagger, \tag{6.15}$$

[2]See appendix C for a definition of the quantity A_m.

which is the simplest non-trivial possibility. This is one of the aspects where the bottom-up model deviates strongly from the top-down model, as there the potential is much more complicated and not even known up to all orders [86]. We will comment on this issue more in section 6.7. To obtain the correct conformal dimension of the dual operator $\mathcal{O}$, $\Delta = 1/2$, the mass M^2 in (6.15) is chosen such that the scalar field saturates the Breitenlohner-Freedman [197] bound in AdS_2. This also causes an instability such that at low temperatures the scalar field shows a tendency to condense, see [266] for a review of the instabilities arising in the $1+1$-dimensional case under consideration here. However, the effectively $1+1$-dimensional case is special in the sense that due to the coupling of the scalar to the gauge field and the asymptotic behaviour (6.14), the scalar's effective mass will get a contribution by $\mathcal{Q}$ [266], leading to the requirement (for the charge $q = 1$) [86]

$$M_{eff}^2 = M^2 - \mathcal{Q}^2 = -\frac{1}{4}. \tag{6.16}$$

This means that in the model under consideration, the mass M^2 has to be fixed to a specific value depending on the choice of the boundary condition $\mathcal{Q}$ in order for the dual operator of ϕ to have the right dimension [86]. With the above value of M^2, the asymptotic near-boundary behaviour of $\phi(z)$ is then

$$\phi(z) = \alpha\sqrt{z}\ln(\Theta z) + \beta\sqrt{z} + ..., \tag{6.17}$$

where we introduced a scale Θ for-dimensional reasons. In order to understand the physical meaning of α and β, we have to remind ourselves that in the discussion of the GKPW formula in section 2.3.3, we dealt with operators that are sourced in the dual CFT by terms $\sim \int d^dx \mathcal{O}\varphi_{(0)}$. In contrast, from (6.6) we can see that the leading contribution of the Kondo coupling to the field theory action in the large N_s limit is the term $\sim \mathcal{O}\mathcal{O}^\dagger$. This is effectively a *double trace deformation* [86, 281–283]. Defining what we will call the *Kondo coupling* [86]

$$\kappa \propto -N_s\lambda_K, \tag{6.18}$$

the holographic prescription to deal with such double trace deformations then yields

$$\alpha \equiv \kappa\beta. \tag{6.19}$$

See also [87] for a detailed discussion of this identification in the Kondo model. Interestingly, one finds that this coupling runs with the energy scale Θ when this scale is changed in (6.17) [282]. In particular, shifting the energy scale as $\Theta_0 \to \Theta_1$ and demanding the physical field $\phi(z)$ to be unchanged in (6.17), we can read off [86]

$$\kappa_1 = \frac{\kappa_0}{1 + \kappa_0 \ln\left(\frac{\Theta_0}{\Theta_1}\right)}. \tag{6.20}$$

Specifically, in the following we will want to use the temperature T as the energy scale describing the RG flow of the Kondo model. To this end we introduce tilded coordinates in which z_H is set to one, i.e. [86]

$$\tilde{z} = z/z_H, \quad \tilde{x} = x/z_H, \quad \tilde{t} = t/z_H. \tag{6.21}$$

As a consequence of these rescalings, we also find [86] that $\tilde{\phi} = \phi$ and $\tilde{a}_t = a_t\, z_H$. Equation (6.14) then yields

$$\tilde{a}_t = \frac{\mathcal{Q}}{\tilde{z}} + \mu_T, \tag{6.22}$$

where we have defined $\mu_T \equiv \mu\, z_H = \mu/2\pi T$ [3]. This means that while keeping z_H fixed in numerical calculations, we can still effectively vary the temperature by varying the coefficient μ_T in the near-boundary expansion of a_t, as only the ratio $\mu_T \sim \mu/T$ is physically meaningful [3, 86]. Similar to (6.17), we define

$$\phi(\tilde{z}) = \alpha_T \sqrt{\tilde{z}} \log(\tilde{z}) + \beta_T \sqrt{\tilde{z}} + \dots \tag{6.23}$$

with $\kappa_T \equiv \alpha_T/\beta_T$ and find

$$\kappa_T = \frac{\kappa(\Theta)}{1 + \kappa(\Theta)\log(\Theta z_H)}. \tag{6.24}$$

This diverges at the Kondo temperature

$$T_{\mathrm{K}} \equiv \frac{\Theta}{2\pi}\, e^{1/\kappa(\Theta)}, \tag{6.25}$$

which satisfies [3]

$$T/T_{\mathrm{K}} = \exp(-1/\kappa_T). \tag{6.26}$$

We hence see that this bottom up-model has the potential to describe the qualitative Kondo-like features expected from a magnetic impurity interacting with a strongly coupled electron system in the large N_s limit, including the formation of a Kondo cloud (condensation of Φ) and the existence of a dynamically generated scale (T_K) [86]. The results to be presented in the following sections will all be derived from this specific model. Hence, although other models for holographic impurities exist [76–85], it will be the bottom-up model discussed above that will for brevity be referred to as *the holographic Kondo model* in this thesis.

6.3 Backreaction in the Kondo model

One of the most interesting aspects about the Kondo effect is the Kondo cloud, and its properties such as size and shape for example. So naturally we should ask how we can investigate the Kondo cloud using the bottom-up model presented in the previous section.

In the heuristic picture 1.1, we have depicted the Kondo cloud as a swarm of electrons surrounding the impurity with anti-aligned spins. Although this is only a naive qualitative picture of the CFT state, it gives us an idea about how the Kondo cloud could manifest itself in terms of objects that can be studied holographically. Namely, in section 3.1 we already saw the simple example of a state (3.8) where two spins are correlated such that they have non-zero entanglement entropy, and similarly we expect that the Kondo cloud should leave an imprint on the pattern of entanglement entropy in the field theory. We have seen in section 3.2 that entanglement entropy is a quantity that can be studied comparably easily in holography, but from the prescription (3.11) it is also clear that we will only obtain non-trivial results on the entanglement entropy in the holographic Kondo model if we include backreaction of the matter fields onto the geometry. How to do this will be the topic of this section, and in the following section 6.4 we will then present and discuss the results that we obtain on the entanglement entropy.

6.3.1 The Israel junction conditions

Looking at the model presented in section 6.2, we first of all note that the only fields that are defined throughout the bulk spacetime are the metric $g_{\mu\nu}$ and the Chern-Simons field A_μ. The latter is topological, and hence does not backreact on $g_{\mu\nu}$. The only remaining matter fields are the scalar Φ and the gauge field a_m which are constrained to live in the worldvolume of a codimension one hypersurface embedded into the bulk spacetime. Naively, they would hence lead to an infinitely thin distribution of mass and energy, or equivalently to an energy-momentum tensor in the three-dimensional Einstein's equations that has a δ-peak like shape. The correct framework to deal with this problem is provided by the *Israel junction conditions* [284], which can be geometrically understood in the following way: The codimension hypersurface on which the matter fields Φ, a_n are defined splits the bulk spacetime into two parts, one to the left of it and one to the right of it, see figure 6.2. To make contact with the topics discussed in chapter 5 (see especially figure 5.1), we will refer to the hypersurface as Q, to the bulk spacetime as N and to the asymptotic boundary as M. Q then splits N into the two parts N_+ and N_- (with metrics $g^\pm$), and similarly M into M_+ and M_-. The embedding of Q into $N_\pm$ is then given by an embedding profile $x_\pm(t,z)$, using coordinates of the Poincaré patch. As in chapter 5, we can choose the boundary condition $x_\pm(0,0) = 0$ without loss of generality, due to the translation invariance of (5.17) in the x-direction.

The Israel junction conditions describe how the two spacetimes $N_\pm$ are glued together along the common hypersurface Q. First of all, the hypersurface Q has to be embedded into the spacetimes $N_\pm$ in such a way that metrics $\gamma^\pm$ on Q that can be induced from the ambient space metrics $g^\pm$ have to be equal: $\gamma^+ = \gamma^- \equiv \gamma$.[3] The equality of the two induced metrics means, amongst other things, that a point on Q given by certain coordinates of N_+ can be identified with a point on Q in terms of coordinates on N_-. It is in this sense

[3] See [285] for an exploration of cases in which this condition is not assumed.

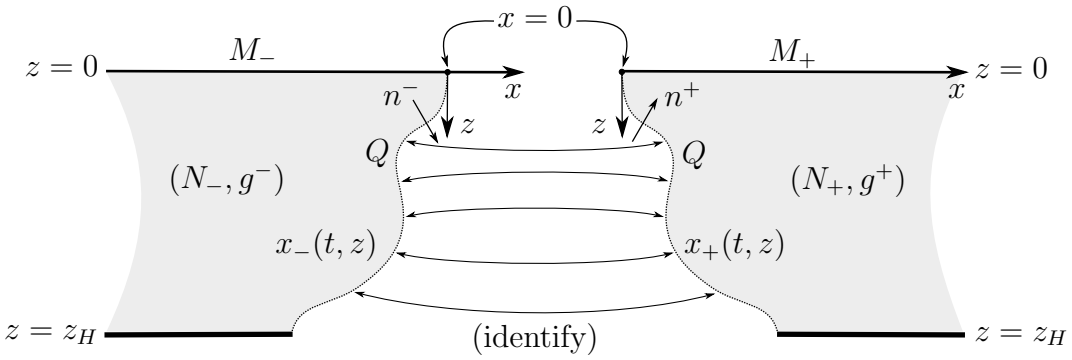

Figure 6.2: Geometric setup of Israel junction conditions. Effectively, two spacetimes are glued together along a common hypersurface Q by identifying points. The figure is presented as in [2].

of identifying points that we claim that the two spacetimes $N_\pm$ are glued together along a common hypersurface Q, see figure 6.2 again.

The role of the "glue" that holds these two spacetimes together along their seam is taken by the energy-momentum of the matter fields living in the worldvolume of Q. Specifically, in the absence of external forces acting on Q, the Israel junction conditions specify that [284, 286]

$$\left\{K^{ij}\right\} S_{ij} = 0, \tag{6.27}$$

$$[K_{ij} - \gamma_{ij} \operatorname{tr} K] = -\kappa_N^2 S_{ij}, \tag{6.28}$$

where $\{A\} \equiv \frac{1}{2}(A^+ + A^-)$, $[A] \equiv A^+ - A^-$ for any tensors $A^\pm$ defined on both sides of the brane. As in chapter 5, S_{ij} is the energy-momentum tensor and γ_{ij} is the induced metric on Q, κ_N^2 the coupling constant in the Einstein equations. See appendix A.2 for a definition of the extrinsic curvature tensor $K_{ij}^\pm$. At this point it is important to point out that equations (6.27), (6.28) are valid for the particular convention that the normal vector of the hypersurface Q is chosen to point from the N_- side to the N_+ side, just as depicted in figure 6.2.

In the following, we will assume the spacetimes $N_\pm$ to be BTZ black holes (5.17) and, crucially, we will assume *symmetric embeddings* with $x_+(t, z) = -x_-(t, z)$, such that $K_{ij}^+ = -K_{ij}^-$. Equation (6.27) is then trivially satisfied while (6.28) reads

$$K_{ij}^+ - \gamma_{ij} K^+ = -\frac{\kappa_N^2}{2} S_{ij}, \tag{6.29}$$

which is identical to (5.2) apart from the factor 1/2. The only difference to the AdS/BCFT models of chapter 5 is then that there, the bulk spacetime was assumed to end on the brane Q, while here we are working with a two sided approach. Hence our results of chapter 5 can be applied to the study of backreaction in the holographic Kondo model.

There are indeed different ways how to derive the Israel junction conditions, and one action-formalism based method (see [287–289]) is to start with an action

$$\begin{aligned}\mathcal{S} = &\frac{1}{2\,\kappa_N^2}\int_{N_+} d^3x\sqrt{-g_+}(R_+ - 2\Lambda_+) + S_{N_+} + \frac{1}{2\,\kappa_N^2}\int_{N_-} d^3x\sqrt{-g_-}(R_- - 2\Lambda_-) + S_{N_-} \\ &+ \frac{1}{\kappa_N^2}\int_{M_+} d^2x\sqrt{-h_+}K^{(h_+)} + S_{M_+} + \frac{1}{\kappa_N^2}\int_{M_-} d^2x\sqrt{-h_-}K^{(h_-)} + S_{M_-} \\ &- \frac{1}{\kappa_N^2}\int_{Q} d^2x\sqrt{-\gamma}K^{(\gamma+)} + \frac{1}{\kappa_N^2}\int_{Q} d^2x\sqrt{-\gamma}K^{(\gamma-)} + S_Q + S_P\end{aligned} \tag{6.30}$$

where we have terms similar to (5.1) both for the N^+ side and the N^- side, coupled to a common boundary Q. This corresponds to our view that the Israel junction conditions describe the gluing of the two spacetimes $N_\pm = M_\pm \cup N_\pm \cup Q_\pm \cup P_\pm$ along the common hypersurface $Q \equiv Q_+ = Q_-$ (intersecting the AdS boundary at $P \equiv P_+ = P_-$, $P_\pm = M_\pm \cap Q_\pm$). The above formula explicitly includes the possibility of matter terms in the ambient spacetime ($S_{N_\pm}$), matter terms on the brane Q (S_Q) as well as boundary and counter terms on the AdS boundary ($S_{M_\pm}$) and on the intersection P, S_P (see [288] and the appendix in [94]). It should also be noted that we have fixed the signs of the extrinsic curvature tensors $K^{(\gamma\pm)}$ according to our usual convention. It can then be shown that (6.30) yields the Israel junction conditions (6.28) [287–289].

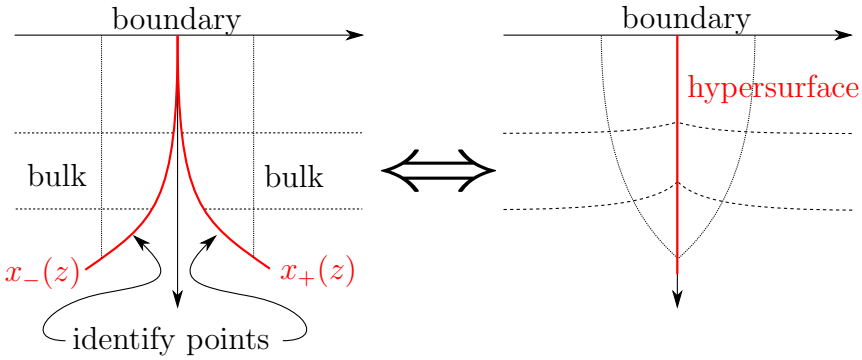

Figure 6.3: Left: Geometric setup with independent coordinate systems on both sides of the brane, as in figure 6.2. Right: Gaussian normal coordinates in which the bulk metric $g_{\mu\nu}$ is continuous at the brane, but not differentiable. The figure is presented as in [3].

As a final comment on the Israel junction conditions, we should note that in the above discussion and derivation it is a priori possible to choose independent coordinate systems in the bulk parts $N_\pm$, as long as the induced coordinate system on Q is the same. This is why the brane has two distinct embedding functions $x_\pm$ with respect to the two bulk parts $N_\pm$ on both sides of it. As an alternative, it is in principle possible to construct *Gaussian-normal coordinates* which cover a vicinity of the brane on both sides of it in a

unified way. To do this, one starts by defining a coordinate system on Q and defines the affine parameter of the geodesics normal to it as the additional coordinate in the higher-dimensional ambient space. This is similar to the construction employed in section 5.3.1. In Gaussian normal coordinates, it is easy to show that the bulk metric $g_{\mu\nu}$ is continuous on the brane, but not differentiable. In fact the discontinuity of the (normal) derivative of the metric on the brane Q is proportional to the expression $K^+_{ij} - K^-_{ij}$. This discontinuity of the first derivative of the metric then leads to a δ-like peak in the curvature tensors at the location of the brane. In Einstein's equations this δ-peak then balances the δ-peak in the bulk energy-momentum tensor $T_{\mu\nu}$ that comes from the worldvolume energy-momentum tensor S_{ij} exactly according to the equation (6.28). See [102] for an extensive discussion of Israel junction conditions in Gaussian normal coordinates. As explained in section 6.2, our bulk spacetime does not only contain the metric $g_{\mu\nu}$ as a dynamical field, but also the CS field A_μ. As this field also couples to the matter localised on the brane, it will enter our calculations with its own junction conditions. These are explained in appendix C, where it is shown that the Chern-Simons field effectively decouples from the fields on the brane.

6.3.2 Equations of motion

The dynamical quantities in the bottom-up bulk model are the fields Φ, a_m, A_μ and, as discussed in the previous section, the embedding profile of the brane $x_+ \equiv -x_-$. The bulk metric $g_{\mu\nu}$ is fixed to be a BTZ background (5.17), which is possible as the CS field does not backreact on the bulk geometry. Furthermore, the CS field A_μ effectively decouples from the rest of the fields as discussed in appendix C. Choosing a static setup where none of the dynamical variables depend on the t coordinate, and choosing a *radial gauge* $a_z = 0$ (which also allows us to set $\psi = 0$, see [3]), the remaining dynamical quantities are then $\phi(z), a_t(z)$ and $x_+(z)$. The equations of motion of this system then read

$$\gamma^{ij}\mathcal{D}_i\mathcal{D}_j\phi - M^2\phi = 0, \tag{6.31}$$

$$\partial_z\sqrt{-\gamma}f^{zt} + J^t = 0, \tag{6.32}$$

$$\mathcal{K}_{ij} - \frac{\kappa_N^2}{2}S_{ij} = 0 \tag{6.33}$$

$$\Leftrightarrow \mathcal{K} = \frac{\kappa_N^2}{2}S \quad \text{and} \quad \mathcal{K}_{L/R} = \frac{\kappa_N^2}{2}S_{L/R}, \tag{6.34}$$

where the current reads $J^m = -2\sqrt{-\gamma}\gamma^{mn}a_n\phi^2$ and the extrinsic curvature quantities $\mathcal{K}_{ij}, \mathcal{K}, \mathcal{K}_{L/R}$ have been defined in (5.26). The energy-momentum tensor following from the worldvolume action (6.12) reads [3]

$$S = \frac{\mathcal{N}}{2}f^{mn}f_{mn} - 2\mathcal{N}V\left(\Phi^\dagger\Phi\right), \quad S_{L/R} = \frac{\mathcal{N}}{2}\widehat{\gamma}^{ij}\left(\mathcal{D}_{(i}\Phi\right)^\dagger\mathcal{D}_{j)}\Phi, \tag{6.35}$$

where $\widehat{\gamma}^{ij}$ was defined in (5.23). At the event horizon, or more accurately at the point where the brane crosses the event horizon, the regularity conditions

$$\phi'(z_H) = -\frac{L^2\, M^2\, \phi(z_H)}{2 z_H}, \quad a_t(z_H) = 0, \quad x'_+(z_H) = \kappa_N^2 \mathcal{N}\, \frac{2L^4 M^2\, \phi(z_H)^2 - z_H^4\, a'_t(z_H)^2}{4L^3} \tag{6.36}$$

have to be imposed [3]. As motivated above, for the study of entanglement entropy we need solutions with non-trivial backreaction, an $\mathcal{K}_{ij}$ that is not perturbatively small. From (6.33), we see that this requires $\kappa_N^2 S_{ij}$ to be of order one in the large N_s limit that the top-down model requires. However, the gravitational coupling constant $\kappa_N^2 = 8\pi G_N$ is of order $1/N_s^2$, and the factor $\mathcal{N}$ in (6.35) is of order N_s. We hence rescale all the fields to be of order $\sqrt{N_s}$, which for consistency is accompanied by a rescaling of the charges q in (6.13). This is effectively the same as fixing $\kappa_N^2 \mathcal{N} = 1$ and $q = 1$, as was done for the numerical calculations of [3]. However, it is important to note that in the next section we will see how the physical properties (specifically energy conditions) of the fields of the bottom-up model constrain the qualitative solutions for the bulk geometry. Consequently, we believe that the solutions found numerically for the choice $\kappa_N^2 \mathcal{N} = 1$ will be qualitatively representative for the behaviour of the system at any value of $\kappa_N^2 \mathcal{N}$. Furthermore, in section 6.5 we will derive a geometrical approximation formula that is only based on the most fundamental geometric properties of the bottom-up Kondo model, and hence does not depend on the specific choices of the parameters made in the numerical calculations of [3].

Solving the equations of motion (6.31)-(6.33), one finds that there is a critical temperature

$$T_c \approx 0.885\, T_K \tag{6.37}$$

below which there is a thermodynamically preferred solution with $\phi(z) \neq 0 \Leftrightarrow \langle \mathcal{O} \rangle \neq 0$, while above T_c the preferred solution is the *normal phase* in which $\phi(z) = 0 \Leftrightarrow \langle \mathcal{O} \rangle = 0$ for any z [3]. This normal phase has an analytical solution due to the normal flow construction, as discussed in section 5.3.1. We then find [3]

$$a_t = \frac{\mathcal{C}}{z_H} \cosh(s) \left(\cosh(s) - \sqrt{(z_H/z)^2 + \sinh^2(s)} \right) \tag{6.38}$$

$$= -\frac{\mathcal{C} \cosh(s)}{z} + \frac{\mathcal{C} \cosh(s)^2}{z_H} \ldots, \tag{6.39}$$

$$x_+(z) = -z_H \operatorname{arctanh} \left(\frac{\sinh(s)}{\sqrt{(z_H/z)^2 + \sinh^2(s)}} \right), \tag{6.40}$$

$$\tanh(s) = \frac{1}{4} \kappa_N^2 \mathcal{N} \mathcal{C}^2, \tag{6.41}$$

where $S_{ij} = -\frac{\mathcal{N}}{2} \gamma_{ij} \mathcal{C}^2$ and $\mathcal{C}$ is the electric flux of the gauge field at the boundary. In the numerical calculations of [3], which lead to the results presented below, we fixed $\mathcal{C} = 1/2$ in order to insure comparability with the results of [86], where the same choice was made.

By comparison with (6.14), we can also read off

$$\mathcal{Q} = -\mathcal{C}\cosh(s) \quad \text{and} \quad \mu = \frac{\mathcal{C}}{z_H}\cosh^2(s) \tag{6.42}$$

from the above near-boundary behaviour. The solution (6.40) satisfies NEC and WEC while violating SEC, as expected from the discussion in section 5.3.1.

It is important to note that for a non-trivial embedding, the line element of the induced metric will read (compare to (6.11))

$$ds^2 = \frac{1}{z^2}\left(-h(z)\,dt^2 + \frac{1 + h(z)\,x'_+(z)^2}{h(z)}\,dz^2\right). \tag{6.43}$$

Equation (6.40) shows that $x'_+(z) \nrightarrow 0$ as $z \to 0$, and consequently the induced metric (6.43) may be asymptotically AdS_2, but the effective AdS radius will depend on $\mathcal{Q}$. This enters the Breitenlohner-Freedman bound of the scalar Φ, and instead of (6.16) we now obtain [3]

$$M^2 = \mathcal{Q}^2 - \frac{1}{4\cosh^2(s)}. \tag{6.44}$$

This reproduces equation (6.16) in the limit of vanishing backreaction, where $\kappa_N^2\mathcal{N} \to 0$.

6.4 Entanglement and defect entropy

Details on how the equations of motion (6.31)-(6.34) can be solved numerically were given in [3] and shall not be repeated here. Instead, we will start right away with the physical interpretation of these solutions in this section. In particular, we will discuss energy conditions and their impact on the geometry in (6.4.2). Section 6.4.2 will then be denoted to a discussion of our findings of entanglement and defect entropy in the Kondo model, while in section 6.4.3 we will discuss the holographic g-theorem.

6.4.1 Energy conditions in the Kondo model

As we have discussed in section 6.3.2 (see also section 5.3.1), the normal phase is described by a gauge field living on Q in the absence of charges, which is effectively a constant tension model (6.40) satisfying WEC and NEC, but violating the SEC. This violation of the SEC is a very important feature of the holographic Kondo model: We want to describe *one* impurity on the boundary which is infinitely extended into the spacelike direction x. This is why in the model without backreaction the brane goes straight from the boundary into the bulk and into the black hole event horizon as depicted in figure 1.1.

If, however, the matter fields living on Q in the holographic model would satisfy both WEC and SEC, we have seen in chapter 5 that this would force the brane to bend back to the boundary in a $\cup$-shaped way, as a consequence of the barrier theorem. This phenomenon of bending back to the boundary would also lead to an effective compactification of the boundary as the x-coordinate would now be restricted to a finite range of values, see [2] for a deeper discussion. Indeed, in section 5.3.2 we have seen several analytic solutions of physical models where precisely this was the case. The fact that the matter fields in the holographic Kondo model of section 6.2 violate the SEC everywhere in the bulk, and the brane consequently shows the phenomenologically desired behaviour of going from the boundary into the event horizon (as a curve of type Q_2 in figure 5.2), should hence be considered a non-trivial consistency check: The model derived and studied in [86] without backreaction in mind still behaves physically reasonable when turning on backreaction. While it is possible to show analytically that the SEC is violated in the normal phase (see section 5.3.1), for the condensed phase this is only possible numerically. We did indeed check that for all numerical solutions discussed in this section, both WEC and NEC are satisfied while the SEC is violated everywhere.

The behaviour of the NEC is especially interesting as we numerically find that $S_{L/R} \to 0$ in both the limits $z \to 0$ and $z \to z_H$. The $z \to 0$ is easy to understand: Near the AdS boundary, the scalar field goes to zero as (6.17)[4] and the contribution of the gauge field (6.39) becomes dominant. Hence we expect that near the boundary, our branes will asymptote to the exact solution for the normal phase (6.40) for any T/T_c. This expectation is indeed verified by our numerical solutions, see figure 6.4. The perhaps more surprising case is the one where $z \to z_H$. Using(6.35), (6.36), (5.23) and (6.43) one indeed finds

$$\widehat{\gamma}^{11} \sim z^2 - z_H^2 = (z - z_H)(z + z_H), \tag{6.45}$$
$$\widehat{\gamma}^{00} \sim (z^2 - z_H^2)^{-1} = (z - z_H)^{-1}(z + z_H)^{-1}, \tag{6.46}$$
$$\phi' \sim const.\,, \tag{6.47}$$
$$\phi \sim const.\,, \tag{6.48}$$
$$a_t \sim z - z_H, \tag{6.49}$$

as $z \to z_H$ and hence $S_{L/R} \to 0$ in this limit. This means that even for $T/T_c \neq 1$ our branes can be approximated by a constant tension brane both in the near-boundary and in the near horizon regime. This will be useful in section 6.5.

The numerically obtained embedding profiles for $x_+(z)$ for different temperatures T/T_c are depicted in figure 6.4. Due to our discussions of sections 5.2.3 and 5.2.4 (see also table 5.1) we have a very clear qualitative understanding of how the energy conditions qualitatively constrain these embedding functions. Due to the violation of the SEC, we will find $x'_+(z) < 0$ everywhere, while due to the NEC the curves bend to the right ($x''_+(z) > 0$) in figure 6.4. Specifically, the more the scalar field Φ condenses, the more positive energy (in the sense of WEC and NEC) the scalar field adds to the worldvolume of the brane, and

[4]Its derivative diverges, but too mildly to make a contribution.

the more the brane bends to the right. This is exactly the behaviour seen in figure 6.4.

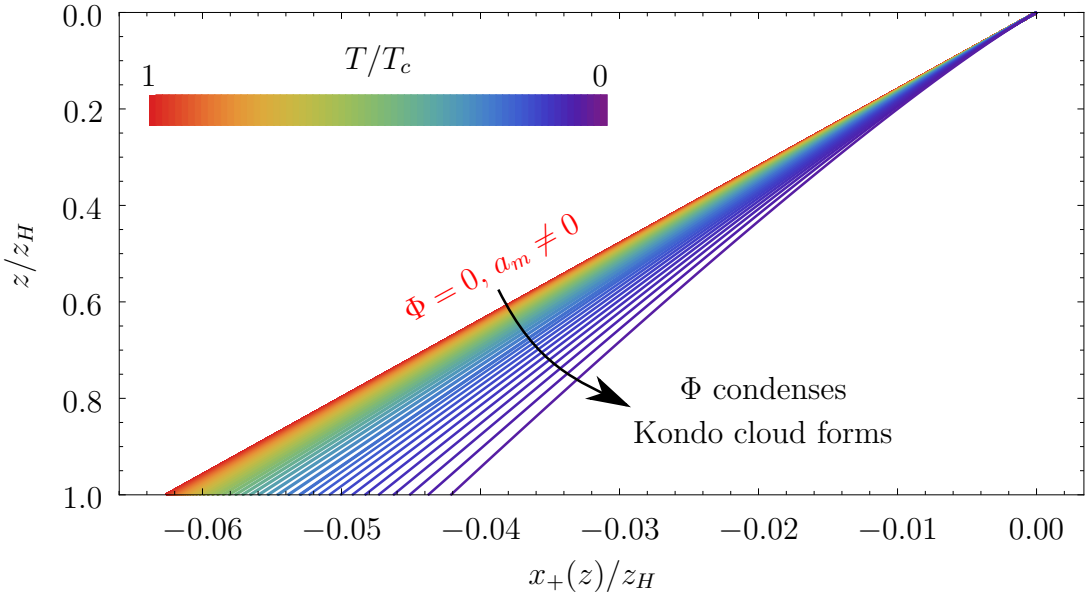

Figure 6.4: Embedding profiles $x_+(z)$ for the embedding of the brane Q into the spacetime N_+, see figure 6.2. At $T = T_c$, the scalar field vanishes everywhere and the embedding is known to be given by the analytical solution (6.40). As the temperature is lowered, the scalar field condenses and the brane bends to the right. The figure is presented as in [3].

6.4.2 Entanglement entropy in the Kondo model

Having numerically calculated the embedding profiles $x_+(z)$ as shown in figure 6.4, it is now possible to holographically calculate entanglement entropy for the holographic bottom-up Kondo model. To do so following the Ryu-Takayanagi prescription introduced in section 3.2, we need to calculate the lengths of spacelike geodesics in the bulk spacetime N. As the bottom-up model includes no backreacting matter in the ambient spacetime parts $N_\pm$, the metrics $g^\pm_{\mu\nu}$ will still be given by the BTZ line element (5.17). In this background, the geodesic equations can be solved analytically, and the only remaining problem is to define correct refraction conditions for curves crossing the brane Q. For example in the setup depicted in figure 6.2, we may be interested in a spacelike geodesic that starts out at a point in M_+, moves through N_+ to a point on Q and then starts moving towards M_- from the corresponding point of Q in N_-. But if the endpoints on $M_\pm$ are fixed as boundary conditions in this geodesic problem, how do we find the correct point on which the geodesic has to cross Q? Alternatively, how do geodesic curves get refracted at Q? Problems like this have indeed been studied before, see for example [290]. Here, we will only employ a very simple geometrical argument: As we have seen in section 6.3.1, it is at least theoretically possible to define a Gaussian normal coordinate system in a neighbourhood to both sides

of the brane, such as on the right hand side of figure 6.3. In such a coordinate system, we would then expect the geodesic curve crossing the brane to be continuous and once differentiable. This means that at the point where the geodesic meets the brane coming from N_+, we decompose its tangent vector into components perpendicular and normal to the brane. On the other side of the brane, the correct refracted tangent vector can then be unambiguously reconstructed from this data and the tangent and normal vectors of the brane in terms of the coordinate system on N_-. As a special case, we note that this implies that curves entering the brane perpendicularly in N_- will also leave it perpendicularly into N_-.

In the following, we will be interested in the entanglement entropy of intervals with length 2ℓ symmetrically centered around the defect, as depicted in figure 1.1. As we also assume a symmetric embedding $x_+(z) = -x_-(z)$ (see figure 6.2), this entire geometrical setup is manifestly mirror symmetric around the defect, and hence the spacelike geodesics then go from the boundary point $x = -\ell$ to $x = \ell$ will cross the brane in a perpendicular manner. As we have seen in section 3.3, the result that we would obtain for an interval of length 2ℓ in a pure BTZ background, where the impurity is absent, is

$$S(\ell)\big|_{\text{Impurity absent}} = S_{BH}(\ell) = \frac{c}{3}\log\left(\frac{1}{\pi\epsilon T}\sinh\left(2\pi T\ell\right)\right). \tag{6.50}$$

In the setup of the holographic Kondo model, by absence of impurity we mean the trivial embedding $x_+(z) = x_-(z) = 0$ of the brane. We can use (6.50) as a reference to compare the entanglement entropy in the holographic Kondo model to, by defining the *impurity entropy*

$$S_{imp}(\ell) \equiv S(\ell)\big|_{\text{Impurity present}} - S(\ell)\big|_{\text{Impurity absent}}. \tag{6.51}$$

This quantity has the useful property of being manifestly finite, as both $S(\ell)\big|_{\text{Impurity present}}$ and $S(\ell)\big|_{\text{Impurity absent}}$ diverge in the same way $\sim \log(\epsilon)$ visible in (6.50) for example. Impurity entropy (6.51) was studied in the field theory literature on the Kondo effect before [88–91], and the approximative result for small temperatures and large interval sizes was derived in [90] to be

$$S_{imp} = \frac{\pi^2 c\,\xi_{\mathrm{K}} T}{6v}\coth\left(\frac{2\pi\ell T}{v}\right) = \frac{\pi^2 c}{6}\frac{T}{T_{\mathrm{K}}}\coth\left(2\pi\frac{\ell}{\xi_{\mathrm{K}}}\frac{T}{T_{\mathrm{K}}}\right) \quad \text{for} \quad T/T_{\mathrm{K}},\ \ \xi_{\mathrm{K}}/\ell \ll 1. \tag{6.52}$$

Here, as before, T_K is the Kondo temperature, v is the Fermi velocity, and $\xi_K = v/T_K$ is the *Kondo scale* [90]. Our numerical results for $S_{imp}(\tilde{\ell})$ are plotted in figure 6.5. As in the numerics of [3] the event horizon coordinate z_H was set to one, we show our results as functions of the tilded coordinates introduced in (6.21). There are several qualitative features in this figure that we can easily interpret based on the findings of the previous sections and chapters.

- First of all, we see that for $T = T_c$ where the scalar field is still uncondensed the impurity entropy $S_{imp}(\tilde{\ell})$ is constant. This is due to the fact that in this case the

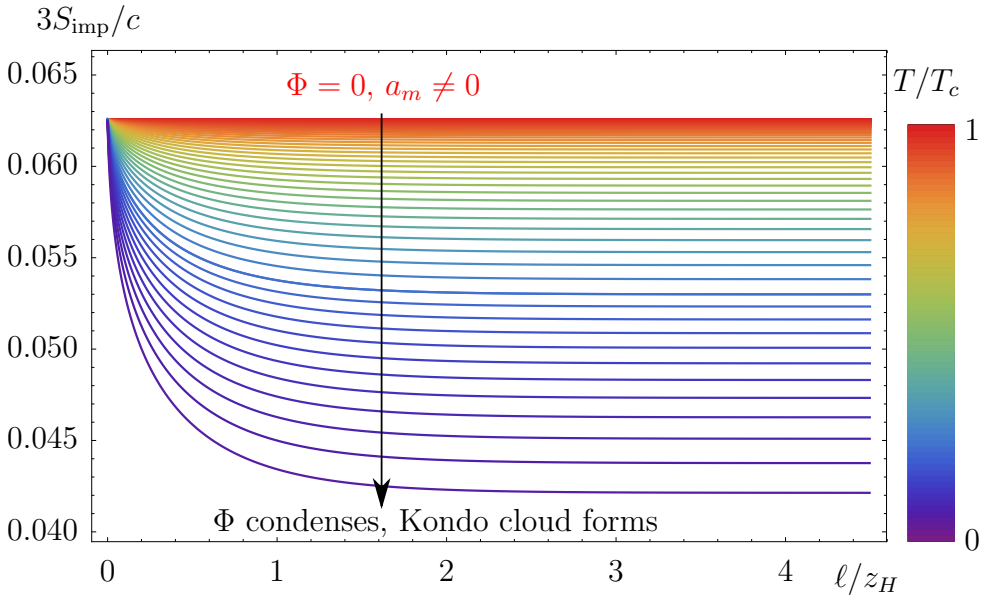

Figure 6.5: Impurity entropy S_{imp} as a function of $\tilde{\ell} = \ell/z_H$ for different values of T/T_c. For $T/T_c = 1$, the embedding profile $x_+(z)$ is given by the constant tension solution (6.40) and consequently $S_{imp}(\tilde{\ell})$ is a constant, see section 5.3.1. As the temperature is lowered, we see that $S_{imp}(\tilde{\ell})$ decreases for fixed $\tilde{\ell}$. The figure is presented as in [3].

embedding is given by the constant tension solution (5.37), see section 6.3.2. We have seen in section 5.3.1 that due to the normal flow construction, the effect of constant tension solutions is to add a tension-dependent extra length to all normal geodesics resulting in (5.38). From (6.40) one can then analytically calculate

$$\frac{3}{c} S_{imp}\left(\tilde{\ell}, T = T_c\right) = \operatorname{arctanh}\left(\frac{\kappa_N^2 \mathcal{N} \mathcal{C}^2}{4}\right) = \operatorname{arctanh}\left(\frac{1}{16}\right) \approx 0.0626 \tag{6.53}$$

for our numerics where we have chosen $\kappa_N^2 \mathcal{N} = 1$, $\mathcal{C} = 1/2$ and $L = 1$. This is precisely the value that can be read off from figure 6.5.

- Secondly, for fixed values of $\tilde{\ell}$ we see that $S_{imp}(\tilde{\ell})$ decreases as the temperature T/T_c decreases. Geometrically, this is clear from figure 6.4. As explained in section 6.4.1, the more the temperature is lowered, the more the scalar field condenses and the more the branes bend to the right in figure 6.4. This is a direct consequence of the NEC satisfied by the scalar field. Note that figure 6.4 shows the embedding profile $x_+(z)$, this means that the points to the right of the branes in that figure are part of the physical spacetime, while the points to the left of it are cut away, as in figures 6.2 and 6.3. This means that, for decreasing temperature, the volume of the bulk spacetime is decreased as bulk points are lost when the brane sweeps past them from the left. In section 6.6 we will investigate this volume loss phenomenon in more detail. As far as entanglement entropy is concerned, it is intuitively clear that as the branes bend to the right, the distance that geodesics travel from the boundary to

the brane decreases. Consequently, the decrease of $S_{imp}(\tilde{\ell})$ as T/T_c is decreased is a direct geometric consequence of the NEC. We interpret this reduction of entanglement entropy as a holographic sign of the Kondo cloud acting as a *screening cloud*. The more the scalar field condenses and the more the Kondo cloud forms, the less impact of the impurity can be seen for a given fixed distance $\tilde{\ell}$.

- Thirdly, we see that in the limit $\tilde{\ell} \to \infty$ the curves for $S_{imp}(\tilde{\ell})$ go to a constant limiting value. This again has a very simple geometrical interpretation. In section 3.3 we saw (see figure 3.3) that for very large boundary intervals, the corresponding bulk entangling curves move almost tangentially to the event horizon. In the limit $\tilde{\ell} \to \infty$ the impurity entropy is then given by the additional strip of the event horizon that appears in the bulk spacetime (compared to the BTZ result) due to the non-trivial embedding of the branes:

$$S_{imp}(\tilde{\ell} \to \infty) = \frac{c}{3} \cdot (-\tilde{x}_+(z_H)). \tag{6.54}$$

  In section 6.4.3 we will interpret this quantity in terms of the *holographic g-theorem*.

- Lastly, by plotting the quantity $S_{imp}(\tilde{\ell}) - S_{imp}(\infty)$ in the log-plot 6.6, we see that the curves in figure 6.5 show an exponential falloff behaviour towards the constant limiting value for large $\tilde{\ell}$. In fact, within very good numerical accuracy this exponential falloff behaviour is of the form $const.(T) \cdot e^{-2\tilde{\ell}}$. This is precisely the behaviour expected from the formula (6.52), see section 6.5 for a more detailed discussion of the geometrical origin of this behaviour and the extend to which we can (hope to) reproduce (6.52) in the holographic Kondo model. The general decrease of $S_{imp}(\tilde{\ell})$ with growing $\tilde{\ell}$ for fixed T/T_c can again be interpreted as a sign of the impurity being screened by the Kondo cloud. The larger the distance to the Kondo cloud, the smaller its effect seems to be on the entanglement entropy. Geometrically, for small interval sizes $\tilde{\ell}$ the corresponding bulk geodesics will cross the brane close to the boundary, while for large $\tilde{\ell}$ they would cross the brane close to the event horizon. As the branes all asymptote to the T/T_c solution near the boundary (see figure figure 6.4 and the discussion in section) but bend increasingly to the right in the bulk as a consequence of the NEC, it is not a surprise that in figure 6.5 the curves all start from the same value for $\tilde{\ell} = 0$ but decrease with growing $\tilde{\ell}$.

We have seen in this section that just as the bulk geometry is qualitatively constrained by the energy conditions of the system and the basic geometric setup of the model, the same statement applies to the impurity entropy. In the next section, we will briefly discuss how the impurity entropy can be used to monitor the RG flow that the Kondo system undergoes as the temperature is lowered, and how this is related to the g-theorem.

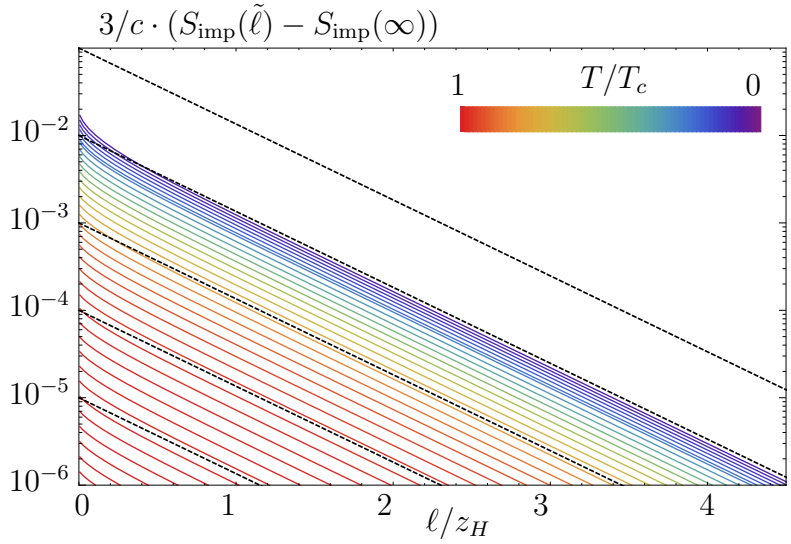

Figure 6.6: Exponential falloff behaviour of $S_{imp}(\tilde{\ell}) - S_{imp}(\infty)$ for large $\tilde{\ell}$. The dashed lines show curves of the form $const. \cdot e^{-2\tilde{\ell}}$ as comparison. The figure is presented as in [3].

6.4.3 The holographic g-theorem

As said in the introduction, there have been numerous holographic studies of RG flows and the corresponding c, a and F-theorems, see for example [45–49]. For BCFTs, a similar statement is the *g-theorem* [92, 257, 291, 292], which states that along the RG flow from the UV to the IR, the effective number of impurity degrees of freedom (measured by the impurity entropy) ought to decrease.

We will now discuss this in the context of the holographic Kondo model. In section 3.3 it was already discussed that in the limit of large boundary intervals ($\tilde{\ell}$) the entanglement entropy reproduces the extensive thermodynamic entropy of the boundary theory. Later in section 6.4.2 we have seen that in the same limit, the impurity entropy goes to a constant limiting value (6.54) proportional to the additional area of the event horizon that appears in the bulk spacetime due to the non-trivial embedding of the brane. This limiting value $S_{imp}(\tilde{\ell} \to \infty)$ should hence be interpreted as the contribution of the impurity to the entropy of the entire system compared to the system without an impurity, and we hence define

$$\ln(g) \equiv S_{imp}(\ell \to \infty). \tag{6.55}$$

From (6.54) we see that this quantity is positive due to the fact that $\tilde{x}_+(z_H) < 0$ (see figure 6.4) which in turn is a direct consequence of the violation of the SEC, see table 5.1. In fact, as we have seen in sections 5.2.3 and 5.2.4, the fact that the brane enters the event horizon at all, and consequently that (6.54) can be defined, is a result of the violation of either WEC or SEC.

Interpreting now the temperature T as the energy scale of the RG flow that the Kondo model undergoes, it was shown in [292] that the g-theorem is equivalent to an increase of

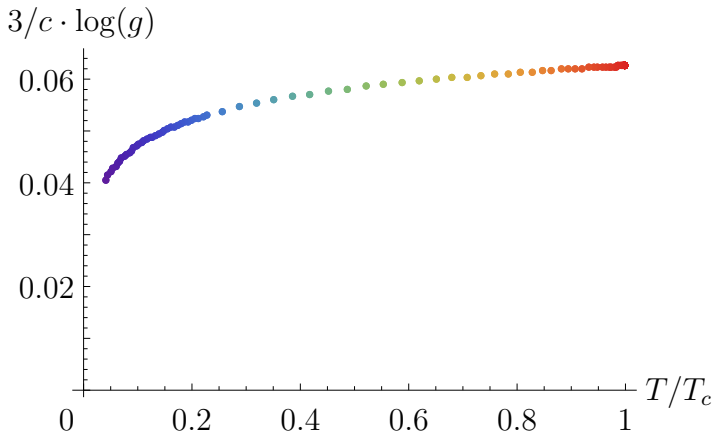

Figure 6.7: Boundary entropy $\ln(g) \equiv S_{imp}(\ell \to \infty)$ as a function of T/T_c. The figure is presented as in [3].

the impurity entropy with T,

$$T \cdot \frac{\partial}{\partial T} \ln(g) > 0. \tag{6.56}$$

As can be seen in figures 6.5 and 6.7, this is indeed the case in the holographic Kondo model. We discussed in section 6.4.2 that in fact $S_{imp}(\tilde{\ell})$ decreases with decreasing temperature for any fixed $\tilde{\ell}$, be it large or small, as a consequence of the NEC. We have hence shown that the holographic Kondo model satisfies the g-theorem which was expected not only from the field theory side, but also from the holographic side. Holographic proofs of the g-theorem were given in [92, 291], both employing the NEC. Especially, the g-theorem was already proven for certain BCFT models of the type introduced in section 5.1 and studied throughout this thesis in [92]. There, it was shown that the NEC implies the g-theorem for branes embedded in locally AdS background spacetimes where the radial bulk coordinate is interpreted as the inverse energy scale of the RG flow, according to the UV/IR connection. As large bulk coordinates z are in the calculation of entanglement entropy related to large boundary intervals $\tilde{\ell}$, and as $S_{imp}(\tilde{\ell})$ are monotonously decreasing functions in figure 6.5, we immediately realise that this interpretation of the g-theorem also holds in the holographic Kondo model, as required by the proof in [92].

6.5 An analytical approximation formula for entanglement entropy

After discussing the numerical results depicted in figure 6.5 in the last section, we will now derive a semi analytical approximation formula for the impurity entropy $S_{imp}(\tilde{\ell})$ for large $\tilde{\ell}$. The core observation motivating this is the one made in section 6.4.1 that the non trace

part of the energy-momentum tensor, $S_{L/R}$, goes to zero both near the boundary and near the black hole event horizon. In this section, we will hence approximate the brane near the event horizon by fitting a constant tension brane (with $S_{L/R} = 0$ for any z) to it as depicted in figure 6.8.

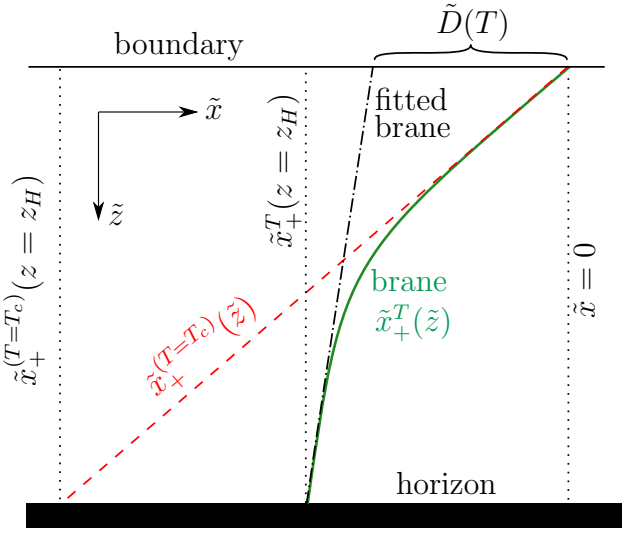

Figure 6.8: Geometrical setup for the derivation of an analytical approximation formula for $S_{imp}(\tilde{\ell})$ for large $\tilde{\ell}$. Although all constant tension branes are curves of the form (6.40) in a BTZ background they are sketched as straight lines in this figure. This is justified because for the scale chosen e.g. in figure 6.4, the curvature of the constant tension solutions would not be visible to the eye. For $T < T_c$, the brane with embedding profile $\tilde{x}_+^T(\tilde{z})$ asymptotes to $\tilde{x}_+^{T=T_c}(\tilde{z})$ near the boundary and can be approximated by a constant tension brane near the event horizon. This fitted brane will reach the boundary at the position $\tilde{x} = -\tilde{D}$. The figure is presented as in [3].

Such a constant tension brane will depend on only two parameters: its tension λ and the position at which it is anchored at the AdS boundary, $\tilde{x} \equiv -\tilde{D}$. Constant tension solutions and the way of constructing them via a geodesic normal flow were already discussed in section 5.3.1. Using the nomenclature suited for the study of the Kondo model in this section, we can write equation (5.38) as

$$S_{EE}^{\lambda}(\ell) = S_{BH}(\ell) + C(\lambda). \tag{6.57}$$

It should be noted however that this formula is only valid for intervals with length 2ℓ symmetrically centered around the defect, which is supposed to be the point where the brane meets the boundary. For convenience, this was chosen to be $x = 0$ so far, see e.g. figure 6.4. In figure 6.8 however, we see that the brane is anchored to the boundary at $x = -D$, effectively broadening distance between the endpoint of the brane and the endpoints of the interval. The correct approximation formula thus reads

$$S_{EE}^{\lambda,D}(\ell) = S_{BH}(\ell + D) + C(\lambda). \tag{6.58}$$

Using this approximation as well as (6.50), the impurity entropy (6.51) can then be written as

$$S_{imp}(\ell) = C(\lambda) + \frac{c}{3}\log\left(\frac{\sinh\left(2\pi T(\ell+D)\right)}{\sinh\left(2\pi T\ell\right)}\right) \tag{6.59}$$

$$\to C(\lambda) + \frac{c}{3}\left[2\pi TD + \left(1-e^{-4\pi TD}\right)e^{-4\pi T\ell} + \mathcal{O}\left(e^{-8\pi T\ell}\right)\right] \quad \text{for} \quad \ell T \gg 1 \tag{6.60}$$

$$\sim C(\lambda) + \frac{2\pi c}{3}TD\left[1+2e^{-4\pi T\ell} + \mathcal{O}\left(e^{-8\pi T\ell}\right)\right] \text{ for } \ell T \gg 1 \text{ and } DT \ll 1. \tag{6.61}$$

As $4\pi T\ell = 2\ell/z_H = 2\tilde{\ell}$, this semi-analytical approximation formula immediately explains the exponential falloff behaviour found in section 6.4.2 and seen in figure 6.6. Furthermore, the temperature dependent prefactor of the exponential falloff of the curves in figure 6.6 is identified to be $1-e^{-4\pi TD}$ by (6.60). This can indeed be checked to be true in our numerical data. Equation (6.60) is hence already an important result, but as (6.61) indicates, this investigation can be brought further by assuming D to be small compared to both ℓ and z_H. We can then even write

$$S_{imp}(\ell) = C(\lambda) + S_{BH}(\ell+D) - S_{BH}(\ell) \tag{6.62}$$

$$\approx C(\lambda) + D\cdot\partial_\ell S_{BH}(\ell) \tag{6.63}$$

$$\approx C(\lambda(T)) + \frac{2\pi c}{3}TD(T)\coth\left(2\pi T\ell\right) \text{ for } \ell T \gg 1 \text{ and } DT \ll 1, \tag{6.64}$$

thereby identifying the series expansion in (6.61) as the one of a coth.[5] In (6.64) we have reinstated that the temperature dependent fit-parameters λ and D are of course also dependent on the temperature. Equation (6.64) lends itself to immediate comparison with the field theory approximation formula [90]

$$S_{imp} = \frac{\pi^2 c\,\xi_{\mathrm{K}}T}{6v}\coth\left(\frac{2\pi\ell T}{v}\right) = \frac{\pi^2 c}{6}\frac{T}{T_{\mathrm{K}}}\coth\left(2\pi\frac{\ell}{\xi_{\mathrm{K}}}\frac{T}{T_{\mathrm{K}}}\right) \text{ for } T/T_{\mathrm{K}},\ \xi_{\mathrm{K}}/\ell \ll 1 \tag{6.52}$$

in four aspects:

- First of all, the formula (6.64) includes the constant offset term $C(\lambda)$ which is not present in (6.52). However, as λ is implicitly dependent on the temperature, it may vanish for small T depending on the details of the model. We will have to say more about the low temperature behaviour of the holographic Kondo model in the remainder of this section as well as in the next one.
- Secondly, we see that the arguments of the coth agree in both (6.64) and (6.52) if the Fermi velocity v is set equal to one, the speed of light, in the latter. This is

[5] Using a Poincaré instead of a BTZ background we can derive a similar approximation formula for the $T=0$ case. In particular, in this case $S_{AdS}(\ell) = \frac{c}{3}\log(\frac{2\ell}{\epsilon})$ and $D\cdot\partial_\ell S_{AdS}(\ell) = \frac{cD}{3\ell}$ lead to a similar formula to the zero-temperature result $S_{imp} = \frac{\pi c}{12}\frac{\xi_{\mathrm{K}}}{\ell}$ for $\ell \gg \xi_{\mathrm{K}}$ derived in [88–91]. Comparing this to (6.52) respectively (6.64), we note that the limits $T\to 0$ and $\ell\to\infty$ do not commute.

precisely the appropriate choice in the Kondo model as it is based on *massless* chiral fermions, see [86]. As is obvious from (6.60), the form of this argument determines the exponential falloff seen in section 6.4.2. In contrast to (6.52) which is valid for $T/T_K \ll 1$, this prediction of our geometrical analysis is expected to be valid for any (not necessarily small) temperature T, an expectation numerically verified by our results in figure 6.6.

- Thirdly, we can compare the prefactors of the coth terms in (6.64) and (6.52). If we set $v = 1$ as discussed above, the comparison of these two factors suggests the identification

$$D(T) \approx \frac{\pi}{4}\xi_{\mathrm{K}} \Leftrightarrow \tilde{D}(T) \approx \frac{\pi^2}{2}\xi_{\mathrm{K}} T \tag{6.65}$$

  for small T, i.e. a proportionality between the geometric bulk length scale D and the Kondo scale ξ_K.

- Lastly, an important aspect of the approximation formulas (6.64) and (6.52) that should be compared are their respective ranges of validity. In (6.64), we have stated the condition

$$\ell T \gg 1 \quad \text{and} \quad DT \ll 1. \tag{6.66}$$

  This is necessary because the constant brane approximation depicted in figure 6.8 only yields reliable results for the entanglement entropy when the bulk entangling curves meet the brane close to the event horizon, i.e. for $\ell T \gg 1$. The condition $DT \ll 1$ is then necessary for the series (6.60) so simplify to (6.61), which is the series expansion of the coth in (6.64). In contrast, (6.52) was derived in [90] under the assumptions

$$T/T_{\mathrm{K}} \ll 1 \quad \text{and} \quad \xi_K/\ell \ll 1. \tag{6.67}$$

  Even with the identification $D \sim \xi_K \sim 1/T_K$ due to (6.65), we see that these sets of inequalities (6.66) and (6.67) are not equivalent. Specifically, while the condition $T/T_K \ll 1$ is part of both (6.66) and (6.67), the condition involving ℓ differs between the two as in (6.66) ℓ is compared to $1/T$ while in (6.67) it is compared to $1/T_K$. From (6.66) it can be shown that

$$T \gg 1/\ell \;\Rightarrow \xi_K/\ell \ll T/T_K \ll 1. \tag{6.68}$$

  This means that with the identification (6.65), (6.67) follows from (6.66), but (6.66) is stronger because it implies the additional hierarchy $\xi_K/\ell \ll T/T_K$.

Of course, the Kondo model studied in this chapter is only a bottom-up model, and is hence only expected to give qualitative insight into the properties of the "real" Kondo effect, nevertheless it is interesting how (6.65) seems to suggest a connection between the length scale ξ_K of the Kondo cloud and the geometrical quantity D defined in figure 6.8. In

fact, the geometrical definition of D is so simple that in principle its approximate values can be read off from figure 6.4 using a straight edge. It hence seems worthwhile to investigate the possible relation (6.65) in more detail. Especially, we should investigate whether in our numerical solutions $\tilde{D}(T)$ becomes a linear function at low T. If this was the case, we could argue that $D(T=0)$ is then a measure for the size ξ_K of the Kondo cloud, up to a factor of order one.

Unfortunately, this is not the case as the plot 6.9 of our numerical values of $\tilde{D}(T)$ shows. However, in order to assess this result we need to find out how the temperature T has to be made before we can even expect a proportionality of the form (6.65). As we will now show, there is an upper bound on the value of $\tilde{D}(T)$ in the holographic model, and consequently, there is an upper bound on the temperatures T for which equation (6.65) can in principle hold. After all, we have stated before that (6.52) and similar formulas only hold for $T/T_K \ll 1$, but in the remainder of this section we will try to answer what the $\ll$ in this expression quantitatively means, i.e. how small is small enough in this context. The argument for this is based on the fact that $\tilde{x}_+(z_H)$ can only increase as T/T_c decreases. This can be seen in figure 6.4, and as discussed in sections 6.4.2 and 6.4.3, this is a direct consequence of the NEC being satisfied by the condensing scalar field. Furthermore, according to table 5.1 the violation of the SEC implies $\tilde{x}'_+(z_H) < 0$. Using these simple facts, it then becomes clear from the sketch 6.8 that

$$\tilde{D}(T) \leq |\tilde{x}_+^{(T)}(z_H)| \leq |\tilde{x}_+^{(T=T_c)}(z_H)|. \tag{6.69}$$

We know from sections 6.4.2 and 6.4.3 that the latter quantity is proportional to the boundary entropy in the uncondensed phase and using (6.53) this yields the bound

$$\tilde{D}(T) \leq |\tilde{x}_+^{(T=T_c)}(z_H)| = \frac{3}{c} \ln\left(g^{(T=T_c)}\right) \approx 0.0626 \tag{6.70}$$

for our numerics. The formula (6.65), predicting $\tilde{D}(T)$ to grow linearly with T for small T can hence *at most* be a good approximation to the behaviour of $\tilde{D}(T)$ until a temperature T^* is reached at which the bound (6.70) is violated. Writing (6.65) as $\tilde{D}(T) \sim const.\frac{T}{T_c}$ with (using (6.37)) $const. = \pi^2 T_c/(2T_\mathrm{K}) \approx 4.37$ this yields that the linear behaviour of $\tilde{D}(T)$ can under no circumstances be seen for temperatures

$$\frac{T}{T_c} \gtrsim \frac{T^*}{T_c} \approx 0.014. \tag{6.71}$$

This is however just a crude estimation, and realistically we would expect that we have to go orders of magnitude below (6.71) in order to numerically check the validity of relation (6.65) in the bottom-up model. See figure 6.9. Unfortunately, as this figure shows it was not possible to investigate the holographic Kondo model at low enough temperatures, due to numerical problems. We can at the present time neither confirm nor exclude a behaviour of the form (6.65) in the holographic Kondo model. We will have to say more about the behaviour of the holographic Kondo model at small temperatures in section 6.7.

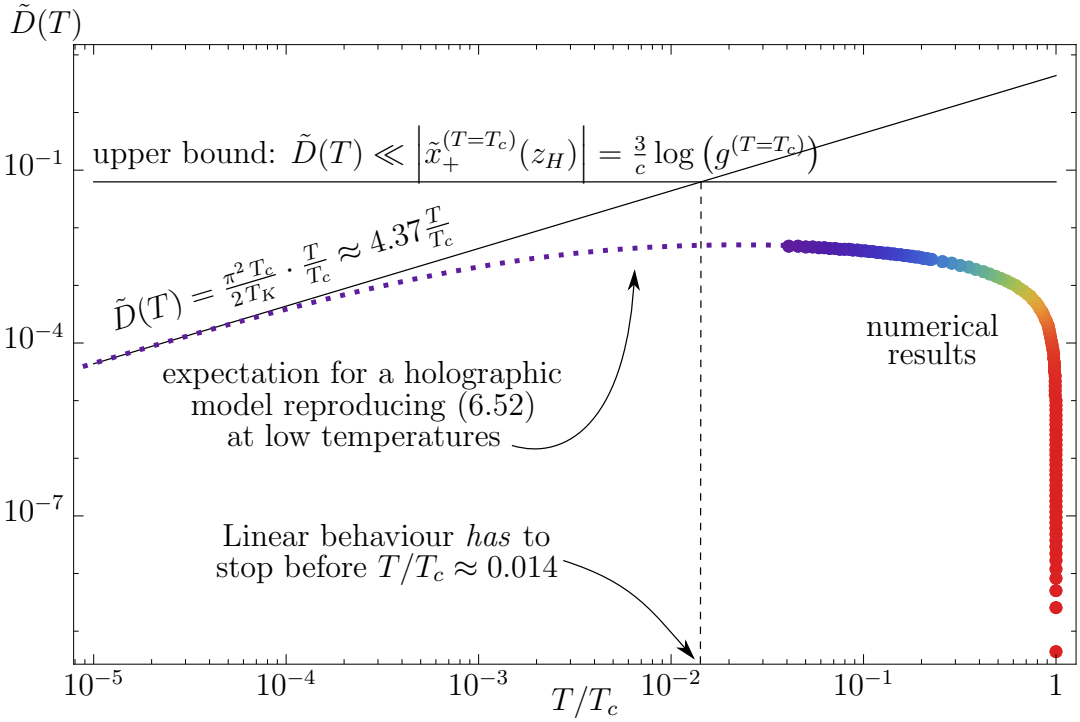

Figure 6.9: The thick points represent the fitted values of $\tilde{D}$ for various temperatures in our numerical results. The dotted line is a sketch of how the behaviour may look like in a realistic Kondo model that exactly reproduces (6.52) at low temperatures. We also indicate the upper bound (6.70), the corresponding temperature bound (6.71) and a line indicating the expected small temperature behaviour $\tilde{D}(T) = \frac{\pi^2}{2}\frac{T}{T_K}$. The figure is presented as in [3].

The bounds discussed in this section are in themselves an interesting result, as they constrain the range of validity of approximation formulas for low temperatures in terms of high temperature quantities such as $\frac{3}{c}\ln\left(g^{(T=T_c)}\right)$. In fact, the temperature bound (6.71) that was derived from the bulk geometry of the holographic Kondo model can equivalently be derived purely in field theory terms. To do so, note that $\coth(x) \to 1$ as $x \to \infty$. The formula (6.52) would hence, if it were valid for any T, predict a linear increase of $\frac{3}{c}\ln\left(g^{T}\right)$ with T. However, by the g-theorem this quantity has to be bounded by $\frac{3}{c}\ln\left(g^{(T=T_c)}\right)$, leading to the realisation that (6.52) cannot be valid above temperatures (6.71).

To end this section, we should point out that although we were not able to numerically investigate the holographic Kondo model at low enough temperatures, both results (6.52) and (6.64) are very general, and not dependent on specific properties of the Kondo system. In fact, (6.52) was derived in [90] by general CFT methods, and the derivation of (6.60) and (6.64) was based on the general geometrical properties of AdS/BCFT approaches of the type proposed in [92–94]. We hence expect that these results are *universal* in the sense that they can be applied to a large range of holographic models, irrespective of their specific details.

6.6 An outlook on complexity

In chapter 3 we have outlined the deep holographic connection between entanglement entropy and bulk geometry. This connection has then be studied and employed in the later chapter 4 as well as in sections 5.2.3 and 6.4.2-6.5. Now, we will look into another quantity related to quantum information in the field theory that can be, according to recent proposals [95–101], calculated from the bulk geometry. This quantity is *computational complexity*.

Ideas relating to computational complexity seem to have entered gravitational physics in discussions concerning the *firewall paradox* [293] in the works [95, 294] where a connection between complexity and bulk geometry was envisioned. See [295] for a review purely from the quantum information theory point of view. Following the definition of [96] (see also [95,98]), *computational complexity* is defined as the minimal number of simple unitary operations that have to be carried out by a quantum computer in order to implement a given unitary operation on a simple initial state, or to create a given state from a simple initial state. Based on the findings of [95, 96], it was then suggested in [98, 99] that holographically, complexity $\mathfrak{C}$ should be measured by the volumes $\mathcal{V}$ of certain spacelike codimension one hypersurfaces, i.e.

$$\mathfrak{C} \propto \frac{\mathcal{V}}{LG_N}. \tag{6.72}$$

In the proposal of [99] for example, in a setup as depicted in figure 3.1, the complexity of the state of the subsystem A would be assumed to be proportional to the volume $\mathcal{V}$ of the spacelike hypersurface $\mathcal{F}$. A proposal similar to (6.72) was made in [101] for a quantity referred to as *quantum information metric* or *fidelity susceptibility*. Interestingly, the paper [101] also employed a thin brane ansatz similar to the AdS/BCFT models introduced in section 5.1, although they used spacelike branes Q. It was argued in [100, 296] that computational complexity $\mathfrak{C}$ should more accurately be calculated from the integral of the bulk action over a certain bulk region. However, the simple approximation formula (6.72) has continued to attract interest in the holography community, see [297–299].

In the above section 6.4.2, we dealt with entanglement entropy in the holographic Kondo model, which is a divergent quantity regulated by the boundary cutoff ϵ. Impurity entropy (6.51) on the other hand was defined in such a way that the divergencies cancel and the leftover quantity is finite and has a well-defined physical meaning. We will now try to obtain a similar notion of *impurity complexity*, or as we will call it, *relative complexity* $\mathfrak{C}_{rel}$. As we see from the definition (6.72), the complexity will be a divergent quantity due to contributions from the part of the bulk spacetime near the boundary. To cancel these contributions, we define

$$\mathfrak{C}_{rel}(T) \propto \mathcal{V}^T - \mathcal{V}^{T=T_c}, \tag{6.73}$$

where $\mathcal{V}^T$ is meant to be the volume of the (codimension one) equal time slices of our bulk geometry. In short, we define the relative complexity to be proportional to the loss of bulk

volume compared to $T = T_c$. We discussed in sections 6.4.1 and 6.4.2 that this loss of bulk volume is a direct geometrical consequence of the NEC satisfied by the scalar field Φ. The overall sign is chosen such that $\mathfrak{C}_{rel}(T)$ decreases with T, due to the hope that there might be a complexity analogue to the g-theorem discussed in section 6.4.3. The induced metric on an equal time slice of the BTZ black hole (5.17) reads

$$ds^2 = \frac{1}{z^2}\left(dx^2 + \frac{dz^2}{1-\frac{z^2}{z_H^2}}\right), \tag{6.74}$$

and consequently we find

$$\mathfrak{C}_{rel}(T) \propto \mathcal{V}^T - \mathcal{V}^{T=T_c} = \int_\epsilon^{z_H} dz \frac{1}{z^2\sqrt{1-\frac{z^2}{z_H^2}}} \int_{x^T(z)}^{x^{T=T_c}(z)} dx \tag{6.75}$$

$$= \int_\epsilon^{z_H} dz \frac{x^{T=T_c}(z) - x^T(z)}{z^2\sqrt{1-\frac{z^2}{z_H^2}}}. \tag{6.76}$$

A priori, this quantity might be divergent in the limit $\epsilon \to 0$[6], but as we have discussed in section 6.4.1 and seen in figure 6.4, the scalar field on the branes falls off so fast near the boundary that the branes all approach $z = 0$ with the same leading (linear) behaviour. This then means that the quantity (6.76) is in fact finite, see figure 6.10 for a plot. Indeed we see that $\mathfrak{C}_{rel}$ decreases monotonously along the RG flow, as expected. Whether this is related to the g-theorem or whether this is a general feature of holographic RG flows might be an interesting question for future research.

It should be noted that although $\mathfrak{C}_{rel}$ is finite in the holographic Kondo model, it is much more sensitive to the near-boundary behaviour of the branes than for example $S_{imp}(\tilde{\ell} \gg 1)$: If the curves $x(z)$ would *not* approach the boundary with the same slope $x'(0)$, S_{imp} would still be a finite quantity, but $\mathfrak{C}_{rel}$ would not. This is due to the possible divergence of the integral (6.76) at the lower bound $\epsilon \to 0$, which does only not contribute due to the well-behaved near-boundary behaviour of the branes. The quantity (6.76) is also more sensitive to the behaviour of the brane at intermediate values of $0 < z < z_H$ than $S_{imp}(\tilde{\ell} \gg 1)$. While our discussion in section 6.5 showed that the behaviour of $S_{imp}(\tilde{\ell})$ for large $\tilde{\ell}$ can be described by an approximation formula only involving the two parameters $C(\lambda)$ and D, no similar universal formula can be derived for $\mathfrak{C}_{rel}(T)$. Although the idea of monitoring the change of complexity along an RG flow is a qualitatively appealing one, the above discussion raises concerns about how useful the investigation of (relative) complexity will in practice be for the holographic study of RG flows. Especially, the absence of a universal approximation formula for low temperatures is problematic, as in bottom-up AdS/CFT it are often the universal features of a system that are of interest, as they can be compared

[6]Near the event horizon the integrand also diverges, but only very mildly and consequently the integral converges at the upper bound.

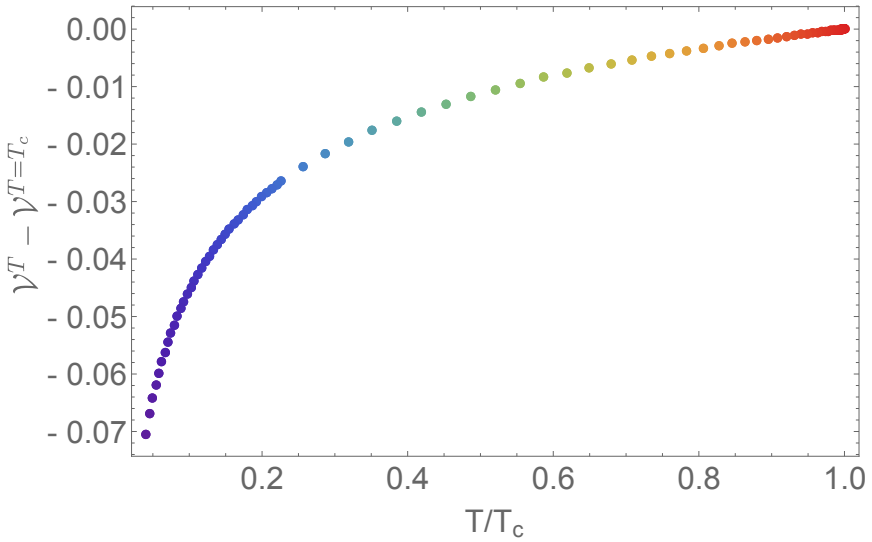

Figure 6.10: Relative complexity as defined in (6.76) shown as a function of T/T_c. Although, as discussed in the text, in the Kondo model this quantity is by definition finite as $\epsilon \to 0$, we have calculated these points using an explicit cutoff $\epsilon = 10^{-10}$ in order to avoid numerical problems.

between gravity and field theory side even if the proposed holographic duality is not exact. We hence leave a further study of holographic computational complexity using either the prescription (6.72) of the more involved action integral proposal of [100, 296] for future research.

Another interesting aspect that we will leave for future research is whether holographic prescriptions of computing computational complexity should be subjected to similar causality constraints as the ones discussed in section 4.4. The way that we have used the definition (6.72) in this section is similar to the RT prescription discussed in section 3.2 in that it explicitly assumes the existence of well-defined equal time slices. One might then call for a causality constraint similar to the one sketched on the left hand side of figure 4.3, which would be satisfied by construction. However, the general case where the prescription of [100] would be more appropriate would also be more complicated in terms of causality constraints.

6.7 $T = 0$ behaviour

As pointed out in section 6.5, it would be very interesting to investigate the behaviour of the bottom-up Kondo model at very low temperatures $T \approx 0$. While this is numerically demanding, we demonstrate in this section that for the $T = 0$ case, where the background spacetime is not a BTZ black hole anymore but instead the Poincaré AdS space, we can

use analytical arguments to assess the properties of the bottom-up model.

The specific question that we want to study is whether in the $T = 0$ case, our system will flow to an IR conformal fixed point. In an AdS/BCFT setting, this would mean that deep in the bulk spacetime we expect the brane to become effectively a constant tension solution [92–94], i.e.

$$S_{ij} \to const. \cdot \gamma_{ij} \quad \text{as} \quad z \to \infty \tag{6.77}$$

$$\Rightarrow S_{L/R} \to 0 \quad \text{as} \quad z \to \infty. \tag{6.78}$$

Due to our field theory intuition that a non-trivial scalar corresponds to the presence of the Kondo cloud, we will also make the assumption

$$\Rightarrow \phi \to const. \neq 0 \quad \text{as} \quad z \to \infty. \tag{6.79}$$

Actually, in section 6.4.1 we saw that in the finite temperature $T \neq 0$ case we automatically get $S_{L/R} \to 0$ as $z \to z_H$ as well as $\phi(z_H) \neq 0$, and as the zero-temperature limit is $z_H \to \infty$, we might be tempted to take this as evidence that at $T = 0$ the behaviour (6.78), (6.79) indeed occurs. This, however, cannot be the case as we will now show.

To do so, we use the equation of motion (5.28) as well as the explicit expression for $\mathcal{K}_{L/R}$ given in table 5.1 to find that (6.78) and (6.78) necessarily imply the set of assumptions that, as $z \to \infty$,

$$\mathcal{K}_{L/R} = \frac{zx''}{2\left(1 + x'^2\right)^{3/2}} \to 0, \tag{6.80}$$

$$\Rightarrow x''(z) \to 0 \text{ faster than } z^{-1} \;\Rightarrow x'(z) \to const. \tag{6.81}$$

Similarly, from the form of $S_{L/R}$ given in (6.35) and using that $\widehat{\gamma}^{ij}$, defined in (5.23), behaves as $\sim z^2$ for large z, we find[7]

$$a_0 \to 0 \text{ faster than } z^{-1}, \;\; \phi' \to 0 \text{ faster than } z^{-1}, \tag{6.82}$$

where we already used the gauge choice of section 6.3.2. Let us now focus on the scalar equations of motion

$$\partial_m \left(\sqrt{-\gamma}\gamma^{mn}\partial_n\phi\right) = \sqrt{-\gamma}\gamma^{00}a_0^2\phi + \frac{1}{2}\sqrt{-\gamma}\frac{\partial V}{\partial\phi}. \tag{6.83}$$

We will now assume that as $z \to \infty$ and $\phi \to const. \neq 0$, the force term $\frac{\partial V}{\partial\phi} \neq 0$ which is necessarily the case in the simple model (6.15). Due to the factor $\sqrt{-\gamma}$, the last term in (6.83) will then, for large z, go to zero exactly as z^{-2} and consequently the equation

[7] As a technicality, we should note that for diagonal $\widehat{\gamma}^{mn}$, $S_{L/R}$ is a sum of two terms, but as $\widehat{\gamma}^{mn}$ is by definition a positive definite matrix, these two terms cannot cancel each other. Hence when $S_{L/R}$ goes to zero, both terms compromising $S_{L/R}$ have to go to zero separately, yielding the above conditions.

(6.83) can only be satisfied if there is another term that also goes as z^{-2} in this limit. The conditions (6.81) and (6.82) however forbid precisely this: All the other terms in (6.83) can be shown to approach zero strictly faster than z^{-2} for large z. We have hence demonstrated a contradiction between the equations of motion (6.83) and the assumptions (6.78) and (6.79), proving the assumptions wrong for simple ansatz (6.15).

There is a loophole in our argument, however. If we would choose a more complicated potential V such that for large z we find $\phi \to \phi^*$ and $\frac{\partial V}{\partial \phi}\big|_{\phi=\phi^*} = 0$, then a zero temperature fixed point might exist. To obtain this result, we could for example add quartic or higher terms to the potential in (6.15). The model studied in this chapter so far would then be a good approximation to this more realistic model at higher temperatures $T \lesssim T_c$ where $\phi(z)$ stays comparably small, and only at lower temperatures $T \approx 0$ where $\phi(z)$ attains larger values for large z would the corrections to the potential become important. In this context, we should note again that in the bottom-up model, the quadratic form (6.15) of the potential was in fact chosen purely for convenience. This is hence one of the features in where the bottom-up model deviates qualitatively from the top-down model discussed in section 6.1.2, and it should consequently not be surprising that one might need a more intricate form of the potential to obtain more realistic results from the bottom-up model at low temperatures.

Let us now try to gain as much insight into the desired properties of the potential $V(\phi)$ as possible. What we already know is that there needs to be a $\phi^* \neq 0$ such that

$$\partial_\phi V\big|_{\phi=\phi^*} = 0 \ , \ V\big|_{\phi=\phi^*} \equiv V^*, \tag{6.84}$$

i.e. there needs to be another extremum or saddle point away from $\phi = 0$. But we can learn more: The geometry that we would expect to get is one where near the boundary, as well as deep in the bulk, the system is effectively described by constant tensions $S = -2\lambda_i \equiv S_i,\ S_{L/R=0}$ (see section 5.3.1), and the brane interpolates between the two corresponding constant tension solutions. By NEC and (5.31), we know that the traces have to increase and by WEC they have to stay non-positive along the brane, hence

$$S_1 < S_2 \leq 0, \tag{6.85}$$

where S_1 is the trace near the boundary (where ϕ falls off to zero) and S_2 is the trace deep in the bulk, for large z. These effective tensions receive different contributions. As already explained in section 6.4.1, near the boundary the main contribution comes from the a-field and its flux $\sim \mathcal{C}^2$. Generally allowing for a non-zero $V(\phi = 0) \equiv V^0$ (equivalent to a non-zero constant tension added to the brane) we find from equation (6.35):

$$S_1 = -\mathcal{N}\left(\mathcal{C}^2 + 2V^0\right). \tag{6.86}$$

Deep in the bulk in contrast, we assume the a-field to vanish because of (6.82), so that the trace is

$$S_2 = -2\mathcal{N}V^*. \tag{6.87}$$

Comparing to (6.85), we immediately find

$$V^* \geq 0 \tag{6.88}$$

$$\mathcal{C}^2 > 2\left(V^* - V^0\right) \equiv 2\Delta V. \tag{6.89}$$

The first equation has a straightforward interpretation: The value of the potential for the field value ϕ^* that the scalar asymptotes to in the bulk has to be non-negative. The second equation is also interesting, it should be discussed separately for the two cases $\Delta V > 0$ and $\Delta V < 0$, see figure 6.11.

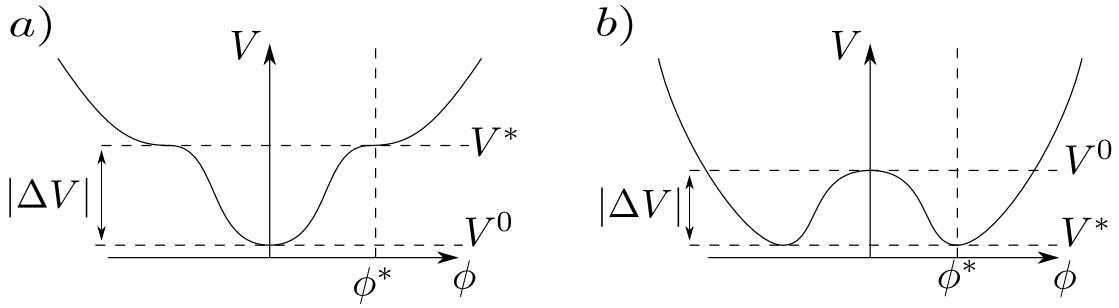

Figure 6.11: Different cases for a possible potential $V(\phi)$, all satisfying (6.88).

In the case $\Delta V > 0$ (figure 6.11*a*)), the new extremum lies higher than the extremum in the middle, and hence $V^0 = 0$ as we had it before is possible. Equation (6.89) is in this case a genuine constraint on the flux of the gauge field of the boundary. Also, in this case we would effectively want the scalar field to go from a "low" region of its potential (V^0) at high temperature to a "high" region of its potential (V^*) at low temperature. This is quite in contrast to the usual field theory intuition. After all, in the large N_s limit, the formation of the Kondo cloud is a phase transition, and the condensed phase needs to be thermodynamically preferred.

The case $\Delta V < 0$ seems more physical. The new extremum lies lower than the extremum in the middle (figure 6.11*b*)), and hence $V^0 > 0$. The equation (6.89) is trivially satisfied. Intuitively, this seems to be the more physical scenario, but it would in its easiest form demand a negative bare mass squared

$$V(\phi) = V^0 + m_{bare}^2\phi^2 + V_2^4\phi^4 \tag{6.90}$$

$$= V^0 - V_1^2\phi^2 + V_2^4\phi^4 \ , \ V_1, V_2 \text{ real.} \tag{6.91}$$

It should be noted that the flux $\mathcal{C}^2$ also enters the calculation of the effective mass at the boundary, hence when we want to ensure the Breitenlohner-Freedman bound (and consequently the correct conformal dimension for the scalar), we get a relation between the bare mass and the flux. Demanding the bare mass to be negative (as in fig. 6.11*b*)) would constrain $\mathcal{C}^2$ depending on the value of the gravitational coupling κ_N^2. Imposing a negative bare mass squared in the backreaction-less case $\kappa_N^2\mathcal{N} = 0$, equation (6.16) would

demand

$$\mathcal{Q}^2 = \mathcal{C}^2 < \frac{1}{4}. \tag{6.92}$$

For finite values of $\kappa_N^2 \mathcal{N}$, this bound gets stricter. Setting $\kappa_N^2 \mathcal{N} = 1$ for example, equation (6.44) and the imposition of a negative bare mass squared would lead to

$$\mathcal{C}^2 < 4\left(\sqrt{2} - \sqrt{2\sqrt{2} - 1}\right) \approx 0.248. \tag{6.93}$$

This concludes our study of how to make the bottom-up Kondo model more realistic in the lower temperature regime by adding higher order terms to the potential $V(\phi)$. As we have seen, this would have to be done under a number of strict constraints on the potential and the asymptotic flux $\mathcal{C}$. We leave a study of such a more realistic model and an investigation into the physical meaning of the constraints derived above to the future.

Chapter 7

Outlook

It is now time to conclude our investigations into the geometrical properties of of entanglement and defect entropies. In the introduction, we explained how *gauge/gravity duality* offers a concrete manifestation of the *holographic principle*, and even generally of the old belief that "physics is geometry". We have then studied concrete formulations and realisations of holography in chapter 2, and the geometrical manifestation of *entanglement entropy* in chapter 3. The original results of the present author summarised in chapters 4-6 were then consequently concerned with this topic of "entanglement from geometry".

Entanglement entropy was studied in higher curvature theories in chapter 4. It is clear that this is an ongoing research topic with steady progress, see [200, 201, 210, 225, 226] for only a partial list of work on this topic published after [1]. In particular, we dealt with new massive gravity in section 4.2 and Gauss-Bonnet gravity in section 4.3. In both cases we found unexpected solutions to the equations for the extremal surfaces that are thought to define holographic entanglement entropy. In section 4.4 we also pointed out the importance of causality conditions such as the *causal influence argument* of [64]. In fact, causality conditions like this one are an important subject even in the absence of higher curvature corrections: If entanglement entropy (or another physical quantity of the boundary theory) is encoded in the bulk geometry in the form of extremal surfaces, it is of interest to find out which part of the bulk spacetime these surfaces have access to [155]. This is related to the ongoing research into such topics as *bulk locality* and *bulk reconstruction*, [154–158], which we briefly commented on in the end of section 2.4.

Chapters 5 and 6 were then devoted to holographic models of $AdS_3/BCFT_2$ in general and of the *Kondo effect* in particular. Specifically, we were able to prove general theorems (in sections 5.2.3 and 5.2.4) that restrict the possible qualitative features of the bulk geometry, depending on whether or not certain energy conditions are satisfied by the matter fields of the model. This, together with the study of exact solutions in section 5.3, gave us a very firm and intuitive understanding of the geometrical properties of the holographic Kondo model, which we put to use in chapter 6. There, we presented numerical and semi-analytical

results on the entanglement entropy in the holographic Kondo model (sections 6.4.2 and 6.5), and compared them to field theory results obtained by Affleck et al. in [90] with good agreement. We also verified that the holographic Kondo model satisfies the g-theorem, as expected, in section 6.4.3. Section 6.6 was devoted to the study of computational complexity in the holographic Kondo model. Finally, the zero-temperature behaviour of the model was investigated more closely in section 6.7, with clear suggestions for improvements of the bottom-up model being made. This work presented in chapters 5 and 6 has opened up some fascinating possible avenues for future research on the junctions of geometry, gravity and quantum theory of impurities:

- As pointed out the introduction, AdS/CFT techniques have been applied to problems in QCD with great success. Interestingly, it has been shown in [300] that a Kondo-like effect can occur in light quark matter, when heavy quarks act as impurities. This is a motivation to ask whether the results derived from the holographic Kondo model of [86] can also be applied to the QCD Kondo effect, or whether a realistic holographic QCD-Kondo model can be constructed.

- In [301], the single impurity Kondo model has been described holographically in terms of a *multiscale entanglement renormalisation ansatz (MERA)* network [302]. In particular, the defect or impurity on the field theory side was holographically described by introducing *boundary tensors* into the tensor network. Assuming that the MERA construction leads to the emergence of an effective bulk geometry (as conjectured in [303]), these boundary tensors bear a striking resemblance to the boundary Q introduced into the bulk spacetime (see figure 5.1) in the holographic Kondo model and similar models of a general AdS/BCFT duality. It would hence be of great interest to compare the Kondo model with the one of [301], to find out whether some of our results and techniques can be applied to the MERA model, and to investigate whether these two types of models are sharing a common physical foundation.

- One important part of our work presented in section 6.4.3 was the study of the g-theorem, proven in the holographic context already in [92,291]. Here, the g-function is a renormalisation group monotone for BCFTs, similar to the c-function for standard CFTs. We found in section 6.6 that the field theory *RG flow* manifested itself in a reduction of the volume of our bulk spacetime due to the loss of certain bulk points, and consequently via the Ryu-Takayanagi approach also in a reduction of entanglement entropy. Indeed, entanglement entropy has been very successfully used before to monitor RG flows e.g. in [46, 304]. The reduction of volume that is visible in the holographic Kondo model on the other hand may be related, as explained in section 6.6, to measures of *computational complexity* or a *quantum information metric* [95–101]. It would certainly be interesting to investigate the interconnection between the boundary RG flow, the loss of bulk points and quantities such as complexity in more detail, as this might yield new insights about how the geometry emerges from the field theory side of the duality.

- Last but not least, in [86] it was pointed out that by using a *higher spin theory* in the $2+1$-dimensional bulk, it may be possible to construct a holographic model that is precisely dual to the large N_s Kondo effect, as this model has an infinite number of conserved currents of arbitrarily high spin. This may be a way around the usual pitfalls of a merely qualitative duality present in many bottom-up holographic models.

We hence see that there are many potential connections between the specific topics presented in this thesis and the important current questions in AdS/CFT research. Without any doubt, the coming years will show a number of remarkable interconnections between such diverse topics as (dynamical) geometry and quantum (information) theory.

Appendix A

Extrinsic curvature quantities

A.1 Codimension two hypersurfaces

As discussed in chapters 3 and 4, the holographic prescriptions for calculating entanglement entropy are based on the geometry of spacelike codimension two extremal hypersurfaces. In this appendix we will define some geometric quantities describing the extrinsic curvature properties of such a hypersurface. Specifically, we will clarify the notation (following [60, 199]) used in equation (4.4) which shall be reproduced here for convenience:

$$S_{EE} = \frac{1}{4G_N}\int_{\Sigma} d^{d-1}y\sqrt{\gamma}\left[1 + 2aR + b\left(R_{\parallel} - \frac{1}{2}k^2\right) + 2c\left(R_{\parallel\parallel} - \mathrm{Tr}(k)^2\right)\right]. \tag{4.4}$$

Here, Σ stands for a spacelike codimension-two hypersurface in a $d+1$-dimensional bulk spacetime, y are the coordinates on this surface and its induced metric is γ_{ij} with positive determinant γ. It is easy to see that in the case $a = b = c = 0$, (4.4) simplifies to the standard *area functional*. We will now define the quantities $R_{\parallel}, R_{\parallel\parallel}, k^2$ and $\mathrm{Tr}(k)^2$. R is just the standard Ricci scalar of the background spacetime $g_{\mu\nu}$.

To begin, we will assume the background metric $g_{\mu\nu}$ to be Euclidean. The codimension two hypersurface Σ will then have two spacelike normal vectors $n^{\mu}_{(\alpha)}$ ($\alpha \in \{1, 2\}$) with

$$n^{\mu}_{(1)}n^{\nu}_{(1)}g_{\mu\nu} = n^{\mu}_{(2)}n^{\nu}_{(2)}g_{\mu\nu} = +1, \quad n^{\mu}_{(1)}n^{\nu}_{(2)}g_{\mu\nu} = 0. \tag{A.1}$$

$R_{\parallel}$ and $R_{\parallel\parallel}$ are derived from the background Ricci and Riemann tensors according to [60, 199]

$$R_{\parallel} \equiv R_{\mu\nu}[g]n^{\mu}_{(\alpha)}n^{\nu}_{(\alpha)}, \quad R_{\parallel\parallel} \equiv R_{\mu\rho\nu\sigma}[g]n^{\mu}_{(\alpha)}n^{\nu}_{(\alpha)}n^{\rho}_{(\beta)}n^{\sigma}_{(\beta)}, \tag{A.2}$$

where we are summing over double bracketed Greek indices like (α). The extrinsic curva-

ture terms k^2 and $\mathrm{Tr}(k)^2$ can be defined according to [60] in the following way:

$$h_{\mu\nu} = g_{\mu\nu} - (n_{(\alpha)})_\mu (n_{(\alpha)})_\nu, \tag{A.3}$$

$$k^{(\alpha)}_{\mu\nu} = h^\lambda_\mu h^\rho_\nu (n_{(\alpha)})_{\lambda;\rho}, \tag{A.4}$$

$$k^2 = (k^{(\alpha)})^\mu_\mu (k^{(\alpha)})^\nu_\nu, \tag{A.5}$$

$$\mathrm{Tr}(k)^2 = (k^{(\alpha)})^\mu_\nu (k^{(\alpha)})^\nu_\mu, \tag{A.6}$$

where again summation over double indices like (α) is implied. In fact, we can imagine such indices to be contracted via a flat Euclidean metric $\delta_{(\alpha)(\beta)}$, although we do not use the convention here that indices (α) are raised and lowered.

For Lorentzian background metrics $g_{\mu\nu}$, we will effectively replace this by a Minkowski metric $\eta_{(\alpha)(\beta)}$. Specifically, we then get

$$n^\mu_{(1)} n^\nu_{(1)} g_{\mu\nu} = -1,\ n^\mu_{(2)} n^\nu_{(2)} g_{\mu\nu} = +1,\ n^\mu_{(1)} n^\nu_{(2)} g_{\mu\nu} = 0, \tag{A.7}$$

$$R_\parallel \equiv R_{\mu\nu} n^\mu_{(\alpha)} n^\nu_{(\alpha)} = -R_{\mu\nu} n^\mu_{(1)} n^\nu_{(1)} + R_{\mu\nu} n^\mu_{(2)} n^\nu_{(2)} \ \text{(similarly for } R_{\parallel\parallel}), \tag{A.8}$$

$$h_{\mu\nu} = g_{\mu\nu} + (n_{(1)})_\mu (n_{(1)})_\nu - (n_{(2)})_\mu (n_{(2)})_\nu, \tag{A.9}$$

$$k^{(\alpha)}_{\mu\nu} = h^\lambda_\mu h^\rho_\nu (n_{(\alpha)})_{\lambda;\rho}, \tag{A.10}$$

$$k^2 = -(k^{(1)})^\mu_\mu (k^{(1)})^\nu_\nu + (k^{(2)})^\mu_\mu (k^{(2)})^\nu_\nu, \tag{A.11}$$

$$\mathrm{Tr}(k)^2 = -(k^{(1)})^\mu_\nu (k^{(1)})^\nu_\mu + (k^{(2)})^\mu_\nu (k^{(2)})^\nu_\mu. \tag{A.12}$$

These definitions ensure that k^2 and $\mathrm{Tr}(k)^2$ are independent of the choice of the $n^\mu_{(\alpha)}$ as long as $n^\mu_{(1)}$ is the timelike and $n^\mu_{(2)}$ is the spacelike normal vector.

A.2 Codimension one hypersurfaces

In the discussions of chapters 5 and 6 we deal with the embeddings of codimension one timelike hypersurfaces into an asymptotically AdS_{d+1} ambient spacetime, as in [92–94]. To be specific, we are interested in the *extrinsic curvature tensor* or *second fundamental form*

$$K_{ij} \equiv \frac{\partial X^\alpha}{\partial \xi^i} \frac{\partial X^\beta}{\partial \xi^j} \nabla_\alpha n_\beta = -n_\alpha \left(\frac{\partial^2 X^\alpha}{\partial \xi^i \partial \xi^j} + \Gamma^\alpha_{\beta\gamma} \frac{\partial X^\beta}{\partial \xi^i} \frac{\partial X^\gamma}{\partial \xi^j} \right), \tag{A.13}$$

where the X^α are the ambient space coordinates ($\alpha \in \{0, ..., d\}$), the ξ^i are the coordinates on the hypersurface ($i \in \{0, ..., d-1\}$) and n_β is the normal form of the hypersurface in the ambient spacetime. Obviously, the sign of K_{ij} needs to be fixed by a convention on the direction of n_β. For one-sided models as the one described in section 5.1 we choose n_β to be pointing *into* the spacetime, which is in contrast to the convention of [92–94]. We choose this convention because it is the more common one in two-sided models based on the Israel junction conditions (6.28), such as the holographic Kondo model of section 6.2. There, for the equations of motion to take the form (6.29), the convention has to be that the normal form n_β points from the $-$ side into the $+$ side, as in figure 6.2.

The trace of the extrinsic curvature tensor can be straightforwardly defined by contraction with the induced metric:

$$K = \gamma^{ij} K_{ij}. \tag{A.14}$$

Let us compare the expressions (A.13) and (A.14) with those presented in appendix A.1. Although the notation used here is a little bit different, we see that the underlying geometric ideas are the same. Both in (A.13) and (A.4) respectively (A.10) we take the covariant derivative of the normal form and project it onto the worldvolume of the hypersurface in question. The difference is that firstly, in appendix A.1 we are dealing with codimension two hypersurfaces, hence there are two independent normal forms and two extrinsic curvature scalars. Secondly, in appendix A.1 we have avoided introducing worldvolume coordinates ξ^i and their indices i. Hence, the induced metric (A.3) respectively (A.9) is effectively a $(d+1) \times (d+1)$ matrix, but a degenerate one. In contrast, the induced metric γ_{ij} used in this section and chapters 5 and 6 is a non-degenerate $d \times d$ matrix.

As a special case, in section 5.2.4 we calculate the extrinsic curvature tensor of a hypersurface embedded into a background of the form (5.17). We assume $\xi^0 = X^0 = t$ and $\xi^1 = X^2 = z$, using the profile function $x(t, z)$ to define the embedding of the hypersurface into the ambient spacetime. The derivatives in (A.13) then simplify considerably. As the brane is defined by the embedding profile $x(t, z)$, i.e. by viewing the x-coordinate as a function of the other coordinates, it is located at the set of zeros of the function $f(t, z, x) \equiv x - x(t, z)$. The normal form n_μ is then proportional (up to its normalisation) to the exterior derivative of f:

$$n_\mu dx^\mu \sim df = dx - \partial_t x(t, z) dt - \partial_z x(t, z) dz. \tag{A.15}$$

Raising the index and calculating the normalisation, we explicitly find

$$n^\mu = \frac{z^2}{\mathcal{N}} \begin{pmatrix} \frac{\partial_t x}{h} \\ -h\partial_z x \\ 1 \end{pmatrix}, \tag{A.16}$$

$$\mathcal{N} = z\sqrt{1 - \frac{(\partial_t x)^2}{h} + h\,(\partial_z x)^2}, \tag{A.17}$$

where the order of bulk coordinates is chosen to be t, z, x. The extrinsic curvature tensor is

$$\begin{aligned} K^{\pm}_{tt} &= \frac{1}{\mathcal{N}}\left(-\partial_t^2 x + \partial_z x\left(\frac{h}{2}\left(h' - \frac{2h}{z}\right) + \frac{h}{z}(\partial_t x)^2\right)\right), \\ K^{\pm}_{tz} = K_{zt} &= \frac{1}{\mathcal{N}}\left(-\partial_t\partial_z x + \partial_t x\left(\frac{h}{z}(\partial_z x)^2 + \frac{h'}{2h}\right)\right), \\ K^{\pm}_{zz} &= \frac{1}{\mathcal{N}}\left(-\partial_z^2 x + \partial_z x\left(\frac{h}{z}(\partial_z x)^2 + \frac{1}{z} - \frac{h'}{2h}\right)\right), \end{aligned} \tag{A.18}$$

and the induced metric reads

$$\gamma_{ij} = \begin{pmatrix} g_{tt} + (\partial_t x)^2 g_{xx} & (\partial_t x)(\partial_z x) g_{xx} \\ (\partial_t x)(\partial_z x) g_{xx} & g_{zz} + (\partial_z x)^2 g_{xx} \end{pmatrix}. \tag{A.19}$$

In the last expression, we made use of the fact that (5.17) is a diagonal metric.

Appendix B

Corollary to the barrier theorem in higher dimensions

This appendix will be devoted to discussing an extension of our findings of section 5.2.3 to higher dimensions. This is non-trivial, but also potentially useful for model building purposes. For example, in [243] a holographic model of the quantum Hall effect was presented using the AdS/BCFT ansatz (5.1) with a $3+1$-dimensional bulk spacetime. There, it was argued (see especially figure 2(d) of [243]) that in a realistic model, the branes should bend back to the boundary in a $\cup$-shaped manner. A better understanding of the implications of the barrier theorem on AdS/BCFT models in higher dimensions might then enable for a more efficient model building yielding such a desired behaviour.

First of all, we see that our results of section 5.2.3 cannot be straightforwardly carried over to higher dimensions as it is possible to construct explicit examples of codimension one branes in $3+1$-dimensional Poincaré space that satisfy both WEC and SEC and yet do not satisfy (5.14). We do not have analytical results on the energy conditions needed to ensure (5.14) in higher dimensions, but by studying a large number of randomly generated energy-momentum tensors[1] for $2+1$-dimensional branes obeying (5.2) we found that (5.14) is ensured by the SEC (generalised to higher dimensions compared to (5.11)) together with the *dominant energy condition* (DEC, [246, 247]) and the *determinant energy condition* (DetEC, [247, 305]). The generalisation of the $\cup$-shaped branes encountered in sections 5.2.3 and 5.3.2 are then bowl shaped surfaces, as sketched on the left hand side of figure B.1.

However, for the phenomenological purposes of [243] one does not need bowl-shaped hypersurfaces, but such ones which are anchored at the boundary in the form of an infinite strip. Such surfaces cannot satisfy the barrier theorem, as shown in figure B.1. But if it

[1] Note that the condition (5.14) as well as all energy conditions are *pointwise* conditions, i.e. they do not depend on derivatives of S_{ij} or K_{ij}. Hence we can check them at any point on the brane separately, and S_{ij} can then be treated as a symmetric matrix with numerical entries.

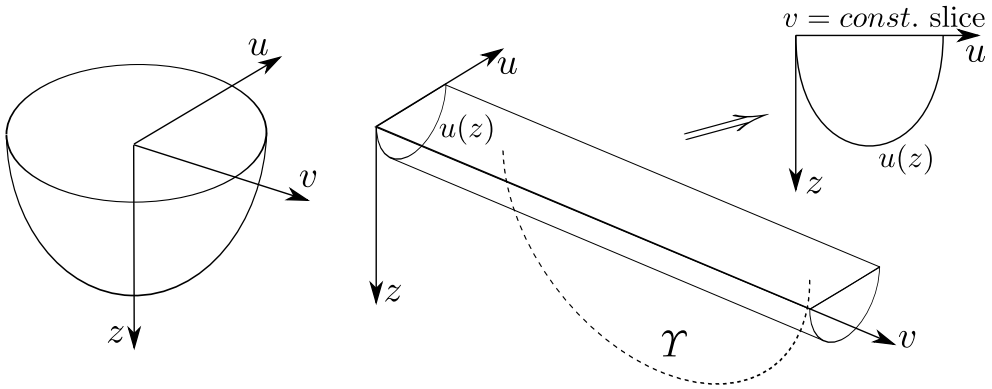

Figure B.1: Left: A bowl shaped hypersurface, anchored to the boundary in a circle. The time direction is omitted in this sketch, u and v are spacelike coordinates on the asymptotic boundary and z is the bulk coordinate, as in Poincaré coordinates. Right: A surface that is anchored on the boundary in a strip-like geometry is not an extremal hypersurface barrier in the sense of section 5.2.3 as it can e.g. be crossed by a geodesic shown as Υ in the figure. Nevertheless, a section of this in the $v = const.$ plane yields a $\cup$-shaped profile. The figure is presented as in [2].

was possible to formulate the barrier theorem only for curves in the z, u-plane, the barrier theorem might tell us how to choose the matter content on the brane such that a $\cup$-shaped profile in the z, u-plane is inevitable. This is what we will study in the remainder of this appendix.

Assuming a strip-like setup for the brane defined by the profile function $U(z)$ as in the right hand side of figure B.1 and a $3+1$-dimensional Poincaré background spacetime (2.11) with $L = 1$, the extrinsic curvature reads (coordinates $x^0 = t, x^1 = z, x^2 = v$)

$$K_{\alpha\beta} = \begin{pmatrix} -\frac{u'(z)}{z^2\sqrt{1+u'(z)^2}} & 0 & 0 \\ 0 & \frac{u'(z)+u'(z)^3-zu''(z)}{z^2\sqrt{1+u'(z)^2}} & 0 \\ 0 & 0 & \frac{u'(z)}{z^2\sqrt{1+u'(z)^2}} \end{pmatrix}. \tag{B.1}$$

Comparing this to (5.18), we can map this to the lower dimensional case by realising that the first two entries on the diagonal of (B.1) are the extrinsic curvature of a brane with profile $u(z)$ embedded in $2+1$-dimensional Poincaré space. Comparing this then to the results in table 5.1 we see that, apart from the trivial case $u'(z) = 0$, $u(z)$ has to be $\cup$-shaped when $u'(z) \geq 0$ and $u'(z) + u'(z)^3 - zu''(z) \leq 0$ hold[2]. This automatically implies $K_{yy} \geq 0$ and hence a violation of (5.14) for spacelike vectors v^i in y-direction. Hence, extremal curves moving in the y-direction such as Υ in figure B.1 may cross the brane.

[2]Note that, due to our convention on the orientation of the normal vector, these expressions only hold for the one branch of the brane that goes into the bulk up to the turning point.

Setting $\kappa_N^2 = 1$ for simplicity, we find from (5.2) that

$$S_{\alpha\beta} = \begin{pmatrix} -\frac{2\left(u'+u'^3\right)-zu''}{z^2(1+u'^2)^{3/2}} & 0 & 0 \\ 0 & \frac{2u'\sqrt{1+u'^2}}{z^2} & 0 \\ 0 & 0 & -\frac{-2\left(u'+u'^3\right)+zu''}{z^2(1+u'^2)^{3/2}} \end{pmatrix}. \tag{B.2}$$

As we are only interested in establishing the brane to be an extremal surface barrier in the u-z-plane, we will in the following only use vectors with vanishing v-component. The NEC then implies $u'' \geq 0$, the WEC implies the NEC together with $2u' + 2u'^3 - zu'' \leq 0$ and consequently $u'' \geq 0$, WEC implies $2u' + 2u'^3 - zu'' \leq 0$ and together, these imply

$$u' + u'^3 - zu'' \leq 0. \tag{B.3}$$

This expression also appears in the zz-component of (B.1). Projecting out the v-component from the tensors above yields

$$K_{ij}^{\perp} = \begin{pmatrix} -\frac{u'}{z^2\sqrt{1+u'^2}} & 0 \\ 0 & \frac{u'+u'^3-zu''}{z^2\sqrt{1+u'^2}} \end{pmatrix}, \tag{B.4}$$

$$S_{ij}^{\perp} = \begin{pmatrix} -\frac{2\left(u'+u'^3\right)-zu''}{z^2(1+u'^2)^{3/2}} & 0 \\ 0 & \frac{2u'\sqrt{1+u'^2}}{z^2} \end{pmatrix}, \tag{B.5}$$

$$\gamma_{ij}^{\perp} = \begin{pmatrix} -\frac{1}{z^2} & 0 \\ 0 & \frac{1+u'^2}{z^2} \end{pmatrix}. \tag{B.6}$$

If we then replace the SEC with the inequality

$$\left(S_{ij}^{\perp} - \gamma_{ij}^{\perp} S^{\perp}\right) v^i v^j \geq 0, \tag{B.7}$$

with $S^{\perp} = \gamma^{\perp ij} S_{ij}^{\perp}$, we get the familiar condition $u'(z) \geq 0$ which together with the WEC ensures that $K_{ij}^{\perp}$ is negative definite. If the matter fields living on the brane are chosen to satisfy the given energy conditions, the branes necessarily have a $\cup$-shaped profile $u(z)$ in the $v = const.$ plane, as desired in [243].

Appendix C

Junction conditions for abelian Chern-Simons fields

The bottom-up Kondo model described in section 6.2 had two fields defined in the entire bulk spacetime (N in the nomenclature of figure 5.1), namely the metric $g_{\mu\nu}$ and the Abelian Chern-Simons (CS) field A^μ. At the locus of the brane, the metric needs to satisfy the *Israel junction conditions*, as discussed in section 6.3.1. Similarly, junction conditions have to be imposed on the CS field, and we will derive these junction conditions in this section. Just as for the Israel junction conditions, there are several ways how to do this, and here we will follow the ansatz of starting with a smoothed out worldvolume current, and then take the limit in which the current is localised at a codimension one hypersurface. This is somewhat related to the study of domain wall solutions in CS theories, see [306,307].

To begin, we assume that we are working in a *Gaussian normal coordinate system*, such that the brane is located at $x = 0$. In the holographic Kondo model, the current is defined by the charged scalar $\Phi = \phi\, e^{i\psi}$ and reads

$$J^m = \gamma^{mn}\, i \left(\Phi \mathcal{D}_n \Phi^\dagger - \Phi^\dagger \mathcal{D}_n \Phi\right) = 2\, \gamma^{mn} \left(A_n - a_n + \partial_n \psi\right) \phi^2 \,, \tag{C.1}$$

which we can write as $J^m \sim \mathcal{Q}(z)\, (\partial_t)^m$ in the static case. As depicted in figure C.1, we now assume the current to be smoothed out by a profile function $f(x)$ with stem-function $F(x)$, such that there exists a well-defined limit in which $f(x) \to \delta(x)$, $F(x) \to \theta(x)$. Here, $\delta(x)$ is the Dirac delta distribution and $\theta(x)$ is the Heaviside step function.

Due to our assumption of staticity, all time-derivatives vanish, and hence the CS equations of motion,

$$\epsilon^{\rho\mu\nu} F_{\mu\nu} = -4\pi\, J^\rho, \tag{C.2}$$

have only the non-trivial component

$$2\, \epsilon^{tz} \left(\partial_z A_x - \partial_x A_z\right) = -4\pi\, J^t = -4\pi\, f(x) \mathcal{Q}(z). \tag{C.3}$$

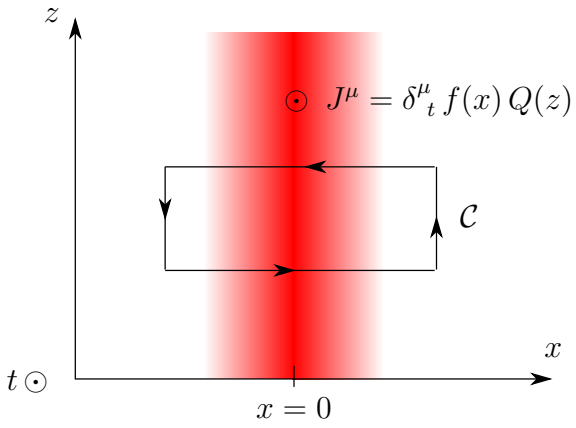

Figure C.1: The static worldvolume current of a brane located at $x = 0$ is assumed to be smoothed out to have a bell-shaped profile $f(x)$. A possible Wilson loop is depicted as $\mathcal{C}$. The figure is presented as in [3].

The worldvolume ϵ-tensor appearing in this equation is defined from the three-dimensional ϵ-tensor via contracting with the normal form of the brane. In Gaussian normal coordinates, this reads $\epsilon^{\rho\mu x} \equiv \epsilon^{\rho\mu}$. We can now solve (C.3) in two simple ways, depending on a gauge choice:

Gauge $A_x = 0$: With this gauge, we find

$$-\epsilon^{tz}\partial_x A_z = -2\pi\, f(x)\mathcal{Q}(z)\,, \tag{C.4}$$

$$\Rightarrow \epsilon^{tz} A_z = 2\pi\, F(x)\mathcal{Q}(z)\,. \tag{C.5}$$

Taking the limit $F \to \Theta,\ f \to \delta$, these equations then tell us that the parallel component of the CS field has a discontinuity proportional to the charge density $\mathcal{Q}$ on the brane.

Gauge $A'_z = 0$: To distinguish this gauge from the one used above, we add primes to the CS field. $A'_z = 0$ leads to

$$\epsilon^{tz}\partial_z A'_x = -2\pi\, f(x)\mathcal{Q}(z) \tag{C.6}$$

$$\Rightarrow -\tilde{\epsilon}^{tz} A'_x = 2\pi\, f(x) \int_0^z \sqrt{-\gamma}\, \mathcal{Q}(\hat{z})\, d\hat{z}\,, \tag{C.7}$$

where $\tilde{\epsilon}$ denotes the Levi-Civita symbol, which is related to the Levi-Civita tensor by $\epsilon^{mn} = \tilde{\epsilon}^{mn}/\sqrt{-\gamma(z)}$. The limit $F \to \Theta,\ f \to \delta$ then implies that the component of the Chern-Simons field normal to the brane acquires a contribution $\sim \delta(x)$ in this gauge convention.

We can explicitly verify that the two results presented in (C.5) and (C.7) are related by a gauge transformation, $d\alpha = A' - A$, with

$$\alpha = \frac{2\pi}{\tilde{\epsilon}^{tz}} F(x) \int_0^z \sqrt{-\gamma}\, \mathcal{Q}(\hat{z})\, d\hat{z}. \tag{C.8}$$

We hence see that even in the step-function limit $F \to \Theta$, this gauge function α need not vanish far away from the brane, i.e. for large $|x|$. Consequently, we see that (open) Wilson lines crossing the brane pick up a phase under this gauge transformation,

$$W(a,b) \to e^{i\alpha(a)} W(a,b) e^{-i\alpha(b)}, \tag{C.9}$$

as expected. Furthermore, simple Wilson loops, such as the one following the rectangular path in figure C.1, can explicitly be calculated in both gauges with agreeing results, as expected. In fact, we can use the equations of motion of the CS field to find the general formula for the static case

$$\oint_{\mathcal{C}} A = \int_{\mathrm{int}(\mathcal{C})} dA \overset{EOMs}{\propto} \int_{\mathrm{int}(\mathcal{C})} \mathcal{Q}\,, \tag{C.10}$$

where $\mathrm{int}(\mathcal{C})$ denotes the interior of $\mathcal{C}$.

Now that we have convinced ourselves that the results (C.5) and (C.7) are physically sensible, we should try to formulate them in a general way that does not depend on the use of Gaussian normal coordinates or a specific gauge choice. When a current J^μ is localised at the infinitely thin brane, then the CS field satisfies its vacuum equations of motion in the ambient space to both sides of the brane and junction conditions on the brane. The physical content (C.5) and (C.7) is that the localised current J^μ leads either to a discontinuity in the parallel component of the A-field or a δ-peak in the normal component, and the two things can be transformed into each other by a gauge transformation. In the case of a discontinuity of the parallel component, we will assume that in (6.13) and (C.1) the scalar field Φ couples to the mean value of the A field when projected from the left and from the right onto the brane, i.e.

$$A_m \equiv \frac{1}{2}\left(\overleftarrow{\mathcal{P}}_m{}^\mu A_\mu + \overrightarrow{\mathcal{P}}_m{}^\mu A_\mu \right). \tag{C.11}$$

where $\overrightarrow{\mathcal{P}}$ is the projector that acts on the A-field from the left hand side of the brane and $\overleftarrow{\mathcal{P}}$ acts from the right hand side of the brane. Complementarily, we define the discontinuity to be

$$C_m \equiv \overleftarrow{\mathcal{P}}_m{}^\mu A_\mu - \overrightarrow{\mathcal{P}}_m{}^\mu A_\mu \tag{C.12}$$

and the δ-peak contribution to the normal component of the A-field via

$$A^0(z,t) \equiv \int_{-\epsilon}^{\epsilon} A^\mu n_\mu\, ds\,, \tag{C.13}$$

where n_μ is the normal form of the brane and we integrate along an integral curve of the vector field n^μ that intersects the brane at coordinates (z,t). The generalised form of (C.5) and (C.7) then reads

$$-2\pi\, J^m = \epsilon^{im}\left(C_i - \partial_i A^0\right). \tag{C.14}$$

Let us comment on the physical properties of this equation. First of all, for the equations of motion of the worldsheet fields Φ and a, as well as for the calculation of the current (C.1), we only need the projection A_m as defined in (C.11), and not the quantities C_m and A^0 which appear only on the right hand side of (C.14). This means that we can first solve the equations of motion of the fields Φ and a assuming the gauge $A_m = 0$, then calculate the current J^m, and then solve the algebraic equation (C.14) for the combination $C_i - \partial_i A^0$. We hence find that the CS field effectively decouples from the dynamics of the brane and its worldvolume fields, just as found in [86] for the case without backreaction on the geometry. Also, it is interesting to note that the current J^m is gauge invariant, and so has to be, due to (C.14), the combination $C_i - \partial_i A^0$. Consequently, in this expression A^0 acts as a gauge function for C_m.

In chapter 5, after introducing the equations of motion (5.2) and studying them in generality in section 5.2, we refined our intuition for this type of setup by studying simple toy-models such as constant tension models and perfect fluids in section 5.3. In order to get a better understanding for the junction conditions (C.14), we will in the remainder of the section apply them to a simple toy model, too. In particular, we will consider a spacetime of the form $T^2 \times \mathbb{R}$, as shown in figure C.2. We assume the torus to be defined by the two non-contractible cycles θ and ϕ. Furthermore, we assume two currents $J^\mu_{1/2}$ (constant in both space and time) to be located at the two equatorial planes $Q_{1/2}$ (defined by $\phi = 0$ and $\phi = \pi$), and a bulk Chern-Simons field to be present which we for simplicity call A_μ above the equator and B_μ below the equator.

In the "bulk", i.e. away from $Q_{1/2}$, there are no currents and hence the CS equations of motion demand $dA = 0, dB = 0$, i.e. A and B to be closed. Due to the cohomology classes of the torus, this means the general bulk solutions can be written as

$$A = a_\phi d\phi + a_\theta d\theta + d\alpha, \tag{C.15}$$
$$B = b_\phi d\phi + b_\theta d\theta + d\beta. \tag{C.16}$$

Here a_ϕ et cetera are assumed to be constants, and it should be noted that the cycles are periodically identified: For example, $\phi \sim \phi + 2\pi$, hence ϕ is not a globally well-defined function, and $d\phi$ is a closed, but not an exact form. The same holds for θ. The form dt, on the other hand, is both closed and exact. The well-defined scalar functions α, β hence have to be periodic in ϕ and θ.

Let us ignore any possible localised A^0 modes for a second. Then the junction-conditions

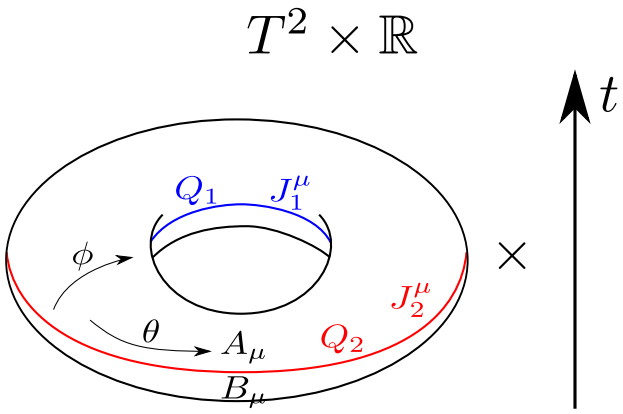

Figure C.2: A simple toy model for the illustration of the junction conditions for the Chern-Simons field. We assume the bulk space to be a three dimensional space with the topology $T^2 \times \mathbb{R}$, and two charge distributions to be confined to the two equatorial circles of the torus.

$C_m \propto \epsilon_{mn} J^n$ give

$$a_\theta - b_\theta + \partial_\theta \alpha - \partial_\theta \beta\big|_{Q_1} = J_1^t, \tag{C.17}$$

$$b_\theta - a_\theta - \partial_\theta \alpha + \partial_\theta \beta\big|_{Q_2} = J_2^t, \tag{C.18}$$

where we have set a numerical proportionality constant to one. We see that if there is a time component in the current, we get a θ component in the jump C_m. While $J_t dt$ is topologically trivial, $const. \cdot d\theta$ is an element of a non-trivial cohomology class of the torus. Being in a different cohomology class, the terms $\partial\alpha$ can hence not contribute to the solution and the previous equations read

$$a_\theta - b_\theta = J_1^t, \quad \partial_\theta \alpha - \partial_\theta \beta\big|_{Q_1} = 0, \tag{C.19}$$

$$b_\theta - a_\theta = J_2^t, \quad \partial_\theta \alpha - \partial_\theta \beta\big|_{Q_2} = 0. \tag{C.20}$$

For the currents, this means

$$J_1^t = -J_2^t, \tag{C.21}$$

i.e. the total charge on the torus has to vanish. This is a result that we would expect on any space with closed spacial sections, also for Maxwell theory for example. Due to dt being an exact form, we do not get these topological complications for the equations involving $J_{1/2}^\theta$, and hence there is no restriction on these components (if time is not compactified). It makes sense that the constraints between $J_{1/2}$ that are conveyed by the CS field only concern conserved charges which have to be fixed once: As the CS field has no propagating degrees of freedom, it cannot communicate dynamical information from Q_1 to Q_2.

We claimed above that the addition of the term $\sim \partial_m A^0$ in the junction condition restores a sense of gauge freedom for C_m. This may be correct on topologically simpler backgrounds,

but in this example it would not be possible to gauge away the jump C_m, as again $\partial_m A^0$ would be in the wrong cohomology class to make C_m vanish.

Bibliography

[1] J. Erdmenger, M. Flory, and C. Sleight, "Conditions on holographic entangling surfaces in higher curvature gravity," *JHEP* **06** (2014) 104, arXiv:1401.5075 [hep-th].

[2] J. Erdmenger, M. Flory, and M.-N. Newrzella, "Bending branes for DCFT in two dimensions," *JHEP* **01** (2015) 058, arXiv:1410.7811 [hep-th].

[3] J. Erdmenger, M. Flory, C. Hoyos, M.-N. Newrzella, and J. M. S. Wu, "Entanglement Entropy in a Holographic Kondo Model," *Fortsch. Phys.* **64** (2016) 109–130, arXiv:1511.03666 [hep-th].

[4] J. Erdmenger, M. Flory, C. Hoyos, M.-N. Newrzella, A. O'Bannon, and J. Wu, "Holographic impurities and Kondo effect," in *The String Theory Universe, 21st European String Workshop and 3rd COST MP1210 Meeting Leuven, Belgium, September 7-11, 2015*. 2015. arXiv:1511.09362 [hep-th].

[5] **LIGO Scientific Collaboration and Virgo Collaboration**, "Observation of gravitational waves from a binary black hole merger," *Phys. Rev. Lett.* **116** (Feb, 2016) 061102.

[6] A. Pais, *Raffiniert ist der Herrgott...: Albert Einstein. Eine wissenschaftliche Biographie*. Spektrum Akademischer Verlag, Heidelberg, 2009.

[7] J. A. Wheeler, "Geons," *Phys. Rev.* **97** (Jan, 1955) 511–536.

[8] J. A. Wheeler and C. W. Misner, "Classical physics as geometry," *Ann. Phys.* **2** (1957) 525–603.

[9] J. Maldacena and L. Susskind, "Cool horizons for entangled black holes," *Fortsch. Phys.* **61** (2013) 781–811, arXiv:1306.0533 [hep-th].

[10] K. Jensen and A. Karch, "Holographic Dual of an Einstein-Podolsky-Rosen Pair has a Wormhole," *Phys. Rev. Lett.* **111** no. 21, (2013) 211602, arXiv:1307.1132 [hep-th].

[11] K. Jensen and J. Sonner, "Wormholes and entanglement in holography," *Int. J. Mod. Phys.* **D23** no. 12, (2014) 1442003, arXiv:1405.4817 [hep-th].

[12] D. Engelhardt, B. Freivogel, and N. Iqbal, "Electric fields and quantum wormholes," *Phys. Rev.* **D92** no. 6, (2015) 064050, arXiv:1504.06336 [hep-th].

[13] N. Bao, J. Pollack, and G. N. Remmen, "Splitting Spacetime and Cloning Qubits: Linking No-Go Theorems across the ER=EPR Duality," *Fortsch. Phys.* **63** (2015) 705–710, arXiv:1506.08203 [hep-th].

[14] J. D. Bekenstein, "Black holes and the second law," *Lett. Nuovo Cim.* **4** (1972) 737–740.

[15] J. D. Bekenstein, "Black holes and entropy," *Phys. Rev.* **D7** (1973) 2333–2346.

[16] J. D. Bekenstein, "Generalized second law of thermodynamics in black hole physics," *Phys. Rev.* **D9** (1974) 3292–3300.

[17] J. D. Bekenstein, "A Universal Upper Bound on the Entropy to Energy Ratio for Bounded Systems," *Phys. Rev.* **D23** (1981) 287.

[18] G. 't Hooft, "Dimensional reduction in quantum gravity," in *Salamfest 1993:0284-296*, pp. 0284–296. 1993. arXiv:gr-qc/9310026 [gr-qc].

[19] L. Susskind, "The World as a hologram," *J. Math. Phys.* **36** (1995) 6377–6396, arXiv:hep-th/9409089 [hep-th].

[20] R. Blumenhagen, D. Lüst, and S. Theisen, *Basic concepts of string theory*. Springer, Heidelberg, Germany, 2013.

[21] M. B. Green, J. H. Schwarz, and E. Witten, *SUPERSTRING THEORY. VOL. 1: INTRODUCTION*. Cambridge University Press, Cambridge, UK, 1988.

[22] M. B. Green, J. H. Schwarz, and E. Witten, *SUPERSTRING THEORY. VOL. 2: LOOP AMPLITUDES, ANOMALIES AND PHENOMENOLOGY*. Cambridge University Press, Cambridge, UK, 1988.

[23] J. Polchinski, *String theory. Vol. 1: An introduction to the bosonic string*. Cambridge University Press, Cambridge, UK, 2007.

[24] J. Polchinski, *String theory. Vol. 2: Superstring theory and beyond*. Cambridge University Press, Cambridge, UK, 2007.

[25] J. M. Maldacena, "The Large N limit of superconformal field theories and supergravity," *Int. J. Theor. Phys.* **38** (1999) 1113–1133, arXiv:hep-th/9711200 [hep-th]. [Adv. Theor. Math. Phys.2,231(1998)].

[26] S. S. Gubser, I. R. Klebanov, and A. M. Polyakov, "Gauge theory correlators from noncritical string theory," *Phys. Lett.* **B428** (1998) 105–114, arXiv:hep-th/9802109 [hep-th].

[27] E. Witten, "Anti-de Sitter space and holography," *Adv. Theor. Math. Phys.* **2** (1998) 253–291, arXiv:hep-th/9802150 [hep-th].

[28] D. A. Lowe and L. Thorlacius, "AdS / CFT and the information paradox," *Phys. Rev.* **D60** (1999) 104012, arXiv:hep-th/9903237 [hep-th].

[29] P. Kovtun, D. T. Son, and A. O. Starinets, "Viscosity in strongly interacting quantum field theories from black hole physics," *Phys. Rev. Lett.* **94** (2005) 111601, arXiv:hep-th/0405231 [hep-th].

[30] D. T. Son and A. O. Starinets, "Viscosity, Black Holes, and Quantum Field Theory," *Ann. Rev. Nucl. Part. Sci.* **57** (2007) 95–118, arXiv:0704.0240 [hep-th].

[31] S. Bhattacharyya, V. E. Hubeny, S. Minwalla, and M. Rangamani, "Nonlinear Fluid Dynamics from Gravity," *JHEP* **02** (2008) 045, arXiv:0712.2456 [hep-th].

[32] M. Rangamani, "Gravity and Hydrodynamics: Lectures on the fluid-gravity correspondence," *Class. Quant. Grav.* **26** (2009) 224003, arXiv:0905.4352 [hep-th].

[33] J. Casalderrey-Solana, H. Liu, D. Mateos, K. Rajagopal, and U. A. Wiedemann, "Gauge/String Duality, Hot QCD and Heavy Ion Collisions," arXiv:1101.0618 [hep-th].

[34] M. Luzum and P. Romatschke, "Conformal Relativistic Viscous Hydrodynamics: Applications to RHIC results at s(NN)**(1/2) = 200-GeV," *Phys. Rev.* **C78** (2008) 034915, arXiv:0804.4015 [nucl-th]. [Erratum: Phys. Rev.C79,039903(2009)].

[35] J. D. Edelstein, J. P. Shock, and D. Zoakos, "The AdS/CFT Correspondence and Non-perturbative QCD," *AIP Conf. Proc.* **1116** (2009) 265–284, arXiv:0901.2534 [hep-ph].

[36] O. DeWolfe, S. S. Gubser, C. Rosen, and D. Teaney, "Heavy ions and string theory," *Prog. Part. Nucl. Phys.* **75** (2014) 86–132, arXiv:1304.7794 [hep-th].

[37] J. Sonnenschein, "Holography Inspired Stringy Hadrons," arXiv:1602.00704 [hep-th].

[38] J. Erdmenger, N. Evans, I. Kirsch, and E. Threlfall, "Mesons in Gauge/Gravity Duals - A Review," *Eur. Phys. J.* **A35** (2008) 81–133, arXiv:0711.4467 [hep-th].

[39] F. Brünner and A. Rebhan, "Nonchiral enhancement of scalar glueball decay in the witten-sakai-sugimoto model," *Phys. Rev. Lett.* **115** (Sep, 2015) 131601.

[40] S. S. Gubser, "Breaking an Abelian gauge symmetry near a black hole horizon," *Phys. Rev.* **D78** (2008) 065034, arXiv:0801.2977 [hep-th].

[41] S. A. Hartnoll, C. P. Herzog, and G. T. Horowitz, "Building a Holographic Superconductor," *Phys. Rev. Lett.* **101** (2008) 031601, arXiv:0803.3295 [hep-th].

[42] A. G. Green, "An Introduction to Gauge Gravity Duality and Its Application in

Condensed Matter," *Contemp. Phys.* **54** no. 1, (2013) 33, arXiv:1304.5908 [cond-mat.str-el].

[43] D. Musso, "Introductory notes on holographic superconductors," *PoS* **Modave2013** (2013) 004, arXiv:1401.1504 [hep-th].

[44] L. Susskind and E. Witten, "The Holographic bound in anti-de Sitter space," arXiv:hep-th/9805114 [hep-th].

[45] D. Z. Freedman, S. S. Gubser, K. Pilch, and N. P. Warner, "Renormalization group flows from holography supersymmetry and a c theorem," *Adv. Theor. Math. Phys.* **3** (1999) 363–417, arXiv:hep-th/9904017 [hep-th].

[46] R. C. Myers and A. Sinha, "Holographic c-theorems in arbitrary dimensions," *JHEP* **01** (2011) 125, arXiv:1011.5819 [hep-th].

[47] R. C. Myers and A. Sinha, "Seeing a c-theorem with holography," *Phys. Rev.* **D82** (2010) 046006, arXiv:1006.1263 [hep-th].

[48] D. L. Jafferis, I. R. Klebanov, S. S. Pufu, and B. R. Safdi, "Towards the F-Theorem: N=2 Field Theories on the Three-Sphere," *JHEP* **06** (2011) 102, arXiv:1103.1181 [hep-th].

[49] H. Casini and M. Huerta, "On the RG running of the entanglement entropy of a circle," *Phys. Rev.* **D85** (2012) 125016, arXiv:1202.5650 [hep-th].

[50] L. Susskind and J. Lindesay, *An introduction to black holes, information and the string theory revolution: The holographic universe*. World Scientific Publishing, Hackensack, USA, 2005.

[51] M. Ammon and J. Erdmenger, *Gauge/gravity duality*. Cambridge Univ. Pr., Cambridge, UK, 2015.

[52] H. Nastase, *Introduction to the ADS/CFT Correspondence*. Cambridge University Press, Cambridge, UK, 2015.

[53] M. Natsuume, "AdS/CFT Duality User Guide," *Lect. Notes Phys.* **903** (2015) pp.1–294, arXiv:1409.3575 [hep-th].

[54] M. Nielsen and I. Chuang, *Quantum Computation and Quantum Information: 10th Anniversary Edition*. Cambridge University Press, Cambridge, UK, 2010.

[55] S. Ryu and T. Takayanagi, "Holographic derivation of entanglement entropy from AdS/CFT," *Phys. Rev. Lett.* **96** (2006) 181602, arXiv:hep-th/0603001 [hep-th].

[56] S. Ryu and T. Takayanagi, "Aspects of Holographic Entanglement Entropy," *JHEP* **08** (2006) 045, arXiv:hep-th/0605073 [hep-th].

[57] R. M. Wald, "Black hole entropy is the Noether charge," *Phys. Rev.* **D48** (1993) 3427–3431, arXiv:gr-qc/9307038 [gr-qc].

[58] T. Jacobson, G. Kang, and R. C. Myers, "On black hole entropy," *Phys. Rev.* **D49** (1994) 6587–6598, arXiv:gr-qc/9312023 [gr-qc].

[59] V. Iyer and R. M. Wald, "Some properties of Noether charge and a proposal for dynamical black hole entropy," *Phys. Rev.* **D50** (1994) 846–864, arXiv:gr-qc/9403028 [gr-qc].

[60] D. V. Fursaev, A. Patrushev, and S. N. Solodukhin, "Distributional Geometry of Squashed Cones," *Phys. Rev.* **D88** no. 4, (2013) 044054, arXiv:1306.4000 [hep-th].

[61] R.-X. Miao, "A Note on Holographic Weyl Anomaly and Entanglement Entropy," *Class. Quant. Grav.* **31** (2014) 065009, arXiv:1309.0211 [hep-th].

[62] X. Dong, "Holographic Entanglement Entropy for General Higher Derivative Gravity," *JHEP* **01** (2014) 044, arXiv:1310.5713 [hep-th].

[63] J. Camps, "Generalized entropy and higher derivative Gravity," *JHEP* **03** (2014) 070, arXiv:1310.6659 [hep-th].

[64] M. Headrick, V. E. Hubeny, A. Lawrence, and M. Rangamani, "Causality & holographic entanglement entropy," *JHEP* **12** (2014) 162, arXiv:1408.6300 [hep-th].

[65] J. Kondo, "Resistance minimum in dilute magnetic alloys," *Progress of Theoretical Physics* **32** no. 1, (1964) 37–49.

[66] L. Kouwenhoven and L. Glazman, "Revival of the Kondo effect," arXiv:cond-mat/0104100.

[67] A. C. Hewson and J. Kondo, "Kondo effect," *Scholarpedia* **4** no. 3, (2009) 7529. revision #91408.

[68] J. Kondo, "Sticking to my bush," *Journal of the Physical Society of Japan* **74** no. 1, (2005) 1–3.

[69] D. K. C. MacDonald, W. B. Pearson, and I. M. Templeton, "Thermo-electricity at low temperatures. ix. the transition metals as solute and solvent," *Proceedings of the Royal Society of London A: Mathematical, Physical and Engineering Sciences* **266** no. 1325, (1962) 161–184.

[70] K. G. Wilson, "The renormalization group: Critical phenomena and the kondo problem," *Rev. Mod. Phys.* **47** (Oct, 1975) 773–840.

[71] P. W. Anderson, "A poor man's derivation of scaling laws for the kondo problem," *Journal of Physics C: Solid State Physics* **3** no. 12, 2436.

[72] H. Ishii, "Spin correlation in dilute magnetic alloys," *Journal of Low Temperature Physics* **32** no. 3, 457–467.

[73] E. S. Sørensen and I. Affleck, "Scaling theory of the kondo screening cloud," *Phys. Rev. B* **53** (Apr, 1996) 9153–9167.

[74] I. Affleck, "The Kondo screening cloud: what it is and how to observe it," *ArXiv e-prints* (Nov., 2009) , arXiv:0911.2209 [cond-mat.mes-hall].

[75] L. Kouwenhoven and C. Marcus, "Quantum dots," *Physics World* **11** no. 6, 35.

[76] S. Kachru, A. Karch, and S. Yaida, "Holographic Lattices, Dimers, and Glasses," *Phys. Rev.* **D81** (2010) 026007, arXiv:0909.2639 [hep-th].

[77] S. Kachru, A. Karch, and S. Yaida, "Adventures in Holographic Dimer Models," *New J. Phys.* **13** (2011) 035004, arXiv:1009.3268 [hep-th].

[78] S. Harrison, S. Kachru, and G. Torroba, "A maximally supersymmetric Kondo model," *Class. Quant. Grav.* **29** (2012) 194005, arXiv:1110.5325 [hep-th].

[79] N. Karaiskos, K. Sfetsos, and E. Tsatis, "Brane embeddings in sphere submanifolds," *Class. Quant. Grav.* **29** (2012) 025011, arXiv:1106.1200 [hep-th].

[80] K. Jensen, S. Kachru, A. Karch, J. Polchinski, and E. Silverstein, "Towards a holographic marginal Fermi liquid," *Phys. Rev.* **D84** (2011) 126002, arXiv:1105.1772 [hep-th].

[81] A. Faraggi and L. A. Pando Zayas, "The Spectrum of Excitations of Holographic Wilson Loops," *JHEP* **05** (2011) 018, arXiv:1101.5145 [hep-th].

[82] A. Faraggi, W. Mueck, and L. A. Pando Zayas, "One-loop Effective Action of the Holographic Antisymmetric Wilson Loop," *Phys. Rev.* **D85** (2012) 106015, arXiv:1112.5028 [hep-th].

[83] P. Benincasa and A. V. Ramallo, "Fermionic impurities in Chern-Simons-matter theories," *JHEP* **02** (2012) 076, arXiv:1112.4669 [hep-th].

[84] G. Itsios, K. Sfetsos, and D. Zoakos, "Fermionic impurities in the unquenched ABJM," *JHEP* **01** (2013) 038, arXiv:1209.6617 [hep-th].

[85] P. Benincasa and A. V. Ramallo, "Holographic Kondo Model in Various Dimensions," *JHEP* **06** (2012) 133, arXiv:1204.6290 [hep-th].

[86] J. Erdmenger, C. Hoyos, A. O'Bannon, and J. Wu, "A Holographic Model of the Kondo Effect," *JHEP* **12** (2013) 086, arXiv:1310.3271 [hep-th].

[87] A. O'Bannon, I. Papadimitriou, and J. Probst, "A Holographic Two-Impurity Kondo Model," *JHEP* **01** (2016) 103, arXiv:1510.08123 [hep-th].

[88] E. S. Sørensen, M.-S. Chang, N. Laflorencie, and I. Affleck, "Impurity entanglement entropy and the kondo screening cloud," *Journal of Statistical Mechanics: Theory and Experiment* **2007** no. 01, L01001.

[89] I. Affleck, N. Laflorencie, and E. S. Sørensen, "Entanglement entropy in quantum impurity systems and systems with boundaries," *Journal of Physics A: Mathematical and Theoretical* **42** no. 50, 504009.

[90] E. S. Sørensen, M.-S. Chang, N. Laflorencie, and I. Affleck, "Quantum impurity entanglement," *Journal of Statistical Mechanics: Theory and Experiment* **2007** no. 08, P08003.

[91] E. Eriksson and H. Johannesson, "Impurity entanglement entropy in kondo systems from conformal field theory," *Phys. Rev. B* **84** (Jul, 2011) 041107.

[92] T. Takayanagi, "Holographic Dual of BCFT," *Phys. Rev. Lett.* **107** (2011) 101602, `arXiv:1105.5165 [hep-th]`.

[93] M. Fujita, T. Takayanagi, and E. Tonni, "Aspects of AdS/BCFT," *JHEP* **11** (2011) 043, `arXiv:1108.5152 [hep-th]`.

[94] M. Nozaki, T. Takayanagi, and T. Ugajin, "Central Charges for BCFTs and Holography," *JHEP* **06** (2012) 066, `arXiv:1205.1573 [hep-th]`.

[95] L. Susskind, "Butterflies on the Stretched Horizon," `arXiv:1311.7379 [hep-th]`.

[96] L. Susskind, "Computational Complexity and Black Hole Horizons," *Fortsch. Phys.* **64** (2016) 24–43, `arXiv:1402.5674 [hep-th]`.

[97] L. Susskind, "Addendum to Computational Complexity and Black Hole Horizons," `arXiv:1403.5695 [hep-th]`.

[98] L. Susskind, "Entanglement is not enough," *Fortsch. Phys.* **64** (2016) 49–71, `arXiv:1411.0690 [hep-th]`.

[99] M. Alishahiha, "Holographic Complexity," *Phys. Rev.* **D92** no. 12, (2015) 126009, `arXiv:1509.06614 [hep-th]`.

[100] A. R. Brown, D. A. Roberts, L. Susskind, B. Swingle, and Y. Zhao, "Complexity Equals Action," `arXiv:1509.07876 [hep-th]`.

[101] M. Miyaji, T. Numasawa, N. Shiba, T. Takayanagi, and K. Watanabe, "Distance between Quantum States and Gauge-Gravity Duality," *Phys. Rev. Lett.* **115** no. 26, (2015) 261602, `arXiv:1507.07555 [hep-th]`.

[102] M. Visser, *Lorentzian wormholes: From Einstein to Hawking*. AIP Press, Woodbury, USA, 1995.

[103] J. D. Brown and M. Henneaux, "Central Charges in the Canonical Realization of Asymptotic Symmetries: An Example from Three-Dimensional Gravity," *Commun. Math. Phys.* **104** (1986) 207–226.

[104] R. Bousso, "The Holographic principle," *Rev. Mod. Phys.* **74** (2002) 825–874, `arXiv:hep-th/0203101 [hep-th]`.

[105] R. M. Wald, *General Relativity*. Chicago Univ. Pr., Chicago, USA, 1984.

[106] S. W. Hawking, "Black hole explosions," *Nature* **248** (1974) 30–31.

[107] S. W. Hawking, "Particle Creation by Black Holes," *Commun. Math. Phys.* **43** (1975) 199–220.

[108] J. M. Bardeen, B. Carter, and S. W. Hawking, "The Four laws of black hole mechanics," *Commun. Math. Phys.* **31** (1973) 161–170.

[109] S. W. Hawking, "Gravitational radiation from colliding black holes," *Phys. Rev. Lett.* **26** (1971) 1344–1346.

[110] S. W. Hawking, "Black holes in general relativity," *Commun. Math. Phys.* **25** (1972) 152–166.

[111] R. D. Sorkin, R. M. Wald, and Z. J. Zhang, "Entropy of selfgravitating radiation," *Gen. Rel. Grav.* **13** (1981) 1127–1146.

[112] W. G. Unruh and R. M. Wald, "Acceleration Radiation and Generalized Second Law of Thermodynamics," *Phys. Rev.* **D25** (1982) 942–958.

[113] S. Hawking and R. Penrose, *The Nature of space and time*. Princeton Univ. Pr., Princeton, USA, 1996.

[114] V. P. Frolov and I. D. Novikov, eds., *Black hole physics: Basic concepts and new developments*. Kluwer Academic, Dordrecht, Netherlands, 1998.

[115] L. Smolin, "Lessons from Einstein's 1915 discovery of general relativity," `arXiv:1512.07551 [physics.hist-ph]`.

[116] G. t. Hooft, "The Cellular Automaton Interpretation of Quantum Mechanics. A View on the Quantum Nature of our Universe, Compulsory or Impossible?," `arXiv:1405.1548 [quant-ph]`.

[117] T. Padmanabhan, "Gravity and/is Thermodynamics," *Curr. Sci.* **109** (2015) 2236–2242, `arXiv:1512.06546 [gr-qc]`.

[118] T. Padmanabhan, "Exploring the Nature of Gravity," 2016. `arXiv:1602.01474 [gr-qc]`.

[119] R. Goswami and G. F. R. Ellis, "The holographic principle in general relativity: the case of Petrov type D vacuum spacetimes," `arXiv:1511.05700 [gr-qc]`.

[120] R. Bousso, "A Covariant entropy conjecture," *JHEP* **07** (1999) 004, `arXiv:hep-th/9905177 [hep-th]`.

[121] V. Faraoni, "Cosmological and Black Hole Apparent Horizons," *Lect. Notes Phys.* **907** (2015) pp.1–199.

[122] R. Bousso, "Holography in general space-times," *JHEP* **06** (1999) 028,

arXiv:hep-th/9906022 [hep-th].

[123] S. Carlip, *Quantum gravity in 2+1 dimensions*. Cambridge University Press, Cambridge, UK, 2003.

[124] O. Coussaert, M. Henneaux, and P. van Driel, "The Asymptotic dynamics of three-dimensional Einstein gravity with a negative cosmological constant," *Class. Quant. Grav.* **12** (1995) 2961–2966, arXiv:gr-qc/9506019 [gr-qc].

[125] A. Strominger, "Black hole entropy from near horizon microstates," *JHEP* **02** (1998) 009, arXiv:hep-th/9712251 [hep-th].

[126] V. Balasubramanian and P. Kraus, "A Stress tensor for Anti-de Sitter gravity," *Commun. Math. Phys.* **208** (1999) 413–428, arXiv:hep-th/9902121 [hep-th].

[127] P. Kraus, "Lectures on black holes and the AdS(3) / CFT(2) correspondence," *Lect. Notes Phys.* **755** (2008) 193–247, arXiv:hep-th/0609074 [hep-th].

[128] S. J. van Albada, "Boundary Dynamics of Three-Dimensional Asymptotically Anti-de Sitter Space-Times," arXiv:1601.07055 [hep-th].

[129] W. Li, W. Song, and A. Strominger, "Chiral Gravity in Three Dimensions," *JHEP* **04** (2008) 082, arXiv:0801.4566 [hep-th].

[130] M. Banados, M. Henneaux, C. Teitelboim, and J. Zanelli, "Geometry of the (2+1) black hole," *Phys. Rev.* **D48** (1993) 1506–1525, arXiv:gr-qc/9302012 [gr-qc]. [Erratum: Phys. Rev.D88,069902(2013)].

[131] M. Banados, C. Teitelboim, and J. Zanelli, "The Black hole in three-dimensional space-time," *Phys. Rev. Lett.* **69** (1992) 1849–1851, arXiv:hep-th/9204099 [hep-th].

[132] R. Blumenhagen and E. Plauschinn, "Introduction to conformal field theory," *Lect. Notes Phys.* **779** (2009) 1–256.

[133] O. Aharony, S. S. Gubser, J. M. Maldacena, H. Ooguri, and Y. Oz, "Large N field theories, string theory and gravity," *Phys. Rept.* **323** (2000) 183–386, arXiv:hep-th/9905111 [hep-th].

[134] E. D'Hoker and D. Z. Freedman, "Supersymmetric gauge theories and the AdS / CFT correspondence," in *Strings, Branes and Extra Dimensions: TASI 2001: Proceedings*, pp. 3–158. 2002. arXiv:hep-th/0201253 [hep-th].

[135] J. McGreevy, "Holographic duality with a view toward many-body physics," *Adv. High Energy Phys.* **2010** (2010) 723105, arXiv:0909.0518 [hep-th].

[136] J. Polchinski, "Introduction to Gauge/Gravity Duality," in *Proceedings, Theoretical Advanced Study Institute in Elementary Particle Physics (TASI 2010). String Theory and Its Applications: From meV to the Planck Scale: Boulder, Colorado, USA, June 1-25, 2010*, pp. 3–46. 2010. arXiv:1010.6134 [hep-th].

[137] A. V. Ramallo, "Introduction to the AdS/CFT correspondence," *Springer Proc. Phys.* **161** (2015) 411–474, arXiv:1310.4319 [hep-th].

[138] V. E. Hubeny, "The AdS/CFT Correspondence," *Class. Quant. Grav.* **32** no. 12, (2015) 124010, arXiv:1501.00007 [gr-qc].

[139] S. de Haro, D. R. Mayerson, and J. Butterfield, "Conceptual Aspects of Gauge/Gravity Duality," arXiv:1509.09231 [physics.hist-ph].

[140] J. Dai, R. G. Leigh, and J. Polchinski, "New Connections Between String Theories," *Mod. Phys. Lett.* **A4** (1989) 2073–2083.

[141] J. Polchinski, "Dirichlet Branes and Ramond-Ramond charges," *Phys. Rev. Lett.* **75** (1995) 4724–4727, arXiv:hep-th/9510017 [hep-th].

[142] E. Kiritsis, *String theory in a nutshell*. Princeton Univ. Pr., Princeton, USA, 2007.

[143] O. Aharony and E. Witten, "Anti-de Sitter space and the center of the gauge group," *JHEP* **11** (1998) 018, arXiv:hep-th/9807205 [hep-th].

[144] G. Hooft, "A planar diagram theory for strong interactions," *Nuclear Physics B* **72** no. 3, (1974) 461 – 473.

[145] S. Weinberg and E. Witten, "Limits on Massless Particles," *Phys. Lett.* **B96** (1980) 59.

[146] S. de Haro, S. N. Solodukhin, and K. Skenderis, "Holographic reconstruction of space-time and renormalization in the AdS / CFT correspondence," *Commun. Math. Phys.* **217** (2001) 595–622, arXiv:hep-th/0002230 [hep-th].

[147] K. Skenderis, "Lecture notes on holographic renormalization," *Class. Quant. Grav.* **19** (2002) 5849–5876, arXiv:hep-th/0209067 [hep-th].

[148] O. Aharony, O. Bergman, D. L. Jafferis, and J. Maldacena, "N=6 superconformal Chern-Simons-matter theories, M2-branes and their gravity duals," *JHEP* **10** (2008) 091, arXiv:0806.1218 [hep-th].

[149] T. Sakai and S. Sugimoto, "Low energy hadron physics in holographic QCD," *Prog. Theor. Phys.* **113** (2005) 843–882, arXiv:hep-th/0412141 [hep-th].

[150] T. Sakai and S. Sugimoto, "More on a holographic dual of QCD," *Prog. Theor. Phys.* **114** (2005) 1083–1118, arXiv:hep-th/0507073 [hep-th].

[151] R. Collier, C. Burkhardt, and L. Lin, *Optical Holography*. Academic Press, New York, USA, 1971.

[152] L. Bergmann, H. Niedrig, and H. Eichler, *Optik: Wellen- und Teilchenoptik*. de Gruyter, Berlin, 2004.

[153] D. V. Khveshchenko, "Contrasting string holography to its optical namesake," *Europhys. Lett.* **109** (2015) 61001, arXiv:1411.1693 [cond-mat.str-el].

[154] A. Almheiri, X. Dong, and D. Harlow, "Bulk Locality and Quantum Error Correction in AdS/CFT," *JHEP* **04** (2015) 163, arXiv:1411.7041 [hep-th].

[155] B. Freivogel, R. A. Jefferson, L. Kabir, B. Mosk, and I.-S. Yang, "Casting Shadows on Holographic Reconstruction," *Phys. Rev.* **D91** no. 8, (2015) 086013, arXiv:1412.5175 [hep-th].

[156] E. Mintun, J. Polchinski, and V. Rosenhaus, "Bulk-Boundary Duality, Gauge Invariance, and Quantum Error Corrections," *Phys. Rev. Lett.* **115** no. 15, (2015) 151601, arXiv:1501.06577 [hep-th].

[157] F. Pastawski, B. Yoshida, D. Harlow, and J. Preskill, "Holographic quantum error-correcting codes: Toy models for the bulk/boundary correspondence," *JHEP* **06** (2015) 149, arXiv:1503.06237 [hep-th].

[158] X. Dong, D. Harlow, and A. C. Wall, "Bulk Reconstruction in the Entanglement Wedge in AdS/CFT," arXiv:1601.05416 [hep-th].

[159] T. Nishioka, S. Ryu, and T. Takayanagi, "Holographic Entanglement Entropy: An Overview," *J. Phys.* **A42** (2009) 504008, arXiv:0905.0932 [hep-th].

[160] S. Ghosh, R. M. Soni, and S. P. Trivedi, "On The Entanglement Entropy For Gauge Theories," *JHEP* **09** (2015) 069, arXiv:1501.02593 [hep-th].

[161] H. Araki and E. H. Lieb, "Entropy inequalities," *Commun. Math. Phys.* **18** (1970) 160–170.

[162] P. Calabrese and J. L. Cardy, "Entanglement entropy and quantum field theory," *J. Stat. Mech.* **0406** (2004) P06002, arXiv:hep-th/0405152 [hep-th].

[163] D. V. Fursaev, "Proof of the holographic formula for entanglement entropy," *JHEP* **09** (2006) 018, arXiv:hep-th/0606184 [hep-th].

[164] M. Headrick and T. Takayanagi, "A Holographic proof of the strong subadditivity of entanglement entropy," *Phys. Rev.* **D76** (2007) 106013, arXiv:0704.3719 [hep-th].

[165] M. Headrick, "Entanglement Renyi entropies in holographic theories," *Phys. Rev.* **D82** (2010) 126010, arXiv:1006.0047 [hep-th].

[166] A. Lewkowycz and J. Maldacena, "Generalized gravitational entropy," *JHEP* **08** (2013) 090, arXiv:1304.4926 [hep-th].

[167] T. Faulkner, "The Entanglement Renyi Entropies of Disjoint Intervals in AdS/CFT," arXiv:1303.7221 [hep-th].

[168] T. Hartman, "Entanglement Entropy at Large Central Charge," arXiv:1303.6955 [hep-th].

[169] V. E. Hubeny, M. Rangamani, and T. Takayanagi, "A Covariant holographic

entanglement entropy proposal," *JHEP* **07** (2007) 062, arXiv:0705.0016 [hep-th].

[170] V. E. Hubeny, H. Maxfield, M. Rangamani, and E. Tonni, "Holographic entanglement plateaux," *JHEP* **08** (2013) 092, arXiv:1306.4004 [hep-th].

[171] A. C. Wall, "Maximin Surfaces, and the Strong Subadditivity of the Covariant Holographic Entanglement Entropy," *Class. Quant. Grav.* **31** no. 22, (2014) 225007, arXiv:1211.3494 [hep-th].

[172] M. Headrick, "General properties of holographic entanglement entropy," *JHEP* **03** (2014) 085, arXiv:1312.6717 [hep-th].

[173] J. M. Maldacena, "Eternal black holes in anti-de Sitter," *JHEP* **04** (2003) 021, arXiv:hep-th/0106112 [hep-th].

[174] E. Witten, "Anti-de Sitter space, thermal phase transition, and confinement in gauge theories," *Adv. Theor. Math. Phys.* **2** (1998) 505–532, arXiv:hep-th/9803131 [hep-th].

[175] M. Mezard, G. Parisi, and M. Virasoro, *Spin Glass Theory and Beyond*. No. Nr. 1993 in Lecture Notes in Physics Series. World Scientific, New Jersey, USA, 1987.

[176] L.-Y. Hung, R. C. Myers, and M. Smolkin, "On Holographic Entanglement Entropy and Higher Curvature Gravity," *JHEP* **04** (2011) 025, arXiv:1101.5813 [hep-th].

[177] J. de Boer, M. Kulaxizi, and A. Parnachev, "Holographic Entanglement Entropy in Lovelock Gravities," *JHEP* **07** (2011) 109, arXiv:1101.5781 [hep-th].

[178] E. A. Bergshoeff, O. Hohm, and P. K. Townsend, "Massive Gravity in Three Dimensions," *Phys. Rev. Lett.* **102** (2009) 201301, arXiv:0901.1766 [hep-th].

[179] E. A. Bergshoeff, O. Hohm, and P. K. Townsend, "More on Massive 3D Gravity," *Phys. Rev.* **D79** (2009) 124042, arXiv:0905.1259 [hep-th].

[180] Y. Liu and Y.-w. Sun, "Note on New Massive Gravity in AdS(3)," *JHEP* **04** (2009) 106, arXiv:0903.0536 [hep-th].

[181] D. Grumiller and O. Hohm, "AdS(3)/LCFT(2): Correlators in New Massive Gravity," *Phys. Lett.* **B686** (2010) 264–267, arXiv:0911.4274 [hep-th].

[182] Y. Liu and Y.-W. Sun, "Consistent Boundary Conditions for New Massive Gravity in AdS_3," *JHEP* **05** (2009) 039, arXiv:0903.2933 [hep-th].

[183] U. Camara dS, C. P. Constantinidis, and G. M. Sotkov, "New Massive Gravity Holography," *Int. J. Mod. Phys.* **A28** (2013) 1350073, arXiv:1009.2665 [hep-th].

[184] A. Sinha, "On the new massive gravity and AdS/CFT," *JHEP* **06** (2010) 061, arXiv:1003.0683 [hep-th].

[185] B. Chen, J.-j. Zhang, J.-d. Zhang, and D.-l. Zhong, "Aspects of Warped AdS_3/CFT_2 Correspondence," *JHEP* **04** (2013) 055, arXiv:1302.6643 [hep-th].

[186] M. Alishahiha, A. F. Astaneh, and M. R. M. Mozaffar, "Entanglement Entropy for Logarithmic Conformal Field Theory," *Phys. Rev.* **D89** no. 6, (2014) 065023, arXiv:1310.4294 [hep-th].

[187] B. Chen, F.-y. Song, and J.-j. Zhang, "Holographic Renyi entropy in $AdS_3/LCFT_2$ correspondence," *JHEP* **03** (2014) 137, arXiv:1401.0261 [hep-th].

[188] S. Deser, R. Jackiw, and S. Templeton, "Topologically Massive Gauge Theories," *Annals Phys.* **140** (1982) 372–411.

[189] S. Deser, R. Jackiw, and S. Templeton, "Three-Dimensional Massive Gauge Theories," *Phys. Rev. Lett.* **48** (1982) 975–978.

[190] E. A. Bergshoeff, S. de Haan, O. Hohm, W. Merbis, and P. K. Townsend, "Zwei-Dreibein Gravity: A Two-Frame-Field Model of 3D Massive Gravity," *Phys. Rev. Lett.* **111** no. 11, (2013) 111102, arXiv:1307.2774. [Erratum: Phys. Rev. Lett.111,no.25,259902(2013)].

[191] M. Bañados, C. Deffayet, and M. Pino, "The Boulware-Deser mode in 3D first-order massive gravity," *Phys. Rev.* **D88** no. 12, (2013) 124016, arXiv:1310.3249 [hep-th].

[192] E. A. Bergshoeff, O. Hohm, W. Merbis, A. J. Routh, and P. K. Townsend, "Chern-Simons-like Gravity Theories," *Lect. Notes Phys.* **892** (2015) 181–201, arXiv:1402.1688 [hep-th].

[193] M. R. Setare and H. Adami, "On the new version of Generalized Zwei-Dreibein Gravity," *Phys. Lett.* **B750** (2015) 31–36, arXiv:1508.00120 [hep-th].

[194] E. Bergshoeff, O. Hohm, W. Merbis, A. J. Routh, and P. K. Townsend, "Minimal Massive 3D Gravity," *Class. Quant. Grav.* **31** (2014) 145008, arXiv:1404.2867 [hep-th].

[195] A. S. Arvanitakis and P. K. Townsend, "Minimal Massive 3D Gravity Unitarity Redux," *Class. Quant. Grav.* **32** no. 8, (2015) 085003, arXiv:1411.1970 [hep-th].

[196] M. R. Setare, "On the Generalized Minimal Massive Gravity," *Nucl. Phys.* **B898** (2015) 259–275, arXiv:1412.2151 [hep-th].

[197] P. Breitenlohner and D. Z. Freedman, "Stability in Gauged Extended Supergravity," *Annals Phys.* **144** (1982) 249.

[198] P. Kraus and F. Larsen, "Microscopic black hole entropy in theories with higher derivatives," *JHEP* **09** (2005) 034, arXiv:hep-th/0506176 [hep-th].

[199] A. Bhattacharyya, M. Sharma, and A. Sinha, "On generalized gravitational entropy, squashed cones and holography," *JHEP* **01** (2014) 021, arXiv:1308.5748

[hep-th].

[200] S. M. Hosseini and A. Véliz-Osorio, "Free-kick condition for entanglement entropy in higher curvature gravity," *Phys. Rev.* **D92** no. 4, (2015) 046010, arXiv:1505.00826 [hep-th].

[201] M. R. M. Mozaffar, A. Mollabashi, M. M. Sheikh-Jabbari, and M. H. Vahidinia, "Holographic Entanglement Entropy, Field Redefinition Invariance and Higher Derivative Gravity Theories," arXiv:1603.05713 [hep-th].

[202] D. Lovelock, "The Einstein tensor and its generalizations," *J. Math. Phys.* **12** (1971) 498–501.

[203] T. Padmanabhan and D. Kothawala, "Lanczos-Lovelock models of gravity," *Phys. Rept.* **531** (2013) 115–171, arXiv:1302.2151 [gr-qc].

[204] X. O. Camanho, J. D. Edelstein, and J. M. Sánchez De Santos, "Lovelock theory and the AdS/CFT correspondence," *Gen. Rel. Grav.* **46** (2014) 1637, arXiv:1309.6483 [hep-th].

[205] J. D. Edelstein, "Lovelock theory, black holes and holography," *Springer Proc. Math. Stat.* **60** (2014) 19–36, arXiv:1303.6213 [gr-qc].

[206] M. Brigante, H. Liu, R. C. Myers, S. Shenker, and S. Yaida, "Viscosity Bound Violation in Higher Derivative Gravity," *Phys. Rev.* **D77** (2008) 126006, arXiv:0712.0805 [hep-th].

[207] M. Brigante, H. Liu, R. C. Myers, S. Shenker, and S. Yaida, "The Viscosity Bound and Causality Violation," *Phys. Rev. Lett.* **100** (2008) 191601, arXiv:0802.3318 [hep-th].

[208] A. Buchel and R. C. Myers, "Causality of Holographic Hydrodynamics," *JHEP* **08** (2009) 016, arXiv:0906.2922 [hep-th].

[209] D. M. Hofman, "Higher Derivative Gravity, Causality and Positivity of Energy in a UV complete QFT," *Nucl. Phys.* **B823** (2009) 174–194, arXiv:0907.1625 [hep-th].

[210] X. O. Camanho, J. D. Edelstein, J. Maldacena, and A. Zhiboedov, "Causality Constraints on Corrections to the Graviton Three-Point Coupling," *JHEP* **02** (2016) 020, arXiv:1407.5597 [hep-th].

[211] S. Banerjee, A. Bhattacharyya, A. Kaviraj, K. Sen, and A. Sinha, "Constraining gravity using entanglement in AdS/CFT," *JHEP* **05** (2014) 029, arXiv:1401.5089 [hep-th].

[212] D. G. Boulware and S. Deser, "String Generated Gravity Models," *Phys. Rev. Lett.* **55** (1985) 2656.

[213] T. Jacobson and R. C. Myers, "Black hole entropy and higher curvature

interactions," *Phys. Rev. Lett.* **70** (1993) 3684–3687, arXiv:hep-th/9305016 [hep-th].

[214] J. T. Wheeler, "Symmetric Solutions to the Gauss-Bonnet Extended Einstein Equations," *Nucl. Phys.* **B268** (1986) 737.

[215] J. T. Wheeler, "Symmetric Solutions to the Maximally Gauss-Bonnet Extended Einstein Equations," *Nucl. Phys.* **B273** (1986) 732.

[216] R.-G. Cai, "Gauss-Bonnet black holes in AdS spaces," *Phys. Rev.* **D65** (2002) 084014, arXiv:hep-th/0109133 [hep-th].

[217] X. O. Camanho and J. D. Edelstein, "A Lovelock black hole bestiary," *Class. Quant. Grav.* **30** (2013) 035009, arXiv:1103.3669 [hep-th].

[218] A. Bhattacharyya, A. Kaviraj, and A. Sinha, "Entanglement entropy in higher derivative holography," *JHEP* **08** (2013) 012, arXiv:1305.6694 [hep-th].

[219] B. Chen and J.-j. Zhang, "Note on generalized gravitational entropy in Lovelock gravity," *JHEP* **07** (2013) 185, arXiv:1305.6767 [hep-th].

[220] S. S. Pal, "Extremal Surfaces And Entanglement Entropy," *Nucl. Phys.* **B882** (2014) 352–385, arXiv:1312.0088 [hep-th].

[221] A. Buchel, R. C. Myers, and A. Sinha, "Beyond eta/s = 1/4 pi," *JHEP* **03** (2009) 084, arXiv:0812.2521 [hep-th].

[222] T. Torii and H. Maeda, "Spacetime structure of static solutions in Gauss-Bonnet gravity: Charged case," *Phys. Rev.* **D72** (2005) 064007, arXiv:hep-th/0504141 [hep-th].

[223] B. Hartmann, J. Riedel, and R. Suciu, "Gauss-Bonnet boson stars," *Phys. Lett.* **B726** (2013) 906–912, arXiv:1308.3391 [gr-qc].

[224] L. J. Henderson, R. B. Mann, and S. Stotyn, "Gauss-Bonnet Boson Stars with a Single Killing Vector," *Phys. Rev.* **D91** no. 2, (2015) 024009, arXiv:1403.1865 [gr-qc].

[225] E. Caceres, M. Sanchez, and J. Virrueta, "Holographic Entanglement Entropy in Time Dependent Gauss-Bonnet Gravity," arXiv:1512.05666 [hep-th].

[226] N. Sircar, J. Sonnenschein, and W. Tangarife, "Extending the scope of holographic mutual information and chaotic behavior," arXiv:1602.07307 [hep-th].

[227] S. Sarkar and A. C. Wall, "Second Law Violations in Lovelock Gravity for Black Hole Mergers," *Phys. Rev.* **D83** (2011) 124048, arXiv:1011.4988 [gr-qc].

[228] V. E. Hubeny and M. Rangamani, "Causal Holographic Information," *JHEP* **06** (2012) 114, arXiv:1204.1698 [hep-th].

[229] V. E. Hubeny, M. Rangamani, and E. Tonni, "Global properties of causal wedges in

asymptotically AdS spacetimes," *JHEP* **10** (2013) 059, arXiv:1306.4324 [hep-th].

[230] J. L. Cardy, "Boundary conditions, fusion rules and the verlinde formula," *Nuclear Physics B* **324** no. 3, (1989) 581 – 596.

[231] J. L. Cardy, "Boundary conformal field theory," arXiv:hep-th/0411189 [hep-th].

[232] E. Wong and I. Affleck, "Tunneling in quantum wires: A boundary conformal field theory approach," *Nuclear Physics B* **417** no. 3, (1994) 403 – 438.

[233] M. Chiodaroli, E. D'Hoker, and M. Gutperle, "Simple Holographic Duals to Boundary CFTs," *JHEP* **02** (2012) 005, arXiv:1111.6912 [hep-th].

[234] M. Chiodaroli, E. D'Hoker, and M. Gutperle, "Holographic duals of Boundary CFTs," *JHEP* **07** (2012) 177, arXiv:1205.5303 [hep-th].

[235] J. Estes, K. Jensen, A. O'Bannon, E. Tsatis, and T. Wrase, "On Holographic Defect Entropy," *JHEP* **05** (2014) 084, arXiv:1403.6475 [hep-th].

[236] J. Estes, "Finite temperature holographic duals of 2-dimensional BCFTs," *JHEP* **07** (2015) 020, arXiv:1503.07375 [hep-th].

[237] G. W. Gibbons and S. W. Hawking, "Action Integrals and Partition Functions in Quantum Gravity," *Phys. Rev.* **D15** (1977) 2752–2756.

[238] M. Alishahiha and R. Fareghbal, "Boundary CFT from Holography," *Phys. Rev.* **D84** (2011) 106002, arXiv:1108.5607 [hep-th].

[239] M. R. Setare and V. Kamali, "Correlation functions of BCFT," arXiv:1109.3849 [hep-th].

[240] Y. Kwon, S. Nam, J.-D. Park, and S.-H. Yi, "AdS/BCFT Correspondence for Higher Curvature Gravity: An Example," *JHEP* **06** (2012) 119, arXiv:1201.1988 [hep-th].

[241] M. Fujita, M. Kaminski, and A. Karch, "SL(2,Z) Action on AdS/BCFT and Hall Conductivities," *JHEP* **07** (2012) 150, arXiv:1204.0012 [hep-th].

[242] Y. Nakayama, "Is boundary conformal in CFT?," *Phys. Rev.* **D87** no. 4, (2013) 046005, arXiv:1210.6439 [hep-th].

[243] D. Melnikov, E. Orazi, and P. Sodano, "On the AdS/BCFT Approach to Quantum Hall Systems," *JHEP* **05** (2013) 116, arXiv:1211.1416 [hep-th].

[244] A. F. Astaneh and A. E. Mosaffa, "Quantum Local Quench, AdS/BCFT and Yo-Yo String," *JHEP* **05** (2015) 107, arXiv:1405.5469 [hep-th].

[245] J. M. Magán, D. Melnikov, and M. R. O. Silva, "Black Holes in AdS/BCFT and Fluid/Gravity Correspondence," *JHEP* **11** (2014) 069, arXiv:1408.2580

[hep-th].

[246] M. Visser and C. Barcelo, "Energy conditions and their cosmological implications," in *Proceedings, 3rd International Conference on Particle Physics and the Early Universe (COSMO 1999)*, pp. 98–112. 2000. arXiv:gr-qc/0001099 [gr-qc].

[247] E. Curiel, "A Primer on Energy Conditions," arXiv:1405.0403 [physics.hist-ph].

[248] M. Parikh and J. P. van der Schaar, "Derivation of the Null Energy Condition," *Phys. Rev.* **D91** no. 8, (2015) 084002, arXiv:1406.5163 [hep-th].

[249] N. Engelhardt and A. C. Wall, "Extremal Surface Barriers," *JHEP* **03** (2014) 068, arXiv:1312.3699 [hep-th].

[250] T. Azeyanagi, A. Karch, T. Takayanagi, and E. G. Thompson, "Holographic calculation of boundary entropy," *JHEP* **03** (2008) 054–054, arXiv:0712.1850 [hep-th].

[251] S. Fischetti, D. Marolf, and A. C. Wall, "A paucity of bulk entangling surfaces: AdS wormholes with de Sitter interiors," *Class. Quant. Grav.* **32** (2015) 065011, arXiv:1409.6754 [hep-th].

[252] J. D. Brown, "Action functionals for relativistic perfect fluids," *Class. Quant. Grav.* **10** (1993) 1579–1606, arXiv:gr-qc/9304026 [gr-qc].

[253] P. W. Anderson, "Localized magnetic states in metals," *Phys. Rev.* **124** (Oct, 1961) 41–53.

[254] I. Affleck, "A Current Algebra Approach to the Kondo Effect," *Nucl. Phys.* **B336** (1990) 517.

[255] I. Affleck and A. W. W. Ludwig, "The Kondo effect, conformal field theory and fusion rules," *Nucl. Phys.* **B352** (1991) 849–862.

[256] I. Affleck and A. W. W. Ludwig, "Critical theory of overscreened Kondo fixed points," *Nucl. Phys.* **B360** (1991) 641–696.

[257] I. Affleck and A. W. W. Ludwig, "Universal noninteger 'ground state degeneracy' in critical quantum systems," *Phys. Rev. Lett.* **67** (1991) 161–164.

[258] I. Affleck, "Conformal field theory approach to the Kondo effect," *Acta Phys. Polon.* **B26** (1995) 1869–1932, arXiv:cond-mat/9512099 [cond-mat].

[259] O. Parcollet, A. Georges, G. Kotliar, and A. Sengupta, "Overscreened multichannel SU(n) kondo model: Large-n solution and conformal field theory," *Phys. Rev. B* **58** (Aug, 1998) 3794–3813.

[260] N. E. Bickers, "Review of techniques in the large-n expansion for dilute magnetic alloys," *Rev. Mod. Phys.* **59** (Oct, 1987) 845–939.

[261] P. Coleman and N. Andrei, "Diagonalisation of the generalised anderson model," *Journal of Physics C: Solid State Physics* **19** no. 17, (1986) 3211.

[262] P. Coleman, "Mixed valence as an almost broken symmetry," *Phys. Rev. B* **35** (Apr, 1987) 5072–5116.

[263] T. Senthil, S. Sachdev, and M. Vojta, "Fractionalized fermi liquids," *Phys. Rev. Lett.* **90** (May, 2003) 216403.

[264] T. Senthil, M. Vojta, and S. Sachdev, "Weak magnetism and non-fermi liquids near heavy-fermion critical points," *Phys. Rev. B* **69** (Jan, 2004) 035111.

[265] A. A. Abrikosov, "Magnetic impurities in nonmagnetic metals," *Soviet Physics Uspekhi* **12** no. 2, (1969) 168.

[266] N. Iqbal, H. Liu, and M. Mezei, "Quantum phase transitions in semilocal quantum liquids," *Phys. Rev.* **D91** no. 2, (2015) 025024, arXiv:1108.0425 [hep-th].

[267] K. Skenderis and M. Taylor, "Branes in AdS and p p wave space-times," *JHEP* **06** (2002) 025, arXiv:hep-th/0204054 [hep-th].

[268] J. A. Harvey and A. B. Royston, "Localized modes at a D-brane-O-plane intersection and heterotic Alice atrings," *JHEP* **04** (2008) 018, arXiv:0709.1482 [hep-th].

[269] E. I. Buchbinder, J. Gomis, and F. Passerini, "Holographic gauge theories in background fields and surface operators," *JHEP* **12** (2007) 101, arXiv:0710.5170 [hep-th].

[270] J. A. Harvey and A. B. Royston, "Gauge/Gravity duality with a chiral N=(0,8) string defect," *JHEP* **08** (2008) 006, arXiv:0804.2854 [hep-th].

[271] J. Pawelczyk and S.-J. Rey, "Ramond-ramond flux stabilization of D-branes," *Phys. Lett.* **B493** (2000) 395–401, arXiv:hep-th/0007154 [hep-th].

[272] J. M. Camino, A. Paredes, and A. V. Ramallo, "Stable wrapped branes," *JHEP* **05** (2001) 011, arXiv:hep-th/0104082 [hep-th].

[273] J. Gomis and F. Passerini, "Holographic Wilson Loops," *JHEP* **08** (2006) 074, arXiv:hep-th/0604007 [hep-th].

[274] S. Yamaguchi, "Wilson loops of anti-symmetric representation and D5-branes," *JHEP* **05** (2006) 037, arXiv:hep-th/0603208 [hep-th].

[275] W. Mueck, "The Polyakov Loop of Anti-symmetric Representations as a Quantum Impurity Model," *Phys. Rev.* **D83** (2011) 066006, arXiv:1012.1973 [hep-th]. [Erratum: Phys. Rev.D84,129903(2011)].

[276] S. Sachdev, "Holographic metals and the fractionalized Fermi liquid," *Phys. Rev. Lett.* **105** (2010) 151602, arXiv:1006.3794 [hep-th].

[277] E. Gava, K. S. Narain, and M. H. Sarmadi, "On the bound states of p-branes and (p+2)-branes," *Nucl. Phys.* **B504** (1997) 214–238, arXiv:hep-th/9704006 [hep-th].

[278] M. Aganagic, R. Gopakumar, S. Minwalla, and A. Strominger, "Unstable solitons in noncommutative gauge theory," *JHEP* **04** (2001) 001, arXiv:hep-th/0009142 [hep-th].

[279] D. Marolf and S. F. Ross, "Boundary Conditions and New Dualities: Vector Fields in AdS/CFT," *JHEP* **11** (2006) 085, arXiv:hep-th/0606113 [hep-th].

[280] A. Castro, D. Grumiller, F. Larsen, and R. McNees, "Holographic Description of AdS(2) Black Holes," *JHEP* **11** (2008) 052, arXiv:0809.4264 [hep-th].

[281] O. Aharony, M. Berkooz, and E. Silverstein, "Multiple trace operators and nonlocal string theories," *JHEP* **08** (2001) 006, arXiv:hep-th/0105309 [hep-th].

[282] E. Witten, "Multitrace operators, boundary conditions, and AdS / CFT correspondence," arXiv:hep-th/0112258 [hep-th].

[283] M. Berkooz, A. Sever, and A. Shomer, "'Double trace' deformations, boundary conditions and space-time singularities," *JHEP* **05** (2002) 034, arXiv:hep-th/0112264 [hep-th].

[284] W. Israel, "Singular hypersurfaces and thin shells in general relativity," *Nuovo Cim.* **B44S10** (1966) 1.

[285] D. Marolf and S. Yaida, "Energy conditions and junction conditions," *Phys. Rev.* **D72** (2005) 044016, arXiv:gr-qc/0505048 [gr-qc].

[286] R. A. Battye and B. Carter, "Generic junction conditions in brane world scenarios," *Phys. Lett.* **B509** (2001) 331–336, arXiv:hep-th/0101061 [hep-th].

[287] G. Hayward and J. Louko, "Variational principles for nonsmooth metrics," *Phys.Rev.* **D42** (1990) 4032–4041.

[288] G. Hayward, "Gravitational action for space-times with nonsmooth boundaries," *Phys.Rev.* **D47** (1993) 3275–3280.

[289] C. Kaeonikhom, "Israel Junction Conditions on Hypersurface from Variational Principle Approach," in *Proceedings of the First National Symposium on Physics Graduate Research*. 2006. see http://www.if.nu.ac.th/sites/default/files/publications/ChakkritNSPG1.pdf.

[290] R. Giambò and F. Giannoni, "Minimal geodesics on manifolds with discontinuous metrics," *Journal of the London Mathematical Society* **67** no. 2, (2003) 527–544.

[291] S. Yamaguchi, "Holographic RG flow on the defect and g theorem," *JHEP* **10** (2002) 002, arXiv:hep-th/0207171 [hep-th].

[292] D. Friedan and A. Konechny, "On the boundary entropy of one-dimensional quantum systems at low temperature," *Phys. Rev. Lett.* **93** (2004) 030402, arXiv:hep-th/0312197 [hep-th].

[293] A. Almheiri, D. Marolf, J. Polchinski, and J. Sully, "Black Holes: Complementarity or Firewalls?," *JHEP* **02** (2013) 062, arXiv:1207.3123 [hep-th].

[294] D. Harlow and P. Hayden, "Quantum Computation vs. Firewalls," *JHEP* **06** (2013) 085, arXiv:1301.4504 [hep-th].

[295] J. Watrous, "Quantum Computational Complexity," *ArXiv e-prints* (Apr., 2008) , arXiv:0804.3401 [quant-ph].

[296] A. Brown, D. A. Roberts, L. Susskind, B. Swingle, and Y. Zhao, "Complexity, Action, and Black Holes," arXiv:1512.04993 [hep-th].

[297] J. L. F. Barbon and E. Rabinovici, "Holographic complexity and spacetime singularities," *JHEP* **01** (2016) 084, arXiv:1509.09291 [hep-th].

[298] D. Bak, "Information metric and Euclidean Janus correspondence," arXiv:1512.04735 [hep-th].

[299] D. Momeni, S. A. H. Mansoori, and R. Myrzakulov, "Holographic Complexity in Gauge/String Superconductors," arXiv:1601.03011 [hep-th].

[300] K. Hattori, K. Itakura, S. Ozaki, and S. Yasui, "QCD Kondo effect: quark matter with heavy-flavor impurities," *Phys. Rev.* **D92** no. 6, (2015) 065003, arXiv:1504.07619 [hep-ph].

[301] H. Matsueda, "Multiscale Entanglement Renormalization Ansatz for Kondo Problem," arXiv:1208.2872 [cond-mat.stat-mech].

[302] G. Vidal, "Class of quantum many-body states that can be efficiently simulated," *Phys. Rev. Lett.* **101** (Sep, 2008) 110501.

[303] B. Swingle, "Entanglement Renormalization and Holography," *Phys. Rev.* **D86** (2012) 065007, arXiv:0905.1317 [cond-mat.str-el].

[304] H. Casini and M. Huerta, "A Finite entanglement entropy and the c-theorem," *Phys. Lett.* **B600** (2004) 142–150, arXiv:hep-th/0405111 [hep-th].

[305] P. Martin-Moruno and M. Visser, "Semiclassical energy conditions for quantum vacuum states," *JHEP* **09** (2013) 050, arXiv:1306.2076 [gr-qc].

[306] A. Antillon, J. Escalona, and M. Torres, "Vortices and domain walls in a Chern-Simons theory with magnetic moment interaction," *Phys. Rev.* **D55** (1997) 6327–6338, arXiv:hep-th/9702118 [hep-th].

[307] M. Torres, "Domain walls in a Chern-Simons theory," in *Solitons: Properties, dynamics, interactions, applications. Proceedings, Workshop, Kingston, Canada,*

July 20-26, 1997. 1997. arXiv:hep-th/9710113 [hep-th].

Acknowledgements

When looking back at the past years and my so far short academic career, I cannot deny that there are a great many people to whom I am deeply indebted.

First and foremost is of course my PhD advisor Johanna Erdmenger, who has not only guided me through these scientific endeavours of the last three years, but who has also provided me with a lot of advice concerning scientific work, publishing papers, giving conference and seminar talks, applying for postdoc positions and many other things.

Similarly, my gratitude goes to all the senior scientists with whom I have interacted during my PhD, be it for research or for other aspects of life and work at the Max Planck institute: Martin Ammon, Andrew O'Bannon, Ralph Blumenhagen, Dieter Lüst, Carlos Hoyos, Ivo Sachs, Jonathan Shock, Frank Steffen, Jackson Wu and the members of my PhD committee.

I would like to thank all the fellow students and young researchers at the MPI, both in the AdS/CFT group and in the other research groups. Without them, life at the institute would most certainly not have been as, well, *lively* as it was, and I certainly learned a lot from all of them. My special gratefulness goes of course to the coauthors of the papers that this work is based on, Andrew O'Bannon, Charlotte Sleight, Max-Niklas Newrzella, Carlos Hoyos, Jackson Wu and Johanna Erdmenger, as well as to the collaborators of all the failed projects and bad ideas of mine that never produced a publishable result: Ann-Kathrin Straub, Daniel Brattan and Abhiram Kidambi.

Last but not least, I would like to thank my friends outside of Munich, my flatmate Max-Josef Hartl and my family for their continued support during these years of hard, yet for an outsider often invisible and inapprehensible work.